Graduate Schools Yearbook 2008

Department of Chemical
and Biochemical Engineering
Technical University of Denmark

Graduate Schools Yearbook 2008

Editors:
Kim Dam-Johansen
Martin Bøjer

Contents

Preface

The research interests of DTU Chemical and Biochemical Engineering span a wide range of topics including chemical product and process design and engineering applied in industrial fields related to chemistry, biotechnology, food technology, pharmaceuticals and energy. The Department collaborates closely with large parts of Danish industry, with international enterprises and with leading universities in Europe, USA and Asia. This intensive and internationally oriented cooperation is documented through our many PhD-projects.

The Chemical and Biochemical Engineering Graduate Schools Yearbook 2008 covers short descriptions of most of the PhD-projects at the department. The yearbook is a platform for our newly matriculated graduate students to present the background and aims motivating their studies while graduate students matriculated for longer time present the progress and status of their research projects.

I hope the readers of the yearbook will find it of value to follow our research and that the content may provide a basis for establishing new contacts and cooperation. The Department is developing very fast these years in most of our research fields and we expect the number of PhD-projects to increase even further in the near future.

I wish you a pleasant reading – and welcome you to contact us for future cooperation.

Kim Dam-Johansen

Head of Department, Professor

Jane Agger

Phone:	+45 4525 2861
Fax:	+45 4525 2906
E-mail:	jag@kt.dtu.dk
WWW:	http://www.kt.dtu.dk
Supervisors:	Anne Meyer
	Hanne Risbjerg Sørensen, Novozymes A/S

PhD Study
Started: March 2007
To be completed: April 2010

Enzymatic Opening of Diferulate Cross Linking in Plant Cell Walls

Abstract
Cereal residues such as e.g. wheat bran, brewers spent grain and corn fiber are rich in arabinoxylan and pose an important resource for the manufacturing of bioactive food ingredients and as raw material for bioethanol production. However, an improved utilization of these residues is highly dependent on efficient enzymatic hydrolysis. The hydrolysis is currently limited for some types of hemicellulose possibly due to the presence of diferulic acid cross linking in the primary cell wall structure. These cross linkings are believed to present a physical/chemical barrier preventing complete enzymatic hydrolysis of the polymers. The aim of this project is to open up diferulate cross linking of polysaccharides via enzymatic hydrolysis. Furthermore, it is the aim to obtain new knowledge regarding the occurrence and influence of diferulates on solubility and enzyme accessibility in plant cell walls.

Introduction

Cereal by-products from e.g. wheat, barley and corn are renewable resources with a potential of being an inexpensive raw material for production of bioethanol or bioactive food components. They are rich in non-starch structural polysaccharides with arabinoxylan being the major hemicellulose compound [1]. However, currently the utilization of these polysaccharides is limited due to inefficient conversion processes and enzymes pose a realistic opportunity for better exploitation. Polymers of arabinoxylan are known to be cross linked in certain plant cell wall materials with dehydrodimers of ferulic acid [1]. These cross linkings present a barrier currently preventing complete enzymatic hydrolysis of the polymers. Esterification of ferulic acid at 0-5-arabinofuranosyl moiety in arabinoxylan can cross link to form dehydrodimers with adjacent polymers and form rigid structures [2]. The extent of ferulic acid dimerization along with the degree of substitution with arabinose, glucuronic acid, acetic acid and monomeric ferulic acid are factors determining the solubility and the enzymatic accessibility of the polymer. Besides cross linking the arabinoxylan polymers, the dehydrodimers of ferulic acid are also believed to cross link to other polymeric structures in the cell wall, for instance lignin and structural proteins

[3]. Figure 1 shows a schematic illustration of the proposed structure of cross linked arabinoxylan.
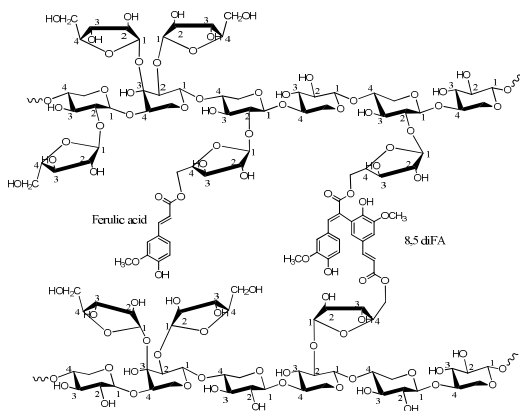
Figure 1: Schematic sketch of arabinoxylan cross linked by dehydrodimers of ferulic acid. The positional substitutions of arabinose are at this point uncertain.

Specific objectives

The project is based upon three major hypotheses, namely that the presence of diferulate cross linking in

the plant cell walls represents a physical/chemical barrier for enzymatic hydrolysis of the structural carbohydrates and in particular the arabinoxylan. Secondly it is believed that identification of enzymes and design of proper reaction conditions will accelerate the efficiency of the enzymatic opening of the cell wall matrix and thereby boost the degradation of structural polysaccharides. Finally, with such a process it will be possible to upgrade non-valuable cereal by-product streams to raw materials for biofuel production or for bioactive components in the food industry.

Results and discussion

Corn fiber is a cereal by-product with large industrial importance, because it is a by-product from the corn based starch production in the United States. It mainly consists of the pericarp cell wall of the corn kernel and the major chemical composition was investigated by acidic and alkaline hydrolysis and analysed by HPAEC and RP-HPLC methods.

Table 1: Monosaccharide composition of corn fiber (mg/g DM). Average of three samples ± standard deviation.

Component	Concentration (mg/g DM)
Glucose	393 ± 13
Galactose	46.7 ± 3.2
Xylose	233 ± 21
Arabinose	158 ± 10

Table 2: Chemical composition of corn fiber (mg/g DM). Average of three samples ± standard deviation.

Component	Concentration (mg/g DM)
Ash	7.91± 0.3
Polysaccharides[a]	831
Protein	89.9 ± 17
Lignin	76.6 ± 2.7
Acetic acid	42.4 ± 3.2
Total phenolics[a]	32.5
Ferulic acid	16.3 ± 0.2
Diferulic acid	14.6 ± 0.3
p-coumatic acid	1.63 ± 0.0
Total[a]	1080

[a]summarized from the individual components.

The content and composition of monosaccharides in corn fiber (Table 1) show that glucose is the major component. Glucose will mainly originate from starch and cellulose and starch determination (HCl hydrolysis) showed that the starch can be quantified to approx. 23% of the total dry matter (data not shown). The starch is most likely residual starch from the endosperm loosely attach to the cell wall surfaces and not an integrated part of the cell wall matrix. Accounting for this amount of starch the cellulose content can be estimated to 16%. The content of xylose, arabinose and galactose will represent the hemicellulosic polysaccharides with arabinoxylan as the major specimen. Using conventional assumptions the total amount of arabinoxylan can be estimated to 36% on a dry matter

basis. Looking into other cell wall components (Table 2) protein and lignin comprises approx. 9% and 7.6% respectively, identifying a relatively complex cell wall matrix. The presence of phenolic compounds other than lignin summarises to approx. 3% of the total dry matter, of which the diferulic acids constitutes 45%. Assuming equal distribution of the diferulic acids on the arabinoxylan polymer every 25 arabinosyl-moiety of the arabinoxylan chain will be substituted with a dehydrodimer of ferulic acid. Furthermore, every 22 arabinosyl-moiety will be substituted with the monomeric ferulic acid. Analysis has revealed that the diferulic acids are mainly composed of the 8,5'-benz, 8-O-4', 5,5' and 8,5' form of the dehydrodimers, which is also consistent with previous findings [4]. p-coumaric acid is only found in minor amounts.

Conclusion

The polysaccharide composition of corn fiber reveals a large potential for use as a raw material for biofuel production or functional food ingredients due to a high content of residual starch, cellulose and a high content of arabinoxylan. However, the high degree of substitution especially with diferulic acids within the hemicellulose polymers complicates the chemical structure of the cell wall matrix and will most likely limit an efficient enzymatic hydrolysis. The presence of several types of compounds in the cell wall will add to the necessity of performing hydrolysis with a complex set of enzyme activities, which again will complicate the reaction condition optimization. However, the identification of key enzyme activities might expose the cell wall structure to already known and optimized enzymes and thereby create the basis for complete or controlled hydrolysis.

References

1. L. Saulnier, C. Marot, E. Chanliaud, J-F. Thibault. Carbohydr. Polym. 26 (1995) 279-287
2. L. Saulnier, M-J. Crépeau, M. Lahaye, J-F. Thibault, M.T. Garcia-Conesa, P.A. Kroon, G. Williamson. Carbohydr. Research 320 (1999) 82-92
3. D.W.S. Wong. Appl. Biochem. Biotechn. 133 (2) (2006) 87-112
4. L. Saulnier, J-F. Thibault. J Sci Food Agric 79 (1999) 396-402

List of publications
No publications yet

Jimmy Andersen

Phone: +45 4525 2838
Fax: +45 4525 2258
E-mail: jia@kt.dtu.dk
WWW: http://www.kt.dtu.dk
Supervisors: Peter Glarborg
Peter Arendt Jensen
Søren Lovmand Hvid, DONG Energy

PhD Study
Started: April 2006
To be completed: April 2009

CFD Modeling of Gas-Phase Combustion and Validation by Bench-Scale Measurements

Abstract
The project concerns development and validation of CFD models with integrated chemical reactions, so that mixing as well as chemical reactions can be predicted in combustion processes. The long term scope of the project is prediction of NO formation and destruction in the freeboard of grate fired boilers. Therefore a model reactor setup has been constructed, that can reproduce the conditions present in the freeboard of grate fired boilers. The setup is to serve as a validation case for the CFD models.

Introduction
Computational Fluid Dynamics (CFD) is a powerful tool to predict mixing and fluid motion, and it have gained increasing popularity in design and trouble shooting industrial combustion installations. It is however challenging to include chemical kinetic models in CFD codes.

The focus of this project is to combine knowledge of chemical kinetic mechanisms with the prediction of mixing and local combustion stoichiometry that commercial CFD codes can provide.

In particular the project focuses on modeling the formation and destruction of NO in the freeboard section of grate fired boilers. For this purpose a bench scale freeboard combustion chamber has been designed and constructed, that will make it possible to provide well controlled and detailed measurements for validation of a CFD freeboard model. At present only limited well controlled measuring data on combustion in non swirled flames that can be used as CFD validation is available in the literature.

Validation of CFD models is essential if the modeling approach is to be the basis of research and design work. The initial objective of this project is therefore to supply reliable and relevant test data for modeling the mixing and gas phase reactions taking place in the freeboard section of grate fired boilers.

Specific objective
The overall objectives of this PhD study are:
- To provide detailed validation data for CFD models.
- To develop and validate a CFD based model of freeboard processes in grate fired boilers.
- To implement and validate a chemical kinetic NO mechanism in a CFD model.

Experimental setup
An experimental setup has been constructed to investigate the chemical reactions taking place in the freeboard section of a grate fired power plant. The setup is designed so that the flue gas from a substoichiometric natural gas flame is mixed with additional natural gas. This gas mixture is supposed to simulate the pyrolysis and primary combustion gasses emerging from a straw layer at grate firing conditions.

The combustion gasses are led through a flow straightner, which can be thought of as the surface of the bed layer, and into the freeboard section, where secondary gas is added to complete the combustion process.

The setup is an almost 3 meter long cylindrical construction that consists of two major sections; a 1st stage and a freeboard section, the diameter in the freeboard section is 49 cm. (see figure 1).
Several ports give entrance to the reactor and thereby make it possible to perform temperature measurements and gas sampling at many different positions, as well as visual access is possible for optical measurements.

Ammonia addition to the reactor is done to simulate fuel nitrogen – a major precursor to NO [1].

Figure 1: Sketch of the experimental setup – a natural gas fired freeboard simulator

Complete mapping of the freeboard combustion chamber is being done for important parameters:

- Temperature – A suction pyrometer provide detailed temperature mapping in the freeboard chamber.

- Velocity – Laser Doppler Anemometry (LDA) measurements provide gas velocity measurements, using a non-intruding particle tracer technique

Figure 2: Picture from the LDA experiments.

- Gas species concentrations - Extractive gas analysis using quenching probes makes it possible to detect and quantify numerous gas phase species (for instance O_2, CO, CO_2, NO

and NH_3) by means of standard analyzing techniques.

Results and Discussion

Figures 3 and 4 compare the CFD predictions of the axial velocity, with measurement data from the LDA measurements at the first and second measurement position (133 and 373 mm down in the FBS).

In the plots, near side experimental measurements should provide the most reliable data. There seem to be a fairly good quantitative agreement between the measured data and the CFD predictions. When taking into consideration the uncertainties connected with seeding (difficult to seed to gas streams in the same concentration) and laser beam measurement area (11 mm radial measurement area) and alignment, the data actually compares well.
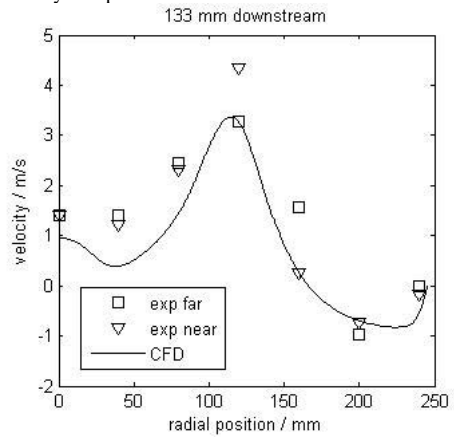
Figure 3: Comparison between measured average axial velocity and predictions from a CFD model with standard k-ε turbulence model.
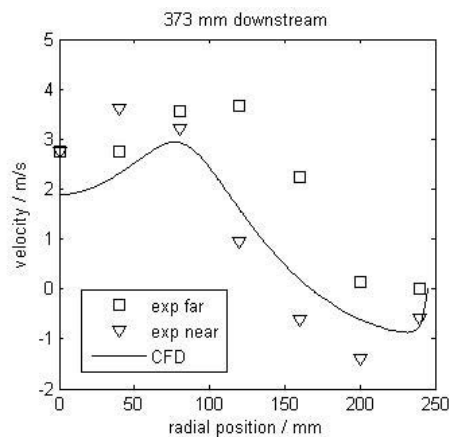
Figure 4: Comparison between measured average axial velocity and predictions from a CFD model with standard k-ε turbulence model.

Figures 5 and 6 compare the CFD predictions of the velocity fluctuations due to turbulence, with measurement data from the LDA measurements at the first and second measurement positions (133 and 373 mm down in the FBS). Although there at the individual measurement positions might be quite large differences between CFD predictions and measured values, it appears that the velocity fluctuation or turbulence level in general is captured satisfactorily. This is very important, when applying the next step in the CFD model, the combustion process.

When implementing species transport and combustion in a CFD model the conversion rate of the reactants are directly correlated with predicted velocity fluctuations.
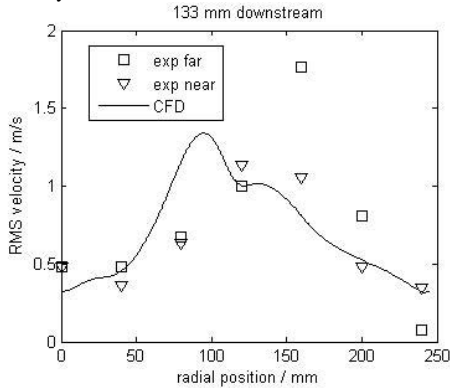
Figure 5: Comparison between measured axial velocity fluctuations and predictions from a CFD model with standard k-ε turbulence model.
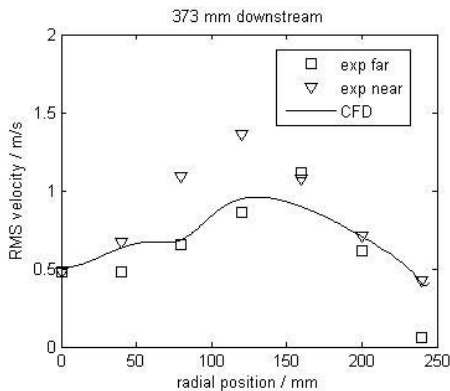
Figure 5: Comparison between measured axial velocity fluctuations and predictions from a CFD model with standard k-ε turbulence model.

In the following the turbulence-chemistry interaction model applied is the eddy-dissipation model [2], which assumes that the chemical reaction rate is governed by the large-eddy mixing time scale

k/ε, where k is the turbulent kinetic energy and ε the dissipation of turbulent kinetic energy.

$$(1) \quad R_i = \nu_i \cdot MW_i \cdot A \cdot \frac{\varepsilon}{k} \cdot \min_r \frac{Y_r}{\nu'_r \cdot MW_r}$$

In eq. 1 R_i is the rate of production of species i due to reaction, ν'_i, is the stoichiometric coefficient, MW denotes the molar weight of either species i, or reactant r. A is an empirical constant (=4,0) and Y_r is the mass fraction of the particular reactant r. The expression $\min_r$ means that the rate is determined from whatever reactant that causes the minimum reactant rate, either oxygen or fuel.
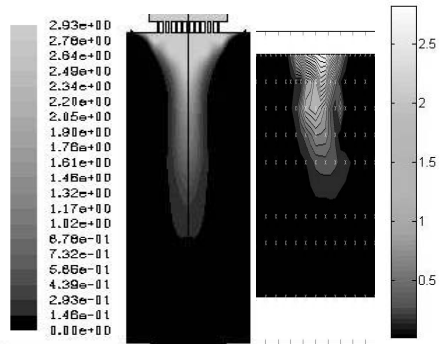
Figure 7: Left: Contours of CO concentrations predicted by the CFD model. Right: Measured CO contours.

Figure 7 shows the predicted CO contours by the CFD model compared with the measured CO levels. CO is an intermediate product in the combustion process, and is therefore representative for the reaction zone. It appears that there is a reasonable agreement also between measured and calculated CO levels.
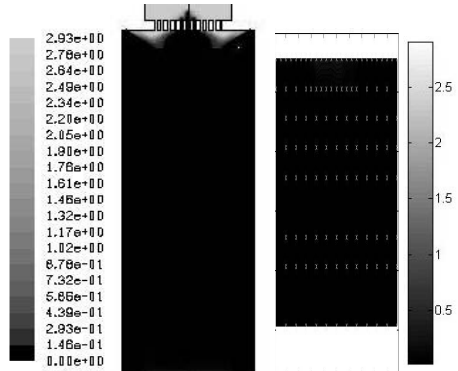
Figure 8: Left: Contours of CO concentrations predicted by the CFD model with maximal secondary air setting. Right: Measured CO contours.

Table 1: Modifed global methane combustion mechanisms with kinetic rate data - units in cm, s, cal, mol.

Reaction #	Reaction	A	β	Ea	Reaction orders
WD1	$CH_4 + 1.5\ O_2 \rightarrow CO + 2\ H_2O$	1.6E13	0	47.8E3	$[CH4]^{0.7}[O_2]^{0.8}$
WD2 (modified)	$CO + 0.5\ O_2 \rightarrow CO_2$	4.0E08	0	10.0E3	$[CO][O_2]^{0.25}[H_2O]^{0.5}$
WD3 (modified)	$CO_2 \rightarrow CO + 0.5\ O_2$	6.2E13	-0.97	78.4E3	$[CO_2][O_2]^{0.5}[H_2O]^{-0.25}$
JL1	$CH_4 + 0.5\ O_2 \rightarrow CO + 2\ H_2$	7.8E13	0	30.0E3	$[CH_4]^{0.5}[O_2]^{1.25}$
JL2	$CH_4 + H_2O \rightarrow CO + 3\ H_2$	3.0E11	0	30.0E3	$[CH_4][H_2O]$
JL3 (modified)	$H_2 + 0.5\ O_2 \rightarrow H_2O$	5.0E20	-1	30.0E3	$[H_2]^{0.25}[O_2]^{1.5}$
JL3 reverse	$H_2O \rightarrow H_2 + 0.5\ O_2$	2.9E20	-0.877	97.9E3	$[H_2]^{-0.75}[O_2][H_2O]$
JL4	$CO + H_2O \leftrightarrow CO_2 + H_2$	2.8E12	0	20.0E3	$[CO][H_2O]$

Another setting was analyzed, where the secondary air flow was put to a maximum (this was the only change).

Surprisingly, almost no CO was measured even in the top section of the FBS. Reassuringly this was low CO level is explained by the CFD results, which predicts an intense recirculation zone in the top of the freeboard section. This results in the fuel being converted almost entirely before the first measurement plane. This is also illustrated by the CO contour plot in Figure 8.

Oxy-Fuel mechanism development

The eddy dissipation concept (EDC) [3] is a more comprehensive turbulence-chemistry interaction model for CFD computations than the eddy dissipation model described above. It takes into consideration finite rate chemistry through the use of ideal reactor modeling, the calculated turbulence levels then determine reactive computational cell fraction and the reactor residence time [3].

As a spinoff of this project, global combustion mechanisms for EDC implementation have been evaluated against a detailed chemical kinetic model [4], under plug flow reactor conditions. This lead to the development of two new mechanisms based on the two-step mechanism of Westbrook and Dryer (WD) [5] and the four-step mechanism of Jones and Lindstedt (JL) [6].

In the modification approach, the initiating reactions involving hydrocarbon and oxygen were retained as in the original references, while modifying the H_2-CO-CO_2 reactions in order to improve prediction of major species concentrations. The main attention has been to capture the trend and level of CO predicted by the detailed mechanism under oxy fuel conditions.

The suggested mechanisms are displayed in Table 1, with an indication of, which reactions have been altered [7].

A CFD analysis of a propane oxy-fuel flame [8] has been performed using both the original and modified mechanisms. Compared to the original schemes, the modified WD mechanism improved the prediction of the temperature field and of CO in the post flame zone, while the modified JL mechanism provided a slightly better prediction of CO in the flame zone. [7]

Conclusions and Future Work

CFD modeling and experimental investigation of the conditions in the FBS have been performed, and a good agreement between numerical calculations and experimental data is observed. Furthermore the CFD model also serves to explain the dramatically different measurement results obtained by changing the experimental settings.

Future work will be to apply NO modeling. The most likely approach is by post-processing more or less comprehensive ammonia oxidation mechanism to perform a validation test of these mechanisms.

References

1. P. Glarborg, A.D. Jensen, J.E. Johnsson, Prog. Energ. Combust. Sci., 29 (2003) 89-113
2. B.F. Magnussen, B.H. Hjertager", Proc. Combust. Inst. 16 (1976) 719-729
3. I.R. Gran, B.F. Magnussen, Combust. Sci. Technol 119 (1996) 171-190
4. P. Glarborg, P, L.L.B. Bentzen, Energy Fuels 22 (2007) 291-296
5. C.K. Westbrook, F.L. Dryer, Combust. Sci. Technol. 27 (1981) 31-44
6. W.P. Jones, R.P. Lindstedt, Combust. Flame 73 (1988) 233-249
7. J. Andersen, C.L. Rasmussen, T. Giselsson, P. Glarborg, *Global combustion mechanisms for use in CFD modeling under Oxy-Fuel conditions*, **submitted to Energy and Fuels (2008)**
8. K. Andersson, F. Johnsson, Fuel 86 (2007) 656-688

Pavle Andrić

Phone:	+45 4525 2842
Fax:	+45 4588 2258
E-mail:	pan@kt.dtu.dk
WWW:	http://chec.kt.dtu.dk
Supervisors:	Kim Dam-Johansen
	Anne Meyer
	Peter Arendt Jensen

PhD Study
Started: October 2005
To be completed: April 2009

Reactor Design for Enzymatic Hydrolysis of Lignocellulosic Biomass for Second-Generation Bio-Ethanol Production

Abstract

Large-scale application of enzymatic hydrolysis of lignocellulose is limited by: a) lack of an appropriate reactor for the complex, heterogeneous and slow reaction, b) high amount of required enzymes (cellulases) per unit weight of substrate, due to their inefficient action on the recalcitrant substrate and loss of activity, and c) resulting too diluted product (glucose) output stream. The main problems related to reactor design lie in the inherently slow reaction and in the mixing of the highly viscous reaction mixture at high dry matter levels, while the activity of enzymes can be lost due to the product inhibition, un-productive adsorption to lignin, temperature de-activation, etc.

Introduction

Bio-ethanol, the ethanol produced from any kind of biomass, is today the world's most widely used transport bio-fuel, accounting for around 90 % of total consumption, and it has a central place in a new EU target for total share of bio-fuels (25 %) by year 2030. Furthermore, in the USA the bio-ethanol is one of the main bio-fuels, and the research focusing on further improving the technology for bio-fuels production will according to several speeches of former and present USA Presidents be intensified.

Production of ethanol from primary biomass, i.e. starch, which can be used as a food or feed, is a well established and known technology. However, this technology is significantly limited by the price of this kind of biomass.

An alternative feedstock to produce ethanol (Figure 1) is lignocellulose which has low or no value as food. Lignocellulosic biomass (Figure 2) includes a variety of relatively cheap agricultural or forestry residues, dedicated crops and different kinds of waste, such as wheat straw, corn stover, wood chips, etc.

Figure 2: One idealistic view of lignocellulose structure: cellulose micro- fibrils protected by lignin and hemi-cellulose [1]. In the lignocelulose, cellulose chains are aggregated together into elementary fibrils of crystalline structures. The bunches of elementary fibrils are embedded in a matrix of hemi-cellulose with a thickness of 7-30 nm, while lignin is located primarily on the exterior of the micro-fibril [2].

Figure 1: Bio-ethanol production from lignocellulosic biomass-simplified scheme of possible process

One of the possible process layouts (Figure 1) for bio-ethanol production from lignocellulose is composed of several main steps: biomass transport and handling, biomass pre-treatment, cellulose and hemi-cellulose hydrolysis, fermentation of sugars and ethanol recovery.

Upon transport to the site of production, biomass is handled using various mechanical operations (separation from dirt and stones, cutting, shredding, milling, conveying, etc.) to facilitate satisfactory heat and mass transfer in the subsequent steps. In the pre-treatment, biomass is usually submitted to high temperature and/or use of chemical agents, in order to open the lignocellulosic structure and make cellulose and hemi-cellulose susceptible to the following hydrolysis step. In hydrolysis, cellulose and hemi-cellulose are depolymerized and solubilized to monosaccharide sugars using enzymes or different acids, while in fermentation sugar-rich syrup is converted by microorganisms to ethanol which will be present in a mixture with water, other fermentation products and residual biomass etc. Ethanol can be further purified using stripping, distillation or pervaporation to obtain fuel grade.

Enzymatic degradation of lignocellulosic biomass
Sugars for fermentation to bio-ethanol can be produced from lignocellulose by using concentrated acid, dilute acid or enzymes. The enzymatic hydrolysis of cellulose seems to be the most promising method. Enzymatic hydrolysis is performed at mild conditions (40-50 $^{\circ}$C, pH 4-5) and utility costs are lower than in acid hydrolysis. Furthermore, since the enzymes (naturally occurring compounds which are biodegradable and environmentally benign) are catalysts that catalyze very specific reactions, a minimal level of undesirable byproducts are formed as well as no corrosion problems are associated with this type of reaction.
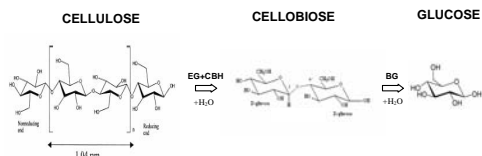
Figure 3: Simplified reaction mechanism of cellulose enzymatic degradation to glucose (saccharification).

However, the use of cellulose degrading enzymes (cellulases) for the hydrolysis of lignocellulosic biomass is a promising, but also a very difficult task and has not been yet demonstrated on a commercial scale, due to technical and economical obstacles. A key element underlying bio-ethanol processing cost reductions is improvement in the pre-treatment and enzymatic hydrolysis technology.

The large-scale application of enzymatic hydrolysis has in general been limited by lack of an effective reactor for the complex bio-catalysis, due to: a) the problems with the inadequate/inefficient stirring of the viscous and heterogeneous feed mixture (pre-treated biomass and enzymes) [3], b) (ligno)cellulose

structure (fibrous, porous, water retaining, partially crystalline and resistant to enzymes), c) enzymes deactivation (by heavy intermediate and final product inhibition, un-productive adsorption to lignin/substrate, shear forces, etc. d) inherent slow reaction rate.

The high glucose concentration from hydrolysis step is one of the main requirements for the feasible overall production of lignocellulosic bio-ethanol, due to the related ethanol concentration in fermentation (desired at least 13 % (v/v), Figure 4).
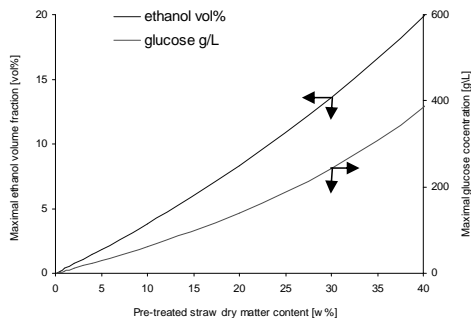
Figure 4: Theoretical (maximal achievable) glucose concentration (g per L of water) in the hydrolysis step and ethanol % (v/v) in the fermentation, in dependence from pre-treated ligno-cellulose dry matter content (DM%). Two lines are based on mass balances for material, reactions stoichiometry, assumption of 100% yield in the hydrolysis and fermentation steps and 50 % (w/w) cellulose fraction in the pre-treated material. It is accounted for the amount of water consumed by the reaction (Cellulose+ $H_2O \rightarrow$ Glucose).

Due to the overall economy of the process, it is necessary to operate hydrolysis at high DM%, which, as seen, is a significant challenge, due to the problematic mixing, pronounced product inhibition and non-productive adsorption to the unconvertible fraction of biomass. Furthermore, the operation of this reactor in a continuous mode with considerable conversion degree and the final glucose concentration is also a difficult task.

Specific Objectives
The main objective of this work is to investigate the enzymatic hydrolysis of lignocellulosic biomass (pre-treated wheat straw) and to develop a reactor concept for enzyme catalyzed cellulose conversion, which is more efficient than the classical batch reactor.

The first part of the study was to quantify and model the glucose product inhibition of commercial cellulases at glucose levels corresponding to high biomass dry matter contents, and evaluate techniques for removal of glucose from the hydrolysis reactor. The second ongoing part is to investigate the influence of mixing of pre-treated biomass during hydrolysis and evaluate related energy consumption. The third part deals with application of different reactor operational strategies in order to increase the conversion rate and final glucose concentration.

Glucose inhibition and removal studies

The enzymatic hydrolysis of lignocellulosic biomass is known to be product inhibited by glucose. In this study, the effects on cellulolytic glucose yields of glucose inhibition and *in-situ* glucose removal were examined and modeled during extended treatment of heat-pretreated wheat straw with the cellulolytic enzyme system, Celluclast® 1.5L, from Trichoderma reesei, supplemented with a β-glucosidase, Novozym® 188, from Aspergillus niger. Addition of glucose (0-40 g/L) significantly decreased the enzyme catalyzed glucose formation rates and final glucose yields, in a dose dependent manner, during 96 hr of reaction (Figure 5).

Although Michaelis-Menten kinetics do not suffice to model the kinetics of the complex multi-enzymatic degradation of cellulose, the data for the glucose inhibition were surprisingly well described by simple Michaelis-Menten inhibition models without great significance of the employed inhibition mechanism. Moreover, the experimental *in-situ* removal of glucose could be simulated by a Michaelis-Menten inhibition model (Figure 7). The data provide an important base for design of novel reactors and operating regimes which include continuous product removal during enzymatic hydrolysis of lignocellulose [5].

Figure 5: Net glucose concentration and net glucose yield (g of formed glucose per g theoretically available glucose) in the hydrolysis reactor at different initial glucose levels (0-40 g/L) [4]. The reaction was performed at 50 °C, pH 5, 350 rpm, 8 FPU/g dry matter and 13 CBU/g dry matter, acting on 2 %DM w/w hydro-thermally pre-treated wheat straw of 4 mm.
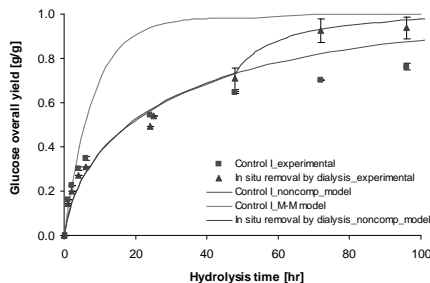
Figure 7: Comparison of experimental and modeling results for *in-situ* removal of glucose by dialysis and Control I [4]. The optimal parameters of the model (non-competitive inhibition) were: k_{cat} = 12 hr^{-1}, K_M = 0.9 mM and K_{IG} = 6.4 mM, determined using glucose addition studies.

When glucose was removed by dialysis during the enzymatic hydrolysis, the cellulose conversion rates and glucose yields increased (Figure 6). In fact, with dialytic *in-situ* glucose removal, the rate of enzyme catalyzed glucose release during 48-72 hr of reaction recovered from 20-40% to become ~70% of the rate recorded during 6-24 hr of reaction.

Mixing studies

The effect of mixing on enzymatic degradation of lignocellulosic substrate is not well understood. We are investigating this effect in experimental set-up consisted of 2x5 batch reactors (Figure 8) designed to apply various levels of shear force on the material. The studies include basic rheological characterization of biomass at different DM%, design of vessels and impellers, application of various stirring programs, determination of energy consumption during hydrolysis and processing of very high DM% reaction mixtures.

Figure 6: Glucose yield in hydrolysis reactor during removal of glucose by [4]: 1) filtration and replenishment of fresh buffer; 2) filtration and replenishment of fresh buffer and enzymes; 3) dialysis membrane, cut-off 1 kDa (*in-situ*).
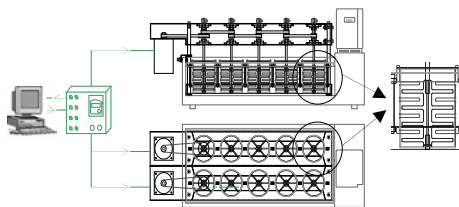
Figure 8: Experimental set-up for investigation of influence of mixing on enzymatic degradation of lignocellulose.

Hydrolysis reactor operational strategies

Due to the inherent slow reaction rate, enzyme inhibition by products and very viscous reaction mixture, the operation of enzymatic hydrolysis of lignocellulose at high DM%, especially in continuous reactor, is difficult assignment. We are currently investigating experimentally and by modeling, application of various methods (stream recycle, product concentration and product removal strategies, enzyme-substrate contact enhancement) in order to improve operation of different reactors (stirred batch, CSTR, packed-bed), to obtain higher conversion rates and final glucose concentrations.

One of the requirements that appear necessary for the reasonably high hydrolysis reaction rate is the continuous removal of the inhibitory glucose, as it is formed.
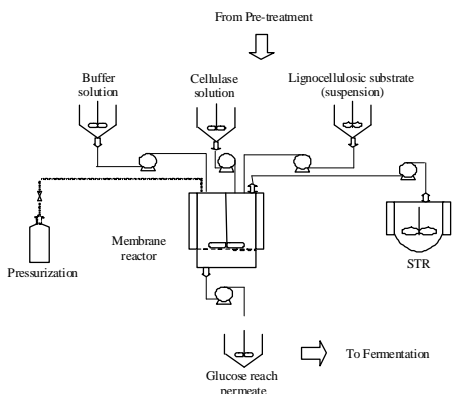
Figure 9: Semi- or continuous enzymatic digestion of lignocellulose in a hydrolysis reactor with simultaneous product removal.

We are temporary analyzing the system for semi- and continuous lignocellulose enzymatic hydrolysis, which central part is the membrane reactor for simultaneous cellulose degradation and glucose removal.

Acknowledgments

References and List of publications

[1] L. Rosgaard, S. Pedersen, A.S. Meyer. Fra halm til alkohol. Aktuel Naturvidenskab. 3 (2005) 11-14.

[2] K. Esau, Anatomy of Seed Plants, 2nd Edition, John Wiley , 1977

[3] L. Rosgaard, P Andrić, K Dam-Johansen, S. Pedersen, A.S. Meyer, Effects of substrate loading on enzymatic hydrolysis and viscosity of pretreated barley straw, Appl. Biochem. and Biotechn., 143 (2007) 27-40.

[4] P. Andrić, A.S. Meyer, P.A. Jensen, K. Dam-Johansen, Effect and modeling of glucose inhibition and in situ glucose removal during enzymatic hydrolysis of pretreated wheat straw. (submitted)

[5] P. Andrić, A.S. Meyer, P.A. Jensen, K. Dam-Johansen, Glucose inhibition of cellulolytic enzymes and lignocellulose hydrolysis reactor design. (in preparation)

P. Andrić, K. Dam-Johansen, A. S. Meyer, P. A. Jensen, Product inhibition of cellulases during enzymatic hydrolysis of the pre-treated ligno-cellulose, ECCE-6, Conference proceedings and poster presentation, Copenhagen, Denmark, 2007

P. Andrić, A. S. Meyer, K. Dam-Johansen, P. A. Jensen, Quantification of glucose inhibition of enzymatic cellulose degradation in pre-treated wheat straw, NordForsk 3rd workshop, Book of abstracts and oral presentation, Lyngby, Denmark, 2007

L. Rosgaard, P. Andrić, K. Dam-Johansen, S. Pedersen, A.S. Meyer, Effect of Fed-Batch Loading of Substrate on Enzymatic Hydrolysis and Viscosity of Pretreated Barley Straw, Conference proceedings and oral presentation, AIChE Annual Meeting, San Francisco, 2006

P. Andrić, K. Dam-Johansen, R. Gani, P. A. Jensen, Retrol vision: Preliminary Techno-Economical Analysis, Conference proceedings and oral presentation, AIChE Annual Meeting, San Francisco, 2006

P. Andrić, K. Dam-Johansen, P. A. Jensen, A. S. Meyer, Bio-ethanol process development: Application of enzymes during hydrolysis of the pre-treated wheat straw, Bio-process Engineering Course, Book of abstracts, poster and oral presentation, Brac-Croatia, (2006)

P. Andrić, K. Dam-Johansen, P. A. Jensen, L. Rosgaard, Bio-Ethanol Process Development: Pre-Treatment and Enzymatic Hydrolysis of Ligno-Cellulose, Book of abstracts and poster, DK$_2$ conference, Lyngby, 2006.

Anis Arnous

Address:	Building 227
Phone:	+45 4525 2966
Fax:	+45 4593 2906
E-mail:	aar@kt.dtu.dk
WWW:	http://www.bioeng.kt.dtu.dk
Supervisors:	Prof. Anne S. Meyer
	BioProcess Engineering

PhD Study

Started:	March 2004
To be completed:	March 2008

Wine and Berry Fruit Juice with Improved Health Potential

Abstract

Fruits skins contribute a main part of produced fruits pomaces which are a rich source of phenolics phytochemicals compounds. Knowledge about fruits skins composition is needed to understand how phenolics phytochemicals are locked inside skin cell wall polysaccharides matrix. Such detailed compositional knowledge is a key issue to upgrades the press residues wine making or valorise the fruit skin for phenolics phytochemicals production as functional food additive. The overall objective is to provide more detailed knowledge on the use of enzymes in pre-press treatments of fruits used in juices and wines processing. This knowledge will be used to improve the release of the phenolics phytochemicals having potential health benefits.

Introduction:

It has been amply documented that phenolic phytochemicals from fruits and berries, including mixed extracts, juice samples, different individual flavonoids and phenolic acids exert antioxidant activity towards human low-density lipoprotein (LDL) oxidation *in* vitro [1-4]. Since oxidation of LDL is a key step in the pathogenicity of atherosclerosis and thus inducive to coronary heart disease, compounds exerting antioxidant activity on LDL may exert protective, disease preventing effects in humans. Enzyme assisted plant cell wall breakdown of press residues, i.e. mainly skins and seeds, from red wine production and black currant juice pressing results in improved release of phenolics that inhibit *in vitro* oxidation of human LDL [5- 7], Fig. 1.

The antioxidant potency of the released phenols varies depending on the enzyme treatment [5, 6], Fig. 2. This suggests that it may be possible to optimize the enzyme treatments to increase concentrations of certain potent antioxidant phenols. Enzymatic pre-press treatments are already widely employed in the berry juice and wine industries. A better understanding of the plant cell wall degrading enzymes action on fruit skin materials for release of potentially health beneficial compounds appear transferable to juice and wine processing operations. The knowledge gained can therefore pave the ground for production of wines and fruit juices with improved health properties.
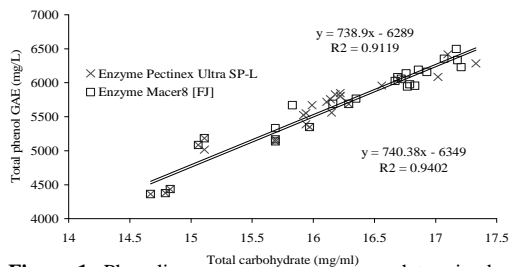
Figure 1: Phenolics determined as gallic acid equivalent (GAE) released when the polysaccharides in the cell wall, notably in the skin fraction, are degraded [7].

Figure 2: Enzyme gives different antioxidant activity.

Specific Objectives

The aim of the proposed Ph.D. project is to explore in detail the enzyme assisted extraction of phenolics from different berry and grape press residues resulting from juice and wine processing. As a part of this, the project will also provide knowledge on how the phenols are bound in the skin polysaccharide-lignin matrix.
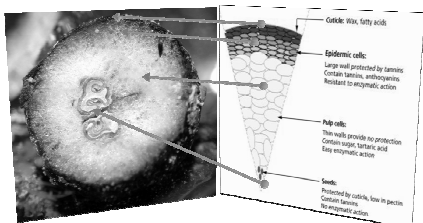
A separate aim is to expand the methods to evaluate possible health benefits to other effects than antioxidant activity on human LDL oxidation.

The main hypothesis to be tested during the PhD study are:

a) Whether it is possible to selectively extract and retain the most potent antioxidants by novel physical and enzymatic treatments of the press residues.

b) Whether it is possible to enzymatically modify the phenolics to optimize their health potential.

Results and Discussion

Practically there is sparse knowledge about the phenolics detailed locations, and how they are bound into the fruit skin polysaccharides matrix. Knowledge about skins composition is needed. As first attempt we used grapes and apples skins as model to understand the relation between skin cell walls polysaccharides and phenolics compounds. Such detailed compositional knowledge is a key issue to upgrades the press residues wine making or valorise the fruit skin for phenolics phytochemicals production as functional food additive. Polysaccharide composition of cell walls fruits skins are usually determined by measuring the monosaccharides released after hydrolysis with acid, alkaline, or enzyme. Chemical hydrolysis is simple, standardised, and an easily repeatable technique. By acid chemical hydrolysis, chromatographic data are simplified and interferences from undesired substances could be minimized. Trifluoroacetic (TFA) and hydrochloric acid (HCl) are commonly used as hydrolysing agents. The difference in monosaccharides and phenolics profiles between grape and apple skins was expected. And it is simply reflects the difference in polysaccharides cell structures between distant plants species [8].

During enzymatic extraction higher phenolics content was released from apples skin (Gold and Red delicious) relative to chemical extraction of phenolics by 60% methanol [8]. This supports the hypothesis: phenols are bound in the skin polysaccharide-lignin matrix and not only present in cell vacuoles. We also

found a strong relation between antioxidant capacity (lag-phase) and the content flavan-3-ols in the different extracts, Fig. 3 suggesting the possibility of selecting and extracting certain antioxidants using specific enzymes treatments.
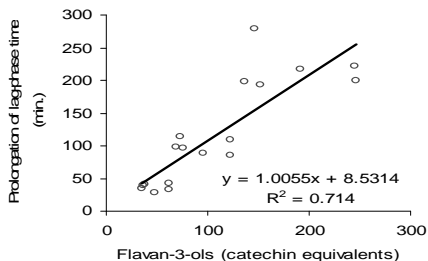
Figure 3: Correlation between antioxidant capacity to inhibit human LDL oxidation *in vitro* and flavan-3-ol content in Red delicious and Golden delicious peel extracts, [8].

Conclusions

A better understanding of the cell walls in fruit skins is needed. We need to know more about how enzymes influence the antioxidant potency of the phenolics. Exploring more specific and mono-active enzymes will help in building the right tailored enzymatic matrix to fit different propose.

References

1. Meyer, A. S.; Heinonen, M.; Frankel, E. N. Food Chemistry 1998, 61 (1-2), 71-75.
2. Meyer, A. S.; Donovan, J. L.; Pearson, D. A.; Waterhouse, A. L.; Frankel, E. N. Journal of Agricultural and Food Chemistry 1998, 46 (5), 1783-1787.
3. Frankel, E. N.; Bosanek, C. A.; Meyer, A. S.; Silliman, K.; Kirk, L. L. Journal of Agricultural and Food Chemistry 1998, 46 (3), 834-838.
4. Meyer, A. S.; Yi, O. S.; Pearson, D. A.; Waterhouse, A. L.; Frankel, E. N. Journal of Agricultural and Food Chemistry 1997, 45 (5), 1638-1643.
5. Meyer, A. S.; Jepsen, S. M.; Sorensen, N. S. Journal of Agricultural and Food Chemistry 1998, 46 (7), 2439-2446.
6. Landbo, A. K.; Meyer, A. S. Journal of Agricultural and Food Chemistry 2001, 49 (7), 3169-3177.
7. Bagger-Jorgensen, R.; Meyer, A. S. European Food Research and Technology 2004, 219 (6), 620-629.
8. Anis Arnous, Rikke A. Trinderup, Manuel Pinelo, and Anne S. Meyer. Journal of Agriculture and Food Chemistry; (in preparation).

Ane Søgaard Avlund

Phone:	+45 4525 2983
Fax:	+45 4588 2258
E-mail:	asa@kt.dtu.dk
WWW:	http://www.ivc-sep.kt.dtu.dk
Supervisors:	Georgios M. Kontogeorgis
	Michael L. Michelsen

PhD Study
 Started:
 To be completed:

August 2007

July 2010

Intramolecular Association within the SAFT Framework

Abstract
The association theory for intermolecular association of Wertheim used in the many different versions of SAFT has been extended to intramolecular association in chain molecules with one site on each terminal segment by two research groups separately. This work summarizes the influences of intramolecular association on the phase behavior of polymers reported by Gregg et al. in four papers on telechelic polyisobutylene, briefly describes the two approaches to modeling intramolecular association with SAFT and discusses the future work needed in order to make the theory useful.

Introduction
The original SAFT equation of state (EoS) was developed from the association theory presented by Wertheim in four papers from 1984-1986 [1-4]. It uses graph theory to describe the formation of clusters due to hydrogen bonding.

The TPT1 (first order thermodynamic perturbation theory) used in SAFT however only includes the smallest order graphs, which describe pair interactions, while higher order interactions are neglected, and the theory therefore only accounts for chain formation. In order to describe ring formation it is necessary to include the graphs corresponding to rings of a specific size.

This is the approach which Sear and Jackson [5] applied to chains with one attractive site on each terminal segment. In this approach inter- and intra-molecular association is considered simultaneously.

Chapman and co-workers [6,7] considered the same system but used a different approach. They found the contribution to the Helmholtz free energy from intermolecular association given that all intramolecular association had occurred and the contribution from intramolecular association given that all intermolecular association had occurred.

Both of these approaches will be further discussed later.

Effects on Phase Equilibrium from Intramolecular Association
Gregg et al. have published four papers [8-11] on the phase behavior of telechelic polyisobutylene (PIB) in

subcritical and supercritical solvents. Experimental cloud-point curves are presented for blank (nonfunctional), monohydroxy and dihydroxy PIB in both nonpolar and polar solvents.

The three most typical types of cloud-point curves are; upper critical solution temperature (UCST), lower critical solution temperature (LCST) and upper-lower critical solution temperature (U-LCST). The three types of curves are sketched in Figure 1. The curve represents the miscibility limit; the solution is stable above it, but splits into two phases below it. If the dissimilarities of the system increases the UCST curve shifts to higher temperatures, and the LCST curve shifts to lower temperatures, this might cause them to merge in to a U-LCST curve. These shifts increase the two-phase region.
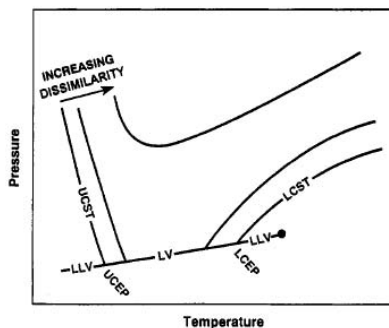
Figure 1: Qualitative cloud-point curves for binary polymer solutions at various degrees of polymer-solvent dissimilarities. Ref. [9]

In the first paper [8] Gregg et al. measured the cloud-point pressure of CH₃-PIB-CH₃, CH₃-PIB-OH and OH-PIB-OH (all with a molecular weight around 1000 g/mol) in 5 different solvents; ethane (non-polar), propane (non-polar), chlorodifluoromethane (polar), dimethyl ether (polar) and carbon dioxide (polar). They found that in non-polar solvents going from CH₃-PIB-CH₃ to CH₃-PIB-OH and from CH₃-PIB-OH to OH-PIB-OH the cloud-point pressure increased. This can be explained by intermolecular association, which results in agglomerate formation. CH₃-PIB-OH forms dimmers, while OH-PIB-OH can form even larger agglomerates. The agglomerate formation increases the size asymmetry, and therefore decreases the solubility.

Figure 2 shows the cloud-point pressure of CH₃-PIB-CH₃, CH₃-PIB-OH and OH-PIB-OH in propane.
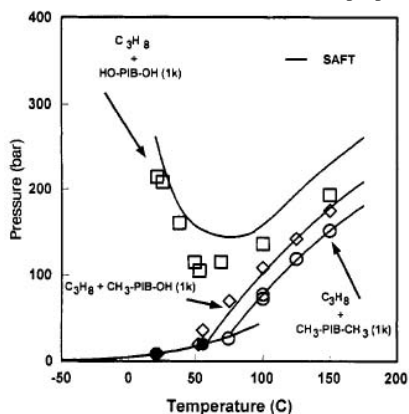
Figure 2: Binary pressure-temperature diagram for C₃H₈ + CH₃-PIB-CH₃ (1000 g/mol), CH₃-PIB-OH (1000 g/mol) and HO-PIB-OH (1000 g/mol). Points are experimental data and curves are calculated by SAFT. Ref. [8].

In the polar solvents the cloud-point pressure of CH₃-PIB-OH is again increased corresponding to that of CH₃-PIB-CH₃ but the experimental points for OH-PIB-OH are almost coinciding with those for CH₃-PIB-CH₃. This cannot be explained with intermolecular association, which as for the non-polar solvent would result in large insoluble agglomerates (see the SAFT curve for OH-PIB-OH in Figure 3).

That OH-PIB-OH has a lower cloud-point pressure than expected can instead be explained with intramolecular association. While intermolecular association occurs between hydrogen bonding sites on different molecules, intramolecular association occurs between hydrogen bonding sites on the same molecule, and only OH-PIB-OH is therefore capable of intramolecular association (and not CH₃-PIB-OH).

In a non-polar solvent the polymer backbone likes the solvent and the molecule will stretch out, and thus increase the distance between the two terminal segments on the molecule. Intramolecular association is therefore not very pronounced in non-polar solvents, and does not

significantly influence the phase behavior of the polymer.

When the polymers are placed in a polar solvent the polymer backbone will curl up to diminish the interactions with the solvent. In this way the likelihood of the two end hydroxyl groups to be in bonding distance is greatly increased resulting in a large degree of ring formation.

Figure 3 shows the cloud-point pressures of the three polymers in dimethyl ether.
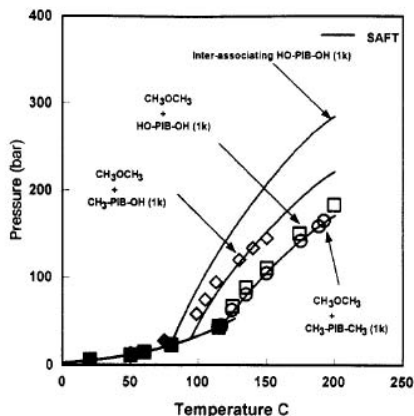
Figure 3: Binary pressure-temperature diagram for CH₃OCH₃ + CH₃-PIB-CH₃ (1000 g/mol), CH₃-PIB-OH (1000 g/mol) and HO-PIB-OH (1000 g/mol). Points are experimental data and curves are calculated by SAFT assuming only intermolecular association. Ref. [8].

Studies of the phase behavior of n-alkanes and the corresponding cycloalkanes have according to Gregg et al. [8] showed that the chain and the ring structure have similar miscibility in polar solvents, but unlike miscibility in non-polar solvents. This confirms that the behavior seen for of OH-PIB-OH is a result of ring formation, and thus of intramolecular association.

Chains with associating sites on the terminal segments

Both of the approaches for describing intramolecular association within the SAFT framework consider chain molecules with one attractive site on each terminal segment. The chains are formed of hard sphere segments, and the attractive sites interact with a square well potential.

This is the simplest model molecule capable of intramolecular association, and a good starting point for the development of a theory to describe this type of association. Figure 4 shows two model molecules with indications of the sites, A and B. A and B sites can associate but A-A or B-B bonds are not allowed.

The association sites can bond either inter- or intramolecularly, and in that way form agglomerates or ring structures respectively.
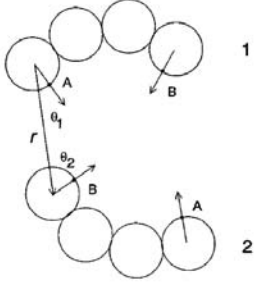
Figure 4: Molecular model for inter- and intramolecular associating tetramer. Ref. [7]

The approach of Sear and Jackson
In their approach Sear and Jackson [5] used the original terminology of Wertheim [1-4]. It considers the four possible bonding states with corresponding number densities: neither of the two sites bonded with the density ρ_0; site A bonded but not B with the density ρ_A; site B bonded but not A with density ρ_B; and both sites bonded with density ρ_{AB}. The following combinations of these densities are used

$$\sigma_0 = \rho_0,$$
$$\sigma_A = \rho_A + \rho_0,$$
$$\sigma_B = \rho_B + \rho_0,$$
$$\sigma_\Gamma = \rho_{AB} + \rho_A + \rho_B + \rho_0 = \rho,$$

where $\rho = N/V$ is the total number density.

According to Wertheim the change in Helmholtz free energy because of association is given by

$$\beta(A - A_R) = \int \left(\sigma_\Gamma(1) \ln \frac{\sigma_0(\bar{1})}{\sigma_\Gamma(\bar{1})} + \sigma_\Gamma(1) - \sigma_A(1) \right.$$
$$\left. - \sigma_B(1) + \frac{\sigma_A(1)\sigma_B(1)}{\sigma_0(1)} \right) d(1)$$
$$- c^{(0)} + c_R^{(0)}.$$

where R indicates that it is the property of the non-associating reference fluid, $c^{(0)}$ is the sum of all irreducible graphs in the system and (1) represents the position and orientation of the molecule as well as the angle subtended by the sites.

Wertheim found that only including the graphs corresponding to chain formation greatly simplified the expression for the graph sum

$$\Delta c^{(0)} = \int \sigma_A(1)\sigma_B(2) F_{AB}(12) y(12) d(1) d(2)$$

where F_{AB} is a measure of the bonding energy between sites A and B, y is the cavity distribution function

To include ring formation it is necessary to include a term for each ring size formed. Sear and Jackson assumed that only rings with n segments would be formed, which results in the following difference in the graph sum:

$$\Delta c^{(0)} = \int \sigma_A(1)\sigma_B(2) F_{AB}(12) y(12) d(1) d(2)$$
$$+ \frac{1}{n} \int \sigma_0(1) \cdots \sigma_0(n) F_{AB}(12) y(12) \cdots$$
$$\times F_{AB}(n1) y(n1) d(1) \cdots d(n).$$

Following a number of derivations they end up with the following expression for the combined change in Helmholtz free energy from association and chain formation:

$$\beta(A - A_R) = \int \left[\sigma_\Gamma(1) \ln \left(\frac{\sigma_B^1(1)}{[\sigma_\Gamma(1)]^n (\lambda y_c)^{n-1} [1 + \sigma_B^1(1^*)\Delta]} \right) \right.$$
$$\left. + n\sigma_\Gamma(1) \right] d(1) \ - \int \sigma_B^1(1) d(1)$$
$$- \int \left(\frac{\sigma_B^1(1)}{1 + \sigma_B^1(1)\Delta} W_{n-1}\Delta \right) d(1)$$

where $\Delta = K F_{AB} y_c$ is the bonding strength between sites A and B, K is the bonding volume and W_{n-1} is the value of the end-to-end distribution function for a freely joined chain of n segments, where the end segments are within bonding range.

This expression is then rewritten in terms of $X = \sigma_B^1/\sigma_\Gamma^1$, the fraction of molecules not bonded at a given site:

$$\frac{\beta(A - A_R)}{N} = -(n-1)\ln(\sigma_\Gamma \lambda y_c) + \ln \left(\frac{X}{1 + X\sigma_\Gamma\Delta} \right)$$
$$+ n - X - \frac{X}{1 + X\sigma_\Gamma\Delta} W_{n-1}\Delta$$

This expression accounts for both inter- and intramolecular association. If the chains are only allowed to intermolecularly association it can be found that

$$1 = X + \sigma_\Gamma X^2 \Delta$$

Using this and realizing that $W_{n-1} \Delta = 0$ in this case we obtain the following expression:

$$\frac{\beta(A - A_R)}{N} = -(n-1)\ln(\sigma_\Gamma \lambda y_c) + \ln X^2 + n - X$$

If instead only intramolecular association is allowed, then

$$1 = X + X W_{n-1}\Delta$$

and the change in free energy is then given as:

$$\frac{\beta(A - A_R)}{N} = -(n-1)\ln(\sigma_\Gamma \lambda y_c) + (n-1) + \ln X$$

The main advantage of this approach is that it is developed completely theoretically and analogue to how the Wertheim association theory was originally developed, but the theory has not been compared to neither experimental nor simulation data.

The approach of Ghonasgi et al.
In the second approach, the one by Chapman and co-workers [6,7], they started by looking at a fluid that could only intramolecularly associate. They found that in that case the change in Helmholtz free energy from association is given by

$$\frac{A^{assoc}}{NkT} = \frac{A - A^R}{NkT} = \ln\left(\frac{\rho_0}{\rho}\right) = \ln X,$$

where X is the fraction of molecules not bonded (fraction of monomers), which they from statistical mechanics and the mass action law found was given as:

$$X = \frac{1}{1 + DF},$$

where $F = \exp(-\varepsilon_{intra}/kT) - 1$ is the Mayer f function for the association potential and D is related to the probability of finding a terminal segment within bonding distance and is given by:

$$D = \frac{1}{(4/3)\pi(m-1)^3\sigma^3} \int_{\substack{Bond \\ Volume}} g_{R,intra}(1m)\,d(1m)$$

They determine the value of D for a tetramer from simulations as a correlation of η, the packing fraction:

$$D = \frac{2 \times 10^{-4}}{(1-\eta)^2}.$$

The theory is then extended to describe the competetion between inter- and intramolecular association by introducing a number of different X's: X_0, the fraction of non-bonded molecules, X_0^{intra}, the fraction of molecules not bonded intramolecularly, X_0^{inter}, the fraction of molecules not bonded intermolecularly, X_A the fraction of molecules not bonded at site A and X_A^{inter} the fraction of molecules not bonded intermolecularly at site A. Again the change in Helmholtz free energy is found from statistical mechanics:

$$\frac{A^{assoc}}{NkT} = \ln X_0 - X_A^{inter} + 1$$

which can be rewritten as

$$\frac{A^{assoc}}{NkT} = \ln X_0 + X_0^{intra} - X_A$$

by realizing that

$$X_A^{inter} + X_0^{intra} - X_A = 1$$

The amount of intermolecular bonding is determined by assuming that all intramolecular bonds have been formed:

$$X_A = \frac{X_0^{intra}}{1 + \rho X_A \Delta_{AB}^{inter}}$$

where Δ_{AB}^{inter} is the intermolecular association strength between site A and B.

Using the theory developed for only intramolecular association and assuming that all intermolecular bonds are formed, they derive the following relationship:

$$\frac{X_0}{X_0^{inter}} = \frac{1}{1 + \Delta^{intra}}$$

where $\Delta^{intra} = DF^{inta}$ is the intramolecular association strength between site A and B.

If Δ_{AB}^{inter} and Δ^{intra} are known the change in Helmoltz free energy can now be determined.

The derivations in this approach are much simpler than those in the approach by Sear and Jackson, and has

the advantage of the distinction between sites bonded inter- and intramolecularly. This could however also be a disadvantage when the equations become more complex in the general expressions. The theory of Ghonasgi et al. was validated against simulation data for tetramers

Conclusions and future work

Experimental results for the phase behavior of telechelic polymers with none, one and two hydroxyl groups have shown the influence of intramolecular association.

Two different approaches to accounting for intramolecular association within the SAFT framework have been presented in the literature, but neither is really used. The theories have been developed for chains with one site on each terminal segment, but for them to be usable, they need to be generalized to an arbitrary number of associating sites that can either inter- or intramolecularly associate or both.

The goal of this project is to get the theory to the next step. There are different possible ways to go, but one option is to look at other model molecules with a fixed number of sites (different from two) or to look at the chain with two sites in n intermolecularly associating solvents.

Based on the knowledge obtained in this way we hope to be able to derive a general expression for intramolecular association, which can be applied to real systems for which intramolecular association is known to be important e.g. glycolethers etc. and compared to experimental data.

The future work in this project will try to compare and utilize both of the approaches presented here, as each has clear advantages.

References
1. M.S. Wertheim, J. Stat. Phys. 35 (1984) 19-34.
2. M.S. Wertheim, J. Stat. Phys. 35 (1984) 35-47.
3. M.S. Wertheim, J. Stat. Phys. 42 (1986) 459-476.
4. M.S. Wertheim, J. Stat. Phys. 42 (1986) 477-492.
5. R.P. Sear, G. Jackson, Phys. Rev. E 50 (1994) 386-394.
6. D. Ghonasgi, V. Perez, W.G. Chapman, J. Chem. Phys. 101 (1994) 6880-6887.
7. D. Ghonasgi, W.G. Chapman, J. Chem. Phys. 102 (6) (1995) 2585-2592.
8. C.J. Gregg, F.P. Stein, M. Radosz, Macromolecules 27 (1994) 4972-4980.
9. C.J. Gregg, F.P. Stein, M. Radosz, Macromolecules 27 (1994) 4981-4985.
10. C.J. Gregg, F.P. Stein, M. Radosz, Macromolecules 98 (1994) 10634-10639.
11. C.J. Gregg, F.P. Stein, M. Radosz, Macromolecules 103 (1996) 1167-1175.

Muhammad Shafique Bashir

Phone:	+45 4525 2853
Fax:	+45 4588 2258
E-mail:	msb@kt.dtu.dk
WWW:	http://www.chec.kt.dtu.dk
Supervisors:	Kim Dam-Johansen
	Peter Arendt Jensen
	Flemming Frandsen
	Stig Wedel
	Johan Wadenbäck, Vattenfall AB

PhD Study
Started: September 2008
To be completed: August 2011

Characterization and Quantification of Deposits Buildup and Removal in Straw Suspension Fired Boilers

Abstract

The use of biomass in power plant boilers is an efficient method to reduce the net CO_2 amount produced. However, during biomass combustion, inorganic matter in the state of vapors, melts and solid particles are transported by the flue gas and form deposits on heat transfer surfaces. During the combustion of straw in suspension fired boilers, fly ash contribution is more than 80% of the total ash generated. The aim of this project is to investigate ash deposition and shedding in suspension fired straw boilers and to provide recommendations for the optimal operation strategy of boilers with respect to minimization of deposit related problems.

Introduction

One of the main sources for sustainable energy now and in the near future are biomass and waste. In Denmark, straw and wood chips are the most abundant biomass sources used for power production. A fairly large surplus of wheat straw exists in certain parts of Denmark, and it can be a substitute for coal [1].

When solid fuel is burned, inorganic material is being released to the flue gas in the form of gases, liquids and solid particles and the fate of the inorganics depend upon the mode of occurrence and local conditions inside the boiler [2]. Dry ash particles, sticky particles and gas phase ash species form deposits on the boiler surfaces. Compared to coal ashes, the biomass-derived ashes contain significant amounts of K and Cl and therefore the use of straw in power plant boilers is a serious technical challenge. The reason is that when straw is burned potassium vapors, salts and silicates with relatively low melting temperatures are formed. These potassium components play a significant role in the deposit formation because they act as glue bonding the individual fly ash particles together [3].

Research on slagging, fouling and shedding has been carried out by researchers but most studies are related to coal-fired boilers. Shedding is a process of removal of deposits by thermal shock, soot blowing, erosion or gravity. Zbogar et al [4] performed experiments in the superheater area of a straw fired grate boiler and the results indicate that surface melting for the inserted probe is the main mechanism of deposit removal for flue gas temperatures greater than 1000°C. The experimental findings indicate that at 1100°C or above, the surface layer is completely melted, at 1000°C it is partially melted and at flue gas temperatures below than 900°C, the deposits contain mainly porous solid phase.

Project Description and Specific Objectives

Shedding of biomass ash deposits naturally or by soot blowing is an area where limited accurate knowledge is available. The objective of this project is to provide recommendations for the optimal operation strategy of suspension fired straw boilers with respect to minimization of deposit related problems. The specific objectives of the project are:

- Understanding removal behaviour of deposits in the boiler chamber and superheater region (convective pass) of biomass fired boilers.
- The influence of load, operation conditions and fuel changes (straw, wood or coal firing) on boiler deposits.
- A model based description of the influence of fuel changes on deposits. The model needs to account for deposit formation and removal with changed temperature, ash composition and flow conditions. The model is intended to

describe the deposit related processes as a function of the local parameters as gas velocity, ash particle size distribution, ash particle composition and gas and surface temperature.

- Provide measuring data that can support activities on fuel characterization and CFD modeling.

Based on the obtained knowledge, innovative ideas for deposit removal will be provided and tested. The practical probe measurements will form the basis for the transient mathematical model for ash deposition and shedding.

Modeling

In order to explain heat transfer in the furnace section of a suspension fired boiler, to predict the deposition of ash particles on the walls of the boiler and to describe the shedding mechanism by accurate models, a mechanistic modeling technique is used. For the assessment of the deposition tendency, mechanistic models can be used for the simplified calculations of combustion and fluid dynamics [5]. These models provide a basement for the development of a more comprehensive mathematical model for ash deposition and heat transfer [5]. A currently used mechanistic model takes into account deposition through condensation, impaction and turbulent eddy diffusion of particles.

(a)   (b)
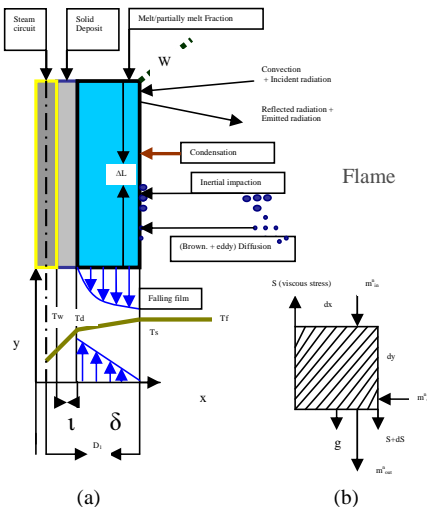
Figure1: a) Furnace wall layout with ash deposition and shedding through surface melting b) Schematic representation of force and mass balances for running ash melt.

Deposits are formed due to accumulation of fly ash particles and aerosols starting from the condensation of inorganic vapors on exposed surfaces in the boiler. The surface temperature increases when the deposit thickness increases and resultantly a melt film of the

outer part of the deposit flows down. A complete schematic representation is shown in figure 1. The overall deposit buildup rate can be written as,

$$\frac{dm_d(t,y)}{dt} = C(t,y) + TH(t,y) + IBD(t,y) - S_h(t,y) \qquad (1.1)$$

In the above equation, m_d corresponds for the deposit buildup rate, C counts for condensation, TH for thermophoresis, IBD for inertial impaction and Brownian eddy diffusion and S_h for the shedding rate. Separate sub-models are developed for each phenomenon. Input data of fly ash particle size distribution, flue gas temperature and chemical composition of fly ash will be used to simulate and predict heat uptake and deposit characteristics.

Experiments

A vertical plate probe is in the development phase which will provide online information of deposit weight and heat uptake. If possible video monitoring and local flue gas measurements will be included. Using both a horizontal (already developed) probe and a vertical probe, a series of full scale measurements will be performed to test influences of boiler operation, sootblowing strategy and fuel changes on the deposit formation and shedding process. The main body of the measurements will be conducted on the Amager Power Plant unit I (suspension fired boiler). This unit will be commissioned early 2009 and can utilize coal, wood and straw as fuels. The initial experiments in late 2008 will be performed on the Amager Power Plant unit II. When possible both a boiler chamber and a convective pass probe will be mounted in areas with severe deposit formation. The probe measurements will be supplemented by pictures of other boiler areas to monitor deposit formation in the whole boiler.

References

1. H. P. Nielsen, Deposition and High Temperature Corrosion in Biomass Fired Boilers. PhD Thesis, (1998), Technical University of Denmark.
2. A. Zbogar, F. J. Frandsen, P. A. Jensen and P. Glarborg, Literature Study: Shedding of Ash Deposits. PSO Project 4106 (2006), CHEC Research Center, Technical University of Denmark.
3. F. J. Frandsen, Fuel. 84 (2005) 1277-1294.
4. A. Zabogar, F. J. Frandsen, P. A. Jensen P. Glaborg, and P. Hansen, Energy Fuel. 20(2) (2006) 512-519.
5. H. Zhou, P. A. Jensen and F. J. Frandsen, Fuel. (86) (2007) 1519-1533.

Matthias Josef Beier

Phone:	+45 4525 2936
Fax:	+45 4525 2258
E-mail:	mjb@kt.dtu.dk
WWW:	http://www.chec.kt.dtu.dk
Supervisors:	Prof. Jan-Dierk Grunwaldt
	Prof. Georgios Kontogeorgis

PhD Study

Started:	February 2008
To be completed:	February 2011

Heterogeneously Catalysed Oxidation Reactions in Liquid Solvents and Supercritical Carbon Dioxide

Abstract

Heterogeneously catalyzed oxidation reactions offer a pathway to various classes of fine chemicals. This Ph.D. project aims at the investigation of new catalysts and catalytic processes suitable for the selective oxidation of alcohols and olefins both in organic solvents and supercritical carbon dioxide. As a catalyst suitable for selective alcohol oxidation, a doped silver on silica catalyst has been found and will be compared to benchmark catalysts, such as other noble metal catalysts and the recently widely studied gold catalysts.

Introduction

Selective oxidation reactions in a condensed phase applied in the production of many industrial key compounds can be accomplished by the use of heterogeneous noble metal catalysts [1]. Heterogeneous catalysts provide the advantage of an easy separation from the reaction product allowing for a continuous production over a catalyst bed. Most oxidative transformations towards fine chemicals are nowadays performed in liquid phase which can be problematic when employing organic solvents – many of which are toxic and/or flammable. As a safe and inert alternative, pressurized "supercritical" carbon dioxide ($scCO_2$) can be used as a solvent being inexpensive and environmentally benign. In addition, it has been proved to feature unique tunability which can be cleverly exploited to improve a catalytic process [2, 3].

This Ph.D. thesis aims at exploring and investigating new catalysts for the selective oxidation of alcohols to aldehydes or ketones and, in the second part, olefins to epoxides thereby assessing the potential of dense CO_2 in comparison to organic solvents. While especially aldehydes serve as artificial flavors and odorants, epoxides are crucial reactive intermediates which can e.g. be used for the production of polymers, agrochemicals or drugs.

Noble metals which are typically applied in the oxidation of alcohols to aldehydes or ketones are platinum, gold, palladium or ruthenium [1, 4] using oxygen as an inexpensive oxidant. Very recently, it has been shown that silver-exchanged hydrotalcites also exhibit a potential for the liquid phase oxidation of

alcohols – interestingly under anaerobic conditions [5].

In many cases, the catalytic activity of a metal depends on its structure. X-ray absorption spectroscopy (XAS), X-ray diffraction (XRD) and transmission electron microscopy (TEM) can be utilized to investigate the structure of a heterogeneous catalyst. Since catalysts often undergo structural changes during reactions, *in-situ* monitoring can establish a deeper understanding for the catalyst reactivity. Due to the highly penetrating nature of X-rays, XAS and XRD allow *in-situ* investigations and can be used to follow structural changes during the catalytic process.

Specific Objectives

The aim of this thesis is to find and investigate new catalysts for the selective oxidation of alcohols and olefins. In case of the alcohol oxidation, silver as a catalyst metal should be explored both in organic solvents as well as $scCO_2$. Since the phase behavior of CO_2 containing mixtures is crucial for the catalytic process, it will be also modeled using SAFT models [6].

For preparation of catalysts both standard and new techniques, especially flame-spray pyrolysis (FSP) will be utilized while a thorough characterization of the catalyst both *ex-situ* and *in-situ* will be done using state-of-the-art analysis techniques such as XRD and TEM with a special focus on XAS.

Results and Discussion

Since noble metals are very expensive, a high surface-to-volume ratio is desired for noble metal catalysts. This can be achieved using a high surface area support.

Additionally, a support can promote the catalytic activity in various ways which makes the efficient test of a number of metal/support combinations essential. Since only an active/inactive classification of tested catalysts was needed, different catalysts were tested "in one pot" for catalytic activity.

Thereby, impregnated Ag/Al_2O_3, Ag/celite, Ag/CeO_2, Ag/MgO, Ag/SiO_2, Ag/activated carbon, Ag/TiO_2 and Ag/kaolin catalysts differing in silver loading and calcination temperature were tested in the oxidation of benzyl alcohol to benzaldehyde in refluxing xylene (Figure 1).
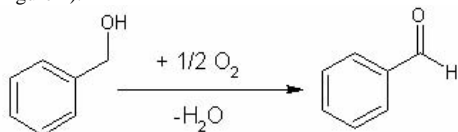
Figure 1: Oxidation of benzyl alcohol to benzaldehyde under aerobic conditions.

A doped Ag/SiO_2 catalyst was identified to be catalytically most active. This catalyst undergoes some deactivation during the course of the reaction, which is at least to a certain degree caused by the reaction products. Specifically water leads to a lower reaction rate.
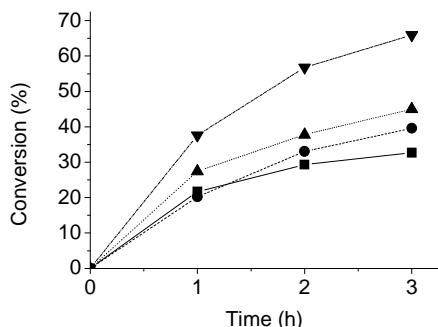
Figure 2: Conversion of benzyl alcohol depending on the addition of drying agent: ■ without drying agent; ● with Na_2SO_4; ▲ with $MgSO_4$; ▼ with molecular sieves 3 Å.. Reaction conditions: 19.3 mmol benzyl alcohol in 40 mL of xylene with 150 mg catalyst in an oxygen atmosphere, reflux.

Upon addition of a drying agent the activity of the catalyst increased. This, however, was bought by a large decrease in selectivity when strong drying agents, i.e. $MgSO_4$ and molecular sieves were used suggesting that water plays a deactivating but also moderating role.

In order to investigate the state of silver in this catalyst, TEM, XRD and XAS data were recorded. Figure 3 shows a XAS spectrum of the fresh silver catalyst revealing silver being in the metallic state.

The performance of the Ag/SiO_2 catalyst was compared to widely acknowledged Gold catalysts. The silver catalyst turned out to be comparable or even better.
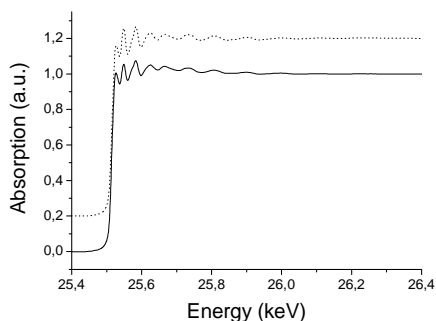
Figure 3: Background corrected XAS spectrum at the Ag K-edge of the Ag/SiO_2 catalyst (solid line) which is similar to the spectrum of a silver foil (dotted line).

Conclusion

Oxidation reactions using molecular oxygen are key reactions in the production of fine chemicals. This research project aims at the investigation of catalysts for the selective oxidation of alcohols and olefins both in "classic" organic and supercritical carbon dioxide.

For the selective oxidation of alcohols a doped silver on silica catalyst has been found. Silver is in the metallic state.

References

1. T. Mallat, A. Baiker, Chem. Rev. 104 (2004) 3037-3058.
2. P.G. Jessop, W. Leitner (Eds.), Chemical Synthesis Using Supercritical Fluids, Wiley-VCH, Weinheim, 1999.
3. J.D. Grunwaldt, R. Wandeler, A. Baiker, Catal. Rev. Sci. Eng. 45 (2003) 1-96.
4. B. Kimmerle, J.D. Grunwaldt, A. Baiker, Top. Catal. 44 (2007) 285-292.
5. T. Mitsudome, Y. Mikami, H. Funai, T. Mizugaki, K. Jitsukawa, K. Kaneda, Angew. Chem. Int. Ed. 47 (2008) 138-141.
6. G. M. Kontogeorgis, M. L. Michelsen, G. Folas, S. Derawi, N. v. Solms, E.H.Stenby, Ind. Eng. Chem. Res. 45 (2006) 4855-4868 and 4869-4878.

List of Publications

1. O.L. Collin, M. Beier, G.P. Jackson, Anal. Chem. 79 (2007) 5468-5473.
2. M.J. Beier, W. Knolle, A. Prager-Duschke, M.R. Buchmeiser, Macromol. Rap. Comm. 29 (2208) 904-909.

Rasmus Risum Boesen

Phone:	+45 4525 2982
Fax:	+45 4588 2258
E-mail:	rrb@kt.dtu.dk
WWW:	http://www.ivc-sep.kt.dtu.dk
Supervisors:	Nicolas von Solms
	Michael L. Michelsen
	Kim G. Knudsen, Haldor Topsøe A/S

PhD Study
 Started:
 To be completed:

March 2007
March 2010

Development of a Component-Based Hydrodesulfurization Kinetic Model for Ultra Low Sulfur Diesel

Abstract
Within recent years many countries have tightened the legislations regarding the sulfur content in diesel oil, and the hydrotreating process has received increased attention. A more detailed understanding of the hydrodesulfurization kinetics at high sulfur conversions, and the effect of inhibitors, such as nitrogen compounds and large aromatics, will be helpful in the development of more active catalysts and in the optimization of the hydrotreating process. It is the purpose of this project to develop a model for a hydrotreating reactor that includes a kinetic model based on the study of individual compounds that can describe the kinetics at a broad range of conversions. The model should also account for physical phenomena such as phase equilibria and mass transfer limitations in the reactor.

Introduction
Due to environmental concerns, many countries have tightened the legislations regarding the sulfur content of diesel to an ultra low sulfur diesel (ULSD) specification of 10-15 ppm S [1].

The sulfur compounds present in diesel oils are mainly thiophenic compounds, and the sulfur is removed through a catalytic reaction with hydrogen, forming H_2S. The typical catalysts used in the hydrotreating process are sulfided $CoMo/Al_2O_3$ and $NiMo/Al_2O_3$. The most important hydrotreating reactions are hydrodesulfurization (HDS), hydrodenitrogenation (HDN) and hydrodearomatization (HDA).

A hydrotreating reactor is a fixed bed catalytic reactor where gas and liquid flow co-currently from the top. It can be described as a trickle-bed reactor in which the liquid trickles from pellet to pellet and the gas forms a continuous phase. Thus equilibrium between gas and liquid phase and internal / external mass transport limitations can influence the performance of the reactor.

During hydrotreating, sulfur is removed from the most reactive compounds first, but in order to meet ULSD specifications, it is necessary to remove some of the most refractive sulfur compounds. Studies have shown that substituted dibenzothiophenes with alkyl groups in the 4 and/or 6 positions are among the most refractive sulfur compounds [2].

It is well-known that certain nitrogen compounds present in diesel oils act as inhibitors for the HDS reactions. The nitrogen compounds present in diesel oil fractions are mainly heterocyclic compounds. Typically one distinguish between basic compounds in which the lone-pair on the nitrogen atom as available for donation, and non-basic compounds in which the lone-pair is delocalized in an aromatic ring. It has been observed that especially basic nitrogen compounds are strong inhibitors of hydrodesulfurization reactions [3].

At high sulfur conversions, the amount of sulfur compounds and nitrogen compounds become comparable, and the inhibition is severe [4]. Understanding of the nature of the inhibition can be helpful in the further improvement of the hydrotreating process when meeting ULSD demands.

Specific Objectives
The purpose of this project is to develop a component-based hydrodesulfurization kinetic model for ULSD. The model should account for the inhibition by nitrogen components and large aromatics.

It is the intention to develop a reactor model where the thermodynamic equilibrium between the diesel oil components and the gaseous compounds (hydrogen, hydrogen sulfide and ammonia) are accounted for. The reactions take place in the liquid phase inside the pores of the catalyst, and the model should be able to describe the diffusion limitations inside the catalyst pellets and any external mass transfer limitations.

The recent work has involved an experimental study of the inhibition effect of some representative nitrogen compounds.

Experimental Work

The effect of different nitrogen compounds on the HDS of 4,6-dimethyldibenzothiophene (4,6-dmdbt) on a NiMo/Al$_2$O$_3$ catalyst has been investigated in a lab-scale fixed-bed reactor. The temperature and pressure was similar to industrial conditions (T= 350 °C and P= 50 barg). Hydrogen and the liquid solution are fed from the top of the reactor, and the liquid product is analyzed in a gas chromatograph. The liquid feeds were solutions of 4,6-dmdbt and nitrogen compounds in n-dodecane, with concentrations similar to what can be found in real feeds.

The nitrogen compounds tested are the basic acridine and the non-basic 1,4-dimethylcarbazole (1,4-dmcbz) and 3-methylindole (3-mein) shown in Figure 1.
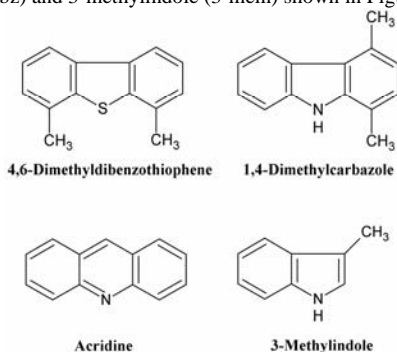
Figure 1: Structures of the model compounds

Table 1 shows the target compositions of the different feeds.

Table 1: S and N concentrations in the liquid feeds

Feed	4,6-dmdbt (ppm S)	Acridine (ppm N)	1,4-dmcbz (ppm N)	3-mein (ppm N)
I	1000	0	0	0
II	1000	300	0	0
III	1000	0	300	0
IV	1000	0	0	300
V	1000	150	150	0

Results

Figure 2 shows the conversion of 4,6-dimethyl-dibenzothiophene as a function of the space time for solutions I-V. It is obvious that all the nitrogen compounds act as inhibitors, by significantly lowering the conversion. The conversions for solution III and IV are very similar, which suggests that the two non-basic compounds 1,4-dmcbz and 3-mein have a very similar inhibition strength. The conversion is lowest in solution II, which shows that the basic compound acridine is the strongest of the inhibitors.

Solution V contains equal amounts of acridine and 1,4-dmcbz. The inhibition effect of the mixture turns out to be very similar to the effect of acridine. A further analysis has shown that acridine inhibits the HDN conversion of 1,4-dmcbz, which might be why the effect of the mixture is stronger than expected. This indicates that the two compounds are competing for the same active sites. Since acridine is removed first, it appears that this compound is more strongly adsorbed, which would also explain why this is the strongest inhibitor.
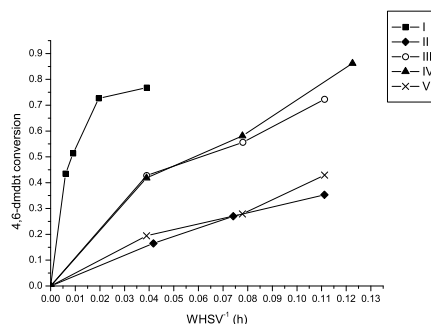
Figure 2: 4,6-dmdbt conversion in solution I-V

Conclusion

The experimental study has shown that basic as well as non-basic nitrogen compounds has a significant inhibiting effect on the HDS of 4,6-dmdbt. The inhibition appears to be due to competitive adsorption of the different compounds on the same active sites on the catalyst.

The basic compound acridine was found to be the strongest of the inhibitors, which is in agreement with litterature observations [3].

Future Work

Based on the experiments with model compounds, simple kinetic expressions should be developed, which can be used in a detailed trickle-bed reactor model. The effect of different inhibitors should be quantified and accounted for in the kinetic models.

Future work on this project involves experimental studies of the hydrotreating of a model diesel feed consisting of 10-15 compounds representing different component classes (paraffins, aromatics, naphthenes, and sulfur and nitrogen compounds).

References

1. T. Song, Z. Zhang, J. Chen, Z. Ring, H. Yang, Y. Zheng, Energy Fuels, 20, (2006), 2344-2349.
2. K. G. Knudsen, B. H. Cooper, H. Topsøe, Applied Catalysis A, General, 189 (1999) 205-215.
3. G. C. Laredo, J. A. De los Reyes H., J. Luis Cano D., J. Jesús Castillo M., Applied Catalysis A, General, 207 (1-2) (2001) 103-112.
4. T. Koltai, M. Macaud, A. Guevara, E. Schulz, M. Lemaire, R. Bacaud, M. Vrinat, Applied Catalysis A, General, 231 (1-2) (2002) 253-261.

Jacob Brix

Phone:	+45 4525 2922
Fax:	
E-mail:	jac@kt.dtu.dk
WWW:	http://www.chec.kt.dtu.dk
Supervisors:	DTU: Anker Degn Jensen
	Peter Arendt Jensen

PhD Study

Started:	October 2007
To be completed:	September 2010

Oxy-Fuel Combustion of Coal and the Evolution of NO$_x$

Abstract

The focus on the environmental role of CO_2 and the following legal legislations and international reduction programs, has increased the interest for a CO_2-friendly use of coal for heat and power generation. A method that can be used both for new and retrofitted plants is Oxy-Fuel combustion. In Oxy-Fuel combustion coal is burned in a mixture of oxygen and recirculated flue gas (RFG), which gives an exit gas consisting mainly of CO_2 and H_2O along with some impurities such as NO$_x$ and SO$_x$. The high content of CO_2 makes this exit gas suitable for sequestration after condensation of H_2O. The purpose of this project is to investigate differences between Oxy-Fuel and air combustion with respect to char combustion kinetics and NO$_x$ evolution.

Introduction

In the recent years there has been an increased focus on the environmental role of CO_2 and this focus has initiated stricter environmental legislations both globally and within the EU [1]. To overcome these legislations and to solve the problems related to CO_2 emission, the energy industry relaying on coal will need to find technological alternatives to the present combustion processes that will utilize coal in a more environmentally friendly way. This technological development is necessary since the dependence on coal as an energy source can be expected to be present for many years to come [1], [2].

One solution that seems to be promising in the nearby to midterm future is Oxy-Fuel combustion [2].

Oxy-Fuel combustion is a combustion technique, which has been shown considerable research attention in recent years [3], [4], [5], [6], [7], [8], [9]. There are several reasons for this continuously increasing interest, among which the following should be emphasized:

- Existing plants can be retrofitted to function under Oxy-Fuel conditions relatively easy using O_2 concentrations of ~ 30 vol. % in the inlet gas [2].
- Oxy-Fuel combustion produces an exit stream with a very high CO_2 content (~90-95 %) [2], [8], [10], which is ready for sequestration. The

CO_2 purity of the exit gas on industrial scale mainly depends on the efficiency of the Air Separation Unit (ASU) and the degree of leakage to the furnace.
- Combustion in an Oxy-Fuel environment has the potential to reduce NO$_x$ emissions, when compared to traditional air-blown plants [2], [3], [4].

As a further benefit all of the Oxy-Fuel combustion unit operations, except the boiler, are in some sense relaying on existing and known equipment [11]. A scheme of the Oxy-Fuel combustion process can be seen in figure 1.
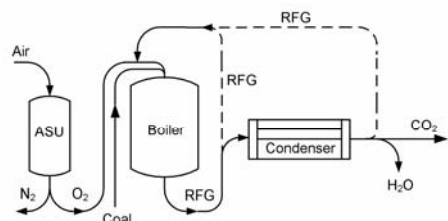
Figure 1: The overall idea behind the Oxy-Fuel combustion process is shown. Units such as desulphurization units and compressors are omitted. The need for desulphurization will depend on the feedstock and if recycle is wet or dry.

Specific Objectives

This project is devoted to the kinetic investigation of char burnout and the evolution of NO_x under Oxy-Fuel combustion.

Combustion of char in oxygen enriched CO_2 atmospheres, such as those prevailing in Oxy-Fuel combustion, is not fully understood, and the influence of gasification at higher temperatures has been observed [12].

The possible differences in combustion behavior between conventional air-blown furnaces and Oxy-Fuel furnaces make a detailed study of the fuel combustion kinetics necessary. Such an investigation will need to focus on both effects arising from increased levels of CO_2 but also on kinetic effects of elevated oxygen concentrations [13]. Along with experiments accurate models predicting and interpreting test results are necessary before large scale plant construction can be initiated.

The NO_x evolution changes between air-blown combustion and Oxy-Fuel combustion [1]. This is mostly due to the recirculation of the flue gas into the flame and the reduction of NO over char. These effects are functions of O_2 concentration, temperature and fuel feed rate [14]. It is also possible that increased levels of CO facilitate an increased reduction of especially NO over the char surface [3].

These dependences on NO_x evolution are important to understand in detail in order to benefit fully from the possibilities Oxy-Fuel combustion gives for reducing the NO_x emission [15].

Experimental

The experimental investigation is mainly carried out in an Entrained Flow Reactor (EFR) located at the department. A schematic representation of the EFR can be seen in figure 2.
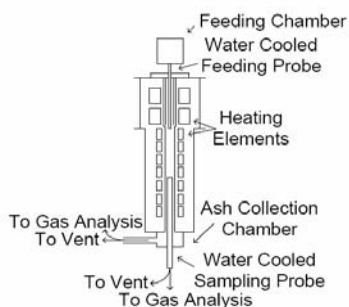
Figure 2: The electrically heated isothermal entrained flow reactor used for experiments.

Using the EFR experiments have been carried out in both CO_2-O_2 and N_2-O_2 mixtures to compare trends in coal conversion profiles. The majority of the experiments have been carried out using bituminous coal particles in the size interval 90 -106 μm, which is a narrow interval chosen to ease the impact of differences in particle size distributions.

To obtain a broad set of experimental data the reactor temperature has been varied from 1073 K to 1673 K along with changes in O_2 concentration from 5 to 28 vol. % corresponding to stoichiometric values ranging from 2 - 16. A constant coal feed flow of 50 g hr^{-1} have been used to avoid temperature increases due to volatile combustion and to ensure a near constant O_2 concentration along the reactor.

To obtain conversion profiles for the different experimental conditions char is sampled through an adjustable water cooled probe. This probe allows isokinetic char sampling and gas analysis at all reactor lengths. For selected particle samples scanning electron microscopy (SEM) is used to characterize particle morphology.

In order to evaluate the fuel consumption due to char conversion devolatilization experiments have been carried out at each of the experimental temperatures using a stoichiometric value of 3 to avoid problems with tar.

Results and Discussion

In figure 3 a devolatilization curve is shown that covers the entire temperature range used in the experiments. The volatile weight percent found by proximate analysis is also included in the figure and it witness of a reasonably accurate data set. The volatile weight fractions at 1573 K and 1673 K are found in both CO_2 and N_2 and shows that no apparent differences exists between the 2 environments. The slight decrease in volatile content from 1473 K to 1573 K and 1673 K is due to a decrease in residence time at the sampling point.
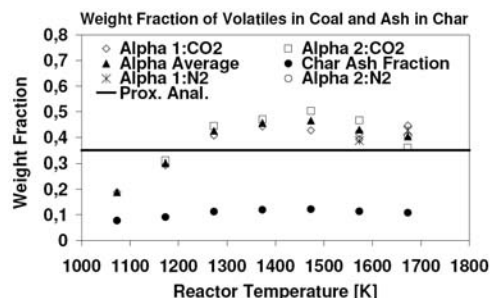
Figure 3: Devolatilization curve. Alphas indicate weight fractions and numbers indicates repetitions in ash tracing. Also included is the weight fraction of volatiles found by proximate analysis. The solid circles are ash content in the fresh chars.

In figure 4 conversions profiles obtained in both N_2 and CO_2 mixtures at 2 reactor temperatures and concentrations of O_2 are shown. The 2 sets of conditions cover scenarios where changes in conversion could be expected when replacing N_2 with CO_2. The first set is high temperature-low O_2 concentration where gasification by CO_2 could be contributing to char conversion. The second set is low temperature-high O_2 concentration where the high O_2 concentration at near pure zone I combustion could reveal differences in intrinsic kinetics. As it is seen in the figure no apparent differences exist for neither of the 2 sets of conditions.
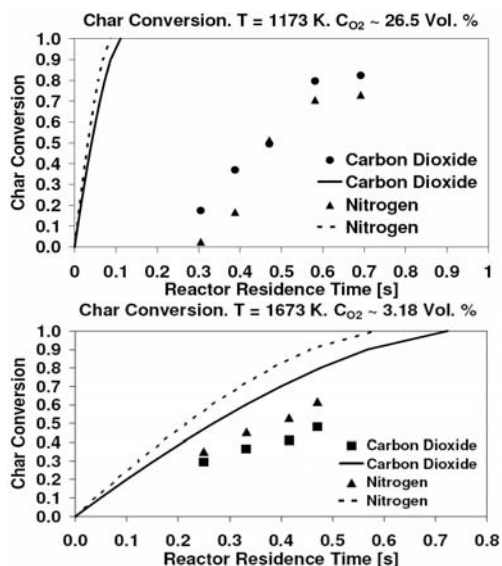
Figure 4: Char conversion profiles for N_2 and CO_2 based combustion under 2 sets of identical conditions. The lines are calculated conversion profiles for combustion under external mass transfer control.

Even though the conversion profiles at 1673 K, shown in figure 4, could indicate that kinetics are slower for CO_2 based combustion the calculated conversions for external mass transfer control reveals that the difference is due to a lower diffusion coefficient of O_2 in CO_2.
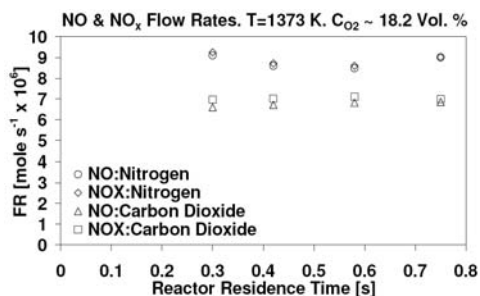
Figure 5: NO and NO_x emission from combustion in O_2-CO_2 and O_2-N_2 mixtures.

As mentioned in the introduction one of the interesting promises of Oxy-Fuel combustion is the potential of significant lower NO_x emissions. This potential is confirmed by figure 5 in which the NO_x emission in O_2-CO_2 combustion can be seen to be significantly lower than in O_2-N_2 under the same conditions. The reduction observed in figure 5 is bound to come directly form changing N_2 with CO_2 since no recirculation of NO_x has been taking place. The mechanism(s) governing this reduction is still being investigated.

Work in Progress
There is still much additional work to be done before Oxy-Fuel combustion can be taken to an industrial scale.

(A)

(B)

(C)
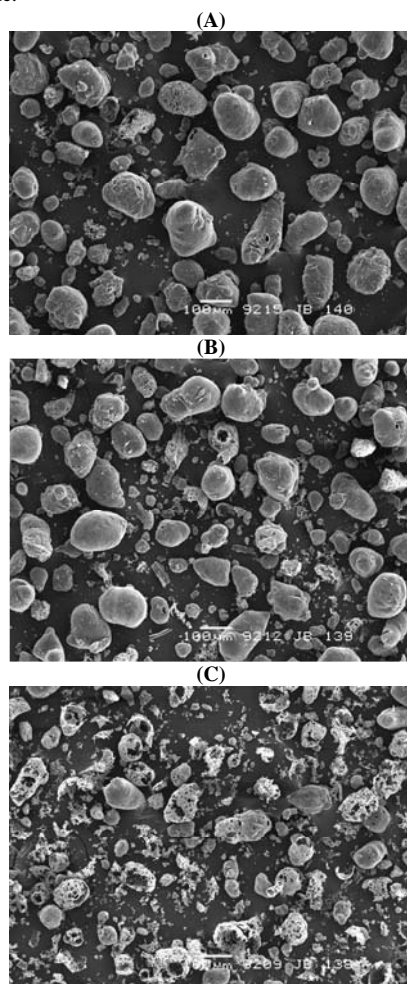
Figure 6: SEM images of char at 3 different degrees of conversion in O_2-CO_2. A = 37 % conversion, B = 50 % conversion, C = 80 % conversion. T = 1173 K and C_{O2} = 27.5 vol. %.

This project will focus on a model describing the char conversion and fuel-NO formation using the experimental data obtained in the EFR and a detailed knowledge from SEM on char morphology.

The task of modeling the char conversion is however not straight forward. As illustrated in figure 6 the char morphology is very complex and changes throughout the combustion process. Efforts are currently being put in to determine what features of the char morphology history that needs to be included in a reliable model.

Besides modeling, experiments are also planned to elucidate the mechanism(s) responsible for the NO_x reduction seen in figure 5 for O_2-CO_2 combustion.

Conclusion

So far the results of this project strongly indicate that no apparent change in kinetics take place when N_2 is substituted with CO_2 under identical conditions. This seems to apply to both high and low temperatures and high and low concentrations of O_2.

A significant reduction in NO_x is found in O_2-CO_2 combustion when compared to combustion in O_2-N_2 under identical conditions. The reason for this reduction is not fully understood and will be a subject of further research throughout the rest of this project.

Acknowledgements

References

1. R. Tan, G. Corragio, S. Santos, Oxy-Coal Combustion with Flue Gas Recycle for the Power Generation Industri, Report No. G 23/y/1, International Flame Research Foundation, 2005.
2. B. J. P. Buhre, L. K. Elliott, C. D. Sheng, R. P. Gupta, T. F. Wall, Prog. Energy Combust. Sci. (31) (2005) 283-307.
3. K. Okazaki, T. Ando, Energy (22) (1997) 207-215.
4. H. Liu, R. Zailani, B. M. Gibbs, Fuel (84) (2005) 2109-2115
5. Y. Q. Hu, N. Kobayashi, M. Hasatani, Fuel (80) (2001) 1851-1855
6. Y. Hu, S. Naito, N. Kobayashi, M. Hasatani, Fuel (79) (2000) 1925-1932
7. K. Andersson, F. Normann, F. Johnsson, B. Leckner, Ind. Eng. Chem. Res. (47) (2008) 1835-1845
8. H. Liu, R. Zailani, B. M. Gibbs, Fuel (84) (2005)
9. P. A. Bejarano, Y. A. Levendis, Combust. Flame (153) (2008) 270-287
10. C. S. Wang, G. F. Berry, K. C. Chang, A. M. Wolsky, Combust. Flame (72) (1988) 301-310
11. L. Strömberg, Combustion in a CO_2/O_2 Mixture for a CO_2 Emission Free Process, Second Nordic Minisymposium on Carbon Dioxide Capture and Storage, 2001, 58-63.
12. T. F. Wall, Proc. Combust. Inst. (31) (2007) 31-47.
13. J. J. Murphy, C. R. Shaddix, Combust. Flame (144) (2006) 710-729.
14. Y. Q. Hu, N. Kobayashi, M. Hasatani, Energy Convers. Manage. (44) (2003) 2331-2340.
15. Y. Tan, E. Croiset, M. A. Douglas, K. V. Thambimuthu, Fuel (85) (2006) 507-512.

Jakob Munkholt Christensen

Phone: +45 4525 2927
Fax: +45 4588 2258
E-mail: jmc@kt.dtu.dk
WWW:
Supervisors: Anker Degn Jensen
                Peter Arendt Jensen

PhD Study
  Started: September 2007
  To be completed: September 2010

Catalytic Conversion of Syngas to Mixed Long Chain Alcohols

Abstract

The catalytic synthesis of higher alcohols from syngas is a promising route to liquid transportation fuels from biomass via gasification. The aim of this project is to optimize the synthesis process and to improve the characteristics of the molybdenum sulfide based alcohol synthesis catalyst. The initial investigations of a K_2CO_3/Co/MoS$_2$/C catalyst indicate that the sulfide catalyst irrespective of the feed sulfur level requires around 10 hours on stream to reach a stabilized behavior. Hydrogen sulfide in the feed lowers the alcohol selectivity by enhancing the hydrocarbon formation, but H_2S also promotes chain growth.

Introduction

In recent years there have been violent fluctuations in the price of oil. Furthermore there is now a widespread consensus that the anthropogenic emissions of CO_2 to a significant extent is contributing to the recent increase in global temperature. A solution that potentially addresses both of these issues could be an increased use of biofuels in the transportation sector. An interesting route to biofuels is a gasification of biomass to form syngas (a mixture of H_2 and CO) followed by a catalytic conversion of the syngas into fuel chemicals.

High octane numbers make alcohols well suited as additives to or substitutes for oil derived gasoline. However the lower alcohols and particularly methanol suffer from a limited miscibility with gasoline, which hampers their introduction as fuel additives. These miscibility problems can largely be avoided by including higher alcohols in the mixture, since the higher species act as co-solvents and stabilize the alcohol/gasoline blend [1]. Such a mixture of methanol and higher alcohols can be produced directly from syngas, and this catalytic synthesis of higher alcohols is the subject of the present PhD-project.

The alcohol synthesis can be conducted over various types of modified methanol [2] or Fischer-Tropsch synthesis catalysts [3]. Another interesting alcohol synthesis catalyst, which is the subject of the present study, is alkali promoted molybdenum sulfide – perhaps additionally promoted with Co or Ni [4]. The strong point of the sulfide catalyst is its ability to produce a significant amount of higher alcohols, while the main limitation for this catalyst is the alcohol selectivity,

since there is a non-negligible side production of short-chained hydrocarbons. One of the main objectives of the present project is indeed to explore the possibilities for improving the alcohol selectivity of the sulfide catalyst.

Experimental Work

The experimental investigations are conducted using a high pressure reactor setup. The setup was originally constructed to investigate homogeneous gas phase chemistry [5]. Recently the reactor has been supplemented with a feeding system that allows normally liquid components to be fed to the high pressure reactor. A simplified diagram illustrating the experimental setup is shown in figure 1.
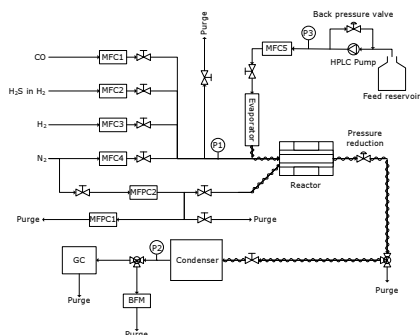
Figure 1: The experimental setup. BFM: Bubble flow meter; GC: Gas Chromatograph; MF(P)C: Mass flow (pressure) controller; P: Manometer; Heat tracing is indicated by sinusoidal curves.

The experimental work is conducted using a K_2CO_3/Co/MoS_2/C catalyst provided by Haldor Topsøe A/S. The catalyst is prepared in the oxide form, and prior to use the catalyst is sulfided in a flow of 2 vol% H_2S in H_2 at atmospheric pressure. The sulfidation is initiated at 100 °C, and the temperature is then increased to 300 °C at a rate of 3 °C/min. A bed of catalyst is placed in a quartz tube contained inside a stainless steel pressure shell. As the inside of the quartz tube is pressurized, nitrogen is dosed to the pressure shell to ensure an equal pressure on both sides of the quartz tube wall. Gases are supplied from pressurized cylinders. Product characterization downstream of the reactor is conducted using a GC-FID/TCD detection system.

Results & Discussion

The initial investigations have focused on the stability of the catalyst in the syngas atmosphere. The catalyst is a sulfide, and the stability investigations include an evaluation of the role of sulfur sources in the syngas feed. Here H_2S has been utilized as the sulfur source.

It is found that irrespective of the presence of H_2S in the feed, the catalyst requires around 10 hours on stream to reach a stabilized behavior in terms of activity and selectivity. During this period the alcohol selectivity increases, while the CO conversion decreases, because the hydrocarbon formation gradually decreases. This is illustrated in figure 2 for the case without H_2S in the syngas feed.
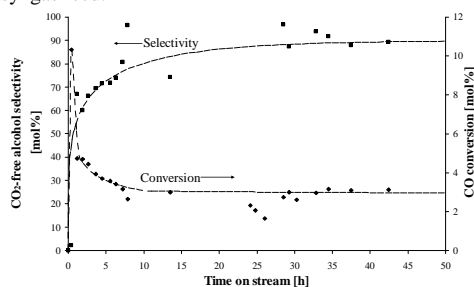
Figure 2: The CO conversion and the carbon based alcohol selectivity (excluding formed CO_2) as functions of the time on stream in a sulfur free syngas. Experimental conditions: T = 327 °C, P = 100 bar, GHSV = 5247 hr^{-1}, H_2/CO = 1/1.

The changes in catalytic properties during the first 10 hours could be due to a loss of sulfur from the catalyst, which is observed to occur during the reaction. Another factor that might be contributing to the initial development in catalytic properties is a gradual spreading of the alkali promoter.

The presence of H_2S in the syngas lowers the alcohol selectivity by enhancing the formation of hydrocarbons. The alcohol production decreases slightly with increasing H_2S level, but this is not a marked effect. The influence of H_2S is however not entirely negative. An important positive effect of H_2S is that it serves to stabilize a substantial fraction of the desired higher alcohols in the product formed over the catalyst.

This is illustrated in figure 3, which shows the ratio of higher alcohols to methanol in the reaction product as a function of time on stream.
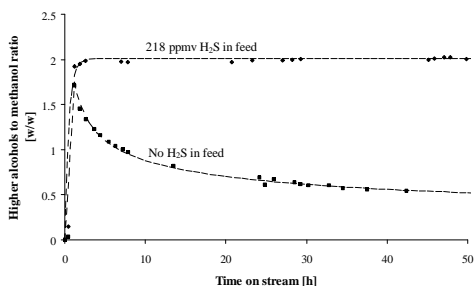
Figure 3: The weight ratio of higher alcohols relative to methanol in the reaction product depicted as a function of the time on stream in syngas with and without co-fed H_2S. The experimental conditions are given in figures 2.

Figure 3 shows that in the presence of 218 ppmv H_2S the ratio of higher alcohols to methanol is stable, but in the absence of feed sulfur the fraction of higher alcohols decreases over time. This is not due to a decreasing production of higher alcohols, but rather due to a gradually increasing production of methanol. In the absence of H_2S the methanol production continues to increase for the first 30-35 hours on stream, but after this time the production appears to be stable.

Conclusion

Irrespective of the H_2S level in the syngas feed a K_2CO_3/Co/MoS_2/C alcohol synthesis catalyst requires around 10 h on stream to stabilize in terms of activity and selectivity. The presence of H_2S lowers the alcohol selectivity by enhancing the hydrocarbon formation. Additionally hydrogen sulfide serves to stabilize a substantial fraction of higher alcohols in the reaction product.

Acknowledgements

References

1. J.L. Keller, Hydrocarbon Process. 58 (1979) 127-138.
2. R.G. Herman, Catal. Today 55 (2000) 233-245.
3. P. Courty, D. Durand, E. Freund, A. Sugier, J. Mol. Catal. 17(1982) 241-254.
4. C.B. Murchison, M.M Conway, R.R. Stevens, G.J Quarderer, in: M.J. Phillips, M. Ternan (Eds.), Proceedings of the 9th International Congress of Catalysis Vol. 2, Chemical Institute of Canada, Canada, 1988, p. 626.
5. C.L. Rasmussen, J. Hansen, P. Marshall, P. Glarborg, Int. J. Chem. Kin., 40 (2008) 423-441.

Martin Ellegaard Christensen

Phone:	+45 4525 2808
Fax:	+45 4593 2906
E-mail:	mec@kt.dtu.dk
WWW:	http://www.capec.kt.dtu.dk
Supervisors:	Jens Abildskov

PhD Study
Started: February 2008
To be completed: January 2011

Some Applications of Fluctuation Solution Theory to Phase Equilibria

Abstract

A goal of this Ph.D. study is to apply the statistical mechanical fluctuation solution theory to phase equilibrium problems. We highlight the applicability to the solubility of solids in mixed solvents and gas solubility in ionic liquids. Further, we seek to develop a group-contribution based equation of state to predict thermodynamic properties of complex liquids.

Introduction and Specific Objectives

This Ph.D. project attempts to describe phase equilibria in complex systems within the framework of the so-called "Fluctuation Solution Theory" (FST). FST is a statistical mechanical theory describing liquid-phase properties. Briefly, FST is based on integrals of molecular pair correlation functions, which leads to simple expressions for useful thermodynamic properties. The formalism is applied to three distinct areas:

1. Solubility of solids in mixed solvent systems.
2. Gas solubility in ionic liquids using a group contribution approach.
3. Group-contribution based equation of state for complex liquids.

In connection with the first item above, the objective is to adequately describe the solubility of a single solid solute in mixed, binary solvent mixtures. This finds great application within the pharmaceutical and agro chemical industries, where an active ingredient frequently is formulated and manufactured in systems comprised of two or more liquid solvents. The solubility behavior in mixed solvent systems is often complex and difficult to describe due to the presence of second and third body interactions between molecular species. A modeling framework has been initiated and the methodology, based on FST, is outlined in [1].

Application of ionic liquids (ILs) for chemical synthesis is an area which is increasingly being investigated. ILs are being considered a new generation of "green" solvents due to favorable physico-chemical properties, including negligible vapor pressure. However, accurate phase equilibria representation is a prerequisite for the design of systems involving ILs. Models for equilibrium thermophysical properties of these solvents, based on group contributions, are beginning to appear in the literature. Here, we seek to develop an equation of state for systems containing ILs. Previously [2], a method has successfully been applied to gas solubility in solvent mixtures of one or two solvents. We wish to expand this method to include ILs with parameterization based on group contributions.

The last area is the core of the project. Here we attempt to model integrals of the pair correlation functions on the basis of group contributions. These integrals may be found from the chemical potential, which is readily accessible from various chemical theories such as SAFT. The concept of SAFT is the construction of molecules from segments (larger than functional groups). This greatly resembles the basic idea of group contributions, which facilitates the concept of a group-contribution based equation of state. Recently, this has been put into practice [2] using a simplified SAFT model. The thermodynamic framework for our method is described in [2] and we propose to further develop modeling by application of SAFT to FST. To this day very little work has been done with a group-contribution based approach to FST.

Results and Discussion

Presently, we are able to show results of the work carried out within the area of mixed solvent solubility.

The theoretical framework will not be repeated here, only a few fundamental definitions are given.

The method requires one parameter characterizing the non-ideality of each solute/solvent pair, as well as parameters for a G^E-model expressing the non-ideality of the solvent mixture. We have used the Wilson equation to represent the activity coefficients of the solvent/solvent non-ideality.

Figure 1 shows examples of four systems, which have been correlated using the method described in [1]. Shown is the 'excess' solubility, a quantity defined for a system of a solid (1) in a mixed solvent (2,3) as

$$\ln x_1^E \; ^\circ \; \ln x_{1,m} - \sum_{j^1 1}^{3} x_j^\phi \ln x_{1,j}. \qquad (1)$$

Here, $x_{1,m}$ is the mole fraction solubility of 1 in the mixed solvent, x_j^ϕ is the solvent mole fraction on a solute-free basis and $x_{1,j}$ is the solubility of 1 in pure solvent j. The figure also shows the experimental data, from which parameters have been regressed. Also provided are error bars indicating the uncertainty of the estimates. These are calculated from error propagation using elements from a variance-covariance matrix. Although not quantitatively in all systems, the method is certainly qualitatively correct.
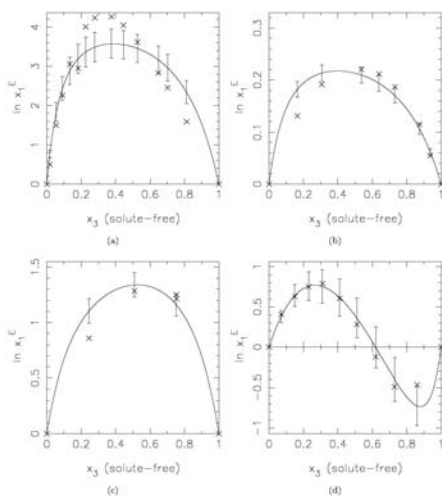
Figure 1. Estimated and experimental excess solubility of solid solutes in binary mixed solvents: (a) Naphthalene(1)/water(2)/acetone, (b) anthracene(1)/n-octane(2)/1-butanol(3), (c) beta carotene(1)/acetone(2)/n-hexane(3), and (d) salicylic acid(1)/ethanol(2)/water(3). The solute-free binary mixture forms a non-ideal solution in all of these systems.

The parameters are regressed from measured, mixed solvent solubilities along with other systems with that solute/solvent pair.

Figure 2 shows examples of systems where the parameters for the solute/solvent interaction have been

predicted using values obtained from mixtures where the solute and each of the solvents are present. The system shown in Figure 2(b) is not very successful, whereas the system in 2(a) is much better. Here, the asymmetry of the excess solubility profile is qualitatively correct.
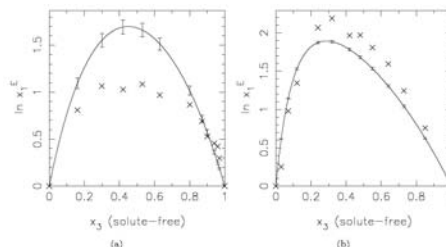
Figure 2. Predicted and experimental excess solubility of paracetamol in binary solvent mixtures: (a) Paracetamol(1)/ethyl acetate(2)/ethanol(3), and (b) paracetamol(1)/water(2)/ethanol(3).

Finally, we have touched upon the connection between the excess solubility and the non-ideality (excess Gibbs energy) of the solvent mixture. The method developed contains an explicit solvent/solvent nonideality term. This means that ideal solvent mixtures will not exhibit excess solubility when the solute is introduced, which is in agreement with experimental data. Furthermore, solvent mixtures with large excess Gibbs energies frequently exhibits large excess solubilities.

Conclusions

Fluctuation Solution Theory (FST) is a suitable methodology for representation of phase equilibrium problems. Extensive, but not exhaustive, comparisons with experimental data show that the method proposed for mixed solvent solubility is capable of describing simple and complex excess solubility behavior.

We expect to further investigate application of FST to systems with supercritical compounds and complex liquids.

References

1. M.E. Christensen, J. Abildskov, J.P. O'Connell, AIChE J. Accepted for publication.
2. E.A. Campanella, P.M. Mathias, J.P. O'Connell, AIChE J. 33 (1987) 2057-2066.
3. A. Lymperiadis, C. Adjiman, A. Galindo, G. Jackson, J. Chem. Phys. 127 (2007) 234903.

Elisa Conte

Phone: +45 4525 2959
Fax: +45 4525 2906
E-mail: elc@kt.dtu.dk
WWW: http://www.capec.dtu.dk
Supervisors: Rafiqul Gani
               Jens Abildskov

PhD Study
  Started: July 2007
  To be completed: July 2010

Innovation in Integrated Chemical Product-Process Design - Development through a Model-Based Systems Approach

Abstract

The chemical industry has recently started to focus attention on 'consumer-oriented' chemical products; for these complex kinds of products, it is important to have the right properties in order to meet the consumer needs. To satisfy these needs, the aim of chemical product and process design is to find a candidate product that exhibits the targeted behaviour and to find a process that can manufacture it for the specified qualities. The objective of this paper is to present a virtual laboratory for chemical product-process design (virtual PPD-lab) where users can test their design ideas on model-based computer-aided tools before performing experiments to validate the designed product. Design alternatives for products and processes matching a priori defined targets can be generated and verified through the PPD-lab. The significance of this virtual laboratory is that the experimental effort in the development of new products and processes can be drastically reduced and attention can be focused on few alternatives; as a consequence, time and resources can be spared. This paper highlights a new feature of the virtual PPD-lab which handles the design of mixtures. Through a case study dealing with a coating formulation, the application of this new feature is illustrated.

Introduction

In design of chemical products and the processes that can manufacture them, one first tries to find a candidate product that exhibits a certain desirable or targeted behavior and then tries to find a process that can manufacture it with the specified qualities. The candidate may be a single chemical, a mixture, or a formulation of active ingredients and additives. The common practice to develop these products is experiment-based trial and error approach, supplemented sometimes with model-based computer-aided tools to speed-up some of the steps. The virtual PPD-lab (Figure 1) is an innovative and more effective approach to product and process design. It contains methods and tools to allow the modeling and simulation of the needed experimental scenarios. For this to work the 'in-house' models need to be reliable and efficient and the architecture of the software needs to include the work-flows related to different product-process design problems. Also, interfaces for efficient data-flow between different tools need to be defined. The architecture has to be flexible to allow changes in work-flow, addition of new models and of new data for future extension of the application range.

The objective here is to quickly and efficiently generate a list of promising candidates for final testing (and selection) by experiments. In this way, rather than use the experiment-based trial and error approach from the start, the experimental resources are reserved for the final selection and verification, while the virtual PPD-lab is used for identifying the promising feasible
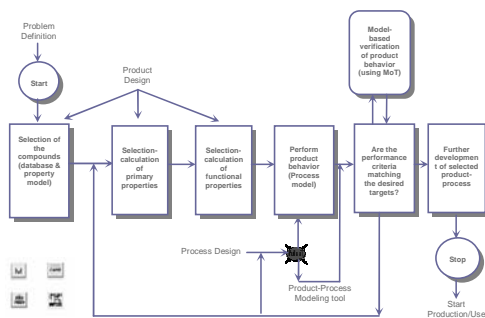
Figure 1. The Virtual PPD-lab, user interface.

candidates, thereby achieving faster to market at reduced cost for any potential chemical product-process. The virtual PPD-lab has been developed using Excel as the simulation environment and provides interconnections between different computational entities, such as databases, property and process models, tools for molecular design and solvent selection, modeling tools, and, templates for guiding the user through product design steps.

An innovative approach
The product-process design problem is solved through the reverse approach that includes a stage to *define the design target*, and a stage to *identify the alternatives that match the target*. This approach is based on the idea that all processes depend on some key properties of the products and on the effect of these properties on the process performance, that is, in the first stage the targets for the product performance are set and the process model is solved with property parameters as the unknown variables. In the second stage, any appropriate property model can be used, including database search, in order to identify a list of product alternatives matching the targets. With this reverse approach it is possible to design products tailormade to suit the process demands by solution of integrated product and process models.

Resident models, methods and tools
From the virtual PPD-lab it is possible to access ICAS[1], an Integrated Computer Aided System consisting of a number of toolboxes that help to efficiently solve a wide range of problems. Some ICAS toolboxes can be launched as standalone applications for the virtual PPD-lab, such as CAPEC DataBase, the Computer Aided Molecular Design tool (ProCAMD), the Property Prediction tool (PropPred), and the Modeling Tool (MoT). These toolboxes can easily be updated with newer and more reliable models[2].
The software architecture is flexible to allow the developer in shaping his own designs (case studies). If new compounds are introduced during the workflow, CAPEC DataBase or ProPred can be employed for the properties calculation. If a new solvent has to be tested, ProCAMD can be helpful in finding a solvent with the desired properties. If different process models have to be tested, MoT can be employed to type in the new model and obtain fast results, statistics and to perform sensitivity analysis.

Templates for Product-Process Design
To guide users in solving product and process design problems, templates defining work- and data-flow for different types of design problems have been developed for the PPD-lab. According to the template, design problems are decomposed into sub-problems: problem definition, selection of involved chemicals, calculation of properties affecting the process, process model solving and, finally, model-based verification of the design (as shown in Figure 1). In each step, the user is

asked to make choices, such as choosing between rigorous models or correlations; choosing between different property or process models. The user can interact with the software through dialog boxes and decide on the direction for the solution of the case study. Currently, two design templates are already available: design of polymeric microcapsules for the controlled release of active ingredients, and, design of pesticide formulations for plant uptake. A third template, which guides the user to design solvent mixtures for formulated products, has been recently added and is presented in this paper.

Mixture Design feature
Many chemicals-based products of everyday life such as sun lotions, shower creams, paints and insect repellents, are formulations. Formulations are complex products constituted of several chemicals (solvents, polymers, pesticides, emulsifiers, pigments, and so on); formulations usually contain a large amount of solvents (single solvents are rare), which have the function of binding all the chemicals together and conferring important end-properties to the product. A tool for designing solvent mixtures in formulations, therefore, has become a template in the virtual PPD-lab environment. It is based on a new algorithm called MixD that has been developed for designing mixtures of solvents, but that can, in principle, be employed for the design of mixture of any kind of chemicals. Currently, MixD considers only binary mixtures, but it can be easily extended to multicomponent mixtures.
The *reverse approach* is applied in the following way: given the mixture target properties, identify the chemicals which could be mixed in order to match the design target and then determine the mixture composition minimizing the cost.
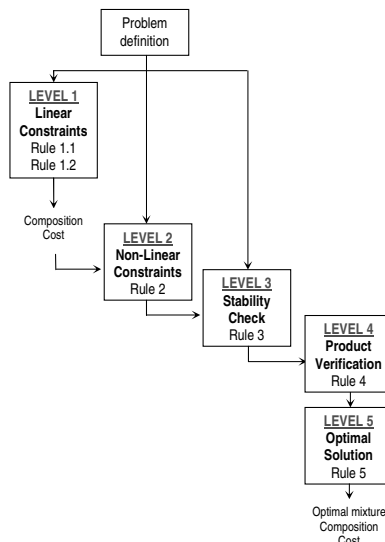
Figure 2. Flow-diagram of the method.

A knowledge-based system helps the user to define the targets.

The MixD algorithm starts by identifying a set of feasible binary pairs of chemicals, then, it reduces the number of feasible candidates through five levels of screening, as highlighted in the flowchart of Figure 2.

The screening starts (level 1) applying the linear constraints for the target properties; linear models are based on linear mixing rules. According to Rule 1.1, any binary mixture is rejected if the pure component property values of both compounds in the mixture are either greater/lower than the upper-/lower-bounds of the target, respectively.

Then, the composition range for each feasible mixture is calculated as shown in Eqs 1 to 4. P_i is a mixture target property, $P_{i,1}$ and $P_{i,2}$ are the pure properties of the chemicals involved in the binary mixture and $P_{i,mix}^{UB}$ and $P_{i,mix}^{LB}$ are the constraints values on P_i (*UB*-Upper Bound, *LB*-Lower Bound).

$$x_{i,1}^{LB} = \frac{P_{i,2} - P_{i,mix}^{UB}}{P_{i,2} - P_{i,1}} \qquad (1)$$

$$x_{i,1}^{UB} = \frac{P_{i,2} - P_{i,mix}^{LB}}{P_{i,2} - P_{i,1}} \qquad (2)$$

$$x_1^{LB} = \max\left(x_{i,1}^{LB}, ...\right) \qquad (3)$$

$$x_1^{UB} = \min\left(x_{i,1}^{UB}, ...\right) \qquad (4)$$

According to Rule 1.2, the binary pairs, which do not have a composition (within 0-1) that satisfies the targets, are rejected. At this point, for each binary mixture, the composition corresponding to the lowest cost is chosen (either x_1^{LB} or x_1^{UB}).

The second level of the design is based on non-linear constraints; non-linear models, which employ rigorous mixing rules to account for excess properties, are now used to further screen the feasible mixtures from level 1 (Rule 2).

The mixtures designed up to this point satisfy all the constraints on the target properties. In level 3, their phase stability is verified (Rule 3); since a solvent mixture for a formulation is being designed, the mixture has to be one single liquid phase. Information about the stability of a liquid mixture can be obtained from the Gibbs energy of mixing ($\Delta G/RT$), and from its first and second derivatives. A new routine for the calculation of the immiscibility gap of partially miscible mixtures with negative $\Delta G/RT$ in the entire composition range, has been developed and tested on various binary mixtures, containing linear, branched and cyclic, aliphatic and aromatic hydrocarbons, and water. The routine employs the tangent plane condition[3,4] and a new numerical solution method. The compositions defining the immiscibility gap have to show two properties: 1) same value of the first derivative of the function $\Delta G/RT$; 2) the straight line connecting the corresponding points on

the $\Delta G/RT$ function is the lowest tangent on the $\Delta G/RT$ curve touching these points.

Level 4 is verification: the performance of the product is tested. Linear property models give good predictions for the properties of mixtures with negligible excess properties of mixing; with large excess properties of mixing it is necessary to calculate mixture properties values with rigorous models accounting for excess properties, and to verify if the mixture properties still match the targets.

Finally, at level 5 the optimal is found applying Rule 5: a performance index (PI) is fixed and the optimal solution is identified by ordering the feasible mixtures in terms of PI.

Case study: coating formulation

A coating is usually constituted by: pigments, solid particles giving the particular coloration; binder, usually a polymer with the function of binding the pigments together; mixture of solvents, with the function of giving structural properties to the final product; finally, additives (usually less than 2% in volume), with different functions (dispersant, emulsifiers, wetting agents).

The paint should have good spreadability to be easily applicable on surfaces; it has to dry in a reasonable time but not too fast for not to be inhaled by the painter; it has to have a low toxicity for the same reason; in addition, it needs to have a competitive price. These performance criteria are achieved through the addition of a solvent mixture, while other additives further enhance the coating performance.

Problem statement and methodology results

Well known binders for paints are Poly(3-hydroxylalkanoates)[5], water insoluble polyesters which can dissolve pigments like titanium dioxide (TiO_2) and Iriodin®. A mixture of solvents for the formulation matching the performance criteria stated above needs to be designed.

The first and most important step is to translate the target performance criteria into target chemical properties. The following properties have been considered: spreadability is related to density, viscosity and surface tension; evaporation rate is associated to the parameter T_{90}, which is the time for the 90% (by weight) of the mixture to evaporate; toxicity is controlled with the parameter LC_{50}, the aqueous concentration causing 50% mortality in a fathead minnow population after 96 hours. In addition, the solvent mixture should be able to dissolve the binder.

Since the binder is water insoluble, it is reasonable to assume that it will be soluble in solvents which dislike water so, in order to ensure the polymer solubility, in this design problem, only solvents that are not miscible with water will be considered. In addition, the mixture solubility parameter should be close to that of the polymer ($\delta_{polymer}$ = 15.67 MPa$^{1/2}$).

For modeling all the target properties linear mixing rules are sufficient, except the evaporation time model[6],

which is based on UNIFAC method. The stability of all binary mixtures composed of a solvent (from the database) and water has been checked. All solvents showing miscibility with water have been excluded from the database. It is worth noting, however, that two solvents which are immiscibile with water may not also form a single liquid phase. Therefore, the stability check of level 4 (see Figure 2) is necessary.

The database used contains 42 solvents which are usually employed for paints/coatings. Since 11 of these solvents show miscibility with water, they are removed from the database, and 31 solvents are left. These solvents can combine in 465 binary mixtures. After the first level of screening, 315 of them are rejected (Rule 1.1 and Rule 1.2). The remaining 150 mixtures are screened in the second level, and only 11 of them satisfy the non-linear constraints (Rule 2). At the third level of screening, the stability of the mixtures is tested. Only one of the mixtures presents two phases in the composition of interest, and it is rejected (Rule 3).

At the fourth level of design, feasible mixtures have been verified in terms of their viscosity and surface tension using more rigorous models (Rule 4) based on UNIFAC[7,8]; the property values calculated in this way were found to be close to the ones calculated with the linear models (Root Square Mean Errors: 0.03 for viscosity, 0.83 for surface tension) and they still matched the design constraints.

Table 1. Mixtures matching the target properties, their compositions (molar fraction) and cost [\$/kg].

n°	Mixtures	x_1	Cost
1	DEGEE+ Toluene	0.05	1.35
2	Toluene + Ethylbenzene	0.56	1.37
3	Toluene + Butyrolactone	0.96	1.60
4	Toluene+ Cyclohexanone	0.95	2.49
5	Ethylbenzene + Ethyl acetate	0.77	3.51
6	Ethylbenzene + Butyl acetate	0.62	3.67
7	Ethylbenzene + Hexane	0.87	3.70
8	Ethylbenzene + Heptane	0.87	3.72
9	Ethylbenzene + Butanone	0.80	3.72
10	Ethylbenzene + Isopropylacetone	0.72	3.91

Table 2. Estimated property values for the feasible mixtures; δ [MPa$^{1/2}$], μ [cP], γ [mN/m], ρ [kg/m^3], LC_{50} [mol/m^3], T_{90} [s].

n°	δ	μ	γ	ρ	LC_{50}	T_{90}
1	18.35	0.71	28.63	0.87	0.40	256.1
2	18.04	0.60	28.41	0.86	0.40	345.8
3	18.49	0.60	28.65	0.86	0.43	255.6
4	18.24	0.63	28.80	0.86	0.40	256.4
5	17.92	0.60	27.18	0.87	0.69	403.8
6	17.68	0.66	27.00	0.87	0.40	448.0
7	17.47	0.60	27.00	0.84	0.52	437.4
8	17.55	0.61	27.00	0.84	0.46	436.1
9	18.09	0.60	27.56	0.85	1.02	427.2
10	17.63	0.63	27.00	0.84	0.84	418.2

The single phase solvent mixtures matching the target criteria are listed in Table 1 (ordered in terms of increasing cost), together with the estimated values of the mixture properties. The mixture DEGEE (Diethylene Glycol Ethyl Ether)-Toluene with a composition of 5% (molar base) of DEGEE is the cheapest (Rule 5).

Additives can be added to the formulation in order to enhance product performance. For instance, sodium dioctyl sulfosuccinate is a wetting, solubilising and dispersal agent; it is not soluble in water and has a solubility parameter close to the ones of Table 1, so it can be a suitable candidate.

Conclusions

The virtual PPD-lab has been introduced and the use of the resident models, methods and tools has been illustrated. A systematic methodology developed for mixture design has been highlighted. A useful feature of the mixture design feature is that it can be employed for the design of formulations, and a case study for paint formulation has been highlighted. Current work is to consider new design problems, for other formulations, through which the methodology can be further tested and validated. Future work is to develop models and design tools for the mixing (process) operation and to enlarge the number of products which can be tested and designed through the PPD-lab.

References

[1] ICAS Documentation, 2003, Internal report, CAPEC, Dep of Chem and Biochem Eng, Tech Univ of Denmark.

[2] Conte, E., Martinho, A., Matos, H. A., Gani, R., 2008, Ind. Eng. Chem. Res., 47(20), 7940-7954.

[3] Baker, L. E., Pierce, A. C., Luks, K. D., 1982, Soc. Petro. Eng. J., 22, 731-742.

[4] Michelsen, M. L., 1982, Fluid Phase Equilibr., 9, 1-19.

[5] Van der Walle, G. A. M., Buisman, G. J.H., Weusthuis, R. A., E. Gerrit, 1999, Int. J. Biol. Macromol., 25, 123–128.

[6] Klein, J. A., Wu, D. T., Gani, R. 1992. ESCAPE-1, S229-S236.

[7] Suarez, J.T, Torres-Marchal, C., Rasmussen, P., 1989, Chem. Eng. Sci., 44(3), 782-786.

[8] Cao, W., Knudsen, K., Fredenslund, A., Rasmussen, P., 1993, IECR, 32, 2088-2092.
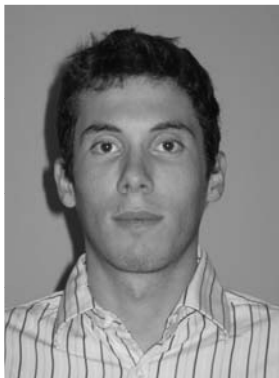
Victor Darde

Phone:	+45 9955 4667
Fax:	+45 4525 2258
E-mail:	vid@kt.dtu.dk
WWW:	http://www.ivc-sep.kt.dtu.dk
Supervisors:	Kaj Thomsen
	Erling H. Stenby
	Willy JM van Well, DONG Energy

Industrial PhD Study
Started: February 2008
To be completed: January 20011

CO$_2$ Capture using Aqueous Ammonia

Abstract

CO$_2$ capture process using aqueous ammonia shows good perspectives for decreasing the energy requirement thanks to the low enthalpy of absorption of CO$_2$ by NH$_3$. However, a scientific understanding of the process is required. The properties of the NH$_3$-CO$_2$-H$_2$O system were described using the Extended UNIQUAC electrolyte model developed by Thomsen and Rasmussen in a temperature range from 0 to 110°C and pressure up to 100 bars. [1] The results show that solid phases consisting of ammonium carbonate and bicarbonate are formed in the absorber at low temperature. The enthalpy calculations show that an energy requirement for the desorber lower than 2 GJ/ton CO$_2$ can be reached.

Introduction

The proportion of carbon dioxide emissions from power production is very significant in industrialized countries. Carbon dioxide capture implies separating the CO$_2$ from the flue gases from a power plant or other industry instead of releasing the CO$_2$ in the atmosphere. Post-combustion techniques separate the carbon dioxide from the flue gas after a traditional combustion process. Amine solutions have been commonly used for the commercial production of CO$_2$. However, such technologies require a large amount of energy, especially in the desorption part of the process. Therefore, new alternatives for post-combustion capture are searched for. Processes using aqueous ammonia as solvent are some of the promising alternatives. They can be found in two variants. The first variant absorbs the CO$_2$ at low temperature (2-10°C) and is called chilled ammonia process. It is a patented process. [2] This process allows precipitation of several ammonium carbonate compounds in the absorber. The second process absorbs CO$_2$ at ambient temperature (25-40°C) and does not allow precipitation.

Specific objective

The purpose of this study is to get a scientific understanding of the CO$_2$ capture process using aqueous ammonia. It is based on the extended UNIQUAC thermodynamic model developed for the CO$_2$-NH$_3$-H$_2$O system by Thomsen and Rasmussen [1]. An updated version of the model is being developed with an enlarged range of temperature by using additional experimental data. The process will then be simulated in order to optimize its configuration and its integration in the power plant process. The rate of absorption will also be investigated by designing and using a wetted wall column apparatus and comparing the rate of absorption of CO$_2$ by ammonia and amine solvents.

Results and Discussion

A study has been made in order to evaluate the process using the original version of the model. It calculates the activity coefficient for the liquid phase using the extended UNIQUAC model, and the gas phase fugacity using the Soave-Redlich-Kwong equation for the volatile compounds. It is based on more than 2000 experimental data points on this system in the IVC-SEP electrolyte data bank, including thermal properties and solid-liquid equilibrium. These data were used to fit the parameters. The analysis of the CO$_2$-NH$_3$-H$_2$O system implies the study of several equilibrium processes. The following reactions are considered in the model:

Speciation equilibria

$$NH_3(aq) + H_2O \longleftrightarrow NH_4^+ + OH^-$$

$$CO_2(aq) + H_2O(l) \longleftrightarrow HCO_3^- + H^+$$

$$HCO_3^- \longleftrightarrow CO_3^{2-} + H^+$$

$$H_2O(l) \longleftrightarrow OH^- + H^+$$

$$NH_3(aq) + HCO_3^- \longleftrightarrow NH_2COO^- + H_2O(l)$$

Vapor-liquid equilibria

$$CO_2(g) \longleftrightarrow CO_2(aq)$$

$$NH_3(g) \longleftrightarrow NH_3(aq)$$

$$H_2O(g) \longleftrightarrow H_2O(l)$$

Liquid-solid equilibria

$$NH_4^+ + HCO_3^- \longleftrightarrow NH_4HCO_3(s)$$

$$NH_4^+ + NH_2COO^- \longleftrightarrow NH_2COONH_4(s)$$

$$2NH_4^+ + CO_3^{2-} + H_2O \longleftrightarrow (NH_4)_2CO_3 \cdot H_2O(s)$$

$$4NH_4^+ + CO_3^{2-} + 2HCO_3^- \longleftrightarrow (NH_4)_2CO_3 \cdot 2NH_4HCO_3(s)$$

$$H_2O(l) \longleftrightarrow H_2O(s)$$
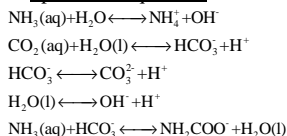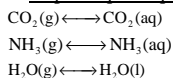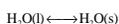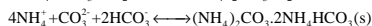
The model is capable of describing accurately the vapor-liquid-solid equilibria and thermal properties for the CO_2-NH_3-H_2O system for a concentration up to 80 molal NH_3, for a temperature in the range of 0-110°C and for a pressure range up to 100 bars. Based on the model and on the information from the patent of the process, the equilibrium composition of the different streams of the process has been studied. The results shown here describe the compositions of the streams in the absorber and in the desorber. A typical initial mass fraction of ammonia in the solvent is 28wt%. This value has been used in this study. Figure 1 shows the nature and amount of solid phase as a function of the CO_2 loading at 10°C, and Figure 2 shows the bubble point pressures as a function of the CO_2 loading at 120°C.
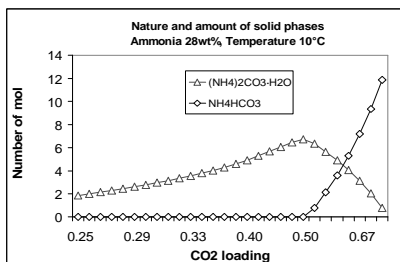
Figure 1: Nature and amount of solid phases of a 28wt% ammonia solvent with a temperature of 10°C as a function of the CO_2 loading
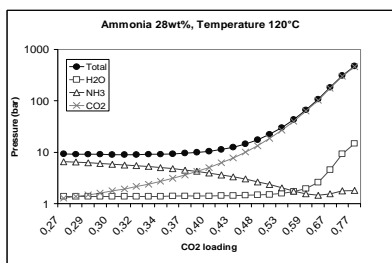
Figure 2: Bubble point pressures of a 28wt% ammonia solvent with a temperature of 120°C as a function of the CO_2 loading

Figure 1 shows that at 10°C, there is a solid phase present at all CO_2 loadings higher than 0.25. For loadings higher than 0.5, two solids are present: ammonium carbonate and ammonium bicarbonate. For lower loadings, the only solid is ammonium carbonate. Figure 2 shows that at high temperature, it is possible to get a pressurized and nearly pure CO_2 stream.

The energy requirement is a key parameter of a capture process. The cost of the capture is strongly linked to the energy that has to be supplied to ensure the desorption. The use of ammonia is supposed to lower the energy requirement. A reference configuration has been set up according to the information from the patent. Then, different parameters were modified individually in order to assess their influence. For the reference configuration, the energy requirement in the desorber was found to be 1830 kJ/kg CO_2 captured. The CASTOR project that consists of a pilot capture plant using aqueous alkanolamines resulted in an energy consumption in the stripper of about 3700 kJ/kg CO_2 captured, with a capture efficiency of 90%. [3] Hence, this study shows that based on the equilibrium calculations, the use of ammonia as a solvent is a way to very significantly decrease the energy consumption in the desorber. In addition, the configuration studied here can be optimized to reduce the energy requirement. Moreover, the CO_2 stream that is obtained at the end of the process is pressurized when ammonia is used, which would result in additional energy savings during compression of the carbon dioxide.

Conclusions

This study showed the presence of precipitates in the absorber, and the formation of ammonium bicarbonate from the ammonium carbonate present in the CO_2-lean stream during the absorption process. It was also shown that the pure CO_2 stream that leaves the desorber column is pressurized. A reference configuration was used to assess the energy requirement both in the absorber and in the desorber. Based on equilibrium calculations, this study showed that the chilled ammonia process allows for a significant reduction of the energy consumption in the desorber compared to the energy consumption of the process using amines.

References

1. K. Thomsen, P. Rasmussen, Modeling of Vapor-liquid-solid equilibrium in gas-aqueous electrolyte system, Chem. Eng. Sci. 54 (1999)1787-1802
2. E. Gal, Ultra cleaning combustion gas including the removal of CO_2, World Intellectual Property, Patent WO 2006022885 (2006)
3. JN. Knudsen, JN. Jensen, O. Biede, Castor SP2: Experiments on Pilot Plant, CASTOR-ENCAP-CACHET-DYNAMIS common Technical Training Workshop (2008)

List of Publications

1. V. Darde, K. Thomsen, W. van Well, EH. Stenby, Chilled ammonia process for CO2 capture, presentation at the Green House Gas Technology 9 (2008)

Anders Egede Daugaard

Address:	Building 423, Room 206
Phone:	+45 4525 6819
Fax:	+45 4588 2161
e-mail:	adt@kt.dtu.dk
www:	http://www.dtu.dk/Centre/DPC.aspx
Supervisor:	Søren Hvilsted

Ph.D. Study
Started: March 2006
To be completed: February 2009

Micro-Sensor Based on Click Chemistry

Abstract

Dendritic macromonomers for application in holographic data storage devices have been prepared. A photopolymer system consisting of a photoinitiator and the functional monomers have been tested in an orthogonally prepared matrix. The use of peripheral groups with a high refractive index resulted in materials with a high data storage capacity. In addition to this, the dendritic properties have been shown to have a beneficial effect on volume shrinkage as well as sensitivity.

Specific Objectives

The project presented here is a result of a research stay at University of California Santa Barbara in the research group of Professor C.J. Hawker. The Ph.D. project is generally focused on the application of click chemistry for the preparation of new functional materials as well as the preparation of sensor materials through this approach.

Introduction

With the increasing demand for higher data storage capacity and flexibility there is a need for development of new storage techniques as well as new materials. Presently used two dimensional techniques like harddrives and other disc media have limits as to how far storage capacity can be extended. In order to achieve sufficient storage capacities in the future one solution is to store data in three dimensions by volume holography. In volume holography data is stored as optical interference patterns throughout a photosensitive material. This interference pattern is created by intersection of two laser beams, where one contains the information to be written and the other is a reference beam used to read out the written holograms afterwards. When the beams intersect they cause chemical or physical changes in the material resulting in a modulation in e.g. the refractive index or the density of the material. Additional holograms can then be recorded by angling of the sample and thereby the storage capacity can be increased.

Presently volume holography still faces some material challenges and thus continued development is still needed. The ideal material should have a high
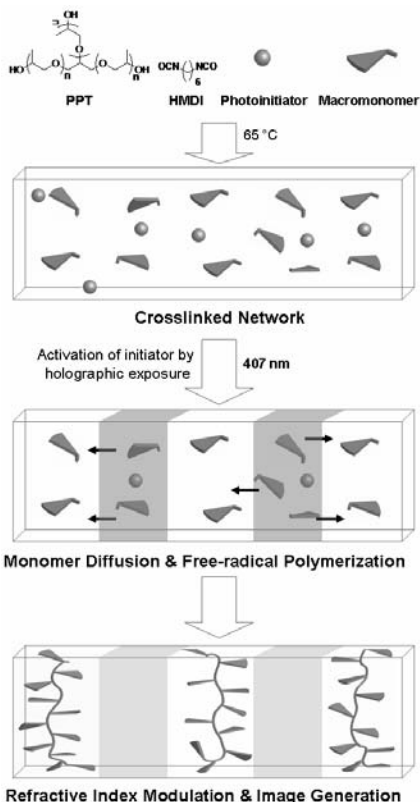
Fig 1: Schematic of the refractive index modulation in a matrix by photopolymerization of dendronized macromonomers.
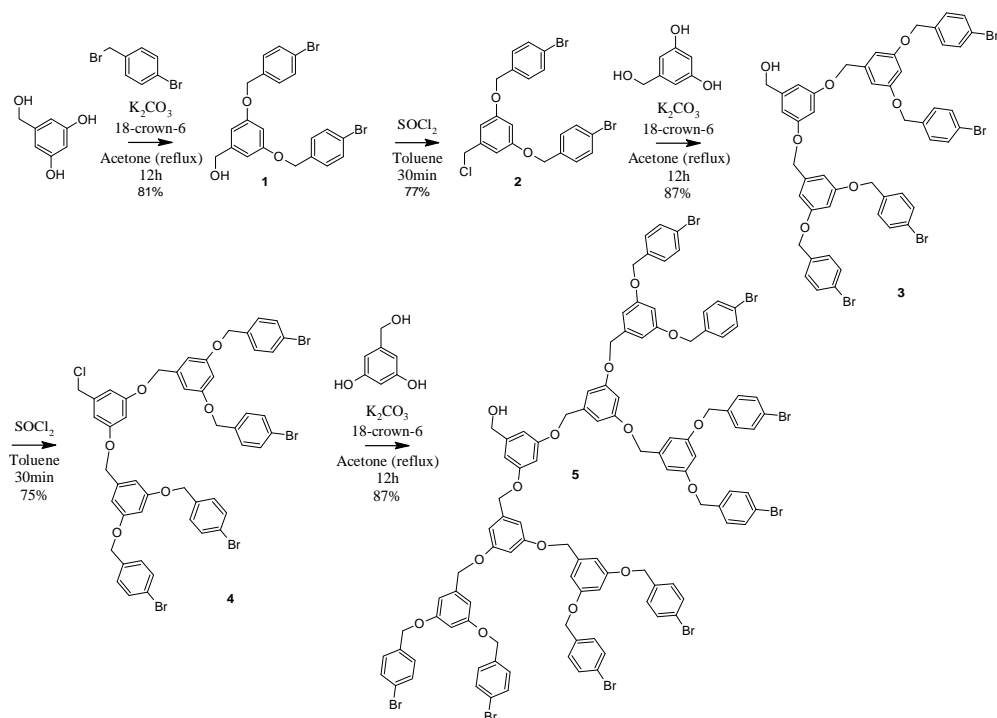
Scheme 1: Convergent synthesis of the first to third generation dendrons with high refractive index.

photosensitivity, high storage capacity, nondestructive readout, dimensional stability, be prepared in milimeter thick samples and be of low cost[1;2].

A photopolymer system[3-5], as outlined in Figure 1, where a monomer is dissolved in an inert matrix together with a photoinitiator and subsequently exposed to light and thereby polymerization in the bright regions fulfills many of these criteria. During the polymerization a concentration gradient is formed in the material as monomer diffuses to the bright areas and that causes a modulation of the refractive index and thereby a hologram is written. Traditionally monomers of low molecular weight have been used and that results in shrinkage upon polymerization as the polymer takes up less volume that the monomers. This writing induced shrinkage causes distortion of the holograms and in practice makes readout impossible. This problem becomes even more important with increasing film thickness and therefore a significant reduction in volume shrinkage is of great importance for the commercial use of photopolymer systems.

New monomers that have low viscosity (good diffusivity), high refractive index (high storage capacity) and low shrinkage upon polymerization therefore needs to be developed.

Here the application of dendritic macromonomers that show low shrinkage upon polymerization without sacrificing sensitivity is presented. The advantage of a dendritic macromonomer is that it contains a number of branches to a functional core that can easily be converted into a polymerizable acrylate. Thereby the concentration of polymerizable group is low in the material. The branches can be of high refractive index, whereby the sensitivity and storage capacity is kept high. Finally the known low viscosities of dendrimers[6] makes diffusion occur easily, maintaining high mobility. Dendritic macromonomers based on benzyl ethers[7] (Fréchet type) were prepared by a convergent approach[8] as shown in Scheme 1. Repeated Williamson ether syntheses and chlorination of the hydroxyl group in the core using thionyl chloride was performed to obtain the first to the third generation dendron.

Subsequent ester syntheses of the hydroxyl functional dendrons with acryloyl chloride gave the respective acrylates **6**, **7**, **8**, and **9** shown in Scheme 2.

Millimeter thick films for the holographic recording was then prepared by mixing the prepared macromolecular acrylates (**6**, **7**, **8** or **9**, 3wt%) with the matrix components hexamethylenediisocyanate (HMDI, 19.5wt%), polypropylene-triol (M_n=1000, 77.2wt%) with the photoinitiator 2,4,6-trimethylbenzoyldiphenylphosphine oxide (Lucirine, 0.3wt%). Initially the mixture is heated, which causes the diisocyanate to react with the triol forming an optical clear polyurethane network with suspended macromonomer and photoinitiator that are unreactive
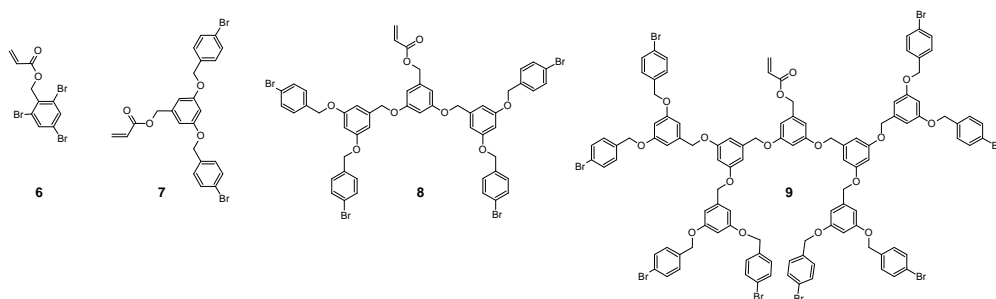
Scheme 2: Prepared dendritic macromonomers of increasing generations from 7 to 9

under these conditions, as illustrated in Figure 1. The crosslinked matrix is then exposed to the laser light and the interference pattern is written into the film. In the exposed areas the laser light initiates polymerization and macromonomers diffuse to the activated areas, as indicated in step 2 in Figure 1. Thereby a modulation of the refractive index is attained and the interference pattern has been created.

The high sensitivity of this system allows at least 60 holograms to be individually recorded in each holographic disc and from this data, the storage capacity (M/#) of holographic systems containing the different macromonomers 6, 7, 8, or 9 was calculated to be 8, 8, 10, and 6, respectively (Table 1). The angular selectivity of the 60 recorded holograms on a disc containing the macromonomer 8 is shown in Figure 2.
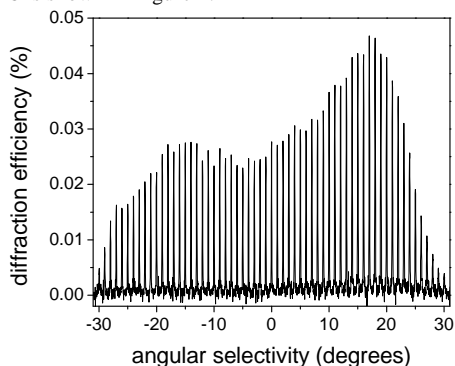
Fig. 2. Angular selectivity curves of the 60 holograms recorded in 0.5 mm thick holographic disc containing the second generation dendritic macromonomer 8.

The change in volume shrinkage as an effect of the different monomers was evaluated in accordance with the method of Dhar and co-workers[9]. The unbranched analogue, 6, was tested and volume shrinkage of 0.23% was observed from recording 60 holograms in the crosslinked film. This corresponds to similar values obtained from other unbranched monomers. Investigation of the first generation

dendronized monomer, 7, showed similar results for the storage capacity, as shown in Table 1. Since 6 and 7 have similar refractive index it was expected that they would also show similar storage capacities. Interestingly volume shrinkage of the dendritic monomer is reduced to only 0.10%. The second generation macromonomer, 8, was then tested. The storage capacity was found to be 10, which is the best result of all the investigated compounds and a result of the higher refractive index of the macromonomer. In addition to this it also showed very low shrinkage with only 0.04%, due to the increased ratio of branching groups to the core acrylate. The monomer also showed the highest sensitivity due to good mobility in the matrix. This clearly shows the beneficial effects of the dendritic structure where increased branching gives the higher storage capacity low shrinkage and still a low viscosity is retained. Continuing to the third generation gave very poor results in the applied matrix as the monomer is poorly soluble. It was decided to prepare a different matrix that could dissolve the third generation monomer. The new matrix was prepared from a blend of polycarbonatediol ($M_n = 800$) and trimethylolpropane (9:1) as well as the HMDI and the photoinitiator from the earlier matrix, referred to as the polycarbonate matrix henceforth. The third generation dendronized monomer, 9, again gave a lower shrinkage with only 0.03%. However both a low sensitivity and a low storage capacity was found compared to the other dendronized monomers.

Table 1: Holographic data from the different systems.

Monomer	Storage Capacity (M/#)	Sensitivity (cm/mJ)	Volume Shrinkage (%)	RI
6[a]	8	0.20	0.23	1.614
7[a]	8	0.37	0.10	1.616
8[a]	10	0.46	0.04	1.647
9[b]	6	0.05	0.03	1.663

[a] Polyurethane matrix
[b] Polycarbonate matrix

A test with the monomers 6, 7 and 8 showed that this was clearly a result of the polycarbonate matrix,

which apparently did not have as good mobility as the polyurethane matrix.

Conclusion

It has been demonstrated that dendronized macromonomers have a beneficial effect on the volume shrinkage in a photopolymer system. In addition to this the outfitting of the periphery of the dendron with high refractive index groups has been shown to be a method to increase the storage capacity. The optimal structure was found to be the second generation dendronized macromonomer, **8.** It had a higher storage capacity, lower shrinkage and higher sensitivity compared to all the other monomers investigated here. An increased storage capacity is very important for the future commercial application of photopolymer systems. The volume shrinkage is negligible allowing for good readout properties and the high sensitivity allows for fast data recording.

1. Acknowledgements

References

1. S.J. Zilker, Chemphyschem 3(4)(2002) 333-334.

2. M. Haw, Nature 422(6932)(2003) 556-558.

3. M.L. Schilling, V.L. Colvin, L. Dhar, A.L. Harris, F.C. Schilling, H.E. Katz, T. Wysocki, A. Hale, L.L. Blyler, and C. Boyd, Chemistry of Materials 11(2)(1999) 247-254.

4. T.J. Trentler, J.E. Boyd, and V.L. Colvin, Chemistry of Materials 12(5)(2000) 1431-1438.

5. M.G. Schnoes, L. Dhar, M.L. Schilling, S.S. Patel, and P. Wiltzius, Optics Letters 24(10)(1999) 658-660.

6. T.H. Mourey, S.R. Turner, M. Rubinstein, J.M.J. Frechet, C.J. Hawker, and K.L. Wooley, Macromolecules 25(9)(1992) 2401-2406.

7. K.L. Wooley, C.J. Hawker, and J.M.J. Frechet, Journal of the Chemical Society-Perkin Transactions 1 (5)(1991) 1059-1076.

8. K.L. Wooley, C.J. Hawker, and J.M.J. Frechet, Journal of the American Chemical Society 113(11)(1991) 4252-4261.

9. L. Dhar, M.G. Schnoes, T.L. Wysocki, H. Bair, M. Schilling, and C. Boyd, Applied Physics Letters 73(10)(1998) 1337-1339.

List of Publications

1. A. D. Thomsen, E. Malmström, S. Hvilsted, Carboxylic Acid Functional Polymers and Copolymers, Nordic Polymer Days, Copenhagen, DK, May 2006.

2. S. Hvilsted, E. Malmström, A. D. Thomsen, Novel Polymers with High Carboxylic Acid Loading, Macro 2006, Rio de Janeiro, BR, July 2006.

3. A. D. Thomsen, E. Malmström, S. Hvilsted, Novel Polymers with a High Carboxylic Acid Loading, Journal of Polymer Science Part A. Polymer Chemistry 2006 (44), 6360-6377.

4. A.E. Daugaard, T.S. Hansen, N.B. Larsen, S. Hvilsted, Conductive Polymer Functionalization by Click Chemistry, Macromolecules 2008 (41), 4321-4327.

5. A.E. Daugaard, S. Hvilsted, The Influence of Pendant Carboxylic Acid Loading on Surfaces of Statistical Poly[(4-hydroxystyrene)-co-styrene]s Macromolecular Rapid Communications 2008 (29), 1119-1125.

6. A.E. Daugaard, T.S. Hansen, N.B. Larsen, S. Hvilsted, Conductive Polymer Functionalization by Click Chemistry, Stipomat, Lacanau, France 2008.

7. A. Khan, A.E. Daugaard, A. Bayles, S. Koga, Y. Miki, K. Sato, J. Enda, S. Hvilsted, G.D. Stucky, C.J. Hawker, Dendronized Macromonomers for Holographic Data Storage, Chemical Communications 2008 (accepted).

Leila Faramarzi

Phone:	+45 4525 2996
Fax:	+45 4525 2258
E-mail:	lef@kt.dtu.dk
WWW:	http://www.ivc-sep.kt.dtu.dk
Supervisors:	Georgios M. Kontogeorgis
	Kaj Thomsen
	Erling H. Stenby

PhD Study
Started:	March 2007
To be completed:	March 2010

Post-Combustion Capture of CO₂ from Fossil Fuel Based Power Plants

Abstract

The extended UNIQUAC model as proposed by Thomsen and Rasmussen [1] was applied to the thermodynamic representation of carbon dioxide absorption in aqueous monoethanolamine (MEA), methyldiethanolamine (MDEA) and varied strength mixtures of the two alkanolamines (MEA-MDEA).

All the essential parameters of the model are simultaneously regressed to a collective set of data on the single MEA and MDEA systems as well as the mixtures of them.

Different types of data are used for modeling and they cover a very wide range of conditions. Vapor-liquid equilibrium (VLE) data for the aqueous alkanolamine systems containing CO₂ in the pressure range of 3-13000 kPa and temperatures of 25-200ºC are used. The model is also regressed with the VLE and freezing point depression data of the binary aqueous alkanolamine systems (MEA-water and MDEA-water). The experimental freezing point depression data down to the temperature of -20ºC are used. Experimental excess enthalpy (H^E) data of the MEA-water and MDEA-water systems at 25, 40, 65 and 69ºC are used as well. In order to enhance the calculation of the infinite dilution activity coefficients of MEA and MDEA, the pure alkanolamines vapor pressure data in a relevant temperature range are included in the parameter estimation process.

The previously unavailable standard state properties of the alkanolamine ions appearing in this work i.e. MEA protonate, MEA carbamate and MDEA protonate are determined.

Using only one set of parameters for correlation of different thermodynamic properties, the model has represented the experimental data with good precision.

Introduction

The reversible process of chemical absorption into aqueous alkanolamine solutions is an established method for separation of acid gases from gaseous streams. This process is considered as a potential perspective for post-combustion capture of CO₂ from fossil fuel based power plants. Accurate thermodynamic modeling of carbon dioxide solubility in alkanolamine solutions is of vital importance for the design of the absorption units. Precision of the thermodynamic properties can pledge that the driving forces for mass transfer can be well defined.

The purpose of the already finished part of the PhD was to apply the extended UNIQUAC model to estimate the essential thermodynamic properties of the alkanolamine systems required for the design of CO₂ capture plants. Moreover, it is tried to demonstrate the capability of the model to precisely represent different types of thermodynamic properties in a quite broad range of conditions using only one unique set of parameters.
.

Chemical and Physical Equilibria

1. Speciation equilibria

CO₂ reacts with alkanolamines in aqueous solutions. The assumed chemical equilibrium reactions in this work are

Aqueous CO₂ system:

$$H_2O(l) \leftrightarrow H^+ + OH^- \tag{1}$$

$$CO_2(aq) + H_2O(l) \leftrightarrow H^+ + HCO_3^- \tag{2}$$

$$HCO_3^- \leftrightarrow H^+ + CO_3^{2-} \tag{3}$$

MEA system:

$$RNHCOO^- + H_2O(l) \leftrightarrow HCO_3^- + RNH_2(aq) \tag{4}$$

$$RNH_3^+ \leftrightarrow H^+ + RNH_2(aq) \tag{5}$$
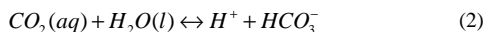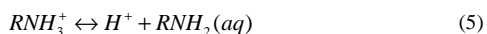
(R: -CH₂CH₂OH)

MDEA system:

$$MDEAH^+ \leftrightarrow H^+ + MDEA(aq) \tag{6}$$

The speciation equilibria can be expressed as

$$-\frac{\Delta G_j^0}{RT} = \sum_i \nu_{i,j} \ln a_i \tag{7}$$

ΔG^0 is the variation in the standard state chemical potential caused by the reaction j at the certain temperature $T(K)$. a_i is the activity of component i and $\nu_{i,j}$ is the stochiometry of component i involved in reaction j.

2. Phase equilibria

For the volatile compounds, the vapor-liquid equilibria can be written as

$$CO_2(g) \leftrightarrow CO_2(aq) \tag{8}$$
$$MEA(g) \leftrightarrow MEA(aq) \tag{9}$$
$$MDEA(g) \leftrightarrow MDEA(aq) \tag{10}$$
$$H_2O(g) \leftrightarrow H_2O(l) \tag{11}$$
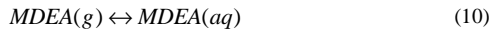
Each of the equilibrium equations 8-11 can be expressed as

$$-\frac{\Delta G^0}{RT} = \ln \frac{y_i \varphi_i P}{x_i \gamma_i P_0} \tag{12}$$

where ΔG^0 is the chemical potential change due to the transfer of one mole of component i from the liquid to the vapor phase. γ_i is the activity coefficient of the component i based on the symmetrical approach for water and asymmetrical for the solute species including alkanolamine. P_0 is the standard state pressure of one bar. y_i and φ_i are the vapor phase mole fraction and the fugacity coefficient of i and P is the total pressure. Equations (1)-(6) should be written in the form of equation (7) and equations (8)-(11) should be expressed in the form of equation (12). In order to calculate the equilibrium composition of the system, equations (1)-(6) and (8)-(11) have to be solved simultaneously.

The bubble point pressure of an electrolyte solution can be found by simultaneously solving equations in the form of equation (12) for all the volatile species.

In this work, the extended UNIQUAC model is also used for the correlation of the pure alkanolamine vapor pressure.

The experimental freezing point depression data available are within the temperature range where the only solid phase formed is ice. Therefore, the condition of solid-liquid equilibria reduces to

$$-\frac{\Delta G^0}{RT} = \sum_i \ln a_w \tag{13}$$

where a_w is the activity coefficient of water and ΔG^0 is the change in chemical potential of liquid water by shifting to ice.

Model

The extended UNIQUAC model as presented by Thomsen and Rasmussen [1] is used for the thermodynamic calculations of this work.

The only parameters of the model are the volume and surface area parameters of the UNIQUAC equation entropic term and the interaction parameters of the UNIQUAC enthalpic term.

The adjustable interaction parameters of the UNIQUAC enthalpic term (u_{ji}) are assumed to be temperature dependent and are fitted to the following function of temperature:

$$u_{ji} = u_{ji}^0 + u_{ji}^T(T - 298.15) \tag{14}$$

The required standard state properties for most of the species present in the solutions studied in this work are obtained from NIST tables [2]. The standard state chemical potentials from NIST tables are mainly reported for 25ºC. At temperatures other than 25°C, they are calculated using the Gibbs-Helmholtz equation and the enthalpy and heat capacity data from NIST tables. For those species that the standard state properties couldn't be found in the standard tables or elsewhere in the open literature, they are determined by adjusting them to experimental data.

The Gibbs-Helmholtz equation is used for calculation of the excess enthalpy of alkanolamine-water solutions. The equation defines the temperature dependence of the excess Gibbs energy and therefore also of the activity coefficients.

To estimate the model parameters, a least square minimization is performed. In this work, the volume and surface area parameters, r and q respectively, for MEA, MEAH$^+$, MEA carbamate, MDEA and MDEAH$^+$ are determined by fitting to experimental data.

The binary interaction parameters that are chosen to be adjusted are regressed to all types of experimental data in order to get a well-rounded model.

Results and Discussion

The results for the correlation of the total pressure of the CO_2-MEA-water system at 40ºC are shown in Fig. 1. It was of paramount importance to include the data of this specific temperature in modeling as, this is the usual operational temperature of the absorber column.

From the available pure MEA vapor pressure data only the points with relevant temperatures were chosen for the regression process and the very high temperature data were simply excluded.

The inclusion of pure MEA data in the regression process led to a notable improvement in the results for the correlation of the total pressure and excess enthalpy of the binary system of MEA-water. Fig. 2 shows the enhanced results for the excess enthalpy of aqueous MEA-water solution.

Freezing point depression data are also very accurately represented by extended UNIQUAC. The results are presented in Fig. 3.

For the MDEA concentration of almost 4 molal and for temperatures in the wide range of 40-140ºC, the model

results are compared to experimental data in Fig. 4. As the temperature of the solution increases, it is expected that the total pressure of the system should increase too. From Fig. 4 it can be observed that both the model and the experimental data behave according to this simple fact.

- ◆ Lee et al. [3] (MEA=1.04 molal)
- ▲ Austgen et al. [4](MEA=2.95 molal)
- △ Lawson and Garst [5] (MEA=2.95 molal)
- ✕ Lee et al. [3] (MEA=2.95 molal)
- ■ Lee et al. [3] (MEA=4.94 molal)
- ✕ Lee et al. [3] (MEA=7.35 molal)
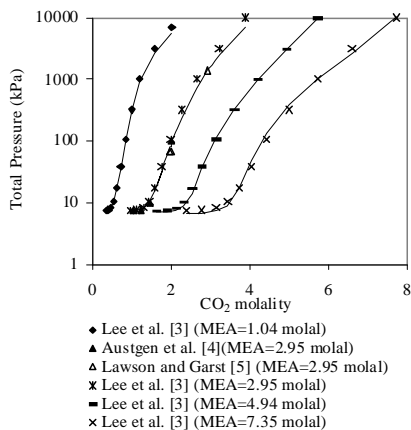
Figure 1: Comparison of the model results (lines) and experimental data for the total pressure of CO_2-MEA-water system at 40ºC.

- ◇ Dohnal et al. [6] (at 25ºC and very low conc. of MEA)
- ■ Touhara et al. [7] (at 25ºC)
- ✕ Posey [8] (at 69.3-69.7ºC)
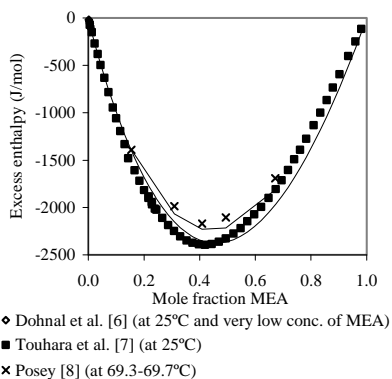
Figure 2: comparison of the model results (lines) and experimental data for the excess enthalpy of the binary MEA-water solution.

No parameters for the MEA-MDEA system are determined. The preliminary results of adjusting the parameters of the blend system showed that they make insignificant contribution to the performance of the model. Fig. 5 presents the total pressure of the quaternary system at 40ºC. Considering that the calculations for the MEA-MDEA system are pure predictions, the results are quite satisfactory.
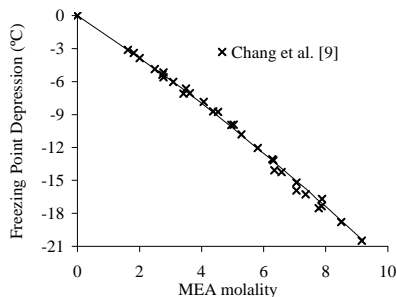
Figure 3: Comparison of the calculated (line) and experimental freezing point depressions (MEA+water).

- ■ Ermatchkov et al. [10] (MDEA=3.94-4.03m & 40ºC)
- ━ Kamps et al. [11] (MDEA=3.95 & 40ºC)
- ◆ Kuranov et al. [12] (MDEA=3.97m & 60ºC)
- △ Kuranov et al. [12] (MDEA=3.95-4.17m & 80ºC)
- ✕ Kuranov et al. [12] (MDEA=3.97m & 100ºC)
- ＋ Ermatchkov et al. [10] (MDEA=3.95-4.04m & 120ºC)
- ◇ Kuranov et al. [12] (MDEA=3.97 & 120ºC)
- ☐ Kuranov et al. [12] (MDEA=3.97 & 140ºC)
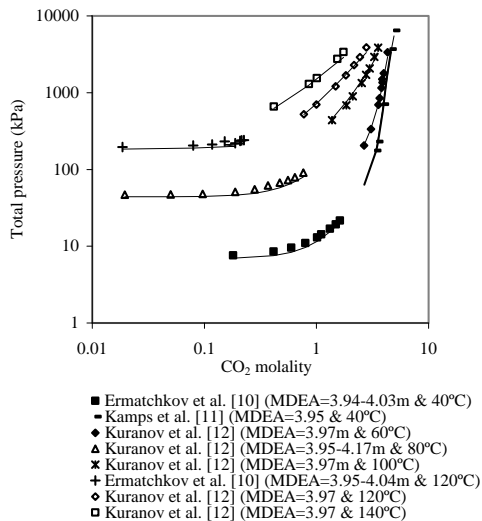
Figure 4: Total pressure of the CO_2-MDEA-water system calculated by the model (lines) and experimental data at approximately 4m MDEA solution.

- ◆ Austgen et al. [4] (MEA=12.2wt%, MDEA=23.8wt%)
- ▲ Shen and Li [13] (MEA=12wt%, MDEA=18wt%)
- ✕ Shen and Li [13] (MEA=24wt%, MDEA=6wt%)
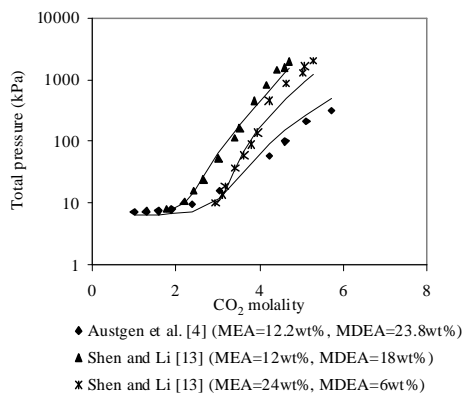
Figure 5: Total pressure of the CO_2-MEA-MDEA-water system calculated by the model (lines) together with the experimental data at 40ºC.

Conclusions

In this work, the extended UNIQUAC model is successfully used for the thermodynamic representation of the aqueous MEA, aqueous MDEA, CO_2-MEA-water, CO_2-MDEA-water and quaternary CO_2-MEA-MDEA-water systems.

The model parameters are volume and surface area parameters of the UNIQUAC entropic term and the interaction parameters of the UNIQUAC enthalpic term. The standard state Gibbs free energy of formation and enthalpy of formation for the alkanolamines and their formed ions in the solution are also determined by adjusting to all the experimental data used in this work.

Compared to other modeling approaches in the literature, a quite extensive range of pressure, temperature and CO_2 concentration in the aqueous phase is addressed. Yet, the model's performance is quite satisfactory for the calculation of VLE of MEA, MDEA and MEA+MDEA systems.

Freezing point depression for the aqueous alkanolamine systems is also calculated very precisely by the model.

The model correlates the excess enthalpy of MEA-water and MDEA-water systems reasonably well considering the scatter of experimental data.

Overall, it has been shown that extended UNIQUAC model can accurately represent various properties (H^E, VLE, SLE) over a wide range of conditions, thus being a valuable thermodynamic model for the design of the CO_2 absorption plants.

References:

1. K. Thomsen, P. Rasmussen, Chem. Eng. Sci. 54 (1999) 1787-1802.
2. NIST Chemical Thermodynamics Database Version 1.1, U.S. Department of Commerce, National Institute of Standards and Technology, Gaithesburg, MD 20899, 1990.
3. J.I. Lee, F.D. Otto, A.E. Mather, J. Appl. Chem. Biotechnol. 26 (1976) 541-549.
4. D.M. Austgen, G.T. Rochelle, C-C Chen, Ind. Eng. Chem. Res. 30 (1991) 543-555.
5. J.D. Lawson, AW. Garst, J. Chem. Eng. Data 21 (1976) 20-30.
6. V. Dohnal, A.H. Roux, V. Hynek, J. Solution Chem. 23 (1994) 889-900.
7. H. Touhara, S. Okazaki, F. Okino, H. Tanaka, K. Ikari, K. Nakanishi, J. Chem. Thermodyn. 14 (1982) 145-156.
8. M.L. Posey, Ph.D. Thesis, The University of Texas at Austin, 1996.
9. H.T. Chang, M.L. Posey, G.T. Rochelle, Ind. Eng. Chem. Res. 32 (1993) 2324-2335.
10. V. Ermatchkov, A.P-S Kamps, G. Maurer, Ind. Eng. Chem. Res. 45 (2006) 6081-6091.
11. A.P-S Kamps, A. Balaban, M. Joedecke, G. Kuranov, N.A. Smirnova, G. Maurer, Ind. Eng. Chem. Res. 40 (2001) 696-706.
12. G. Kuranov, B. Rumpf, N.A. Smirnova, G. Maurer, Ind. Eng. Chem. Res. 35 (1996) 1959-1966.
13. K-P Shen, M-H Li, J. Chem. Eng. Data 37 (1992) 96-100.

José M. S. Fonseca

Phone:	+45 4525 2858
Fax:	+45 4588 2258
E-mail:	jfo@kt.dtu.dk
WWW :	http://www.ivc-sep.kt.dtu.dk
Supervisor:	Nicolas von Solms

PhD Study
Started: January 2007
To be completed: January 2010

Multiphase Equilibrium in Natural Gas / Hydrate Inhibitor Systems

Abstract

A considerable amount of money is currently spent in the so-called "production chemicals", used in order to increase or facilitate production from a reservoir and in pipelines. Examples of such chemicals are methanol and glycols, used as inhibitors to prevent the formation of gas hydrates. As the oil price raises, the use of new, more expensive and exotic chemicals become viable, further complicating the prediction of phase equilibria and increasing environmental concern. A better knowledge of the phase equilibria in these systems will allow the reduction of the amounts used to the strictly necessary, with the inherent economical and environmental advantages. Therefore, we are working on the improvement of our experimental techniques with the designing of a new vapor-liquid-liquid-equilibria (VLLE) set-up, which will allow the collection of more accurate and reliable data in a wider range of conditions.

Introduction

Gas hydrates are crystalline compounds formed by inclusion of low molecular weight compounds in lattice structures formed by water on hydrogen bonds. Small molecules from light gases like nitrogen, carbon dioxide, hydrogen sulphide, methane, ethane, propane, n-butane or i-butane stabilize the lattice structure with the formation of stable solids at temperatures above the freezing point of water. Additionally, hydrates form more readily from real natural gas mixtures than from the pure constituent components of natural gas, representing a frequent problem for the gas industry, especially at the high pressures and low temperatures typical in North Sea gas reserves.

Blocking of lines due to the formation of hydrates presents serious issues in what safety is concerning and it has disastrous economic consequences.

Because of this, hydrate inhibitors such as ethylene glycol (MEG) or methanol are injected to the natural gas well stream, in order to prevent the formation of hydrates during transportation and further processing. In the case of offshore production, these inhibitors are transported through pipelines to the well. When a mixture of gas, water, MEG and condensate arrives onshore, all the components are distributed through all the phases, and it is essential to evaluate the amount of glycol lost in the gas phase, for environmental and for economical reasons. Also for environmental reasons it is necessary to determine the solubility of aromatics in the glycol rich phase, due to possible emissions during the regeneration process of the glycol.

However the amount of inhibitor needed is not well known and in order to avoid accidents, an excess of inhibitors is regularly used in the processes, with the inherent economical and environmental consequences.

A better knowledge of the phase equilibrium in these systems can allow the reduction of the amounts used to the strictly necessary.

This project will focus on the study of the phase equilibria in these systems, through the improvement of our experimental techniques, with the designing of a new vapor-liquid-liquid-equilibria experimental set-up which will allow the collection of more accurate and reliable data in a range of temperatures and pressures that can allow for example the replication of the polar conditions under which some pipelines are operated.

The methods for phase analysis will include the use of gas chromatography (GC), gas chromatography associated with mass spectroscopy (GC-MS), Karl Fisher and the use of adsorption columns (ATD).

This experimental part will allow establishing the basis for the posterior modeling of these systems with equations of state.

Experimental

In order to fulfill our goals, an existing experimental set-up was improved, in order to overcome several of the existing limitations and adapting this set-up to a new range of temperatures.

A new experimental set-up will allow measurements at high pressures (up to 40 MPa) and low temperatures (down to -60ºC or 213 K). The experimental conditions will be controlled and monitored with the high accuracy necessary to the production of high quality results. Finally, our goal is to achieve a full characterization of all the phases, including the quantification of traces of water and inhibitors in the gas phase.

The fundamental part of the experimental set-up is the equilibrium cell, depicted in Figure 1.
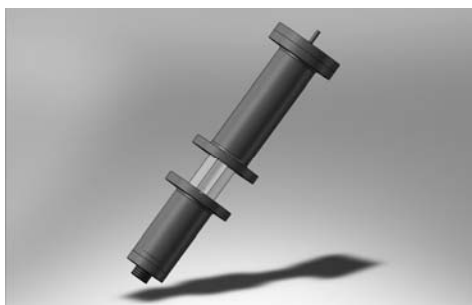
Figure 1: Three-dimensional computer generated image of the new equilibrium cell.

It is a variable volume cell specially designed for this project, equipped with two moving pistons and a 360º sapphire window. The position of the piston in the lower part of the cell can be set manually before a series of experiments, and it allocates in its interior a magnetic stirrer, while the position of the piston in the upper part is computer controlled, compensating for the pressure drop usually associated with the gas sampling.

Figure 2 shows a cut of the cell where is possible to observe the positioning of the pistons inside.

Figure 2: Cut of the new equilibrium cell, where it is possible to see the pistons inside.

The 360º window allows a good visibility of what is happening inside the cell at any moment, also permitting for example the study of phase interfaces, through optical or other kinds of measurements. The metal parts of this cell have already been built in the workshop of the department.

The cell will be placed inside a temperature controlled chamber, capable of keeping the whole system at a stable temperature down to -60ºC (213 K). This chamber is being specifically developed in a close collaboration with a company specialist in this area.

Another big progress in this new set-up is the online sampling of all the phases, directly for the GC carrier gas stream. This is possible by the use of the ROLSI[TM] system (Rapid On Line Sampler Injector), represented schematically in Figure 3.
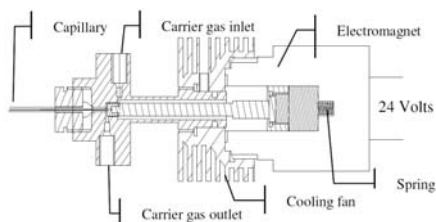
Figure 2: Schematic representation of a ROLSI[TM] electro-pneumatic sampler.

This system consists of electro-pneumatic valves, controlled by computer, with the ability of sampling very small amounts of liquid or gas, making possible to sample directly for the GC carrier gas without the need for dilutions.

Finally, the analysis of the samples will include different methods and techniques, in order to obtain precise results. The assessment of the composition of some of the phases will be possible by more than one method in order to test the respective accuracies.

Other necessary parts for this set-up are also currently being designed and built.

Wenjing Fu

Phone:	+45 4525 2947
Fax:	+45 4525 2906
E-mail:	wfu@kt.dtu.dk
WWW:	http://www.bioeng.kt.dtu.dk
Supervisors:	John M Woodley
	Anders Riisager (DTU Chemistry)

PhD Study
Started:	March 2008
To be completed:	February 2011

Process Design of Chemo-Enzymatic Synthetic Cascades

Abstract

Limited fossil resources and the unstable oil price make it increasingly important to create new chemical processes based on renewable resources. For many of these new processes a combination of enzymatic as well as heterogeneous and homogeneous catalysis will be required to direct the reaction toward the desired products. Hence there is a need to create a suitable process model to manage a range of technologies and products in the optimal way starting from renewable resources, such as glucose. In particular this project will focus on the design of chemo-enzymatic synthetic cascades from glucose.

Introduction

Enzymatic synthesis is now becoming an accepted means of achieving selective catalysis for many classes of reaction where conventional approaches are very difficult. However in industrial biocatalysis the reaction operates far away from natural conditions and therefore inevitably some changes to catalyst and process are required. This project focuses on the latter issue and in particular the selection, operation and design of a suitable scaleable process. The focus of design here is on chemo-enzymatic processes and their integration.

The project examines the use of renewable resources as new, versatile feedstocks for the chemical industry. As an example, the project targets the production of a new building block for the polymer industry, 2,5-furandicarboxylic acid (FDA), from glucose via the intermediate 5-hydroxymethyl furfural (HMF) and employs a combination of chemical and enzymatic catalysis as well as novel reactor design. The new polymer building block has applications and properties similar to terephthalic acid (PTA) which is derived from fossil resources and is the main building block for polyester (PET) resins and fibers. The annual growth of the PTA market is approximately 10%. By 2006, global purified terephthalic acid (PTA) demand had exceeded 30 million tones per annum.

HMF is an important intermediate product, which can be oxidized to FDA. In aqueous media, HMF may also be hydrolyzed to levulinic acid and formic acid. Both FDA and levulinic acid are listed in the top 12 value-added chemicals for building blocks for industry[1]. HMF can be obtained by dehydration of hexoses. The dehydration of fructose to HMF is reported to have good conversion and selectivity[2]. Although in principle, glucose can also be converted HMF directly, due to the low selectivity and long reaction time, dehydration of glucose is much harder than that of fructose. However, by using the enzyme glucose isomerase, glucose can be easily converted to fructose

The process starts with glucose since this can be readily obtained from starch and involves isomerization, dehydration and oxidation to synthesize FDA. Figure 1 shows the pathway of the process to produce FDA from glucose. The reaction conditions for the three main reactions are listed in Table 1. There are many alternative technologies in the route from glucose to FDA. Some give a limited yield and selectivity, some have problems for integration and some give difficulties for scale-up. The challenge is to develop a modeling framework to evaluate all the alternatives in an effective way.

The initial flowsheet (base case) is based on the three individual reactions, without recycle of integration. Initial work is focusing on collecting suitable data to characterize the reactions and obtain suitable property data. For many reactions of this type such data is scarce.
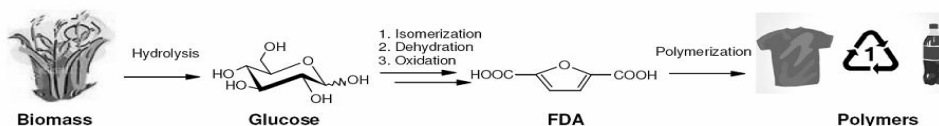
Figure 1: Main pathway of synthesis FDA from glucose.

Table 1: Typical reaction conditions for three main reactions involved in synthesis FDA.

Reaction	Temperature (°C)	pH	Catalyst
Isomerization	50 – 60	7 – 8	Glucose isomerase
dehydration	80- 200	acidic	Heterogenous, Homogeneous
oxidation	room	basic	Noble metal

Specific objectives
The objective of this project is to addresses the necessary definition and design of an optimal process to produce FDA from glucose within specification and economic constraints as an example of the process design for chemo-enzymatic syntheses. The identification of a suitable reactor and product recovery scheme will form the basis of a pilot-plant process for the production of HMF and later FDA. Likewise the process will form the basis of process / cost models for sensitivity analysis and to set targets for catalyst and process improvement.

Different flowsheets according to different process alternatives will be identified. Based on the flowsheets, mathematical models will be established to describe the alternative process configurations for FDA synthesis from glucose. Sensitivity to cost and scale-up issues will also be addressed.

Methodology
The methodology of this study is shown in Figure 2.

1) Modeling base flow sheet
Once the base case flowsheet is generated, collection of property data of all the chemicals involved in the base case will be required in order to set up the model in ProII. Software will be used to predict the property data which are not available in literature.

2) Sensitivity and bottleneck identification
Mass and energy balance models are used to evaluate the bottlenecks in the base-case process. Costing and modelling software will therefore be used to identify the parts of the base flowsheet which need improvement.

3) Identification of process alternatives
Other alternative process flowsheets based on the base case modelling results will be developed. These process alternatives may also include process integration.

Models based on alternative flowsheets will then be created to allow evaluation.

4) Cost analysis of different flowsheets
Cost analysis will be used to compare different process alternatives and identify the most likely process.
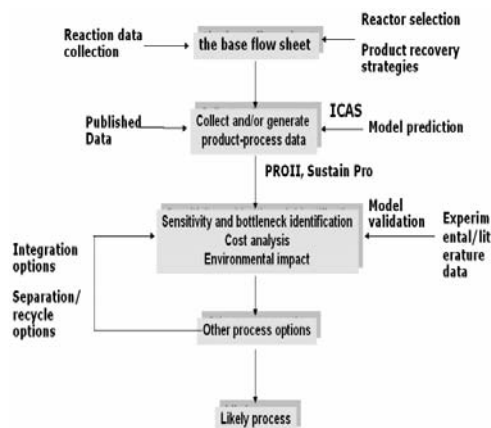
Figure 2: Plot of methodology of the study.

References
1. T. Werpy, and G. Petersen. Top Value Added Chemicals from Biomass: Volume 1 - Results of Screening for Potential Candidates from Sugars and Synthesis Gas. 2004 [cited; Report No. NREL/TP-510-35523]. Available from: Available electronically at http://www.osti.gov/bridge.
2. C. Moreau, , M. N. Belgacem, ,A. Gandini, , 2004, Recent catalytic advances in the chemistry of substituted furans from carbohydrates and in the ensuing polymers, Topics in Catalysis, 27(1–4): 11-30.

Fengxiao Guo

Phone: +45 4525 6821
Fax: +45 4525 2161
E-mail: feg@kt.dtu.dk
WWW: http://www.dtu.dk/Centre/DPC
Supervisors: Martin E. Vigild
Sokol Ndoni (DTU Nanotech)
Katja Jankova

PhD Study
Started: November 2006
To be completed: November 2009

Hydrophilic Nanoporous 1,2-polybutadiene via Surface-Initiated Atom Transfer Radical Polymerization

Abstract

Hydrophilic nanoporous polymers were obtained via surface-initiated atom transfer radical polymerization (ATRP) of different acrylates onto the pore surface of nanoporous 1,2-polybutadiene precursors. The precursor material was prepared from diblock copolymer melts by first cross-linking the major block of 1,2-polybutadiene (1,2-PB) and then etching the minor block of polydimethysiloxane (PDMS) from a 1,2-PB-*b*-PDMS copolymer of gyroid morphology. The ATRP bromoester initiator was immobilized onto the pore walls through two different methodologies. Following ATRP-grafting of polyacrylates the originally hydrophobic samples transformed to hydrophilic nanoporous materials.

Introduction

The self-organization of block copolymers has attracted considerable attention in relation to "bottom up" nanotechnology because it enables various highly ordered structures at nanometer length scale. Specific removal of a minority component from an ordered block copolymer allows for the preparation of nanoporous materials. Potential applications of nanoporous polymeric materials include nanoobject templates, separation membranes, sensors, and substrates for catalysis [1]. A variety of applications would require the nanoporous polymers to work in an aqueous environment. Only a limited number of nanoporous polymers with hydrophilic pores have been reported to date [2-4].

Recently we have created hydrophilic nanoporous poly(acrylic acid)-*b*-polystyrene by using the combination of living anionic polymerization and ATRP. Two different morphologies, lamellae and cylinders have been achieved [4]. We also demonstrated the preparation of nanoporous cross-linked 1,2-polybutadiene (1,2-PB) from 1,2-polybutadiene-*b*-polydime-thylsiloxane (1,2-PB-*b*-PDMS) diblock copolymer precursors [5]. Gyroid morphology can be formed with specific composition of 1,2-PB and PDMS blocks and cross-linking temperature, Here we describe two approaches, both leading to grafting of polyacrylates onto the pore walls of 1,2-PB with gyroid morphology. As a result hydrophilic nanoporous polymers of predetermined morphology were obtained.

Experimental Work

Two different kinds of ATRP bromoester initiator were produced and assigned as initiator A and initiator B.

Initiator A: Epoxidation of the double bonds of in the1,2-PB precursor was firstly attempted: Nanoporous 1,2-PB films, meta-chloroperoxybenzoic acid (*m*CPBA) and dry toluene were charged into a round flask with stirring. The solution was stirred for 6 hours at room temperature. The epoxidized films (1,2-PB-ep) were washed with toluene and THF and vacuum-dried. The hydroxylation of 1,2-PB-ep films was then performed according to ref. 6. Once 1,2-PB films with OH groups (1,2-PB-OH) are formed, bromoisobutyrate initiator was attached to 1,2-PB films by the same method as described previously [4]. The synthesis of initiator A is outlined in Scheme 1.
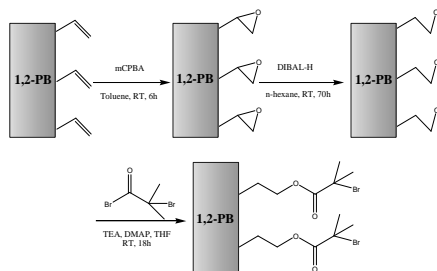
Scheme 1: Synthesis of initiator A through 3-step wet chemistry.

Initiator B: Benzophenonyl bromoisobutyrate (BPBriBu) was synthesized according to literature [7]. The nanoporous 1,2-PB precursors were submerged into BPBriBu 170 mg/ml toluene solution for 4 hours. The films were then placed into transparent glasses filled with nitrogen. After irradiation under UV of wavelength 365 nm at 32°C for 1 hour, the films were washed with toluene and THF. The synthesis of initiator B is outlined in Scheme 2.
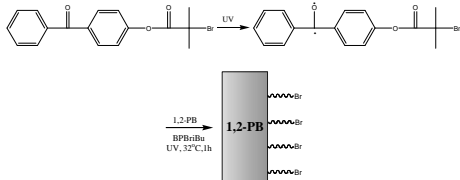
Scheme 2: Synthesis of initiator B through photo-chemistry.

After immobilization of the initiator onto the surface of nanoporous 1,2-PB film, the thus modified 1,2-PB film, CuBr, 2,2'-bipyridyl (bpy), poly(ethylene glycol) methacrylate (PEGMA) with M_n of 360 g/mol and methanol were added into a Schlenk flask. Oxygen was removed by three freeze-pump-thaw cycles. The reactions were carried out at room temperature under nitrogen. The polymerization was stopped after desired time and the films were rinsed with methanol and THF. Scheme 3 shows the route leading to grafting PPEGMA onto nanoporous 1,2-PB. Similar procedures were followed for the ATRP of 2-hydroxyethyl methacrylate (HEMA)
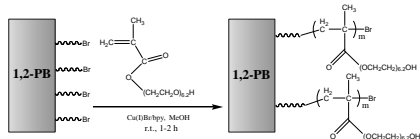
Scheme 3: ATRP of PEGMA

Results and Discussions

Surface-Initiated Polymerization by Initiator A: The three-step chemical immobilization of initiator A was confirmed by FT-IR after each step. Figure 1 shows FT-IR spectra of the original 1,2-PB, the epoxidized sample 1,2-PB-ep, the hydroxyl group containing sample 1,2-PB-OH and finally the initiator immobilized film 1,2-PB-Br.
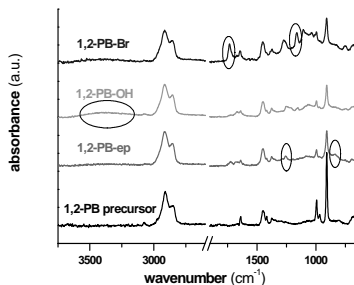
Figure 1: FT-IR spectra of 1,2-PB precursor, 1,2-PB-ep, 1,2-PB-OH and 1,2-PB-Br.

The characteristic absorption peaks related to epoxy groups at 1250 and 800 cm^{-1} appear and intensity of the peak for double bonds at 908 cm^{-1} is reduced after the epoxidation. The appearance of a broad signal at 3400-3200 cm^{-1} indicates the formation of hydroxyl groups in the film after hydroxylation. Finally, the peaks corresponding to ester groups at 1730 (C=O) and 1230 cm^{-1} (ester C-O) confirm the immobilization of the bromoisobutyrate initiator onto the 1,2-PB film.

The obtained monolith initiator 1,2-PB-Br was used to polymerize HEMA and PEGMA by ATRP. The use of methanol as solvent in ATRP is advantageous, as methanol exclusively penetrates the porous volume of nanoporous 1,2-PB [5]. As a result most of the grafted polymer chains are expected onto the pore-wall surface, but attachment onto the film surface was also registered (see data in contact angle measurement). FT-IR spectroscopy confirms the presence of PHEMA and PPEGMA in the nanoporous 1,2-PB as shown in Figure 2. Compared to the spectrum of the 1,2-PB precursor, additional characteristic peaks associated with ester groups and ethylene oxide units in the grafted polymers appear in the case of the modified film: at 1730 cm^{-1} (C=O), 1230 cm^{-1} (ester C-O) and 1110 cm^{-1} (C-O-C).
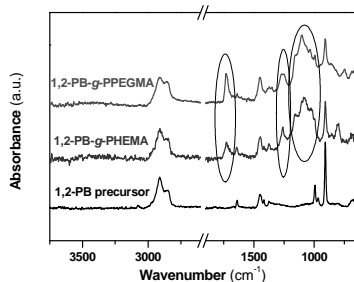
Figure 2: FT-IR spectra of 1,2-PB precursor, 1,2-PB-*g*-PHEMA and 1,2-PB-*g*-PPEGMA.

The three nanoporous samples: 1,2-PB precursor, 1,2-PB-*g*-PHEMA and 1,2-PB-*g*-PPEGMA were placed into glass vials containing distilled water. After soaking in water for 5 minutes, the two modified samples started

to sink down to the bottom of their respective vials. However, the 1,2-PB precursor floated on the surface of the water and was not able to take any water for 3 months. The spontaneous uptake of water was a direct proof of hydrophilicity for the nanoporous materials.

The hydrophilicity of the modified nanoporous 1,2-PB films was also substantiated by water contact angle measurements. Figure 3 compares the water contact angle of the original and the two functionalized nanoporous polymers. The initial water contact angle for 1,2-PB was around 119° and seems to remain constant after 2 min. Due to the evaporation of water the drop leaves a small water trace on the surface of 1,2-PB after 20 min. After modification the films became hydrophilic, which lead to an initial contact angle of about 76° for 1,2-PB-*g*-PHEMA and 60° for 1,2-PB-*g*-PPEGMA. The contact angles for the two functionalized samples decreased further to 59° and 26° after 2 min, and the water drops entirely disappeared from the surfaces after 10 min and 3 min 45 sec respectively, due to capillary suction into the nanoporous films. Because each repeating unit of PPEGMA contains more than 6 (6.2 in average) ethylene oxide units while for that of PHEMA there is only 1 ethylene oxide unit, that is why 1,2-PB-*g*-PPEGMA exhibited a stronger hydrophilicity as compared to 1,2-PB-*g*-PHEMA as shown in Figure 3.
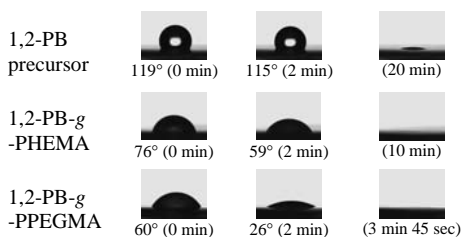
Figure 3: Water contact angle measurements for 1,2-PB precursor, 1,2-PB-*g*-PHEMA and 1,2-PB-*g*-PPEGMA.

The morphologies of the nanoporous 1,2-PB samples during the modification steps and the functionalized sample in water were investigated by small angle x-ray scattering (SAXS) and Figure 4 shows the resulting data for 1,2-PB-*g*-PPEGMA. The 1-D scattering curves are indexed to match the reflections of the gyroid morphology [8]. The positions of the scattering peak for the modified samples do not change; this proofs that the gyroid structure and lattice spacing of the sample were preserved during the modification. Nevertheless due to the additional layer of grafted PPEGMA, a so called core-shell gyroid morphology [9] associated with air-core, PPEGMA-shell onto the 1,2-PB-matrix is formed. That is why the peak at 0.63 nm^{-1} for the 1,2-PB-g-PPEGMA is significantly pronounced as compared to 1,2-PB precursor. When water penetrates the sample and fill up all the pores, electron density contrast between the pores and the polymers is reduced, which leads to weaker scattering. The study of detailed reasons for intensity of peaks at 0.63 and 0.52

nm^{-1} becoming more enhanced after soaking in water is still in process. So far we have confidence to say that it is caused by the change of form factor of core-shell structure when PPEGMA-shell is expanded by surrounding with water.
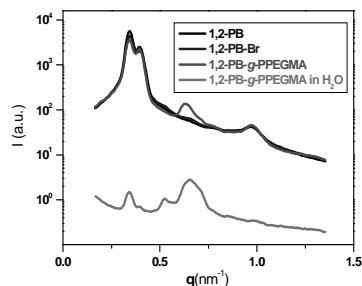
Figure 4: SAXS 1D profiles of 1,2-PB precursor, 1,2-PB-Br, 1,2-PB-*g*-PPEGMA and 1,2-PB-*g*-PPEGMA in H$_2$O.
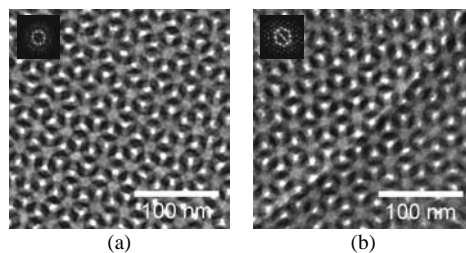
Figure 5: TEM images of (a) 1,2-PB precursor and (b) 1,2-PB-*g*-PPEGMA.

Transmission electron microscopy (TEM) was employed to elucidate the structure of the samples. Figure 5 shows images of nanoporous 1,2-PB precursor and 1,2-PB-*g*-PPEGMA. Both images were observed nearly along the [111] direction. The center to center distances in the "wagon wheel" pattern (36±2 nm for 1,2-PB precursor and 37±1 nm for 1,2-PB-*g*-PPEGMA) calculated by using the trigonometric relationships had good agreement with those obtained from SAXS analysis (twice the spacing of the {211} planes, 37 nm for both samples). As seen in the figure, the gyroid morphology was preserved after modification and array of pores for the functionalized sample has the same regular pattern as the precursor. Due to the complicity of gyroid structure and not the exact same projections, the pore sizes of sample before and after modification can not be determined directly by examining the TEM images.

Surface-Initiated Polymerization using initiator B: The successful creation of hydrophilic nanoporous polymer by applying this method was monitored by FT-IR and water uptake measurements. Detailed information on

the chemical composition changes for 1,2-PB before and after modification was acquired by the FT-IR spectra shown in Figure 6.
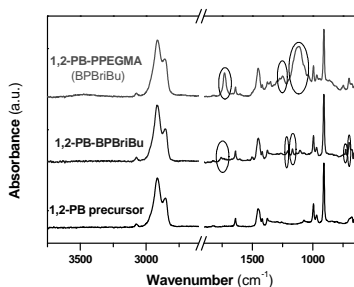
Figure 6: FT-IR spectra of 1,2-PB precursor, 1,2-PB-BPBriBu, and 1,2-PB-*g*-PPEGMA (BPBriBu).

New absorbance bands at 1758 cm^{-1} (aromatic ester C=O), at 1206 cm^{-1} (aromatic ester C-O), at 1170 cm^{-1} (tertiary alcohol), and at 740 and 700 cm^{-1} (benzene group) appear in the initiator immobilized sample. This proves that the BPBriBu initiator had been successfully grafted onto the film. The enhanced absorption peaks at 1730 cm^{-1} (C=O), 1230 cm^{-1} (ester C-O) and 1110 cm^{-1} (C-O-C) indicate the formation of PPEGMA-modified 1,2-PB.

After contact with distilled water for 5 minutes, the modified sample sank down to the bottom of the vials. This confirms that hydrophilic nanopores were created in the 1,2-PB sample by using photochemistry as well.

Conclusions

Hydrophilic nanoporous polymer samples were successfully prepared by surface-initiated atom transfer radical polymerization (ATRP) of various acrylates onto the pore surface of hydrophobic nanoporous 1,2-PB. Two different methods were applied to immobilize the ATRP bromoester initiator onto the pore walls: 1) three-step chemical conversion of double bonds of 1,2-PB into bromoisobutyrate, and 2) photochemical functionalization of cross-linked 1,2-PB with bromoisobutyrate groups. The water contact angle measurements show that the PPEGMA-modified sample 1,2-PB-*g*-PPEGMA has stronger hydrophilicity than the PHEMA-modified sample 1,2-PB-*g*-PHEMA.

References

1. M.A. Hillmyer, Adv. Polym. Sci. 190 (2005) 137.
2. G. Liu, J. Ding, S. Stewart, Angew. Chem. Int. Ed. 38 (1999) 835.
3. J. Rzayev, M.A. Hillmyer, Macromolecules 38 (2005) 3.
4. F. Guo, K. Jankova, L. Schulte, M.E. Vigild, S. Ndoni, Macromolecules 41 (2008) 1486.
5. F. Guo, J.W. Andreasen, M.E. Vigild, S. Ndoni, Macromolecules 40 (2007) 3669.
6. J. Marchand-Brynaert, N. Jongen, J.L. Dewez, J. Polym. Chem. 35 (1997) 1227.
7. J.Y. Huang, H. Murata, R.R. Koepsel, A.J. Russell, K. Matyjaszewski, Biomacromolecules 8 (2007) 1396.
8. S. Ndoni, M.E. Vigild, R.H. Berg, J. Am. Chem. Soc. 125 (2003) 13366
9. T.A. Shefelbine, M.E. Vigild, M.W. Matsen, D.A. Hajduk, M.A. Hillmyer, E.L. Cussler, F.S. Bates, J. Am. Chem. Soc. 121 (1999) 8457.

List of Publications

1. F. Guo, K. Jankova, M.E. Vigild, S. Ndoni, Polymer Peprint 49 (2008) 540.
2. F. Guo, K. Jankova, L. Schulte, M.E. Vigild, S. Ndoni, Macromolecules 41 (2008) 1486.
3. F. Guo, J.W. Andreasen, M.E. Vigild, S. Ndoni, Macromolecules 40 (2007) 3669.

Mohd. Kamaruddin bin Abd. Hamid

Phone:	+45 4525 2912
Fax:	+45 4593 2906
E-mail:	mka@kt.dtu.dk
WWW:	http://www.capec.kt.dtu.dk
Supervisors:	Rafiqul Gani
	Gürkan Sin

PhD Study

Started:	July 2007
To be completed:	June 2010

Integrated Process Design and Control of a Single Reactor System

Abstract

This paper presents a model-based methodology to solve an integrated process design and control (IPDC) problem of a single reactor. The IPDC problem is formulated as a mixed-integer dynamic optimization (MIDO) model in which the economic performance is optimized in order to design a cost effective and highly controllable process. The methodology is organized into four hierarchical stages based on decomposition of a MIDO model. By applying decomposition method, IPDC MIDO model is decomposed into four sub-problems, which are relatively easy to solve. The concept of attainable region (AR) and driving force (DF) technique are used within this methodology, to find the optimal design-control decision as an alternative to the use of optimization/search algorithms. Accordingly, the optimal solution to the design-control problem is to be found by locating the maximum value of AR and DF for reactor and separator units respectively. In this paper, we demonstrate successfully the potential use of the model-based methodology in solving IPDC problem of a single reactor for synthesis of ethylene glycol.

Introduction

Traditionally, chemical process design and process control are two separate engineering problems that are performed sequentially. The chemical process is designed first to achieve the design objectives, and then, the operability and control aspects are analyzed and resolved. This traditional-sequential approach has some limitations such as dynamic constraint violations, process overdesign or under performance, and does not guarantee robust performance (Seferlis and Georgiadis, 2004). Another drawback has to do with how process design decisions influence the control performance of the system. To assure that design decisions give the optimum economic and best control performance, the control aspects should be considered at the design step. By considering control aspects together with the economic issues in the process design stage, the integration of process design and control (IPDC) can be achieved.

A number of methodologies and tools have been proposed for addressing the interactions between process design and control. Sakizlis et al. (2004) presented an overview of the state of the art of optimization-based methods of IPDC. They classified optimization-based methods into two categories, multi-objective approach and dynamic optimization approach. In the former, the control cost and the design cost are accounted for by different objective functions requiring

the solution of complex optimization problems. Whereas, latter considers a single economic objective but the system operation is represented with dynamic models. Thus, this approach can be formulated as a mixed-integer dynamic optimization (MIDO) problem. However, their drawback is the MIDO problem will give rise to a highly nonlinear optimization formulation, in which case, requires an effective global search algorithm to find the optimal solution.

Alternatively, simpler approaches have been proposed, which are founded on the premise of using process knowledge about chemical system in question. This method is based on the use of model-based analysis for solving IPDC problems (Ramirez and Gani, 2007; Kiss et al., 2007). Russel et al. (2002) propose a systematic analysis of the model equations as pre-solution step for IPDC problems. By using model analysis the relationships between the design and control variables can be identified, which help to understand, define and address issues related to IPDC problems.

Therefore, a methodology of IPDC for chemical process, based on model analysis is proposed (Hamid and Gani, 2008). In this paper, the potential use of this methodology in solving IPDC problem of a single reactor for synthesis of ethylene glycol is presented.

Problem formulation

IPDC in this work is treated as a mixed-integer dynamic optimization (MIDO) problem, where the economic performance is optimized in order to design a cost effective and highly controllable process. A general formulation for IPDC problem can be presented below:

$$\min J(x,u,y) \tag{1}$$

s.t.

$$h_1(x,u,y) = dx/dt \tag{2}$$

$$h_2(x,u,y) = 0 \tag{3}$$

$$g(x,u,y) \leq 0 \tag{4}$$

$$x_L \leq x \leq x_U \tag{5}$$

$$u_L \leq u \leq u_U \tag{6}$$

$$y \in \{0,1\} \tag{7}$$

where x is the vector of design variables and u the vector of control variables. In the objective function, Eq. (1), J, represents the expected total annualized cost (TAC) of a system. The system dynamics is described by a set of differential equations given in Eq. (2). The steady-state system is described by a function given in Eq. (3). In Eq. (4), the possible inequality constraint is expressed. The bounds on design and control variables are represented in Eqs. (5)-(6), respectively. In Eq. (7), y comprises the binary variables for the process and the control structure (corresponding to whether a manipulated variable is paired with a particular controlled variables or not).

Once the MIDO model has been defined, the next step is solving this model by applying a decomposition-based approach, where the MIDO model is decomposed into a number of sub-problems.
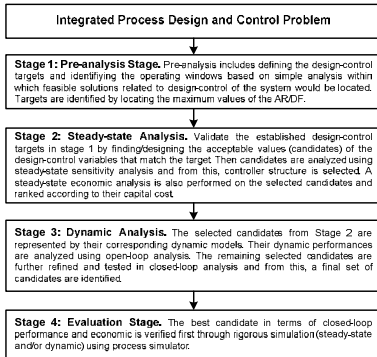
Figure 1: Decomposition method for IPDC problems. (Hamid and Gani, 2008).

Decomposition-based solution strategy

In IPDC problem, combinatorial in nature, can be solved in many ways. However finding a solution may become cumbersome especially when the constraints are nonlinear and/or the number of variables are large, which causes difficulties in convergence and high computational cost. Since typically a number of constraints is involved, the feasible region can be very

small compared to the search space. All of the feasible solutions to the problem may lie in that relatively small portion of the search space. The ability to solve such problems depends on the ability to identify and avoid the infeasible portion of the search space. Hence, one approach to solve this IPDC problem is possible by applying decomposition method, in which the problem is decomposed into sub-problems, which are relatively easy to solve.

Figure 1 shows a decomposition method for IPDC problem (Hamid and Gani, 2008). Accordingly the problem is decomposed into four sequential hierarchical stages: (1) pre-analysis, (2) steady-state analysis, (3) dynamic analysis, and (4) evaluation stage.
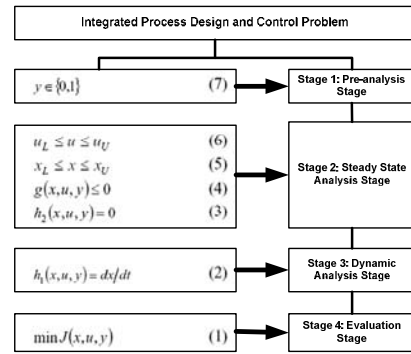
Figure 2: Solution methodology for IPDC: MIDO type IPDC problem (left) and its correspondence to the four sequential hierarchical stages of the decomposed IPDC problem (right).

Figure 2 shows how the general IPDC problem (MIDO) corresponds to the four hierarchical stages of the model-based methodology. It shows how the model-based methodology is equivalent to the general IPDC problem formulation in Eqs. (1)-(7). However with a single exception that the problem in decomposition methodology is rearranged in the reverse order compared to the general IPDC problem (Eq. 1 to 7). As each sub-problem is being solved, a large portion of the infeasible part of the search space is identified and hence eliminated, thereby leading to a final sub-problem that is significantly smaller MIDO or DO problem, which can be solved more easily.

In this contribution, we demonstrate the concept of AR (and DF) to find the optimal design decisions as an alternative to the use of search algorithms. Accordingly, the AR (and DF) are used in the first stage of the model-based methodology to select the optimal design and control structure. Since decision of design and control structure are representing by y (binary variable) in Eq. (7), the use of AR and DF techniques enumerate the decision (binary) variables is stage 1, in which assisting the optimal design decisions.

Attainable region and driving force techniques

Within this model-based methodology, concepts from AR and DF techniques are used, although differently than their original purpose, in order to assist in selection

of the optimal design. The AR concept is used for dimensioning reaction units, while DF concept is applied for separation units in chemical systems. For the reactor design problem, the idea is to locate the maximum value of AR for design feasibility, and from there the operating conditions in terms of residence time, temperature, volume, etc. are identified. The same idea is used to solve separator design problem using DF technique. DF is defined as a measure of the relative ease of separation (Gani and Bek-Pedersen, 2000). When DF is zero, no separation is possible. When DF is large, separation becomes easy. By employing this technique, one can determine values of design variables for separation systems at the largest value of DF.

For control problem, the value of the derivative of AR/DF with respect to manipulative variables will determine process sensitivity and flexibility as well as the controller structure selection. According to Russel et al. (2002), derivative of the constitutive variables (e.g. reaction rate or equilibrium constant) with respect to manipulative variables influences the process operation and controller structure selection. Basically, reaction rate and equilibrium constant are used to determine the value AR and DF, respectively. If values of the derivative are small, the process sensitivity is low and process flexibility is high. Therefore, by using AR/DF technique to solve the design and control problem, insights can be gained in terms of controllability and resiliency, and IPDC problems can be solved in an integrated manner. This is demonstrated below.

Application – Integrated process design and control of an ethylene glycol production process

The new model-based methodology is generic in character and applicable to chemical processes with reactor (R), separator (S) and/or reactor-separator-recycle (RSR) systems. A reaction (R) system has been selected to evaluate the capability of the methodology. For S and RSR systems, the procedure would be exactly the same. In this case study, the IPDC problem of a single reactor for ethylene glycol (EG) production is presented.

Case Study: Reaction (R) System

The objective is to determine the optimal design (with respect to controllability and economic) that gives the highest yield of the desired product at given feed flow rate and concentrations. The process reactions are given as:

$$EO + W \xrightarrow{r_1} EG \qquad (8)$$

$$EO + EG \xrightarrow{r_2} DEG \qquad (9)$$

$$EO + DEG \xrightarrow{r_3} TEG \qquad (10)$$
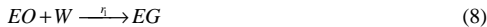
In Eq. (8), ethylene oxide (EO) and water (W) react to produce ethylene glycol (EG). Eqs. (9)-(10) are side reactions where the excess EO react with EG and DEG to produce diethylene glycol (DEG) and triethylene glycol (TEG), respectively. The reaction rates for the above reacting system are:

$$r_1 = k_1 C_{EO} C_W, \quad r_2 = k_2 C_{EO} C_{EG}, \quad r_3 = k_3 C_{EO} C_{DEG}$$

with kinetic parameters; $k_1 = 5.238\exp^{30.163-10583/T}$ [m^3/kmol h], $k_2 = 2.1k_1$ and $k_3 = 2.2k_1$ are taken from Parker and Prados (1964).

Stage 1: Pre-analysis Stage

In this stage, the design-control target and operational windows within which all feasible solutions related to design-control would be located are determined. The starting range for temperature is defined between the minimum melting point and maximum boiling point of components (161<T(K)<562). For a single reactor, design should satisfy the sizing and costing constraints (3<V(m^3)<30) as defined in Table 6.2 of Sinnot (2005). Therefore, the dimension of the design space is a plane with (161 x 562) by (3 x 30). The AR analysis was carried out and the design-control target is selected by locating the maximum value of the AR (point A) as shown in Figure 3(top). The optimum value of the attainable yield of EG of 0.16671 kmol/m^3 is obtained at C_W=0.59 kmol/m^3. Other concentrations are also identified.
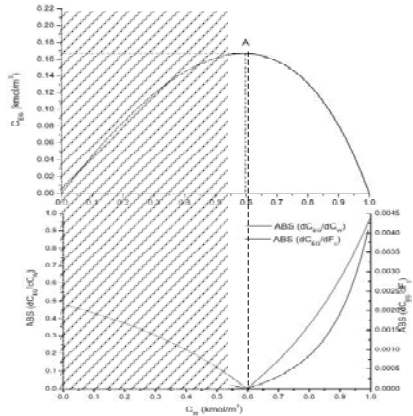
Figure 3: Top: AR diagram for concentration of EG and W; Bottom: Corresponding derivatives of the AR with respect to W and F$_c$. (The shaded area represents the infeasible region where the concentration of EO is exhausted, thereby, turning-off the operation).

Stage 2: Steady-State Analysis

In this stage, the search space defined in stage 1 is further reduced using steady state analysis. The established target (point A) is now validated by finding the feasible values (candidates) of the design-control variables (temperature, residence time, volume, etc.) that match the target. If feasible values cannot be obtained, a new target is selected and variables are recalculated until satisfactory matching is found. At point A, the allowable operating temperature is calculated using Eq. (11).

$$\sum_i x_i T_i^m < T(K) < \sum_i x_i T_i^b \qquad (11)$$

where, x_i is the mole fraction, and T_i^m and T_i^b are the melting and boiling point, respectively. The search space for temperature is now reduced to (251 x 406)

from (161 x 562). With this range, the range of the residence time (0.017< (h)<108,199) and the volume ($11.78 < V(m^3) < 1.082e^8$) are calculated using their corresponding steady state models. However, the upper limit of the volume is more than what defined in stage 1. Therefore, volume that is more than 30 m³ and its corresponding temperature are eliminated. For that reason, the search space for temperature is further reduced to (394 x 406). After stage 2, the dimension of the design space is now a plane with (394 x 406) by (11.78 x 26.89). Candidates of design-control variables for stage 2 together with their total annualized cost (TAC) are tabulated in Table 1.

Table 1: Candidates of design-control variables for stage 2.

Candi-dates	C_W (kmol/m³)	C_{EG} (kmol/m³)	T (K)	r (h)	V (m³)	F_c (m³/h)	TAC ($)
1	0.59	0.16671	406	0.0107	11.78	1388	53,300
2	0.59	0.16671	402	0.0143	15.76	1388	59,700
3	0.59	0.16671	398	0.0187	20.53	1388	67,000
4	0.59	0.16671	394	0.0244	26.89	1388	83,700

Next, sensitivity and flexibility as well as the controller structure selection of all candidates are analyzed by taking the derivative of the AR with respective to manipulative variable (MV) as shown in Eqs. (12)-(13). Results are shown in Figure 3(bottom).

$$\frac{dAR}{dMV} = \frac{dC_{EG}}{dC_W} = 0 \qquad (12)$$

$$\frac{dAR}{dMV} = \frac{dC_{EG}}{dF_c} = \left(\frac{dC_{EG}}{dC_W}\right)\left(\frac{dC_W}{dT}\right)\left(\frac{dT}{dF_c}\right) = 0 \qquad (13)$$

From Figure 3(bottom), values of dC_{EG}/dC_W and dC_{EG}/dF_c of all candidates are zero, since they are at the maximum value of AR (point A). According to Russel et al. (2002), at the minimum value of derivatives, the process sensitivity is low and process flexibility is high. Therefore, by designing a reactor at the maximum value of AR leads to process with higher flexibility and lower sensitivity. Since $dC_{EG}/dF_c = 0$, it also indicates that composition of *EG* can be controlled by manipulating F_c.

Stage 3: Dynamic Analysis
Here, the search space is further refined using dynamic analysis. Candidates from stage 2 are now represented by their corresponding dynamic models. Transfer function-based models are then developed for every candidates and from that, the controller tuning parameters are calculated. Closed loop dynamic responses for all candidates are shown in Figure 4. Candidate with the best closed loop performance and the lowest cost is verified through rigorous simulation using an appropriate simulator in the final stage. As shown in Figure 4, candidate 1 shows the best closed loop performance in terms of set point tracking and also has the lowest cost (Table 1). Therefore, candidate 1 is the optimal design that gives the best economic and control performances.
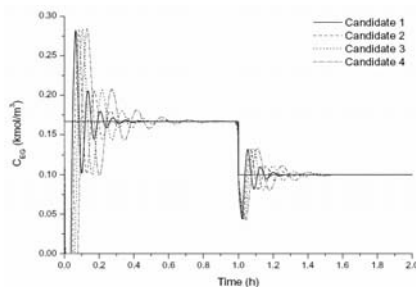
Figure 4: Closed loop dynamic analysis – response of C_{EG} to its set point change.

Conclusions and Future Work

In this contribution, the capability of a new model-based methodology has been successfully evaluated for the design of reaction system for the synthesis of ethylene glycol. The results demonstrates the potential use of the decomposition method in solving IPDC problems particularly its ability to reduce the huge dimension of the design space. The use of AR technique is shown to provide an optimal design with respect to design and control for reactor. As future perspective, this promising methodology will be further applied to solve IPDC problems for separation and reactor-separator-recycle systems.

Acknowledgement

References

Bahri, P. A., Bandoni, A., Romagnoli, J. (1996). Operability assessment in chemical plant. *Comput. Chem. Eng.,* 20, 787-792.

Gani, R., Bek-Pedersen, E. (2000). A simple new algorithm for distillation column design. *AIChE J.*, 46(6), 1271-1274.

Hamid, M. K. A., Gani, R. (2008). A model-based methodology for simultaneous process design and control for chemical processes. *In Proceedings of the FOCAPO 2008*, Massachusetts, USA, 205-208.

Kiss, A. A., Bildea, C. S., Dimian, A. C. (2007). Design and control of recycle system by non-linear analysis. *Comput. Chem. Eng., 31,* 601-611.

Ramirez, E., Gani, R. (2007). Methodology for the design and analysis of reaction-separation systems with recycle. 2. Design and control integration. *Ind. Eng. Chem. Res., 46,* 8084-8100.

Russel, B. M., Henriksen, J. P., Jørgensen, S. B., Gani, R. (2002). Integration of design and control through model analysis. *Comput. Chem. Eng.,* 26, 213-225.

Sakizlis, V., Perkins, J. D., & Pistikopoulos, E. N. (2004). Recent advances in optimization-based simultaneous process and control design. *Comput. Chem. Eng.,* 28, 2069-2086.

Seferlis, P., Georgiadis, M. C. (2004). *The integration of process design and control*. Amsterdam: Elsevier B. V.

Sinnot, R. K. (2005). *Chemical Engineering Design, Volume 6,* Elsevier, Butterworth-Heinemann, 4th. Ed.

Michael Lykke Heiredal

Phone: +45 4525 4828
Fax: +45 4525 2258
E-mail: mlh@kt.dtu.dk
WWW: http://www.chec.kt.dtu.dk
Supervisors: Professor Anker Degn Jensen
                 Associate professor Flemming J. Frandsen
                 Joakim R. Thøgersen, Haldor Topsøe A/S

Industrial PhD
  Started: September 2006
  To be completed: August 2009

Particle Dynamics in Monolithic Catalysts

Abstract

Emission of nitrogen oxides from pulverized coal combustion is a major environmental problem today. The most used method for reduction of nitrogen oxides in the flue gas from coal fired power stations is Selective Catalytic Reduction (SCR) of nitrogen oxides with ammonia as reducing agent. A major problem using the SCR process is the risk of plugging and erosion/attrition of the monolithic catalysts because of fly ash particles in the flue gas. The objective of this Ph.D. project is to develop a model that in combination with Computational Fluid Dynamics can simulate the degree of plugging in monolithic catalysts with flue gas containing high fly ash concentration. The model should be a function of particle properties, gas velocities, angle of incidence to the monolith, geometry of the catalyst, and characteristics of the surfaces.

Introduction

The formation of nitrogen oxides (NO_x) during combustion processes takes place partly because of reaction between oxygen and nitrogen in the combustion air and partly because of reaction between oxygen in the air and nitrogen in the fuel. The formation of NO_x is an unwanted reaction because it contributes to acidifying the rain water and also is unhealthy for human beings.

Figure 1: Illustration of a high dust SCR reactor with monolithic catalysts.

The most used method for reducing NO_x in the flue gas from coal fired power stations is Selective Catalytic Reduction (SCR) of NO_x, where ammonia (NH_3) is used as reduction agent. Figure 1 shows an illustration of a high dust SCR reactor with monolithic catalysts. The global reactions for the SCR process are:

$$4NO + 4NH_3 + O_2 \rightarrow 4N_2 + 6H_2O$$

$$6NO_2 + 8NH_3 \rightarrow 7N_2 + 12H_2O$$
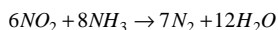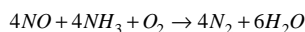
where the products are free nitrogen (N_2) and water (H_2O) which are harmless to the environment.
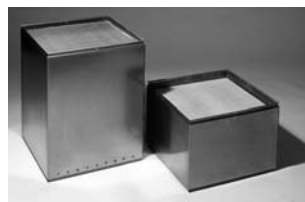
Figure 2: Picture of Haldor Topsøe A/S DeNOx SCR catalysts with corrugated monolith.

Generally industrial catalysts consist of vanadium and wolfram (V_2O_5/WO_3) dispersed on a titanium oxide (TiO_2) carrier. Figure 2 shows a picture of two Haldor Topsøe A/S DeNOx catalysts with corrugated monoliths. The high dust zone in the stationary power

stations is usually preferred for the SCR reactor. The operating temperature in the high dust zone is in the range from 300 to 400°C which is ideal for the catalytic activity. The content of NO_x in the flue gas is typically about 300 to 700 ppm, and NO_x can thereby be reduced by 80 to 90% over the SCR catalyst with an ammonia slip of a few ppm.

A major problem using the SCR DeNOx process under high dust conditions is the risk of plugging and erosion/attrition of the monolithic catalysts because of fly ash particles in the flue gas. The content of fly ash formed by the combustion processes is usually about 5-20 g/Nm^3 [1]. Monolithic catalysts are generally designed as a collection of catalytic channels, where the flue gas flows parallel to the wall to minimize the risk of plugging. Despite regular soot blowing, it is observed that a major part of the channels in the catalysts have been deactivated due to plugging. The plugging can be minimized by using larger channel diameters but as a consequence the catalyst volume has to be larger to obtain the same conversion which makes the reactor more expensive. One of the main design criteria is that the catalysts should be able to operate under heavy dust load and be compact to reduce cost, and at the same time function effectively without plugging.

Objective
To meet these design criteria it is necessary with a fundamental study (both experimental and numerical) of the particle dynamics in monolithic catalysts in order to understand the mechanisms that transport and deposit fly ash particles on the surface of the catalyst. Depending on the size of the particles, the transport can be due to Brownian diffusion [7], particle inertia, aerodynamic forces [2], turbulent diffusion [8] or thermophoresis [6].

Today a lot of models exist in the literature for transport of particles and aerosols in duct flow including deposition of these. It is also possible to use CFD to simulate transport and deposition of particles and aerosols in turbulent gas flow [3, 4]. CFD models also exist that can simulate the performance of the SCR reactor down stream in coal fired power stations regarding pressure loss, temperature and mixing of chemical species [5]. But none of these models take deposition and plugging into account in the channels of the monolithic catalysts.

The objective of this Ph.D. project is to develop a model that e.g. in combination with Computational Fluid Dynamics (CFD) can simulate the degree of plugging in monolithic catalysts with flue gas containing high fly ash concentrations. The model e.g. should be a function of particle properties, gas velocities, angle of incidence to the monolith, geometry of the catalyst and characteristics of the surface.

Methods
An experimental setup has been built for measuring deposition of submicron particles in a pipe, see Figure 3 and Figure 4. The experimental setup consisted of a Six-

Jet Atomizer Model 9306A *TSI Incorporated*, a Diffusion Dryer Model 3062 *TSI Incorporated*, an Aerosol Neutralizer Model 3054 *TSI Incorporated*, a 3m long electro polished stainless steel tube[1] for deposition of aerosol particles and two sampling lines for Scanning Mobility Particle Sizer (SMPS) measurements. The pipe was bent in 4 sections of about 0.75m. The flow rate in the deposition pipe was 300 ml/min, giving an average velocity of 0.18 m/s corresponding to a Reynolds number of about 72, to ensure enough residence time for deposition of submicron particles.
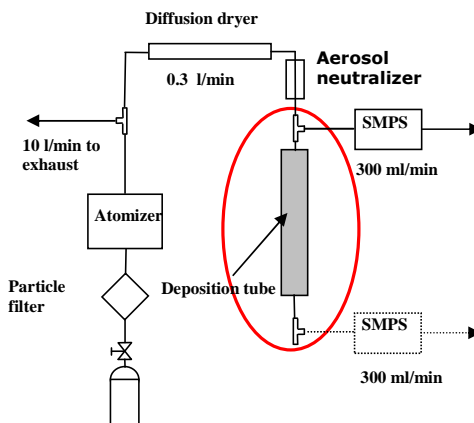
Figure 3: Experimental setup for measuring deposition of submicron particles in a 3m long electro polished bent pipe with a diameter of 6mm.

All fittings in the setup were Swagelok® and tubes were made of carbonized silicon material to prevent deposition due to electrostatic forces. Dimensions of the fittings and tubes in the setup were ¼" inch except for connections to the atomizer, where ½" fittings and tubes were used.

The principle of the setup was as follows. Pressurized atmospheric air at 5 bar controlled by a valve was fed to the atomizer through a particle filter. The atomizer was set to a pressure at about 4 bar giving a flow rate of about 10 l/min per nozzle which was connected to the exhaust system. Because the SMPS system was set to a flow rate of 300 ml/min controlled by an internal vacuum pump, a side stream of 300 ml/min was drawn from the atomizer main aerosol stream through the diffusion dryer and through the deposition pipe. The surplus of the aerosol stream from the atomizer was led to the exhaust system. To minimize deposition losses through the sampling lines, these were made as short as possible giving a maximum length of about 10 cm. To minimize deposition in the system due to electrical charges the setup was grounded using stainless steel and carbonized tubes.

---

[1] The stainless steel pipe had a surface roughness of less than 200 nm.

Figure 4: Experimental setup for measuring deposition of submicron particles in a 3m long electro polished bent pipe with a diameter of 6mm.

The Scanning Mobility Particle Sizer (SMPS) system consisted of a Condensation Particle Counter (CPC) model 3775 *TSI Incorporated*, and a Long Differential Mobility Analyzer (LDMA) model 3081 *TSI Incorporated* or a Nano Differential Mobility Analyser (NDMA) model 3085 *TSI Incorporated* depending on the system settings. The SMPS system measured the size distribution of a poly-dispersed aerosol in the size range between 4.4-833nm using the NDMA for particles in the size range between 4.4-168nm and the LDMA for particles in the size range between 13-833nm. The CPC counted the different classes of particles classified by respectively the NDMA and LDMA.

CFD modeling of Brownian diffusion and electrostatic dispersion

Figure 5: CFD model of 3m bent pipe.

Deposition of submicron particles in the size range between 3 nm and 1 μm in laminar pipe flow, due to Brownian diffusion has been simulated using Fluent 6.3. Additionally, electrostatic dispersion and deposition due to space charge of the submicron particles have been modelled using User Defined Scalars (UDS) in Fluent and thereby taking deposition of charged aerosol particles into account. This has been done by solving transport equations for the particle number concentration and the Poisson equation for the

electrostatic potential due to space charging (induced by the charged aerosol particles) together with the Navier-Stokes equation for laminar air flow at room temperature. The transport equation for the particle number concentration including electrostatic forces is given as follows:

$$\frac{\partial n}{\partial t} + \vec{\nabla} \cdot \left(\vec{v} n + Z n \vec{E} \right) = D \vec{\nabla}^2 n$$

where n is the particle number concentration, v the velocity field, Z the electrical mobility of the particles, E the electrical field strength and D the particle diffusion coefficient. The transport equation for the potential is given as:

$$\vec{\nabla}^2 \Phi = -\frac{ie\,n}{\epsilon_0}$$

where $q=ie$ is the total charge carried by a particle. The CFD model in Figure 5 consisted of a grid with 855540 cells. Discretization was modelled using second-order schemes. Flow was laminar and incompressible.

Results and discussion

The particles that were generated by the atomizer were produced by a 0.002 wt% salt solution consisting of potassium chloride KCl. The size distribution of the polydisperse KCl aerosols between 4.4-168nm was measured using the NDMA. The measurements were carried out at the top and bottom of the deposition pipe, see Figure 3 and Figure 4. In order to analyze the effect of particles carrying a charge, the measurements were carried out both with and without using the Aerosol Neutralizer in the setup as shown in Figure 3. Using the Aerosol Neutralizer discharges the particles to a Boltzmann charge equilibrium. The size distributions of the poly-disperse KCl aerosols at the top and the bottom of the deposition pipe are shown in Figure 6.
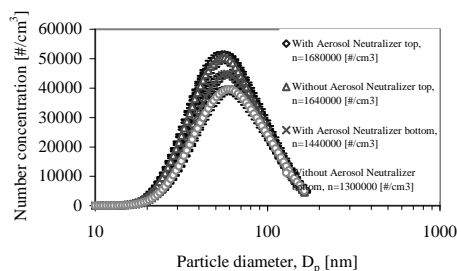
Figure 6: Size distribution of the charged and discharged polydisperse KCl aerosols at the top and the bottom of the deposition pipe consisting of a 3m long electro polished with a diameter of 6mm. The pipe was bent in 4 sections of about 0.75m

Comparison of CFD simulations for neutral (zero charge) KCl particles with experimental data for deposition of particles with a Boltzmann equilibrium charge distribution and low initial concentration, n_0 is shown in Figure 7. The figure also shows the

importance of secondary flow in a bent pipe compared to a straight pipe without secondary flow, because the particle deposition is enhanced due to secondary flow which is superimposed on the main flow. The reason for this is that the secondary flow transports particles from the core of the pipe to the near-wall region where it is deposited due to diffusion.
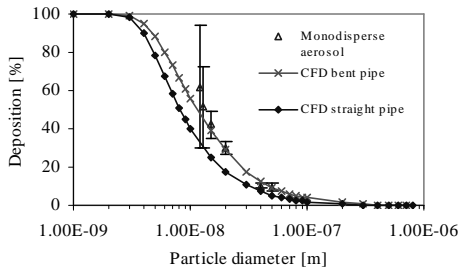
Figure 7: Deposition efficiency for very low concentrations of charged KCl particles with a Boltzmann equilibrium charge distribution and CFD simulation of neutral particles (zero charge).

Figure 8 shows CFD simulations of neutral KCl particles compared with experimental data for deposition of high concentrations of particles with e.g. a Boltzmann equilibrium charge distribution and KCl particles as delivered by the atomizer thereby carrying a high charge due to the atomization process. The initial concentration of the KCl particles was, n_0=1.7e6 [#/cm^3]. Higher deposition is seen for the highly charged particles due to an additional electrostatic dispersion induced by the space charging compared to a Boltzmann equilibrium charge distribution. Figure 8 also shows a comparison of CFD simulation for unipolar particles carrying an average of 2 elementary charges and for neutral particles.
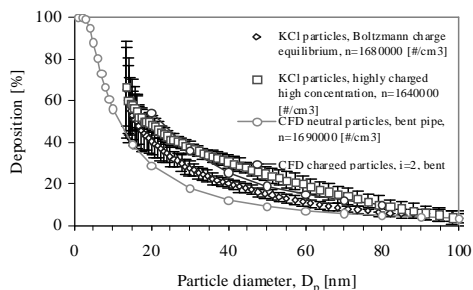
Figure 8: Deposition efficiency for charged and discharged KCl particles including CFD simulation of neutral and charged particles.

Conclusion
Particle size distribution and deposition rate of highly charged aerosol particles generated by an atomizer from a 0.002 wt% KCl solution were measured at the top and bottom of a 3m long pipe with a diameter of 6mm. The pipe was bent in 4 sections of about 0.75m Size distribution and deposition rate were compared with particles which have been discharged to a Boltzmann charge equilibrium using an Aerosol Neutralizer. The size distribution shows that concentrations of the discharged particles at the bottom of the deposition pipe are substantially higher than the concentration of the particles which have not been discharged. The discharged particles show a lower deposition rate in the range between about 20-80nm than particles which have been discharged. This is due to an additional deposition from electrostatic forces (space charging) as a result of the higher charge that the particles are carrying. CFD simulations of the deposition of submicron particles carrying zero charge in the particle size range between 3-800nm in a 3m long smooth pipe (bent in 4 sections of about 0.75m) with a diameter of 6mm show lower deposition than simulations of unipolar particles carrying an average of 2 elementary charges. CFD simulations shows that secondary flow in a bent pipe enhances the particle deposition by transporting particles from the core of the flow to the near-wall region and thereby enhancing deposition due to Brownian diffusion.

Future work
In the next period plugging experiments using a pilot plant will be carried out. Further experiments will be made with the experimental setup for measuring deposition of submicron particles in a 3m straight pipe in order to experimentally confirm the higher deposition due to secondary flow. A setup will be build in order to investigate the deposition of large particles in the micro meter range. The experimental result will be used to evaluate a model for particle deposition of micron particles in a single pipe taking the particle/wall interaction into account.

References
1. E. Raask, Minerals Impurities in Coal Combustion. Behavior, Problems and Remedial Measures, Taylor & Francis, 1 edition, U.K., 1985.
2. P.G. Saffman, Journal of Fluid Mechanics, 22 (2) (1965) 385-400.
3. C.M. Winkler, S.L. Rani & S.P. Vanka, Powder Technology, 170 (2006) 12-25.
4. R. Maniero & P. Canu, Chemical engineering Science 61 (2006) 7626-7635.
5. K. Rogers, M. Albrecht & M. Varner. Babcock & Wilcox, Technical Paper (2000).
6. C-J. Tsai, J-S. Lin, S.G. Aggarwal & D. Chen, Aerosol Science and Technology, 38 (2004) 131-139.
7. J.M. Frey, P. Schmitz, J. Dufreche & I.G. Pinheiro, Transport in Porous Media, 37 (1999) 25-54.
8. A. Kitamoto & Y. Takashima, Bulletin of the Tokyo Institute of Technology, No. 127 (1975).

Jesper Holck

Phone: +45 4525 2979
E-mail: jeh@kt.dtu.dk
WWW   http://www.bioeng.kt.dtu.dk

Supervisors: Anne S. Meyer

                Jørn Dalgaard Mikkelsen

PhD Study
  Started: November 2007
  To be completed: December 2010

Enzymatic Production of Prebiotics from Sugar Beet Pectin

Abstract

The potential importance of dietary fibres and oligosaccharides in modulating the microbial ecology of the human colon to exert beneficial health effects is currently receiving significant attention. By targeting dietary fibre structures and prebiotics by selective enzymatic hydrolysis of complex plant substrates, such as pectin, defined poly- and oligomers can be derived.

Introduction

Dietary fibres and prebiotics are non-digestible dietary carbohydrate structures that can be health promoting by supporting the growth of beneficial bacteria in the human colon, such as *Bifidobacterium sp*. and via other mechanisms [1]. This PhD project builds on that a significant potential exists for targeting dietary fibre and prebiotics structures by selective enzymatic hydrolysis of pectinaceous plant cell wall structures present in sugar beet pulp – the byproduct stream left over from industrial production of sugar.

Project outline

The focus of the project will be on enzyme assisted modification of sugar beet pectin in order to manufacture target oligomer products which can have a potential beneficial effect. The production is made via an intelligent reaction optimisation and combination of monoactive experimental enzymes available in the Prebiotics Center. A particular focus area will be on characterising the action of these enzymes in modification of pectin rhamnogalacturonan I (RG I) (see Figure 1).

Figure 1: schematic structure of rhamnogalacturonan I

RG I is a heteropolysaccharide composed of a rhamno-galacturonan backbone with arabinan, galactan, and arabinogalactan side chains. The design of optimal enzyme reactions, including only the required activites for the particular target substrate and target product, will be done via an iteration of advanced structural substrate and product analyses in systematic enzymatic treatments using monoactive enzymes. The research will include reaction parameter optimisations of selected reactions. The experimental work will be conducted to allow obtainment of new realizations about enzyme cascade action patterns on RG I and other pectin structures, including quantitative kinetics on branched plant cell wall polysaccharides.

Specific objectives

In order to tailor the enzymatic treatment, the first challenge is to establish methods for thorough analysis of the substrate structure and the product oligomers. Therefore initial experiments on the monocomponent composition are required.

Results

A monocomponent composition analysis of modified high molecular weight pectin extracted from sugar beet pulp has been performed using standard acid hydrolysis followed by HPAEC-PAD analysis. The results on mole basis are compared to other published data for sugar beet pectin composition [2] on figure 2. These results showed a lower level of arabinose which might be due to loss of arabinan sidechains during the extraction. The decrease in arabinose content gives a relatively higher content of galacturonic acid. The ratio between

rhamnose and galacturonic acid indicate that a relatively large amount of the pectin consists of homogalacturonan.
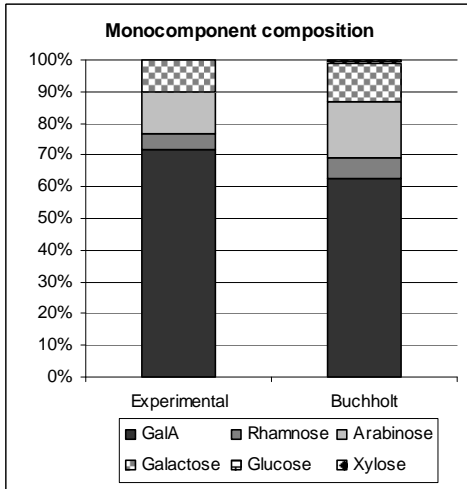
Figure 2: Comparison of composition on mole basis of modified sugar beet pectin from experimental data and [2].

These results is the first step in the progress of designing a properly targeted enzyme biocatalysis followed by construction of statistically designed combinations of monoactive experimental enzymes for contriving optimal "minimal" enzyme cocktails.

References

[1] Rastall, R.A., Gibson, G.R., Gill, H.S., Guarner, F., Klaenhammer, T.R., Pot, B., Reid, G., Rowland, I.R. and Sanders, M.E. (2005). Fems Microbiology Ecology 52, 145-152.

[2] Buchholt, H.C., Christensen, T.M.I.E., Fallesen, B., Ralet, M.C. and Thibault, J.F. (2004). Carbohydrate Polymers 58, 149-161.

Norazana binti Ibrahim

Phone:	+45 4525 2922
Fax:	+45 4588 2258
E-mail:	nbi@kt.dtu.dk
WWW:	http://www.chec.kt.dtu.dk
Supervisors:	Prof. Kim Dam-Johansen
	Assoc.Prof. Peter Arendt Jensen

PhD Study
  Started: July 2007
  To be completed: June 2010

Flash Pyrolysis of Wheat Straw for Bio-oil Production: The Influence of Feedstock Moisture Content on the Product Yields

Abstract

The influence of the initial moisture content on the flash pyrolysis of the wheat straw for producing bio-oil has been studied and is reported in this paper. The aim is to study how initial moisture content of wheat straw will influence the yield of the flash pyrolysis products, namely bio-oil, char and gas, in the temperature range of 475-575 °C. Bio-oil is made up of liquid organics and 'produced water'. Samples of straw with different moisture content (6.20 wt % and 15.0 wt %) were fed to a bench scale Pyrolysis Centrifuge Reactor (PCR) to study the effect of the moisture content on the pyrolysis products. The results show that at the higher moisture content of 15.0 wt %, the maximum liquid organics yield of approximately 53.0 % (wt, daf) was attained at the reactor temperature of 525 °C compared to only 48.0 % (wt, daf) at the moisture content of 6.20 wt % when subjected to the same conditions. At the higher moisture content also, the char yield was about 6 yield % higher in the reactor temperature domain of 475-525 °C but beyond the reactor temperature of 550 °C the char yield was almost the same for the different initial moisture content. The production of gas and water of reaction were higher at the lower moisture content (6.20 wt %) by as much as 7 yield % and directly proportional to increasing reactor temperature due to the liquid organics and char were being converted into gases and water through secondary cracking. The hot gas residence time in the reactor was 0.21±0.04 s.

Keywords: Flash pyrolysis, moisture content, wheat straw, bio-oil

Introduction

Flash pyrolysis process has been the subject of intense research in the last decades (Sipila et al, 1996). The main features are the very rapid or high heating rate of biomass particles and a short residence time at temperature of 450 - 600°C (Acikgoz and Kockar, 2007) required to obtain the highest possible liquid yield. Generally, flash pyrolysis processes produce 50-75 wt% of liquid bio-oil (including water), 15-25 wt% of solid char and 10-20 wt% of noncondensable gases, depending on the feedstock used (Mohan et al, 2006 and IEA 2006). The flash pyrolysis process is a promising thermal conversion route for producing ash-free liquid fuels with a high volumetric energy density from bulky biomass. During pyrolysis, biomass is thermally decomposed without oxidizing agent to solid charcoal, liquid oil and gases. The char is the only residual solid carbon. The gas component consists mainly of carbon monoxide, carbon dioxide and light hydrocarbons. The liquid oil is a condensable component composed of a large variety of higher molecular weight species,

organic acids, aldehydes, alcohols, phenols and other oxygenates. This liquid oil also is known as a pyrolysis liquid, bio-oil or tar and has a lower heating value of about half that of conventional fuel oil (Bridgwater et al, 2000) which is approximately 17 MJ/kg, due to the high oxygen content in bio-oil. The tar can undergo secondary reactions to be further broken down into gas, refractory tar and water. The quality and the yields of the products of pyrolysis depend on several operating parameters including temperature, types of biomass, particle size, reaction condition, and reactor configuration, as well as the extraneous addition of catalysts (Bridgwater, 1994).

Over the last two decades, extensive studies have been conducted to understand the complexity of flash pyrolysis to obtain the optimal conditions for producing bio-oil with a high quality. The effect of biomass properties has been identified recently as one of the key research area but only little attention has been focused on the effect of feedstock moisture content on the flash pyrolysis of woods (Gray et al, 1985) and none on

wheat straw has been found. Previous studies indicated that moisture may change or enhance some pyrolysis behaviour or reactions. Shafizadeh, (1968) found that the decomposition rate of wet cellulose was much faster than dry cellulose when subjected to the same conditions in a closed system at 200 °C. Gray and co-workers, (1985) found that the presence of moisture increased the char yield by as much as 5 yield % (relative to dry sample). Recent studies investigated the effect of moisture content on the conventional pyrolysis and found that the oily products increased with increasing moisture content (Demirbas, 2004). This paper reports the results of studies on the effect of moisture content of wheat straw on the pyrolysis behaviour and its products distribution.

Table 1: Analysis of wheat straw

Analysis	Wheat straw
Proximate	
Volatile matter, %db	74.7
Ash, %db	5.9
Moisture, %wt	5.9
HHV (MJ/kg, dry basis)	18.75
Ultimate (wt %, dry ash free basis)	
Carbon	49.4
Hydrogen	6.2
Nitrogen	1.11
Sulphur	0.17
Oxygen (by difference)	43.12
Ash Composition (wt %)	
Cl	14.4
Si	22.03
Al	0.51
Fe	0.27
Ca	3.9
Mg	11.02
Ti	0.02
Na	1.19
K	25.4
P	2.37
O (by difference)	18.89

db: dry basis

Specific Objectives

The main objective of the current study is to investigate the effect of initial moisture content of wheat straw on the flash pyrolysis products, namely bio-oil in the reactor temperature domain of 475-575 °C.

Experimental Section

Material. In this study, wheat straw with a particle size of less than 1400 μm was used. The characteristics of the wheat straw are given in Table 1. A moisture content of 6.20 %wt ('as received') and 15.0 %wt ('wet') were used. Wet straw samples were prepared by sprinkling water on them to achieve a moisture content of 15.0 ± 1 %wt. The mixture was stored for 3 to 4 days to ensure that the water had been fully distributed.

Apparatus and Procedures. The flash pyrolysis experiments were conducted in a bench scale Pyrolysis Centrifuge Reactor (PCR) as depicted in Figure 1. The biomass was introduced by a screw feeder into a horizontally oriented Ø 82 x 200 mm tubular reactor. Here, a three-blade rotor with close clearance of 2 mm to the reactor wall rotated at a fixed speed of 14784 rpm which creating a centrifugal force at the pipe wall of 10 x 10^3 g, provides a rotation of the gas phase and the biomass particles. The reactor wall was heated electrically by four independent heating zones located inside the reactor. A Proportional Integral Differential (PID) temperature controller was used, which allowed for a better temperature control and minimized the temperature deviation from the set point. While undergoing reaction, the particles moved down the reactor pipe before leaving suspended in the gas through the tangential outlet. Larger char particles were removed by change-in-flow separator and whereas fines particles were collected by the following cyclone. Vapors were condensed in a direct condenser (bubble chamber) filled with previously produced bio-oil and cooled by water. The temperature in the condenser was controlled to 55 to 75 °C by means of a pipe coil cooled by tap water. Aerosols that were not retained by the condenser were collected in a coalescer filled with ROCKWOOL (insulation material). In this coalescer, droplets of bio-oil were formed and removed by gravity force. The gas was pumped to a preheater at temperature of 450 °C before it recirculates to the reactor in order to maintain the gas residence time and to avoid condensation of liquid products within the reactor. The excess gas was measured by a temperature compensated gas meter and collected. Before the gas was metered, it was cooled to ambient temperature in order to remove water. The gas residence time in the reactor was calculated based on the performance curve of the positive displacement gas pump and the yield data. Details about the reactor descriptions were presented in previous work (Bech, 2008).

In this work, samples of straw with different moisture content (6.20 wt % and 15.0 wt %) were tested to investigate its effect on the pyrolysis products, namely bio-oil, char and gas. A 500.0 g sample of straw was placed in the feeder and the system was purged with nitrogen. The tracing/heater was turned on and after the reactor reached the temperature set point, then the rotor speed was adjusted to the required set point at 14784 rpm. The obtained feed rate was approximately 23 g/min. The experiment was run for 14-20 minutes and stopped just before the coalescer meter reading reached the pressure of -400 mbar, to avoid severe blockage in the nozzle where the bubble chamber is placed. After the system had cooled, liquid and char yield in addition to spend raw material was determined gravimetrically. Gas yield was calculated on the basis of the measured gas volume and the molecular weight measurement obtained immediately after the run in order to minimize the potential effect of light gasses diffusing through the gas bag. Liquid samples were filtered through a Whatman #4 filter paper on a Buchner funnel. The char left on the filter was washed

thoroughly using ethanol and acetone and dried under an infrared light bulb for 7 to 10 minutes. Then the residual mass was determined and added to the char yield. Water content in the liquid products from the bubble chamber and the conical flask below the coalescing filter was determined by refractive index measurement and an empirical correlation valid for wheat straw and pine wood (Bech, 2008). The fraction left in the coalescer was assumed to be similar in composition to the fraction condensed in the bubble chamber and was determined by weighing the coalescer before and after the run.
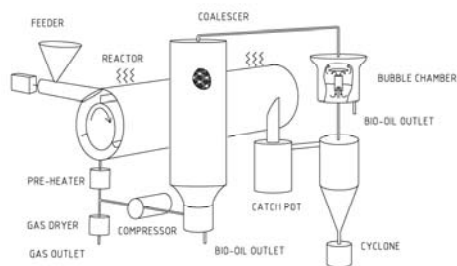
Figure 1: Schematic diagram of the developed ablative pyrolysis bench reactor system (Bech, 2008).

Results and Discussion

Effect of reactor temperature on the yields

Figure 2 shows the pyrolysis products distribution at different reactor temperatures. The pyrolysis products are char, gas and bio-oil and the latter is subdivided into the liquid organics and produced water. The organics yield increases with increasing reactor temperature and the maximum yield is obtained at reactor temperature of 525 °C and then it decreases afterwards. On the other hand, the char yield decreases as the temperature increases. Meanwhile, both the gas and water yield increase with increasing reactor temperature. The reason for the higher char yield and lower organics yield at a lower temperature might be due to the fact that the reaction temperature is not high enough for complete flash pyrolysis. Furthermore, at low temperature, the char formation is favoured due to the dehydration reactions of cellulose is dominant. Besides, at high temperature, cellulose depolymerizes rapidly producing levoglucosan resulting in a high tar yield (Balat, 2008). In addition, at high temperature and high heating rates the time for dehydration reaction to take place is much shorter which result in more unstable material left for depolymerization to primary volatiles and therefore lower final char yields (Zanzi, 2001). The increasing of gas and water yield with increasing temperatures might be due to pyrolysis vapor and char being converted into gases and water through secondary cracking (Radlein, 2002).

Effect of moisture content of the feedstock

The effect of the moisture content of the feedstock on the yields of bio-oil, char and gas is depicted in Figure 2. All data points presented are averages of two or three experiments. It has been observed that with increasing moisture content, the liquid organics and char yield increase by as much as 8 yield % and the produced water and gas yield decrease. Gray et al. also observed that more moisture in the feedstock results in an increased char yield. The increasing of the char yield with increasing moisture could be explained by the energy consumption and partly at the particle level during the pyrolysis reactions.

The presence of moisture could slow down the particle surface temperature rise because more energy is consumed for heating and water evaporation and thus a smaller portion of the energy is transferred into the solid. Consequently the effective particle temperature is lower than the reaction temperature which increase the char yield. Another reason is the wet straw produces more condensate during the pyrolysis progress and therefore the pyrolysis reactions in wet straw proceeded in the presence of higher concentration of water vapor than the dry straw. Hence, this water vapor may interact with tar formation to increase the char yield.

Meanwhile the increasing of liquid organics and decreasing in gas yield with increasing moisture content may relate to the residence time in the reactor. The presence of moisture would increase the volume of volatiles escaping from the straw and this would reduce the residence time in the reactor resulting high organic yield and low gas yield.

(a)

(b)

(c)

(d)
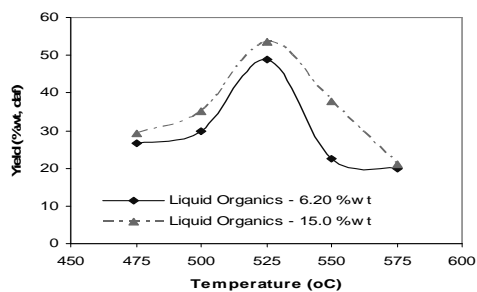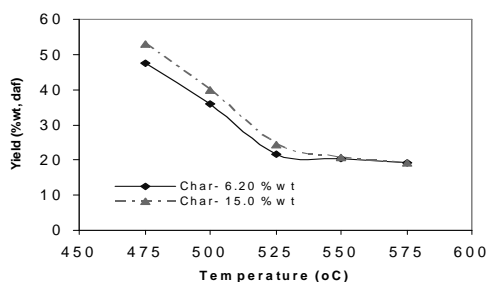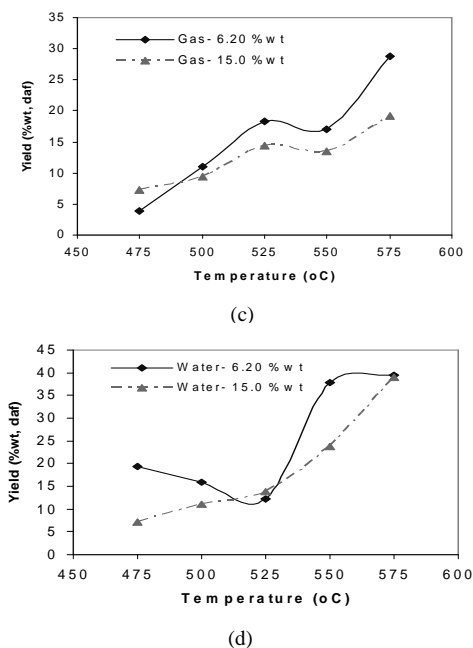
Figure 2: Effect of moisture on the yield of (a)
Liquid organics, (b) Char, (c) Gas and (d) Water

Conclusion

The influence of moisture content on the flash pyrolysis
product yields has been experimentally investigated. In
general, the yield of liquid organics increase with
increasing pyrolysis temperature from 475 °C to 525 °C
and then it decreases afterwards. The gas yield also
keeps increasing as temperature increases and the yield
of water increases after temperature of 525 °C. At
reactor temperature of 525 °C, the maximum organic
yield is obtained for both moisture contents. The yield
of organics is increased from 48.0 wt% (moisture
content: 6.20 wt %) to 53.0 wt% (moisture content: 15.0
wt %) at this temperature. Overall, the organic yield
increases with increasing moisture content by as much
as 8.0 yield %. In contrast, the char yield decrease with
increasing reactor temperatures. The water and gas yield
increase with temperature due to secondary thermal
cracking proceeded at higher temperatures which in turn
lead to a reduction of liquid organics and increase a
production of gaseous products and light hydrocarbon
gases.

It can be concluded that the presence of moisture in
straw influences its behaviour during pyrolysis
reactions. Further investigation should be carried out to
determine which chemical interactions or reactions
occurred during the course of pyrolysis process.

References

Acikgoz, C and Kockar, A.M. (2007). Flash pyrolysis of
Linseed (Linum usitatissimum L.) for production of
liquid fuels. Journal of Analytical and Applied
pyrolysis, 78. 406-412.

Balat, M. (2008). Mechanism of thermochemical
biomass conversion processes. Part 1: Reactions of
pyrolysis.

Bech, N. (2008). PhD Thesis: In situ flash pyrolysis of
straw. Technical University of Denmark, Denmark.

Bridgwater, A.V. (1994). Catalysis in thermal biomass
conversion. Applied Catalysis. A, General 116, 5–
47.

Bridgwater, A.V., and Peacocke, G.V.C. (2000). Fast
pyrolysis process for biomass. Renewable &
Sustainable Energy Reviews, 4, 1–73.

Demirbas, A. (2004). Effect of initial moisture content
on the yields of oily products from pyrolysis of
biomass. Journal of analytical and Applied paralysis,
71, 803-815.

Gray, M.R., Corcoran, W.H., and Gavalas. G.R. (1985).
Pyrolysis of a wood – derived material. Effect of
moisture and ash content. Ind.Eng.Chem. Process
Des, 24, 646-651.

IEA-International Energy Agency (2006),
www.ieabioenergy.com

Mohan, D., Charles, U., Pittman, J., and
Philip,H.S.(2006). Pyrolysis of wood/biomass for
bio-oil: Critical Review. Energy & Fuels, 20, 848–
889.

Radlein, D. (2002). In fast pyrolysis of biomass: A
Handbook,Vol.2; Bridgwater, A.V., Ed,;CPL
Press: Newbury,UK:p.165.

Shafizadeh, F. (1968). Adv.Carbohydr.Chem, 23, 419.

Sipilae` K., Kuoppala E., and Fagernae`s L. (1998).
Characterization of biomass–based flash pyrolysis
oils. Biomass and Bioenergy, 14, 103–13.

Zanzi, R. (2001). PhD Thesis: Pyrolysis of biomass.
Royal Institute of Technology, KTH, Stockholm,
Sweden.

Irakli Javakhishvili

Phone:	+45 4525 6817
Fax:	+45 4588 2161
E-mail:	irj@kt.dtu.dk
WWW:	http://www.polymers.dk
Supervisors:	Prof. Søren Hvilsted

PhD Study

Started:	September 2007
To be completed:	August 2010

Gold Nanoparticles Protected with Thiol-Derivatized Amphiphilic Poly(ε-caprolactone)-*b*-poly(acrylic acid)

Abstract

Amphiphilic poly(ε-caprolactone)-*b*-poly(acrylic acid) (HS-PCL-*b*-PAA) with a thiol functionality in the PCL terminal has been prepared in a novel synthetic cascade. Initially, living anionic ring-opening polymerization (ROP) of ε-caprolactone (ε-CL) employing the difunctional initiator, 2-hydroxyethyl 2-bromoisobutyrate (HEBI), followed by esterification with 2,4-dinitrophenyl- or 4-monomethoxytrityl-protected mercaptoacetic acids (Prot-) provided well-defined PCL macroinitiators capped with protected thiols. The macroinitiators allowed atom transfer radical polymerization (ATRP) of *tert*-butyl acrylate (*t*BA) in a controlled fashion by use of $NiBr_2(PPh_3)_2$ catalyst to produce Prot-PCL-*b*-P*t*BA with narrow polydispersities (1.17-1.39). Subsequent mild deprotection protocols provided HS-PCL-*b*-PAA. Reduction of a gold salt in the presence of this macroligand under thiol-deficient conditions afforded stable, aggregation-free nanoparticles as evidenced from UV-vis spectroscopy and transmission electron microscopy (TEM), the latter revealed nanoparticles with a mean diameter of 9.0±3.1 nm.

Introduction

Gold nanoparticles (AuNPs) are envisioned to be superior to polymeric micelles as candidates for constructing drug delivery devices. Encapsulation and controlled release of drugs, as well as adequate masking from reticuloendothelial system (RES) remain as a challenge in case of the polymeric micelles[1]. On the contrary, monolayer protected AuNPs offer improved stability, low toxicity, versatility of surface functionalities, and small size, rendering them unrecognizable by RES, and thus may serve as excellent reservoirs for hydrophobic drugs. Tailoring the surface properties of the AuNPs bestows the system site-specificity and prolonged circulation time.[1,2] Antibody conjugated AuNPs provide high contrast for noninvasive imaging of targeted cancer tissues.[3] AuNPs with tunable optical properties find application in thermal ablative therapy for cancer.[4]

AuNPs are generally prepared by reduction of $HAuCl_4$ in a boiling sodium citrate solution, or in the presence of thiol capping ligands.[5] Numerous studies were reported where amphiphilic block copolymer micelles were utilized for stabilization of AuNPs.[5,6] Biocompatible and biodegradable poly(ε-caprolactone)-*b*-poly(ethylene oxide) has been end-functionalized with disulfide moiety, and employed as the ligand for protection of AuNPs, which may be exploited as drug delivery device as well as for subcellular localization studies.[7]

Zhang et al. have prepared water miscible shell cross-linked nanoparticles based on diblock copolymers of PCL and poly(acrylic acid) (PAA), and obtained nanoscale cage-like membranes after hydrolysis of PCL core.[8]

Our work covers the synthesis of thiol-functionalized amphiphilic diblock copolymer HS-PCL-*b*-PAA and the demonstration of its capacity in passivation of AuNPs. PCL, comprising the core of the nanoparticle, is biocompatible and exhibits high permeability to small drug molecules[9], whereas PAA, constituting the shell, is biocompatible and mucoadhesive.[10] Therefore, the AuNPs may have potential as drug carriers in bladder cancer therapy.

Results and Discussions

For preparation of HS-PCL-*b*-PAA dual initiator strategy combining different living polymerization techniques has been utilized.[11] ROP of ε-CL from double-headed initiator - HEBI[12] afforded heterotelechelic PCL bearing hydroxy and bromoester end groups (Scheme 1, a). The polymerization was catalyzed with tin octoate ($Sn(Oct)_2$). Undesirable side effects that could originate from high initial catalyst concentration (~0.05 M) and low initial initiator to

catalyst ratio (~2.2) was counteracted by conducting the polymerization at low temperature (62 °C) and thus suppressing collateral esterification and transesterification reactions involving HEBI and liberated octanoic acid.[13,14] The monomer conversion determined gravimetrically is about 59.6 %, which corresponds to the degree of polymerization (DP) of 32. The DP estimated from ^{1}H NMR experiment is approximately 30. This, together with symmetrical size exclusion chromatography (SEC) trace and narrow polydispersity index (PDI) (Table 1), indicates almost quantitative incorporation of the dual initiator and minimal share of side reactions.

Incorporation of a protected thiol functionality was attained by esterification of hydroxy chain end of PCL with α-(2,4-dinitrophenylthio)acetic acid (dNPTAA) using diethyl azodicarboxylate (DEAD) and triphenylphosphine (TPP) in modification of the synthetic protocol which had previously been exercised by Trollsås et al.[15] (Scheme 1, b).

Scheme 1: Synthetic Pathway for Preparation of PCL Macroinitiators (**1**, **2**). (a) Sn(Oct)$_2$, 62°C, THF; (b) dNPTAA, DEAD, TPP, THF; (c) MmtTAA, DEAD, TPP, THF

Br-PCL-dNPTA **1** with near to quantitative functionalization (estimated from ^{1}H NMR data), and narrow polydispersity was obtained (Table 1, **1**).

Table 1: Characteristics of Br-PCL-OH and PCL Macroinitiators (**1**, **2**) Estimated by SEC and ^{1}H NMR

Compound	$M_n{}^b$	$M_n{}^c$	$M_w/M_n{}^c$
Br-PCL-OH^a	3640	6100	1.09
1	3880	6200	1.08
2a	3990	6300	1.09
2b	3990	7100	1.08

^{a} DP of PCL estimated by ^{1}H NMR is 30; ^{b} By ^{1}H NMR; ^{c} By SEC

Br-PCL-dNPTA **1** was employed as macroinitiator in subsequent ATRP of *t*BA (Scheme 2, a). ATRP of *t*BA mediated by NiBr$_2$(PPh$_3$)$_2$ was carried out in bulk at 90 °C. Less than stoichiometric amount of the catalyst was taken as advocated by Hedrick et al.[16] to avoid unsymmetrical SEC traces. High monomer concentration overpowered otherwise sluggish polymerization.[17] Ratio of the initial molar concentrations of the monomer and initiator [M]$_0$:[I]$_0$ was decreased from 210 for **3a** to 170 for **3b**. This significantly decreased polymerization time necessary to attain similar monomer conversion (Table 2). SEC revealed narrow molecular weight distribution and no

Scheme 2: Synthetic Pathway for Preparation of HS-PCL-*b*-PAA (**5**, **6**). (a) *t*BA, NiBr$_2$(PPh$_3$)$_2$, 90°C; (b) CH$_3$CH$_2$SH, TEA, CHCl$_3$; (c) TFA, TES, CH$_2$Cl$_2$

unreacted macroinitiator indicating good control over the reaction (Fig. 1). ^{1}H NMR spectrum of **3b** (Fig. 2) confirmed successful formation of the P*t*BA block, and preservation of protected thiol functionality. The results for diblock copolymers prepared from the macroinitiator Br-PCL-dNPTA **1** are summarized in Table 2 (**3a**, **3b**).

Removal of 2,4-dinitrophenyl protecting group from **3** was conducted in CHCl$_3$ using large excess of ethanethiol in the presence of triethylamine (TEA) according to the procedure reported by Carrot et al.[18] This provided HS-PCL-*b*-P*t*BA (Scheme 2, I b). Full deprotection was confirmed by ^{1}H NMR and FT IR spectroscopy. Selective cleavage of *tert*-butyl ester groups of **3** was carried out in CH$_2$Cl$_2$ employing

Figure 1: SEC trace of PCL-*b*-P*t*BA **3b**
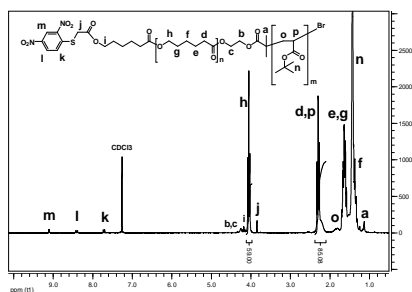
Figure 2: ^{1}H NMR spectrum of PCL-*b*-P*t*BA **3b**

trifluoroacetic acid (TFA)[19] and triethylsilane (TES) as the cation scavenger[20] (Scheme 2, I c). Under these

relatively mild conditions (2 M TFA) almost complete deprotection of P*t*BA was achieved.

However, thiols are inclined to auto-oxidation and disulfide formation under basic conditions[21] as well as when in contact with air, which may decrease the effectiveness of the macroligand in stabilization of AuNPs.[22] Moreover, removal of 2,4-dinitrophenyl protecting group is reversible, and demands large excess of low molecular weight thiol to shift the equilibrium to the macrothiol.[18] Therefore, it would be an advantage to make use of thiol protecting group deblocking of which could be irreversibly carried out concurrently with the cleavage of *tert*-butyl ester groups. Such a reaction would be run under acidic conditions, and would limit the time of contact of the macrothiol with air as well.

Table 2: Conditions of ATRP and Characteristics of PCL$_n$-*b*-P*t*BA$_m$ (**3**, **4**) Estimated by SEC and ^{1}H NMR

Compound	$[M]_0$:$[I]_0$:$[Cat]_0^a$	Reaction Time, h	n	m	M$_n$ (^{1}H NMR)	M$_n$ (SEC)	M$_w$/M$_n$ (SEC)
3a	210:1:0.8	48	30	31	7900	10800	1.27
3b	170:1:0.8	20	30	24	7000	10200	1.17
4a	220:1:0.8	42	30	70	13000	15300	1.39
4b	170:1:0.8	20	30	50	10400	14000	1.29

[a] Ratio of initial molar concentrations of the monomer to initiator and catalyst

4-Monomethoxytrityl (Mmt) group has been successfully employed in peptide synthesis as sulfhydryl protection for mercapto acids: It is very acid-labile, succumbs to irreversible deprotection, and can be removed simultaneously with *tert*-butyl ester groups when treated with TFA in CH$_2$Cl$_2$/TES.[23] Indeed, it proved to be an efficient and convenient protecting group in the synthesis of thiol-derivatized HS-PCL-*b*-PAA.

Esterification of PCL with α-(4-monomethoxytritylthio)acetic acid (MmtTAA) gave Br-PCL-MmtTA **2** with near to quantitative functionalization and low PDI (Scheme 1, c, Table 1, **2a**, **2b**). Br-PCL-MmtTA **2** was successfully chain-extended by ATRP of *t*BA resulting in block copolymer **4** (Scheme 2, a). Interestingly, under similar conditions, macroinitiator **2** afforded higher DP of *t*BA than macroinitiator **1** (Table 2). This may be attributed to hypothetical interaction of the thiol protecting groups with catalytic center in ATRP. However, SEC analysis produced monomodal trace with fairly narrow molecular weight distribution, which proved absence of any undesirable side reactions, and high efficacy of the macroinitiator (Fig. 3). ^{1}H NMR spectrum of the block copolymer **4a** (Fig. 4) reveals all characteristic resonances: **k** and **l** (overlap with the residual solvent peak) as well as **m** correspond to the thiol-protecting Mmt moiety. Methylene group next to the sulfur atom gives rise to singlet **j** indicating that no deblocking reaction took place. Simultaneous deblocking of Mmt and *tert*-butyl ester groups by treating PCL-*b*-P*t*BA **4** with TFA (2 M) in CH$_2$Cl$_2$/TES provided **6** (Scheme 2, II c). ^{1}H NMR data confirmed the preservation of PCL backbone:

Figure 3: SEC trace of PCL-*b*-P*t*BA **4b**

ratio of integrals of the resonances originating from PCL and P*t*BA repeating units remained almost unaltered after deprotection. Signals attributed to the protecting species disappear completely, while the resonance originating from the methylene group next to the sulfur atom, shifts downfield and is split into
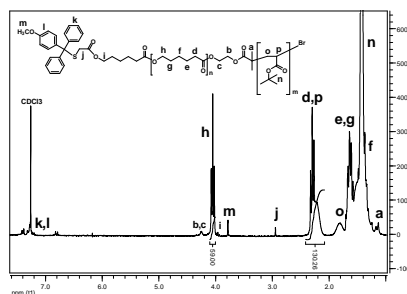
Figure 4: ^{1}H NMR spectrum of PCL-*b*-P*t*BA **4a**

doublet. Approximately 5 % of the residual *tert*-butyl ester units have been detected.

AuNPs were synthesized according to a modified literature procedure[7]: To the solution of **6a** (0.054 mmol) and gold (III) chloride trihydrate (0.165 mmol) in THF (16.2 ml) was quickly added freshly prepared solution of lithium borohydride (0.825 mmol). Reduction was marked with immediate change of color from yellow to purple and vigorous gas evolution. Thus, gold nanoparticles were formed employing threefold excess of the gold salt compared to the macrothiol. No insoluble matter was observed under these thiol-deficient conditions. UV-visible spectrum of water solution of the nanoparticles (Fig. 5, A) exhibits
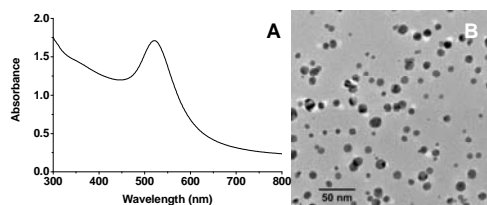
Figure 5: UV-visible spectrum (A) and TEM image (B) of the gold nanoparticles

absorption at 522 nm – characteristic for aggregation free AuNPs.[24] TEM image shows well-separated AuNPs with moderate dispersity. The particles shown in Fig. 5, B have mean diameter of 9.0 ± 3.1 nm.

Conclusions

In summary, we have demonstrated the ease of preparation of well-defined amphiphilic diblock copolymer bearing thiol end group, HS-PCL-*b*-PAA, which affords reliable stabilization of the gold nanoparticles. Synthetic protocol of ROP of ε-CL initiated by HEBI has been optimized to yield the macroinitiator with narrow molecular weight distribution, and high degree of functionality. 4-monomethoxytrityl protecting group has proved to be advantageous for this particular system because it allows deprotection of thiol and P*t*BA block in one pot. Reduction of the gold salt with relatively mild reducing agent provides stable, well-separated nanoparticles, which signifies fairly high efficiency of HS-PCL-*b*-PAA in the passivation of the gold nanoparticles.

References

1. J. D. Gibson, B. P. Khanal, E. R. Zubarev, J. Am. Chem. Soc. 129 (2007) 11653-11661.
2. R. Hong, G. Han, J. M. Fernández, B.-j Kim, N. S. Forbes, V. M. Rotello, J. Am. Chem. Soc. 128 (2006) 1078-1079.
3. A. Agarwal, S. W. Huang, M. O'Donnell, K. C. Day, M. Day, N. Kotov, S. Ashkenazi, J. Appl. Phys. 102 (2007) 064701.
4. L. R. Hirsch, R. J. Stafford, J. A. Bankson, S. R. Sershen, B. Rivera, R. E. Price, J. D. Hazle, N. J. Halas, J. L. West, Proc. Natl. Acad. Sci. U.S.A. 100 (2003) 13549-13554.
5. J. Shan, H. Tenhu, Chem. Commun. (2007) 4580-4598.
6. S. Abraham, I. Kim, C. A. Batt, Angew. Chem. Int. Ed. 46 (2007) 5720-5723.
7. T. Azzam, A. Eisenberg, Langmuir 23 (2007) 2126-2132.
8. Q. Zhang, E. E. Remsen, K. L. Wooley, J. Am. Chem. Soc. 122 (2000) 3642-3651.
9. P. P. Ghoroghchian, G. Li, D. H. Levine, K. P. Davis, F. S. Bates, D. A. Hammer, M. J. Therien, Macromolecules 39 (2006) 1673-1675.
10. B. S. Lele, A. S. Hoffman, J. Controlled Release 69 (2000) 237-248.
11. C. J. Hawker, J. L. Hedrick, E. E. Malmström, M. Trollsås, D. Mecerreyes, G. Moineau, Ph. Dubois, R. Jérôme, Macromolecules 31 (1998) 213-219.
12. W. Jakubowski, J.-F. Lutz, S. Slomkowski, K. Matyjaszewski, J. Polym. Sci., Part A: Polym. Chem. 43 (2005) 1498-1510.
13. A. Kowalski, A. Duda, S. Penczek, Macromol. Rapid Commun. 19 (1998) 567-572.
14. H. R. Kricheldorf, Macromol. Symp. 153 (2000) 55-65.
15. M. Trollsås, C. J. Hawker, J. L. Hedrick, G. Carrot, J. Hilborn, Macromolecules 31 (1998) 5960-5963.
16. J. L. Hedrick, M. Trollsås, C. J. Hawker, B. Atthoff, H. Claesson, A. Heise, R. D. Miller, D. Mecerreyes, R. Jérôme, Ph. Dubois, Macromolecules 31 (1998) 8691-8705.
17. G. Moineau, M. Minet, Ph. Dubois, Ph. Teyssié, T. Senninger, R. Jérôme, Macromolecules 32 (1999) 27-35.
18. G. Carrot, J. G. Hilborn, M. Trollsås, J. L. Hedrick, Macromolecules 32 (1999) 5264-5269.
19. Q. Ma, K. L. Wooley, J. Polym. Sci., Part A: Polym. Chem. 38 (2000) 4805-4820.
20. A. Mehta, R. Jaouhari, T. J. Benson, K. T. Douglas, Tetrahedron Lett. 33 (1992) 5441-5444.
21. J. Hu, M. A. Fox, J. Org. Chem. 64 (1999) 4959-4961.
22. J. Shan, M. Nuopponen, H. Jiang, E. Kauppinen, H. Tenhu, Macromolecules 36 (2003) 4526-4533.
23. S. Mourtas, D. Gatos, V. Kalaitzi, C. Katakalou, K. Barlos, Tetrahedron Lett. 42 (2001) 6965-6967.
24. J. Raula, J. Shan, M. Nuopponen, A. Niskanen, H. Jiang, E. Kauppinen, H. Tenhu, Langmuir 19 (2003) 3499-3504.

List of Publications

I. Javakhishvili, S. Hvilsted, Biomacromolecules (2008) 10.1021/bm800860t

Lars Jensen

Phone:	+45 4525 2858
Fax:	+45 4588 2258
E-mail:	lje@kt.dtu.dk
WWW:	http://www.ivc-sep.kt.dtu.dk
Supervisors:	Nicolas von Solms
	Kaj Thomsen

PhD Study

Started:	March 2007
To be completed:	June 2010

Methane Hydrate Growth Kinetics and the Effect of Adding Different Types of Ice-Structuring Proteins

Abstract

Ice-structuring proteins have been shown to be quite effective in inhibiting ice nucleation and growth in the plasma of fish and insects living in cold climates. Gas hydrates are ice-like compounds formed from gas and water at low temperature and high pressure and, these can cause flow assurance problems for the petroleum industry, in particular, which is why efficient inhibitors of gas hydrates have to be used.

In this work, we investigated experimentally whether ice-structuring proteins are also capable of inhibiting the growth of methane hydrate forming structure I hydrate.

Introduction

Gas hydrates are crystalline compounds formed as a result of combination of water and suitably sized guest molecules at elevated pressure and low temperature. Light hydrocarbons; methane-pentane, carbon dioxide and hydrogen sulphide are the guest molecules of interest to the oil and natural gas industry [1]. Depending on the pressure and gas composition, gas hydrates may build up where water coexists with natural gas at temperatures as high as 300 K. Especially long gas transmission lines at cold weather conditions and process equipment are vulnerable to being blocked by hydrate formation causing potential hazards or economical loss.

Inhibition of gas hydrates is a necessity in the oil and gas industry in order to assure a continuous flow of reservoir fluids from the production well to the platform. Traditionally methanol or glycol has been used to inhibit the formation of gas hydrates by shifting the hydrate equilibrium to lower temperatures and higher pressures. Due to the relative large amounts (10-50 wt%) of methanol or glycol needed in the process of hydrate prevention [2] other chemicals capable of inhibiting hydrate formation at much lower doses (<1 wt%) have gained interest [3]. These impact the kinetics of hydrate formation, in contrast to the thermodynamic inhibitors, thus the chemicals are known as kinetic inhibitors.

Kinetic information of hydrate formation is very important if kinetic inhibition is applied as a mean of preventing hydrate formation in transmission lines, valves etc.

Ice-structuring proteins (ISPs) found in animals living at sub-cooling conditions and known to retard the nucleation and growth of ice might have the potential to work as kinetic inhibitors of gas hydrates.

In this work, we experimentally investigated the effect of types of ISPs on the growth of methane hydrate. The ISPs investigated were type III ISP from fish and mealworm, and glycopeptide from Greenland cod. The effectiveness of these ISPs as hydrate inhibitors was evaluated against polyvinyl pyrrolidone (PVP); a well known kinetic inhibitor.

Methods and Equipment

The growth of hydrate is investigated in a high-pressure stainless steel cell. This is done by stirring water and gas at high pressure and low temperature. Formation of gas hydrate will cause the pressure in the cell to drop. The cell has for this reason been attached with a pressure transducer and an electronic mass flow meter which in combination work as a backpressure control system. This will assure that the pressure in the cell will maintain constant during the experiment. The temperature of the cell was controlled by circulating coolant in a jacket surrounding the cell. The temperature was monitored by a platinum resistance probe. The cell was placed on a stir plate thereby allowing a magnet bar to rotate within the cell. Data (P, T and ml gas injected
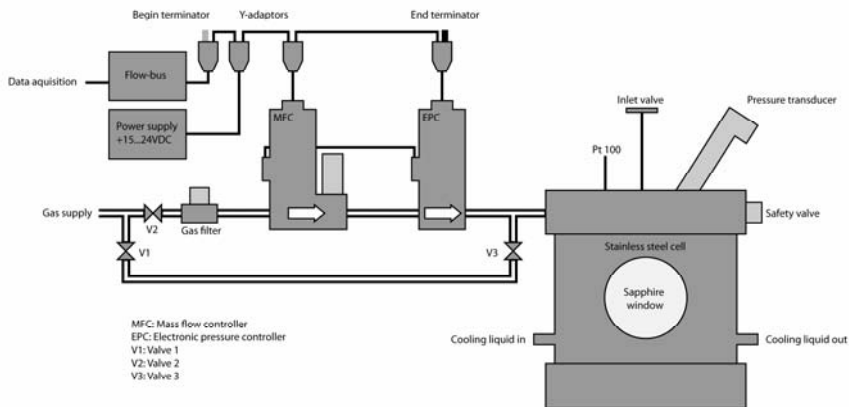
Figure 1: Experimental set-up showing the hydrate cell and the back pressure control and flow measurement system.

to the cell) was recorded continuously on a computer. In figure 1 a schematic of the experimental set-up is shown.

Results

All the experiments were performed at 276.9 K and under constant pressure. The back pressure control system ensured that the maximum deviation between the experimental pressure and the set-point pressure was never more than 0.25 %.Figure 2 shows the methane absorption curve due to methane hydrate growth. The solid points are based on the data obtained from 3 different experimental runs. For visual reasons, not all data points are represented. As expected, the data shows linearity and in general low scattering among the data points is observed. The dashed line indicates the average moles of methane absorbed as found using linear regression. Figure 3 shows the growth pattern of methane hydrate from an aqueous solution containing 0.05 wt% type III fish ISP. We note that two growth periods are quite apparent in the plot and the interface between the periods is found at around 300 min. The dashed line present in growth period 1 indicates the average mole absorption and is based on a second-order polynomial. The dashed line present in growth period 2 indicates the average mole absorption found by linear regression. This growth pattern is in very good agreement with the findings of Al-Adeel and co-workers [4]. In table 1 all experimental results are provided. We note that only the type III fish ISP causes an initial slow growth period to appear.

Figure 2: Moles of methane absorbed into the aqueous phase over time due to the growth of methane hydrate at T = 276.9 K and P = 56 bars. Solid points are the data combined from 3 experiments and the dashed line indicates the average mole absorption. For visual reasons the number of data points presented here has been reduced compared to the number of data points obtained experimentally.

Figure 3: Methane hydrate growth from an aqueous solution containing 0.05 wt% type III fish ISP at T = 276.9 K and P = 56 bars. Solid points are the data combined from 3 experiments and the dashed lines indicate the average mole absorption.

Table 1 Experimental conditions, measured growth rates of methane hydrate (numbers in parenthesis indicate the standard error) and the percentage inhibition of the growth rates by the ice– structuring proteins. The degree of sub-cooling is 4.1 K at 56 bars (Found using the CSMHYD software).

Solution	[C] wt%	Stirring rate (rpm)	Growth period 1 ($y=bx+cx^2$)			Growth period 2 ($y=\alpha x$)		
			Period occurrence (min)	b	c	Period occurrence (min)	Growth rate (mol/min)	Inhibition (%)
Dist. water	-		-	-	-	0-65	$3.16\cdot10^{-4}$ $(1.26\cdot10^{-7})$	-
Dist. water + Type III fish ISP	0.01	450	0-85	$1.21\cdot10^{-4}$ $(6.05\cdot10^{-7})$	$2.61\cdot10^{-8}$ $(8.48\cdot10^{-9})$	85-120	$2.63\cdot10^{-4}$ $(2.12\cdot10^{-6})$	17
	0.05		0-300	$1.06\cdot10^{-5}$ $(6.92\cdot10^{-8})$	$5.65\cdot10^{-8}$ $(3.15\cdot10^{-10})$	300-430	$9.34\cdot10^{-5}$ $(1.99\cdot10^{-7})$	70
	0.1		0-620	$3.63\cdot10^{-6}$ $(2.08\cdot10^{-8})$	$1.00\cdot10^{-8}$ $(4.32\cdot10^{-11})$	620-820	$7.79\cdot10^{-5}$ $(1.53\cdot10^{-7})$	75
Dist. water + Type III Mealworm ISP	0.1	450	-	-	-	0-100	$2.20\cdot10^{-4}$ $(4.41\cdot10^{-7})$	30
Dist. water + Greenland cod ISP			-	-	-	0-100	$2.06\cdot10^{-4}$ $(1.81\cdot10^{-7})$	35
Dist. water + PVP			-	-	-	0-105	$1.92\cdot10^{-4}$ $(3.04\cdot10^{-7})$	39

We note that type III fish ISP decreases the second growth period most extensively while PVP and ISPs of mealworm and Greenland cod has a minor effect on the growth rate. In figure 4 the regressed growth curves of methane hydrate at different concentrations of type III fish ISP and at different stirring rates are presented. It is observed that growth period 1 is prolonged quite substantially when the concentration of type III fish ISP is increased. The ISP also decreases the growth rate of growth period 2 a pattern that seems to also be depending on the ISP concentration. Also we note that the amount of methane absorbed during the non-linear growth period decreases with increasing protein concentration. Another interesting effect observed is that changing the stirring rate will cause both changes to growth period 1 and 2.
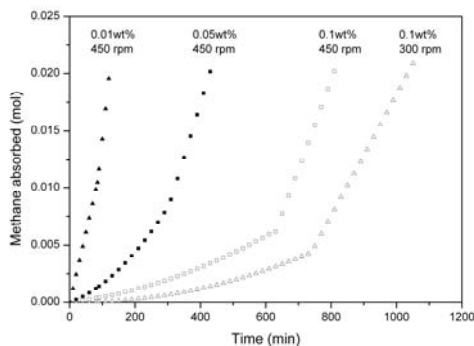
Figure 4: Regressed growth curves of methane hydrate at T = 276.9 K and P = 56 bars at different concentrations of type III fish ISP and at different stirring rates.

Discussion

The slowest growing plane of sI hydrate is the {110} plane whereas the growth along {111} and {100} is more rapid [5, 6]. Different reasons why the {110} plane is slowest have been proposed. Smelik and King [5] argues that since large cages is a result of packing of the smaller cages it is likely that the construction of 5^{12} cages is critical to the formation of hydrate crystals. Because the {110} face has the highest density of 5^{12} cages it therefore results in the slowest growing face. In contradiction to this other studies have shown that it is the completion of the hexagonal ring in the large cages that is the rate determining step. In total there are 48 pentagonal and 6 hexagonal rings per hydrate unit cell leaving a very limited number of hexagonal faces to be represented in the {110} growth plane. This also explains why nucleation and growth of sI hydrate is faster than sII hydrate since sII hydrate has more hexagonal faces [7, 8]. In figure 5 the structure of methane hydrate is represented by linking of five small cages to two large cages looking down on the {001} plane. The small 5^{12} cage has a radius of around 0.4 nm while the larger $5^{12}6^2$ cage has a radius of around 0.43 nm. Whether we assume that growth of methane hydrate is limited by either completion of small or large cages it is obvious that the resulting structure leaves many possibilities for docking of ISPs through hydrogen bonding. The case of binding to incomplete small cages is problematic because it would leave a very high number of possibilities for hydrogen bonding between ISPs and pendant hydrogen atoms in hydrate lattice. To simplify the case we will limit our selves to focus only on the hexagonal face of the large cages.
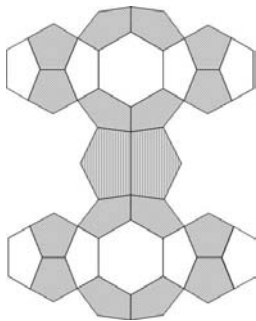
Figure 5: Crystal structure of methane hydrate here represented by linking of five small cages to two large cages in the {001} direction.

Assuming that closure of the hexagonal ring is the rate determining step for growth of hydrate the ISPs have to dock on those faces, and with as many of the repeating threonine groups as possible (These have been found to be responsible for retarding ice growth). The distance from the center of the hexagonal face in the lower large cavity in figure 5 to the center of the hexagonal face in the upper large cage is approximately 1.65 nm. This will give a very good match for docking the 2 repeating threonine groups (0.98 nm between them) of type III fish ISP. It is likely that mealworm ISP will be more restricted in the orientation due to a much smaller distance between the threonines. The results suggest that ISPs with threonine repeating units close to the distance between hexagonal faces exhibits higher inhibitory effect compared to ISPs that does not posses this property.

Conclusion

The result of the study revealed that the ice-structuring protein type III from fish is the overall best inhibitor of methane hydrate growth decreasing the growth rate by up to 75%. The ice-structuring proteins of Greenland cod and mealworm only caused growth rate reductions of around 35 % while polyvinylpyrrolidone in comparison caused a reduction of 39%. Besides being the most efficient growth inhibitor the type III fish ISP also caused the growth profile to change. At constant pressure and temperature growth of hydrates in general exhibits a linear trend however in presence type III fish ice-structuring protein an initial growth period showing second-order polynomial behavior appear followed by a linear growth period. The extension and profile of this initial growth period is concentration dependent. The changed growth profile is attributed to massive adsorption of ice-structuring proteins on the surface of the growing hydrate crystals limiting the surface area available for growth.

To clarify what might cause the differences in the growth patterns observed for the different ice-structuring proteins a comparison study of the structure of the different proteins and their preferred binding planes on ice was performed. In connection to this we carried out a study on the mechanism of hydrate growth identifying what might be the rate determining step, namely the hexagonal ring closure of the large cage. These studies directed us to propose that ice-structuring proteins having threonine repeating groups close to the distance between the centers of each hexagonal face in the hydrate lattice are better growth inhibitors than proteins with a distance between threonine repeating unit that is shorter.

References

1. E.D. Sloan, Clathrate hydrates of natural gases, Marcel Dekker, New York, 1998.
2. Kelland, M., (1995). Studies on New Gas Hydrate Inhibitors, SPE 30420, 531-539.
3. Sloan, E.D., Lederhos, J.P., Long, J.P., Sum, A., Christiansen, R.L. (1996). Effective Kinetic Inhibitors for Natural Gas Hydrates, Chem. Eng. Sci., 51, 1221-1229.
4. Al-Adel, S,. Dick, J.A.G., El-Ghafari, R., Servio, P. (2008). The effects of biological and polymeric inhibitors on methane gas hydrate growth kinetics, Fluid Phase Equilibria, 267, 92–98.
5. Smelik, E.A., King, H.E. (1997). Crystal-growth studies of natural gas clathrate hydrates using pressurerized optical cell, American mineralogist, 82, 88-98.
6. Larsen, R., Knight, C.A., Rider, K.T., Sloan, E.D. (1999). Melt growth and inhibition of ethylene oxide clathrate hydrate, Journal of crystal growth, 204, 376-381.
7. Makogon, T.Y., Sloan, E.D. (2002). Mechanism of kinetic hydrate inhibitors, Proceedings of the 4th International Conference on Gas Hydrates, Yokohama, Japan, May 19-23.
8. Chihaia, V., Adams, S., Kuhs, W.F. (2005). Molecular simulation of properties of a (001) methane clathrate hydrate surface, Chemical physics, 317, 208-225.

Mette Krog Jensen

Phone:	+45 4525 6809
Fax:	+45 4588 2161
E-mail:	mkj@kt.dtu.dk
WWW:	http://www.dtu.dk/Centre/DPC
Supervisors:	Ole Hassager
	Anne L. Skov
	Anders Bach, Global R&D, Coloplast A/S

PhD Study

Started:	November 2006
To be completed:	November 2009

Elongation Tests of Cross-Linked Poly(Propylene Oxide) – Towards the Application as Pressure Sensitive Adhesives

Abstract

The present work focuses on the use of polymer networks as pressure sensitive adhesives (PSA). The purpose is to achieve a tool for the optimization of PSAs by understanding the material response in rheological tests, especially in elongation experiments. It is presumed that uniaxial- and planar elongation are the two types of deformation that are dominating in the removal process of adhesives. In order to measure planar elongational stresses a new test device has been designed as a detachable part to the filament stretch rheometer. It is designed to measure on hollow cylindrical samples in such a way, that only the height and sample thickness changes, while the perimeter remains constant. The new test method was validated with apritcle tracking, where it was found that by a proper balance of the two aspect ratios, $\Lambda_1 = h/d$ and $\Lambda_2 = D/h$, pure planar elongation was indeed obtained. Here d is the initial sample thickness, h the initial height and D the diameter if the cylindrical fixture.

Introduction

Pressure Sensitive Adhesives (PSAs) are probably the most common class of adhesives in consumer products, e.g. self-adhesive tapes and labels of all kinds are ubiquitous products in everyday life. However, the understanding of the rheological properties of the material upon application is limited [1]. It is especially the rheological properties upon removal/debonding of the adhesive that remain as a challenge, and although several studies have focused on such relations there is still a lack of knowledge on the field of interfacial failure mode upon debonding [2].

Most modern PSAs are made of cross-linked polymers to avoid flow. The unique property is simply that there is a difference in the energy gained in forming the interfacial interactions and the energy dissipated during debonding.

The major focus on this study is to achieve a tool for the optimization of PSAs by understanding the material response in rheological tests. In particular it is of interest to understand the behavior in uniaxial and planar elongation since these types of deformation are expected to occur in the removal process. This process is illustrated in a 2D side view in figure 1, where it is seen that the peel front is deformed rather severely.

Researchers have since the 1970's worked on developing instruments for measuring elongational flows [3]. Despite this, experimental work is still dominated by shear flows [4]. In particular the selection of instruments for measuring planar elongation is limited. A new experimental setup has therefore been developed to measure planar elongation on soft polymeric networks which are classified as PSAs.
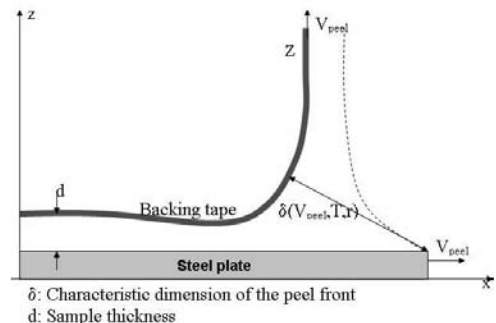
Figure 1: Draft of an idealized peel experiment. The adhesive is peeled in a 90˚ angle from a rigid surface.

Planar Elongation

Planar elongation is a special type of shear free deformation where the velocity field is given by the following:

$$\dot{x} = -\frac{1}{2}\dot{\varepsilon}(1+b)x$$
$$\dot{y} = -\frac{1}{2}\dot{\varepsilon}(1-b)y \qquad (1)$$
$$\dot{z} = \dot{\varepsilon}z$$

$b = 1$ for planar elongation, and thus $\dot{y} = 0$. Hence the fluid elements will only move in the x and z directions. The deformation is illustrated in figure 2 where the height and thickness of the sample change while the length is fixed.
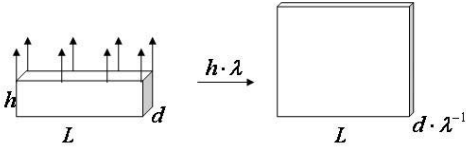
Figure 2: Illustration of planar elongation. Only the height and thickness of the sample changes while the length remains fixed.

In order to achieve this type of deformation a cylindrical fixture as shown in figure 3 is designed. A film of the sample is then wrapped around the fixture, as illustrated, to form a hollow cylinder. The device is designed as a detachable fixture on a filament stretch rheometer (FSR). When applied in the rheometer the upper plate will move with a given strain rate to elongate the cylindrical sample.

Particle tracking will be used to validate the experiments, and to show that it is possible to measure this type of deformation on the fixture.

Sample Preparations

A vinyl-terminated linear poly(propylene oxide) (PPO) is cross-linked with a silyl-terminated f-functional cross-linker with $f \geq 5$. A test sample is prepared such that it will form a gel, i.e. the degree of cross-linking, r, defined as the ratio of silane to vinyl groups, $r = silane/vinyl$, is larger than the lower critical degree of cross-linking [5, 6, 7] given by eq. 2. In order to have a sample that is both very sticky but also coherent enough to handle when it is being applied on the fixture r is set to 0.6.

$$r > r_c = \frac{1}{f-1} \qquad (2)$$

The sample is prepared in a static mixer to avoid air-bubbles in the films. It is hereafter pressed in desired thicknesses in a 100 C hot-press between two sheets of silicone release liner. The sample is then cured at 100 C for one hour to make sure that it is fully reacted before further analysis.

Particle Tracking

Particle tracking is used to determine the local strain rate, $\dot{\varepsilon}^*$, on the sample surface. If the deformation is not planar $\dot{\varepsilon}^*$ will deviate from the imposed strain rate, $\dot{\varepsilon}$. Hence the distinguishing feature of elongational flow, that neighboring fluid elements move relative to each other at an exponential rate, is used. If $\dot{\varepsilon}^* = \dot{\varepsilon}$ then the following is valid [4]:

$$\frac{l(t)}{l_0} = \frac{h(t)}{h} = \exp(\dot{\varepsilon} \cdot t) \qquad (3)$$

$h(t)$ is the plate distance at time t, while $l(t)$ is the distance between two neighboring particles at time t. Four experiments are performed with different aspect ratios, defined as:

$$\Lambda_1 = \frac{h}{d} \qquad \Lambda_2 = \frac{D}{h} \qquad (4)$$
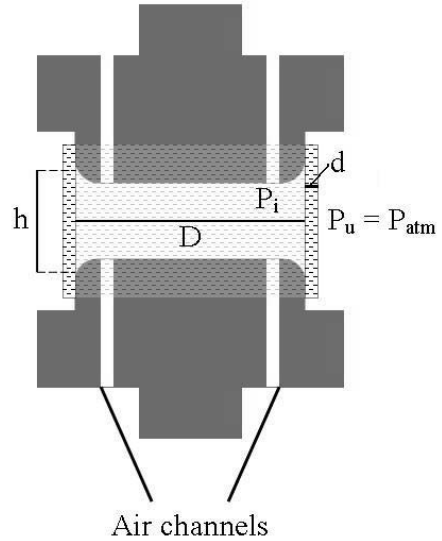
Figure 3: Draft of the planar elongation fixture. D is the cylinder diameter, h the initial sample height and d is the initial sample thickness.

The sizes of the aspect ratios are given in table 1.

Table 1: Test conditions for the four planar elongation experiments performed.

	TEST 1	TEST 2	TEST 3	TEST 4
Λ_1	5	9	27	54
Λ_2	7	4	7	4

The snapshots given in figure 4 are from test 3 at 0, 1, 1.5 and 2 Hencky strain. From this little series of pictures it is possible to see how the diameter changes with time, and it is seen that in this case it barely changes. Red particles are placed on the sample surface and the distance between them will be examined over time. The results obtained from test 1 and 3 are shown in figures 5 and 6. It is seen that as Λ_1 increases the local strain approaches the imposed one. The results for test 2 and 4 show a similar trend with respect to Λ_1. It has now been proved how to obtain a local strain rate that is equal to the imposed one; however it is also important to check whether the cylinder diameter remains constant throughout an experiment. This is tested by changing Λ_2, which also have an influence on the deformation. It is therefore important not to naively increase Λ_1 since it might change Λ_2 in a bad way as well.

In figure 7 it is found how the cylinder diameter changes over time. It is seen that there is a significant difference from test to test. It is especially seen that by increasing Λ_1 in such a way that Λ_2 decreases the diameter will change more compared to the initial outer diameter, which is the fixture diameter plus two times the sample thickness.

Comparing the results obtained in figures 5-7 shows that test 3 gives the best replication of planar elongation. That is because the local strain rate is equal to the imposed strain rate and because the diameter only decreases with approximately 3 % which is negligible.
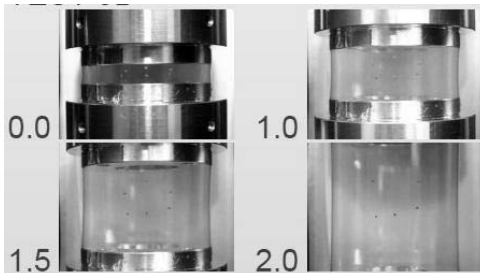
Figure 4: Snapshots of a planar elongation experiment. The snapshots is taken at 0, 1, 1.5 and 2 Hencky strain, .
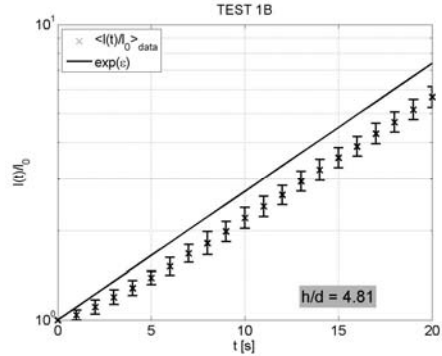
Figure 5: Particle tracking with $\Lambda_1 = 4.81$ and $\Lambda_2 = 7.34$.
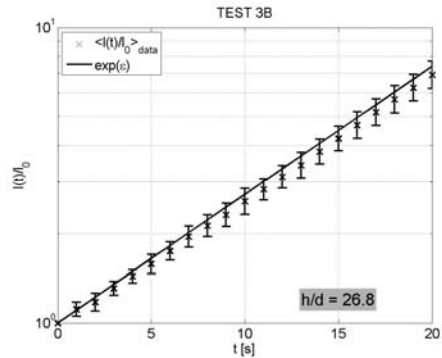
Figure 6: Particle tracking with $\Lambda_1 = 26.8$ and $\Lambda_2 = 7.34$.
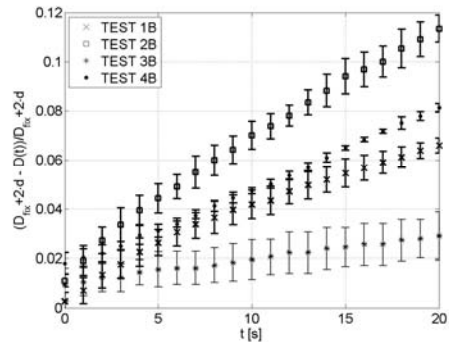
Figure 7: The decrease in cylinder diameter during the four experiments. The diameter is compared to the initial outer diameter, which is the fixture diameter plus two times the sample thickness.

Conclusion

A new test fixture has been designed as an add-on to the FSR. It is made such that the sample to be deformed is a hollow cylinder. Different test conditions have been tested to find an appropriate geometric balance such that the perimeter remains constant and the local strain rate is equal to the imposed strain rate.

Two predefined aspect ratios determined from the relative sizes of the sample and the instrument, Λ_1 and Λ_2 were used for this analysis. And it was found that by increasing Λ_1 it was possible to obtain a local strain rate given by the imposed one. No significant difference was observed when increasing Λ_1 with a factor of two. Hence there is some upper limit where a further increase does not have a visible effect.

It was furthermore observed that by increasing Λ_1 in such a way that Λ_2 decreases could be a bad solution. The reason for this is that the cylinder diameter is sensitive to the size of Λ_2, and the smaller it is the more will the diameter deviate from the initial outer diameter. This means that in order to obtain planar elongation it is important to have a proper balance between Λ_1 and Λ_2. In this case the best result was obtained in test 3, where $\Lambda_1 = 26.8$ and $\Lambda_2 = 7.34$ respectively.

Acknowledgements

References
1. C. Creton, Mrs. Bulletin, 28(6):434-439, 2003
2. C. Verdier, G. Ravilly, J. Pol. Sci. B, 45:2113-2122, 2007
3. J. Meissner, Polymer Engineering and Science, 27(8): 537,1987
4. R. B. Bird, R. C. Armstrong and O. Hassager, Dynamics of Polymeric Liquids, Vol 1: Fluid Dynamics. Whiley Interscience, New York, 1987
5. P. J. Flory , 63:3083–3090, 1941
6. C. W. Macosko and D. R Miller, 9(2):199–205, 1976.
7. D. R Miller and C.W. Macosko, 9(2):206–211, 1976.

List of Publications
1. M. K. Jensen, A. L. Skov, A. Bach, O. Hassager and H. K. Rasmussen, Dansk Kemi, 89(10):14-17, 2008
2. M. K. Jensen, A. Bach, O. Hassager and A. L. Skov, J. of Adhesion and Adhesives, accepted November 2008.
3. M.K.Jensen, O.Hassager, A.L.Skov, A.Bach, Rheology and Adhesive Performance of Soft Polymeric Networks, Proceedings of the XVth International Congress on Rheology, Monterey 2008.
4. M.K. Jensen, O. Hassager, A. Bach, Polymer Networks as Pressure Sensitive Adhesives – Viscoelastic Guidelines, Proceedings of The 31st Annual Meeting in the Adhesion Society.

Dorte Møller Larsen

Phone:	+45 4525 2979
Fax:	+45 45932906
E-mail:	dml@kt.dtu.dk
WWW:	http://www.kt.dtu.dk
Supervisors:	Jørn Dalgaard Mikkelsen
	Jens Christian Frisvad
	Uffe Hasbro Mortensen

PhD Study
Started: August 2008
To be completed: July 2011

Discovery of Thermostable Enzymes for Production of Dietary Fiber and Prebiotics from Plant Material Residues

Abstract

In order to be able to hydrolyze plant materials into specific oligomers, new monocomponent enzymes with high thermostability are needed. The enzyme discovery is going to be fulfilled using approaches involving 1) Fungal screening processes 2) Post-genomic and proteomic data analysis. Uncharacterized proteins are identified, their corresponding genes are generated and expressed. Increased thermostability is obtained by selective mutagenesis from predictive protein modeling. Enzymes are applied in synergy studies for production of prebiotics.

Introduction

The dietary fibre hypothesis implies that a high intake of fibre containing foods is related to a low incidence of many disorders and diseases related to Western lifestyle (e.g. chronic bowel disease, diabetes, coronary heart disease and colon cancer) [1]. Even though, a dietary intake of 25 to 35g per day is recommended, it has been shown that the actual food consumption of dietary fiber tends to be only half of the recommended [2]. A way to overcome this problem is to add specific healthy fiber so-called prebiotics to food products and thereby increase the health for many people.

Conversion of waste materials into useful products such as fibers, oligosaccharides, hydrocolloids and bioethanol is promising concerning transformation of byproduct streams from sugar beet pulp into dietary fibers and prebiotics [3, 4]. In order to obtain those compounds from substrates under reduced energy consumption, hydrolytic enzymes can be used as catalysts. Sugar beet pulp consists of approximately 35% pectin including rhamnogalacturonan I (RGI). In this case, it has already been shown that arabino-oligosaccharides extracted from sugar beet pulp are potential prebiotics. Especially low molecular weight arabino-oligosaccharides (AOS) have proven to increase the growth of beneficial gut bacteria [5].

For controlled production of specific candidate prebiotics, it is a requisite to use monocomponent enzymes to avoid enzymatic side activities that can destroy potential prebiotic structure. RGI is mainly composed of rhamnogalacturon backbone substituted with arabinan side chains of different length and structure [6]. Thus the structure is potential with respect to production of AOS.

An obvious main source of enzymes can be derived from fungi that have been adapted to degrade plant cell walls using their hydrolytic enzyme apparatus as a way to penetrate the plant working either as pathogens or decomposers [7]. Another source of enzymes is post-proteomic data. Their corresponding genes can be generated and expressed in production hosts.

As thermostable enzymes are desired in biorefinery processes reasoned that high temperature gives rise to lower substrate viscosity, easy mixing, better substrate solubility and lower the risk of contamination [8], why it is crucial to focus on optimization hereof.

Specific objectives

- To discover new RGI degradable enzymes by *in silico* and fungal screening approaches focusing on rhamnogalacturonan lyase and arabinase
- To express selected genes in *Pichia patoris* and *Bacillus subtilis*
- To characterize enzymes and elucidate synergistic properties.
- To optimize enzyme thermostability

Characterization and application of enzymes is worked out in corporation with other work packages of The Strategic Research Center "Biological Production of Dietary Fibers and Prebiotics".

References

1. Brennan C.S. and Cleary L.J 2005. The potential use of cereal (1->3, 1->4)-beta-D-glucans as functional food. *Journal of cereal Science* 42:1-13
2. Fagt S.J, Matthiessen A., Biltoft-Jensen M., Velsing Groth T., Christensen H.J., Hinsch H., Hartkopp E., Trolle N., Lyhne N and Møller A. (2004). Udviklingen I danskernes kost 1985-2001 – med focus på sukker og alkohol samt motivation og barrier for sund livstil. *The National Food and Veterinary Institute*, DK.
3. Olano-Marin E., Williams M.R., Gibson G.R. and Rastall R. A. (2003). Pectins and pectic-oligosaccharides inhibit *Escherichia coli* O157:H7 Shiga toxin as directed towards the human colonic cell line HT29. *FEMS Microbiology Lett.* 218:101-105
4. Vernazza C.L., Gibson G.R. and Rastall R.A. 2006. Carbohydrates preference, acid tolerance and bile tolerance in five strains of Bifidobacterium. *Journal of Appl. Microbiology* 100: 846-853
5. Al-Tamimi M.A.H.M., Palframan R.J., Cooper J.M., Gibson G.R. and Rastall R.A. (2005). *In vitro* fermentation of sugar beet arabinan and arabino-oligosaccharides by the human gut microflora. *Journal of Appl. Microbiology* 100: 407-414
6. Buchholt, H. C., Christensen, T. M. I. E., Fallesen, B., Ralet, M. C., & Thibault, J. F. (2004) Preparation and properties of enzymatically and chemically modified sugar beet pectins. *Carbohydrate Polymers,* 58, 149-161.
7. Reignault P.H., Valette-Collet O. and Boccara M. (2007). The importance of fungal pectinolytic enzymes in plant invasion, host adaptability and symptom type. *European journal of Plant pathology* 120:1-11
8. Turner P, Mamo G., Karlson E.N. (2007). Potential and utilizing of thermophiles and thermostable enzymes in biorefinery. *Microbial cell factories* 6:9

LI LI

Phone:	+45 4525 6825
Fax:	+45 45882161
E-mail:	li@kt.dtu.dk
WWW:	http://dpc.kt.dtu.dk
Supervisors	Martin E. Vigild
	Sokol Ndoni, DTU Nanotech
	Lydia D. Clausen, Radiometer Medical ApS
	Kristian M. Hansen, Radiometer Medical ApS

Industrial PhD Study

Started:	Feb 2008
To be completed:	Jan 2011

Nanoporous Polymer Membrane for Biosensors

Abstract

Nanoporous materials derived from self-assembled block copolymers have attracted great interest due to particular features and advantages in various fields. The aim of this project is to investigate thin membranes of nanoporous polymer with adjustable transport properties and develop their potential application as a diffusion-regulating membrane in biosensors. The preliminary work was performed with nanoporous polymers of gyroid morphology. The results obtained from N_2 permeation and glucose diffusion measurements are presented here.

Introduction

Generally, a biosensor consists of two essential parts, a bio-element (that creates a recognition event) and a sensor-element (that transduces the recognition event) [Ref 1-5]. In any case, ultrafiltration plays a critical role in a biosensor and the membrane is a key to implement the function. Biological fluids are often complex mixtures of proteins, electrolytes and cells etc. The interference by unexpected molecules can often happen in the detection process, which negatively influences the desired biochemical and electrochemical reactions. Therefore, it is important to separate the interfering components from the targeted components to alleviate the interference. Permeability and selectivity are important membrane properties in terms of the performance of membranes.

For instance, a glucose enzyme-based membrane system consists of an outer membrane, an enzyme layer and an inner membrane. The outer membrane is expected to protect the sensor against protein adsorption or interferents fouling, filter out certain interfering substances, regulate analytes diffusion, and control passage of oxygen and so on. Especially, the preference is to obtain a linear response of the biosensor via the diffusion limitation.

Many current ultrafiltration membranes are made by phase inversion [Ref 6-8], in which non-solvent components congregate to form particular domains in the matrix. This provides the possibility to control and adjust the diffusion process. The track-etched polymers are also a selection for outer membrane, since the simple characteristic of structure. The particular membrane studied here were nanoporous polymer membrane of gyroid morphology as shown in Figure 1. SEM and N_2 adsorption experiments [Ref 9], were performed to characterize the structure of the gyroid nanoporous membrane. The pore diameter is around 15 nm and the specific inner area 278 m^2/g [Ref 9]. The porosity is around 40% estimated by methanol uptake.
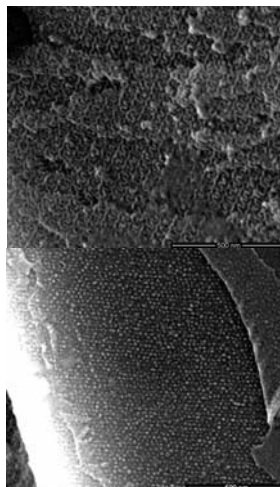
Figure 1: SEM micrographs of the morphology of gyroid nano-porous 1,2-polybutadiene (1,2-PB) membrane. Top panel: The fracture surface parallel to top surface; Bottom panel: The top surface.

In the preliminary work, we started to measure the gas permeation and glucose diffusion properties. We expect

to explore the possibility and even particular advantages of the nanoporous membrane for outer membrane applications in a biosensor. A polyester membrane was used as a reference for this initial work.

Experimental

Membrane preparation:

We used gyroid nanoporous membranes (Figure 1) in the preliminary experiments. The nanoporous membranes are derived from a precursor— diblock copolymer 1,2-PB-b-PDMS. Chemical incompatible 1,2-PB-b-PDMS can undergo phase separation and self-assemble to a gyroid morphology where PDMS is the removable component by selective etching and 1,2-PB is the surviving nanoporous matrix.

To fit to the particular application a thin nanoporous membrane with a thickness of < 10 µm is required. In the early work, we decided to make a composite membrane where the nanoporous membrane is a ~10 µm top layer, dominating the transport performance. The sublayer is a macroporous substrate which has a negligible effect on the performance of the derived composite membrane. A thin free-standing nanoporous membrane is expected in the future work. The main steps of membrane preparation go through film drawing, cross-linking and etching to produce the nanoporosity, and finally an optional step of UV treatment to modify some properties of the nanoporous material. Here, we used a filter paper Whatman 50 (Sigma Aldrich, used as received) as the substrate to support the nanoporous membrane. A 10-µm aluminum foil was used as a spacer to control the thickness of polymer in the drawing step. The details of the fabrication of the composite membrane and nanoporous membrane are described in the previous work [Ref 10-11].

The transport properties of the resulting membranes from each step (denoted as cross-linked, etched, and UV-treated samples) were measured in the gas permeation and glucose diffusion experiments, respectively.

The thickness of the prepared membranes was examined with a micrometer (precision 0.0001 mm). The average thickness of polymer layer is 2 ~ 5 µm, which indicates part of polymer submerged into the filter paper. This might be due to both the roughness of the substrates and the drawn polymer layers. In the analysis of data from the gas permeation and glucose diffusion measurements, the thickness of all the samples are considered as an extreme range of 1 ~ 10 µm.

Gas permeation measurements:

The membranes prepared as described above were used in the N_2 diffusion experiments. The set-up is illustrated in Figure 2. A membrane (red) is placed in the plastic holder (green) to separate the cylinder chamber from the outside. The active diameter of the membrane is 9 mm. It is sealed with rubber ring (blue) and the cylinder tightly closed with metal screws. The top of chamber connects with the source of inlet gas. The applied pressure is controlled by regulator and monitored by manometer (not shown in Figure 2). Soap meter or U-tube is used as detectors to measure the volume of outlet gas through the membrane with time.
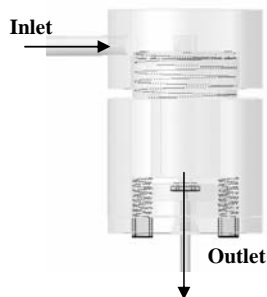
Figure 2: The schematic drawing of the gas permeation set-up.

The permeability of nanoporous membranes is determined from Knudsen flow mechanism.

$$J = \frac{D_K}{RT}\frac{\Delta P}{l} \quad , \qquad D_K = 0.66r\sqrt{\frac{8RT}{M_w}}$$

where J is the gas flux across the membrane of thickness l under applied pressure ΔP.   is the surface porosity and   the tortuosity of membrane. D_K is Knudsen diffusion coefficient, and M_W molecular weight of the measured gas.

The resulting permeability is simply taken as

$$P = \frac{D_K}{RT}$$

From these equations, the theoretic value can be predicted and will be compared with the experimental data in the next section.

Glucose diffusion measurements:

The membrane prepared as above was clamped into the diffusion cells as shown in Figure 3. The set-up contains two chambers separated by the membrane with an active diameter of 4 mm.

As an initial state, the feed cell is filled with 4 ml, 0.5 M glucose solution ($C_0 = C_1(t)$ at t=0). Over time the solution concentraton changes in the permeate cell ($C_2(t)$). For each certain time interval, 50 µl solutions were respectively extracted from both cells and the solutions were analyzed with a reference analyzer provided by Radiometer.

The equations of mass transfer and flux are used to derive the equation which determines the effective diffusion coefficient of the measured membranes.

$$\ln\left(\frac{C_1 - C_2}{C_0}\right) = -\left(\frac{1}{V_1} + \frac{1}{V_2}\right)\frac{AD_{effective}}{l}t$$
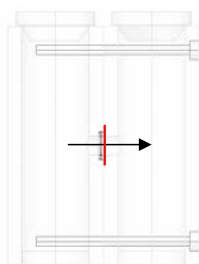
Figure 3: The schematic drawing of diffusion cells. The membrane (red) is clamped between two cells. The rubber ring is used for sealing and four screws are used to tighten the two cells.

The measurement data is plotted as $\ln((C_1-C_2)/C_0)$ *vs.* t, and the effective diffusion coefficient $D_{effective}$ is calculated from the slope.

Results and Discussion

The representative data for N_2 diffusion across the cross-linked and cross-linked + etched (etched) samples are shown in Figure 4.
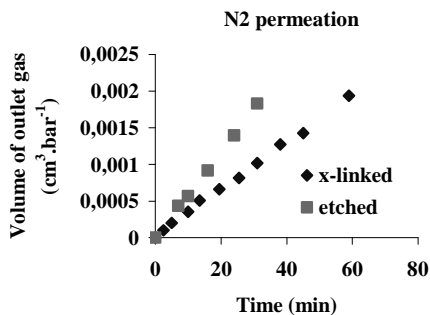
Figure 4: Typical N_2 permeation data for the cross-linked and etched samples.

For the cross-linked and etched membranes without UV treatment, the volume of outlet gas increases linearly with time, which implies the permeability is constant with time and proportional to the slop. However, for the UV-treated membranes, both cross-linked and etched, the volume of outlet gas shows more complex dependence with time. A typical data for UV-treated etched membrane is shown in the Figure 5. Apparently, the permeability of UV-treated samples is much greater than the non-UV-treated samples. In addition, the permeability increases within the measurement time.

The reason is not well-known yet. The experimental permeability for these membranes are summarized in Table 1 and compared with the data given by theoretic prediction.
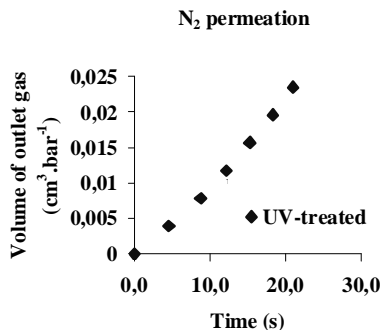
Figure 5: Typical N2 permeation data for the UV-treated etched sample.

The experimental results fall into the range of reference polyester bulk membrane and show potential for using nanoporous polymers as diffusion-limiting membranes. For the cross-linked and etched membranes without UV treatment, the reproducibility of the experiments can be reached within 10% for the same sample, and 23% for the same batch. It is mostly like that the active thickness is not well-defined as mentioned above. Basically, all the results fall in the same order for the same type of membrane.

Table 1: Experimental and theoretic N_2 permeation coefficient for the cross-linked, UV-treated cross-linked, etched, and UV-treated etched membranes.

Membrane	Experimental cm³ cm cm⁻² s⁻¹ Pa⁻¹	Knudsen
Polyester	10^{-15}	-
cross-linked [c]	$10^{-15} \sim 10^{-14}$	-
cross-linked-UV [a, c]	$10^{-13} \sim 10^{-12}$	-
Etched [c]	$10^{-15} \sim 10^{-14}$	10^{-8} [b]
Etched-UV [a, c]	$10^{-13} \sim 10^{-12}$	10^{-8} [b]

[a] The experimental data for UV-treated samples are taken from results at the initial time.
[b] Assuming $= 0.54$, $= 0.29$.
[c] Assuming thickness of membrane within the range of 1 µm~ 10 µm.

It is worth noting that a large discrepancy exists between the experiments and theoretic predictions. When using the Knudsen equation, the surface porosity of nanoporous membrane is assumed to be 0.54 which is calculated from the bulk porosity by $0.4^{2/3}$ and the resulting permeability is 10^{-8}. However, the experimental permeability is 6 or 7 order less than the

values expected from the Knudsen flow equation. This implies that there is a dense layer present in the composite membrane which blocks the porosity, and becomes a diffusion-limiting layer.

Actually, we can also take one data of experimental permeability and use the Knudsen flow to calculate the surface porosity. Other parameters are kept constant. We found that the resulting surface porosity is very little, around 10^{10}. From this aspect, it confirms the presence of a dense layer which probably resides at the surface of the polymer. This assumption is consistent with the SEM micrographs (Figure 1)

The data obtained from the glucose diffusion experiments are plotted as suggested by the equation above, as shown in Figure 6.
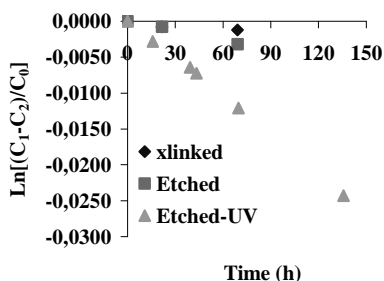
Figure 6: Typical glucose diffusion data for the cross-linked, etched and UV treated etched membranes.

The effective diffusion coefficient is proportional to the absolute value of slope. The slopes for the cross-linked and etched samples are almost zero, because the cross-linked is a non-porous membrane and the diffusion across the bulk material itself is too little to be detected, The effective diffusion coefficient of UV-treated nanoporous membrane is in the order of 10^{-10} which is in agreement with that of track-etched polyester membrane.

Conclusions

From the preliminary work, the composite membrane system shows the positive opening and promise of the nanoporous membrane derived from the block copolymers for biosensor applications. The values of N_2 permeability and glucose diffusion coefficient are within the orders of magnitudes which are requested for these applications. This implies that the nanoporous polymer might provide an interesting alternative material which gives a proper diffusion-limiting separation of analytes.

However, important issues must be investigated and clarified in the future work. For example, the structure characterizations of the composite membranes, the effect and influence of UV treatment seperation functions, and the manufacture of free-standing thin membranes.

References
[1] J. E. Pearson, A. Gill and P. Vadgama, Review article: Analytical aspects of biosensors. Ann Clin Biochem (2000), 37, 119-145.
[2] Saraju P. Mohanty, and Elias Kougianos. Biosensors: A tutorial review. IEEE POTENTIALS (2006), March/April, 35-40.
[3] Seamus P.J.Higson, Subrayal M.Reddy and Pankaj M.Vadgama. Enzyme and other biosensors: Evolution of a technology. Engineering Science and Education Journal Feb 1994.
[4] E. Wilkins and P.Atanasov. Review: Glucose monitoring: state of the art and future possibilities.
[5] S.Zhang, G.Wright and Y.Yang. Materials and techniques for electrochemical biosensor design and construction. Biosensors & Bioelectronics 15 (2000) 273-282.
[6] Mulder, M (2003) Basic principles of membrane technology, Kluwer.
[7] William A. Phillip, Javid R., Jounal of Membrane Science 286 (2006) 144-152.
[8] SiXun,Z. Journal of Polymer Science, Vol.37, 2412-2419 (1999).
[9] Anne Grydgaard and Mathilde Rosendahl Jakobsen, Bachelor Thesis, Characterization of Nano Cavities in Polymeric Materials, (2006).
[10] Ndoni, S., Vigild, M.E., Berg, R.H. J Amer Chem Soc, 125, 44, 13366-7 (2003).
[11] Li Li, report: Surface Modification of Nanoporous Cavities in Crosslinked 1, 2-Polybutadiene Matrices, 2006.

Rasmus Lundsgaard

Phone:	+45 4525 2869
Fax:	+45 4525 2258
E-mail:	RAL@kt.dtu.dk
WWW:	http://www.ivc-sep.kt.dtu.dk
Supervisors:	Georgios M. Kontogeorgis
	Bjarne Nielsen, Danisco A/S
	Ulrik Aunskjær, Danisco A/S

PhD Study
Started: July 2007
To be completed: July 2010

Migration of Plasticisers from PVC and Other Polymers

Abstract

The major objective of this project is to develop an enhanced understanding of the mechanism of migration of plasticisers and similar polymer additives from PVC (and other polymers) into various environments and under varying conditions. The final deliverable of the project will be a model which can not only describe existing experimental migration data but also predict the migration of existing and new plasticisers with very little or no experimental data, thus assisting in the development of new formulations. A qualitative and quantitative understanding of the effect of various factors on migration will be achieved.

Introduction

The ability to estimate diffusion coefficients and migration of plasticisers in highly plasticised Polyvinyl Chloride (PVC) was evaluated against experimental data, based on a migration experiment carried out by the Danish food additive company Danisco A/S in 2005[1]. Migration experiments for estimating diffusion coefficients are very time consuming, so the ability to estimate diffusion coefficients with very little or no data is therefore very important.

Good migration models exist ("KTS-SML" or "FABES-MIGRATEST®EXP"[2]), but they are only as good as the parameters used (i.e. diffusion coefficients and partition coefficients). A new semi-empirical model has been proposed by Dr. Otto Piringer for estimating "worst case scenario" diffusion coefficients, using only three parameters[2].

Experimental

Three plasticiers:
1. GRINDSTED® ACETEM CO 95 (Acetem)
2. GRINDSTED® SOFT-N-SAFE (SNS) [figure 1]
3. Epoxidised soybean oil (ESBO)
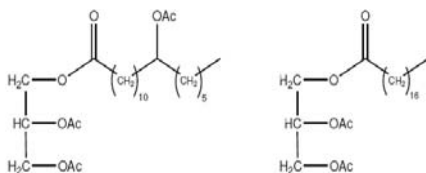
Figure 1: Fully acetylated glycerol monoester based on 12-hydroxystearic acid (85%, left) and on stearic acid (10%, right), the two main components of GRINDSTED® SOFT-N-SAFE[1].

where tested in three different PVC types at three temperatures (20°C, 40°C and 60°C). The sampling was from 30 minutes to 96 hours[1].

The model

The dependence between temperature and diffusion coefficient is normally seen to follow an Arrhenius type equation (equation 1), where D_0 is the temperature independent diffusion constant, E_d is activation energy of diffusion, R is the ideal gas constant and T is the temperature.

$$D = D_0 \exp\left(\frac{-E_d}{RT}\right) \tag{1}$$

The diffusion coefficients of SNS and Acetem seemed to be independent of temperature, when correlated by an Arrhenius type equation. ESBO followed very well the expected tendency of lower diffusion coefficient at higher temperatures, as illustrated in figure 2.

With the semi-empirical model of Piringer it should be possible to estimate diffusion coefficients from only three parameters:

T Temperature
M_r Molecular weight of the migrating additive
A_p Specific polymer matrix parameter

Figure 2: The correlation between experimentally derived diffusion coefficients and temperature for ESBO. Compounds 1,2,3 are the three PVC types used in the experiments.

So knowing the temperature and molecular weight from the ESBO migration experiments it should be possible to obtain the polymer specific parameter for this system, and hence use this parameter to fully estimate diffusion coefficients for Acetem and SNS.

$$D = 10^4 \, exp \left(A_p' - 0.1351 M_r^{2/3} \; 0.003 M_r - \frac{\tau + 10454}{T} \right) \quad (2)$$

In equation 2 the polymer specific parameter A_p is split into to two parts: A'_p and τ ; T is in Kelvin and M_r in g/mol and D is in cm^2/s.

As it can be seen in figure 3 the estimated diffusion coefficients at 20°C is very close to the experimental derived diffusion coefficients (the lower line and circled points). As no temperature dependence was seen for the diffusion coefficients of SNS and Acetem, it was expected that the data points at 40ºC and 60ºC would not follow the model. This can however be explained because of the fast depletion of plasticiser at the higher temperatures. For this reason it is not possible to obtain diffusion coefficients through experiments for these systems.

Figure 3: The estimation of diffusion coefficients of Acetem(M_r = 330g/mol) and SNS (M_r = 500g/mol) from the data of ESBO (M_r = 905g/mol).

	A_p	τ
PVC 1	-4.5	-5140
PVC 2	-5.5	-5667
PVC 3	-6.5	-6160

Table 1: The fitted polymer specific parameters for the Piringer model

	PVC 1		PVC 2		PVC 3	
	D_{calc} [cm^2/s]	Err [%]	D_{calc} [cm^2/s]	Err [%]	D_{calc} [cm^2/s]	Err [%]
20ºC	[·10^{-10}]					
Ace	62.68	-0.09	169.32	0.98	275.71	0.63
SNS	13.44	-0.12	29.84	3.69	59.01	0.06
ESBO	0.71	-0.09	1.61	-1.11	3.18	-0.12
40ºC	[·10^{-9}]					
Ace	19.97	-6.02	39.57	-1.05	70.33	-0.36
SNS	4.28	-6.56	8.47	-1.92	15.04	-4.98
ESBO	0.23	0.25	0.46	2.21	0.81	0.75
60ºC	[·10^{-8}]					
Ace	5.54	19.11	9.92	-20.65	16.03	-16.27
SNS	1.18	-7.85	2.21	-10.47	3.43	-10.09
ESBO	0.06	-0.13	0.11	-1.37	0.18	-0.18

Table 2: The calculated diffusion coefficients of Acetem, SNS and ESBO and the logarithmic error to the experimental diffusion coefficient in percent

Conclusion

With the use solely of migration data from ESBO it was possible to estimate the polymer specific parameters (table 1) and thereby diffusion coefficients of Acetem and SNS for this particular PVC matrix (table 2). As highly plasticised PVC is a very complex system it should be noted that the estimated diffusion coefficients of this method is only of the worst case scenario type, and not necessarily the physically true diffusion coefficients of the system. The EU legislation has approved to use this type of calculation for estimating diffusion coefficients for migration estimation[3].

References

[1] Jensen, T.F., *Migration of plasticizers from PVC to iso-octane*. Danisco research report **2006**.

[2] Piringer, O.G.; Baner, A.L. *Plastic packaging materials for food: barrier function, mass transport, quality assurance and legislation*. Wiley-VCH: Weinheim, **2000**.

[3] Kyprianou, M. *Commission Directive 2005/79/EC of 18 November 2005 amending Directive 2002/72/EC relating to plastic materials and articles intended to come into contact with food*. Official Journal of the European Union. **2005**, *302*, 35

Karin Madsen

Phone: +45 4525 2826

E-mail: kam@kt.dtu.dk
WWW: http://www.chec.kt.dtu.dk
Supervisors: Anker Degn Jensen
                   Flemming Frandsen
                   Joakim Reimer Thøgersen, Haldor Topsøe

Industrial PhD Study
  Started: May 2008
  To be completed: May 2011

Mercury Chemistry in Flue Gas

Abstract
The speciation of mercury in flue gases from combustion processes is important to understand in order to optimize the mercury removal in the flue gas cleaning. An oxidized form favors a high degree of removal because $HgCl_2$ is soluble in water and is effectively removed in a wet scrubber. The vanadium-based selective catalytic reduction (SCR) catalyst has been shown to have catalytic activity in the mercury oxidation. This project is devoted to examining the catalytic oxidation of mercury across the SCR catalyst.

Introduction
Mercury emissions from coal-fired utility plants range from 1-20 $\mu g/Nm^3$ depending on the type of coal applied, the flue gas composition, operating conditions and the air pollution control devices (APCDs) [1].

Three mercury species are normally considered: elemental Hg^0, oxidized Hg^{2+} and particle bound Hg^p. The speciation in flue gasses is important to understand in order to optimize the mercury removal in the flue gas cleaning. Oxidized mercury is soluble in water and is effectively removed in a wet scrubber or by adsorption on fly ash in fabric filters. Elemental mercury is in contrast difficult to capture in existing APCDs due to its high volatility and low solubility.

Figure 1 shows the average partitioning of mercury in different process streams based on studies of power plants in the Netherlands.
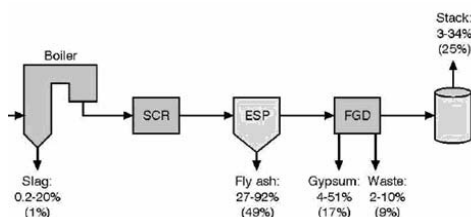
Figure 1: Typical partitioning of mercury in process streams from power plants [2].

Coal mercury is converted to gaseous Hg^0 in the combustion flame and is subsequently partially oxidized as the combustion gas cool. According to thermodynamic calculations all mercury should exist in the oxidized form for temperatures lower than 400°C [3]. Various full-scale and laboratory measurements show that the fraction of oxidized mercury ranges from 35-95%, which indicates that the conversion is kinetically controlled [1].

Mercury chlorination, $HgCl_2(g)$ is generally considered to be the most dominating mercury transformation mechanism. The degree of mercury oxidation is also strongly correlated with the chlorine content in the coal, but many other parameters have been demonstrated to influence the mercury speciation. A fundamental understanding of the reactions taking place in the flue gas is needed in order to predict the mercury speciation.

International research of this type is under way and can generally be broken down into the study of homogeneous gas-phase reaction during quenching of the flue gas and heterogeneous gas/solid reactions with the fly ash. Furthermore, the vanadium-based selective catalytic reduction catalyst (SCR) has been shown to have catalytic activity in the mercury oxidation [4,5].

Specific Objectives
This project is devoted to examining the mercury oxidation across the SCR.

The SCR catalyst in lab-scale experiments has the effect of rendering the mercury speciation at the outlet close to equilibrium. Yet in full scale experiments, mercury in the flue gas does not appear to come as close to equilibrium [6].

The mechanism for the catalytic oxidation across the SCR is not fully understood. In both lab- and full-scale experiments, a positive effect of chlorine and an inhibitory effect from ammonia has been reported [4,5,6]. However, the influence of other flue gas constituents and also of operating conditions is not as unambiguously reported in literature. A better understanding of this complex interplay is needed in order to optimize the oxidation.

Methodology

The work will involve a literature survey on the subject above.

The catalytic reaction will be studied in a laboratory setup at Haldor Topsøe A/S. Here a simulated flue gas containing elemental mercury is passed through an SCR-reactor. The influence from the flue gas constituents HCl, SO_2, NO, NH_3, O2 and H_2O on the oxidation and also the influence of temperature, space velocity and catalyst age will be examined.

Full-scale experiments will be carried out at Plant Crist in Pensacola, Fl, where the mercury conversion across an SCR catalyst will be measured in a slipstream.

Kinetic and thermodynamic modeling will be performed in order to get a better understanding of the mechanism for mercury oxidation on the catalyst.

Conclusions

An increased understanding of the mercury oxidation across the SCR catalyst can potentially be a means of optimizing the mercury removal from flue gasses in existing air pollution control devices.

References

1. J.H Pavlish, E.A. Sondreal, M.D. Mann, E.S. Olson, K. C. Galbreath , D.L. Laudal, S.A. Benson, Fuel Processing Technology 82 (2003) 89-165.
2. R. Meij, H. Winkel, Sci. Total Environment (2006), 368-393.
3. F. Frandsen, K. Dam-Johansen, P. Rasmussen, Prog. Energy Combustion Science 20 (1994), 115-138.
4. R. Mei, L.H.J Vredenbregt, H. te Winkel, Air & Waste Management Association 52 (2002), 912-917.
5. Pilot-scale screening evaluation of the impact of selective catalytic reduction for NOx on mercury speciation, EPRI, Palo Alto, U.S. Department of Energy, Morgantown, Wv, and U.S. Environmental Protection Agency, Raleigh, NC: 2000. 1000755.
6. Communication with C. Senior (2004), Reaction Engineering International, Salt Lake City, UT.

David Mogensen

Phone:	+45 4525 2922
Fax:	+45 4525 2258
E-mail:	dam@kt.dtu.dk
WWW:	http://www.chec.kt.dtu.dk
Supervisors:	Prof. Kim Dam-Johansen
	Prof. Jan-Dierk Grunwaldt
	Jens U. Nielsen, Topsøe Fuel Cell A/S
	Peter Vang Hendriksen, Risø

PhD Study
Started: November 2007
To be completed: October 2010

Mathematical Modeling of Solid Oxide Fuel Cells

Abstract

Solid Oxide Fuel Cells (SOFC) technology is on the brink of commercialization. In order to facilitate continuous optimization of the SOFC stack operation, improve its competitiveness and to integrate it with other technologies, an experimentally verified model is required. The aim of this project is to obtain such a model and implement it in a commercial simulation program. One important aspect embraces internal steam reforming where only little data is available on real Ni-YSZ anode catalysts. Because of this steam reforming kinetics is also investigated in this project.

Introduction

The fossil fuel reserves are limited and because of this, it is necessary to investigate technologies that can be used to make our society independent of fossil fuels [1][2]. SOFC technology is highly versatile since it can use a large number of different fuels either from fossil or renewable sources, such as H_2, CH_4 and NH_3, methanol, dimethylether and diesel [3]. In this way the technology facilitates the transition between these energy sources. SOFCs combined with a gas turbine, which utilizes the high temperature exhaust gasses from the SOFC, can achieve electrical efficiencies of 65%-70% and about 90% total efficiency for a cogeneration plant [4][5][6]. It can also be in a decentralized power supply system since even relatively small units can provide high efficiencies i.e. 60% electrical efficiency and 80% total efficiency for a 3-400 kW system [7].

A SOFC is an electrochemical cell, which is continuously supplied with separated streams of gaseous fuel and air/oxygen. The species that is transported through the solid electrolyte is O^{2-}. Both electrolyte and electrodes in the cell are made of ceramic materials and in order to obtain a sufficient rate of oxygen ion transport through the electrolyte a temperature in the range 600 K to 1000 K is needed. The configuration and materials of a SOFC can be seen in Figure 1. In this case the cathode is composed of strontium doped $LaMnO_3$ (LSM) and LSM on yttria-stabilized zicronia (YSZ), the electrolyte of YSZ, and the anode side of NiO/YSZ [8].
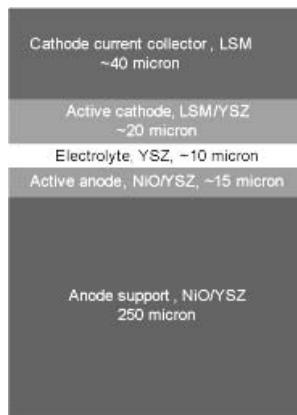
Figure 1: A schematic illustration of an SOFC as produced by Topsøe Fuel Cell A/S [8].

The two main electrode reactions taking place in the cell are shown below.

Anode:
$$H_2 + O^{2-} \rightarrow H_2O + 2e^-$$
Cathode:
$$\tfrac{1}{2}O_2 + 2e^- \rightarrow O^{2-}$$
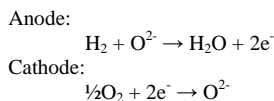
If methane is used as the fuel, it has to be catalytically converted into hydrogen internally in the SOFC by the NiO present in the anode material. [9]

Specific Objectives

The objective of this project is to obtain an experimentally validated model of a SOFC with internal steam reforming. Since the data, from literature, on steam reforming kinetics over Ni-YSZ is very limited, the current objective are to determine the kinetics experimentally.

Results and Discussion

The experiments where conducted in a differential packed bed reactor. The bed consisted of powder from a crushed industrial SOFC anode diluted with Mg-Al-spinel powder. The setup was tested for mass transport effects by varying total flow rate and the particle size of the catalyst powder.

Figure 2 shows the concentrations of CO and CO_2 at the outlet of the reactor for a typical rate determination experiment. The grey reproducibility lines indicate the standard conditions that are used as reference between each set of concentration variations.
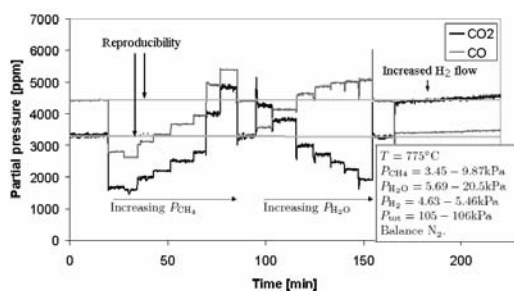
Figure 2: Rate determination experiment.

These experiments have been used to find an expression for the steam reforming kinetics as suggested by Wei & Iglesia [10], for Ni on Mg-Al-spinel, see equation 1.

$$(1) \qquad r = k P_{CH_4} P_{H_2O} \cdot \left(1 - \frac{Q}{K}\right)$$

Where k is the rate constant K is the equilibrium constant and Q is the reaction quotient for the steam reforming reaction. The factor (1-Q/K) accounts for the distance from equilibrium.

α	β	E_a	A
1	0	124 ± 6 kJ/mol	$0.0115 \frac{mol}{g\,Pa\,s}$
0.899	-0.155	123 ± 3 kJ/mol	$0.102 \frac{mol}{g\,Pa\,s}$

Table 1: two possible sets of values of the constants for the kinetic expression

The rate constant is described by an Arrhenius type expression and table 1 shows the values of the activation energy and the pre exponential factor, both for a best fit, and for α=1 and β=0. It should be noted

that a dependence on the hydrogen partial pressure was also observed, this has not yet been fully investigated since a long term dynamic effect occurs after a change in hydrogen partial pressure. This can be seen in the rightmost part of Figure 1. A similar dynamic effect is observed during startup and after temperature changes.

This kind of behavior has not previously been reported on Ni catalysts for steam reforming, even though this system has been thoroughly investigated. It should however be noted that the vast majority of the studies concerning the catalytic activity of Ni with regard to steam reforming, did not use YSZ as the support material [11][12]. Because of this, we expect that the observed dynamic behavior is caused by YSZ and experiments are currently being conducted in order to investigate this possibility.

The primary objective of the project at the moment is to explain this dynamic behavior and also to measure steam reforming kinetics on a SOFC structure.

References

1. M. Asif, T. Muneer, Renewable and Sustainable Energy Reviews 11 (2007) 1388-1413.
2. http://www.iags.org/futureofoil.html, 30/11-2007.
3. N.Christiansen, J. B. Hansen, H. Holm-Larsen, S. Linderoth, P.H. Larsen, P.V. Hendriksen, M. Mogensen, Fuel Cells bulletin 8 (2006) 12-15.
4. A. Selimovic, Solid Oxide Fuel Cell Modelling for SOFC/Gas Turbine Combined Cycle Simulations, doctoral thesis, Lund University, 2002.
5. J. Pålsson, A. Selimovic, L. Sjunneson, Combined solid oxide fuel cell and gas turbine systems for efficient power and heat generation, Journal of Power Sources 86 (2000) 442-448.
6. V. Dorer, R. Weber, A. Weber, Energy and Buildings 37 (2005) 1132-1146.
7. A. F. Massardo, Transactions of the ASME. Journal of Engineering for Gas Turbines and Power 124 (2002) 110-116.
8. http://www.topsoefuelcell.com/, 27/11-2007.
9. W. Vielstich et al., Handbook of Fuel Cells, John Wiley & Sons Ltd, 2003 ISBN: 0-471-49926-9.
10. J. Wei, E. Iglesia, Journal of Catalysis 224 (2004) 370-383
11. S. H. Clarke et al., Catalysis Today 38 (1997) 411-423
12. J. R. Rostrup-Nielsen, J. Sehested, and J. K. Nørskov., Advances in Catalysis 47 (2002) 65–139,

Merlin Alvarado-Morales

Phone:	+45 4525 2981
Fax:	+45 4593 2906
E-mail:	mal@kt.dtu.dk
WWW:	http://capec.dtu.dk
Supervisors:	Rafiqul Gani
	John M. Woodley
	Krist V. Gernaey

PhD Study

Started:	April 2007
To be completed:	March 2010

Sustainable Bioprocess Synthesis, Design and Analysis

Abstract

Biorefineries have an important role to play in sustainably supplying the chemical and energy needs of society and in mitigating the environmental effects of fossil fuels and their rapid depletion. There is an urgent need to bring commercially viable and technically effective biorefineries on stream as quickly as possible, in order to address these concerns, and to ease the transition from an oil-profligate to an oil-depleted world. The use of a systematic methodology to analyze and improve processing routes for a specific biorefinery product is therefore a useful first step in the evaluation of the biorefinery product tree. A systematic methodology supported by computer aided methods and tools for synthesis, design and analysis of bioprocess is proposed.

Introduction

Biorefineries have an important role to play in sustainably supplying the chemical and energy needs of society and in mitigating the environmental effects of fossil fuels and their rapid depletion. There is an urgent need to bring commercially viable and technically effective biorefineries on stream as quickly as possible, in order to address these concerns, and to ease the transition from an oil-profligate to an oil-depleted world. However, in competing with existing petrochemical and energy industries, biorefineries face a double disadvantage. First, despite unstable oil prices, oil and other fossil fuels remain cheaper than alternative biomass-based feedstocks. Secondly and less well recognised, oil refineries and the chemical industries to which they supply feedstocks have benefited for several decades from the application of process integration principles and approaches and the availability of sophisticated software packages embodying these design principles. This makes oil refineries and many chemical processes highly efficient, benefiting from cost and energy savings through extensive integration within complex processes. Emergent biorefineries do not have access to equivalently sophisticated process design and integration tools and do not yet enjoy this cost and energy benefit. In this respect, oil refining provides both the competition and the model for the design of biorefineries. There is a need for a systematic methodology capable of evaluating an integrated process in order to identify the optimal set of products and the best route for producing them enhancing the energy efficiency and economic competitiveness of the whole process. Hence, the use of a systematic methodology to analyze and improve processing routes for a specific biorefinery product is therefore a useful first step in the evaluation of the biorefinery product tree. In this project, we highlight the use of a systematic methodology for design and analysis supported by a collection of computer aided methods and tools particularly suitable for calculations involving biorefinery processing routes. In order to illustrate these tools we have selected bioethanol production from lignocellulose as an example. We have chosen this example due to the wealth of data already available. Here we discuss the essential features of a biorefinery, describe a systematic design methodology and introduce some of the tools prior to an analysis of the bioethanol production from lignocelullose. Although we have illustrated the methodology on one single example, we believe the tools to be generic.

Systematic Methodology for Design/Analysis

The goal for the systematic methodology we propose is to determine more sustainable alternatives to an established production route of a biorefinery product. The main stages in the proposed methodology are depicted in figure 1 and briefly described below.

- Available process knowledge data collection (**establish base case design**)
- Modelling and simulation of the base case design (**generate data for analysis**)

- Analysis of important issues (**define targets for design alternatives**)
- Process synthesis and design (**generate design alternatives, that match the targets**)
- Performance evaluation and selection (**identify sustainable design alternatives**)
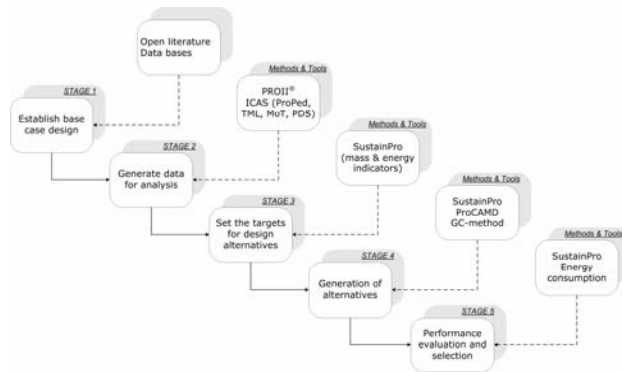
Figure1: Main stages in the systematic methodology.

Case study: Bioethanol production process

The base case design corresponds to a bioethanol production process documented by National Renewable Energy Laboratory (NREL) (Wooley *et al.*, 1999). The main process operations are highlighted in figure 2 and a briefly description is given below.
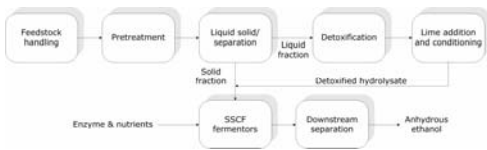
Figure2: Base case: bioethanol production process flowsheet from lignocellulosic biomass based on the NREL process [9].

Feedstock handling: The feedstock, in this case hardwood chips, is delivered to the feed handling area for storage and size reduction.

Pretreatment: The goal is to make cellulose more accessible to enzymatic hydrolysis by using dilute sulfuric acid at elevated temperature and solubilize the hemicellulose sugars. After the pretreatment the hydrolysate slurry is separated into liquid and solid fractions. Detoxification is only applied to the liquid fraction.

Detoxification, lime addition, and conditioning: The goal is to eliminate the inhibitor compounds formed in the pretreatment area by ion exchange and then adjust the pH by means of lime addition for the subsequent processing step.

Simultaneous Saccharification and Co-Fermentation (SSCF): Two different operations are performed in this area, saccharification of the remaining cellulose to glucose using enzymes and the fermentation of the resulting glucose and other sugars to ethanol using an inoculum of bacteria.

Downstream separation: This step consists of separation of ethanol from water and some residual solids. A mixture of nearly azeotropic composition ethanol and water resulting from a first distillation step is further purified to anhydrous ethanol using molecular sieves.

Generate data for analysis

The overall flowsheet was simulated using the PROII® simulator supported by ICAS-tools (Gani, 2002). Part of the physical property data for simulation were obtained from Wooley *et al.* (1999), and others were estimated by the method of Marrero and Gani (2001) for pure component property estimation. The feedstock composition and operation conditions were taken from Wooley *et al.* (1999), as well as the description of the chemical and biochemical reactions taking place during the process. Each part of the process (see figure 1) has been analyzed in detail, including also a breakdown of the operating and capital costs of the different parts of the bioethanol production process. Once the operational and equipment costs were determined, the manufacturing cost of the bioethanol production process was calculated. First, process economy and process points where the base case design can be improved were analyzed.

Define targets for design alternatives

Economic analysis: The main characteristics of the base case are summarized in table 1 and figure 3 shows the breakdown of the total manufacturing cost where each percentage represents the contribution of each process area to the total manufacturing cost. Based on economic analysis, it has been identified that the economic feasibility of the process for ethanol can be improved through higher product yields and/or more efficient product recovery.

Table 1: Main characteristic of the base case design.

Ethanol Production rate	52.7	Mgal/y
Purity	99.95	% wt
Operating hours	8406	h/y
Enzyme cost	1.5	$/kg
Total equipment cost	49.05	M$
Total manufacturing cost	101.39	M$/y
Total manufacturing cost	1.92	$/gal

The option of increased product yield in the reaction is beyond the scope of this work as it involves the design/selection/testing of new enzymes and microorganisms.
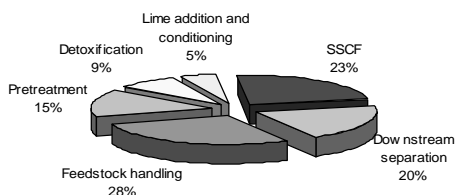
Figure3: Breakdown of the total bioethanol manufacturing cost.

Indicator-based analysis of process flowsheet: The *SustainPro* software has been applied to the base case to generate sustainable alternatives. *SustainPro* performs a flowsheet decomposition based on identification of component mass and energy "paths" (open- and closed-paths) in order to calculate a set of mass and energy indicators that trace the paths of the component "mass-flows" and "energy-flows" as they enter and leave the process. *SustainPro* then identifies the points that allow the best improvements in the process through sensitivity analysis. In this way the target indicators are selected and local sensitivity analysis is subsequently performed to determine the design and the operational parameters that influence the targets. For the process flowsheet and the results of the mass and energy balances, *SustainPro* calculated 3437 Open-Path (OP) indicators. Since the process flowsheet does not have any recycle streams, there are no Closed-Path (CP) indicators. Table 2 lists the indicators for the OPs with the highest (absolute) indicator values (highest sensitivity). The second line of each path states the component and OP it refers to.

Table 2: List of the most sensitive indicators for the Open-Paths (OP's).

		Indicators		
Path	Prob.	MVA (10^3\$/y)	EWC (10^3\$/y)	TVA (10^3\$/y)
OP-576 Lignin 1-51	High	-2146		
OP-1807 H_2O 14-51	High	-107.2	8084	-8191

Analyzing the indicators from table 2, it can be seen that there is a large waste of the raw material and utilities. For example, the MVA (material value added) indicator corresponding to OP 576 indicates that the raw material in the form of lignin is being wasted (because the MVA has a large negative value). For OP 1807, the EWC (energy and waste cost) is 8084 while the TVA (total value added) is -8191. This indicates that water in this stream uses a lot of energy (positive EWC) and is losing its value (negative TVA) as it enters and leaves the process. The *SustainPro* sensitivity analysis then indicates that the OP 1807 is the most likely to result in an improvement in terms of TVA (water use) and EWC (energy and waste cost due to use of water).

Generate design alternatives
Based on economic and sustainability analysis, two options have been considered reduction of water (in order to reduce the open-path MVA values) and alternatives for downstream separation (in order to improve process energy and operating costs, without increasing the environmental impact).

Reduction of water: The first attempt to generate alternatives was to identify possibilities of reducing the TVA in OP 1807 (see table 2) by reducing the amount of water leaving the system (that is, minimizing the fresh water requirement with respect to OP 1807). A feasible solution for reduction of fresh water consumption is by treating the water after the beer distillation, and by recycling the treated water to the process. After adding this recycle and water recovery step, and recalculating the indicators, *SustainPro* confirms that the TVA for water has indeed been improved, thereby improving the sustainability metrics related to waste. Table 3 lists the new values of the OPs for the MVA, TVA, and EWC indicators.

Table 3: New values of the indicators for the new flowsheet alternative (with water recycle).

		Indicators		
Open-path	Compound	MVA (10^3\$/y)	EWC (10^3\$/y)	TVA (10^3\$/y)
1297[†]	Water	-6.1	288.5	-294.6
1807[‡]	Water	-107.2	8084	-8191

[†]New design; [‡]Base case design

Note that the amount of water needed by the pre-treatment, detoxification and SSCF operations has not been reduced. As a consequence the EWC indicator has not been reduced, indicating that this process improvement (with respect to recycling water) will not improve the energy efficiency, and therefore, the subsequent life cycle assessment (which is primarily based on energy usage).

Downstream separation: The downstream separation can be defined in this case as the separation task related to obtaining anhydrous ethanol from an ethanol-water

mixture. Two options to be considered (and evaluated) are the use of organic solvents and ionic liquids. The calculated energy consumption for different alternatives for the solvent-based separation problem using the group contribution (GC) method is listed in table 4. The results from table 4 show that two of the solvents reported by Seiler *et al*. (2004) have also been independently found in this work through the application of the CAMD technique (Harper *et al*. 2000). In the case of alternative 1 the energy consumption predicted by the GC method is slightly better than the one reported by Seiler *et al*. (2004). Compared to alternative 3, using the GC-method, a better option (alternative 4) than the one reported by Seiler *et al.* (2004) has been found. This is because alternative 4 uses a higher driving force than alternative 3 as it can be seen in figure 4, representing a reduction of 10.2% with respect to energy consumption. Among the generated (feasible) alternatives, the best alternative in terms of energy consumption is predicted by the combined driving force-process group method of d'Anterroches and Gani (2005) and corresponds to alternative 6. This alternative represents in terms of energy consumption a reduction of 21.9 % in
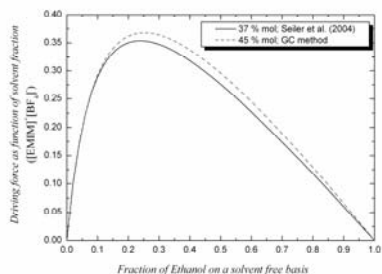
Figure4: Driving force comparison between alternative 3 and 4.

comparison with alternative 3. However, it is not practical to implement this alternative due to its high environmental impact. In this case, alternative 7 would be a better option.

Table 4: Design alternatives results.

| Alternative | x_{sol} | df | Energy consumption (MkJ/h/kmol) | |
			Predicted energy[†]	[‡]Energy demand
EG (1)	0.52	0.48	0.0317	0.0335
Glycerol (2)	0.63	0.48	0.0322	
[EMIM][BF$_4$] (3)	0.37	0.35	0.0352	0.0333
[EMIM][BF$_4$] (4)	0.45	0.37	0.0299	
[BMIM][Cl] (5)	0.30	0.37	0.0402	
[BMIM][Cl] (6)	0.45	0.42	0.0260	
[EMIM][EtSO$_4$] (7)	0.40	0.31	0.0386	

[†]Predicted energy by GC method; [‡]Energy demand [9].

Conclusions

The proposed systematic methodology provides a useful approach in the search for more sustainable alternatives to already established biorefinery production routes. On the one hand, the use of the group contribution method in the generation and test of feasible downstream separation design alternatives for the bioethanol production process has been highlighted. The ability to predict a flowsheet property of a flowsheet structure, in this case the energy consumption without any rigorous simulation offers many advantages as it opens the possibility to screen a lot of process alternatives very quickly and with a good accuracy as it demonstrated. On the other hand, the use of sustainability metrics has been highlighted as set of performance criteria in the search of more sustainable alternatives.

Although we have only illustrated the methodology with one case-study, it should be emphasized that the presented tools are generic. Thus, the production route for many new biorefinery products can now be systematically analyzed and improved using this methodology. Therefore, the future work is mainly related to test the methodology with case studies representing challenging product-process design problems from bioindustries.

References
[1] L. d' Anterroches and R. Gani, 2005, Fluid Phase Equilib., 228-229: 141–146.
[2] A. Carvalho, H. Matos, R. Gani, 2008, Process Saf. Environ. Prot., 86: 328-346.
[3] R. Gani, 2002, ICAS documentation. CAPEC, Technical University Of Denmark
[4] R. Gani, E. Bek-Pedersen, 2000, AIChE J., 46(6), 1271-1274.
[5] P.M. Harper, R. Gani, 2000, Comput. Chem. Eng., 24(2), 667-683.
[6] J. Marrero and R. Gani, 2001, Fluid Phase Equilib., 183-184: 183-208.
[7] PROII User's Guide (2006) Simulation Sciences Inc, Brea, USA.
[8] M. Seiler, C. Jork, A. Kavarnou, W. Arlt, R. Hirsch, 2004, AIChE J., 50(10): 2439–2454.
[9] R. Wooley, M. Ruth, J. Sheehan, K. Ibsen, H. Majdeski, A. Galvez, 1999, NREL, Golden, CO.

List of Publications
[1] M. Alvarado-Morales, N. Al-Haque, K. V. Gernaey, J. M. Woodley, R. Gani, ESCAPE 18, CAPE Methods and Tools for Systematic Analysis of New Chemical Product Design and Development, Lyon, France, 2008.

Ricardo Morales Rodríguez

Phone:	+45 4525 2911
Fax:	+45 4525 2906
E-mail:	rmr@kt.dtu.dk
WWW:	http://www.capec.kt.dtu.dk/
Supervisors:	Rafiqul Gani

PhD Study
Started: February 2006
To be completed: January 2009

Multiscale Modelling Framework for Chemical Product-Process Design

Abstract

The objective of this project is to present a novel computer-aided model-based framework for product-process design that also includes multiscale modelling features. To develop this framework, a combination of different computational tools, such as, property prediction packages, modelling tools, simulation engines, solvent selection software, etc, are necessary together with a set of established systematic work-flow and data-flow for various types of design problems. This framework allows the user to cover a wide range of problems at different scales (of length and time) and disciplines of chemical engineering and science in a easy and efficient manner; achieving in this way the development of a product-process with the desired end-use characteristics. Development of a pesticide formulation, fuel cell design and microcapsules controlled release are employed to highlight the work-flow and data-flow in the multiscale modelling framework.

Introduction

The design, development and reliability of a chemical product and the process to manufacture it, need to be consistent with the end-use characteristics of the desired product. One of the common ways to match the desired product-process characteristics is through trial and error based experiments which can be expensive and time consuming. An alternative approach is the use of a systematic model-based framework according to an established work-flow in product-process design, replacing some of the time consuming and/or repetitive experimental steps. Furthermore, for many chemical products the appropriate models for product-process design need to have multiscale features as the properties defining the chemical structure and the product end-use characteristics are dependent on parameters of different size and time scales. The advantages of the use of multiscale modelling approach in this case is that in the design, development and/or manufacturing of a product-process and knowledge of the applied phenomena, can be provided at diverse degrees of abstractions and details; furthermore of the multidiciplinary approach in product-process design and identified design issues related to different scales of size, time and complexity.

The development of a computer-aided framework for product-process design including a multiscale modelling option is very important for analysis, design, and/or identification of feasible chemical product candidates because it allows one to consider processing issues during the development of the product. The multiscale modelling framework should include the product and process design components, modelling tools and templates (work-flow) for guiding the user through the appropriate design steps. The integration of computational tools is also necessary to increase the application range of the computer-aided product-process framework; where the connection between computational tools could be established through well-defined COM-objects or the CAPE-OPEN standards.

Objective of the PhD

A novel computer-aided model-based framework for product-process design, that also includes multiscale modelling features, is developed in this project. To develop this framework, a combination of different computational tools, modelling tools, simulation engines, molecular and mixture design software, solvent selection software, etc, are integrated within a set of established systematic work-flow and data-flows for various types of design problems. This framework allows the user to cover a wide range of problems at different scales (of length and time) and disciplines of chemical engineering and science in a easy and efficient manner; achieving in this way the development of a product-process with the desired end-use characteristics. The performance of the multiscale model-based framework, the associated models and the work-flow for a specific product-process design is illustrated through a

case study involving the modelling and design of a pesticide product (pesticide uptake inside the leaf is designed and evaluated through the use of the framework) and a direct methanol fuel cell, where a model-based, database of properties and compounds as well as modelling tools are employed.

Multiscale Modelling Framework for Chemical Product-Process Design: Needs

Figure 1 illustrates the multiscale modelling framework for chemical product-process design where four main parts can be found: problem definition, product design, product-process modelling and product-process evaluation; each of them have sub-steps that guide the user through a systematic work-flow and data-flow.
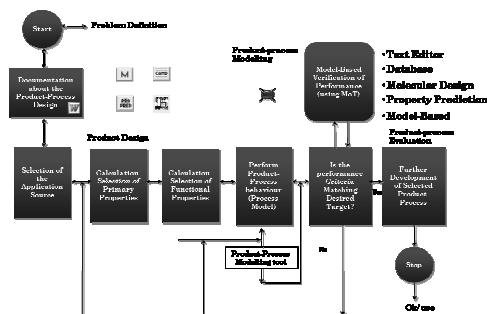
Figure 1: Multiscale Modelling Framework for chemical product-process design

Multiscale modelling framework for chemical product-process design starts with the definition of the design problem, which concerns setting the desired characteristics of the product, its properties, special qualities, etc., that might apply for a new product or even for existing products that needs to be improved.

The next part is the product design step where a sub-step of data/knowledge generation of appropriate documentation related with the needs, ingredients, etc., of the product are written down for future examination; other sub-steps in this second part consists of the selection of the materials for the product, the main ingredients, solvents, etc., as well as the calculation of the necessary product properties to be used during the prediction of the product performance. A lack of information needed to perform the product behavior analysis, is however frequently encountered. To overcome these gaps of information, computer-aided methods and tools are employed. That is, the use of specialized computer-aided tools such as, databases of property compounds, property prediction packages, molecular and mixture design software, solvent selection tools, etc. (all these computational tools can be found in ICAS software developed by CAPEC at Technical University of Denmark).

Once, the necessary information for evaluating the performance of the product behavior has been retrieved, a modelling tool can assist for the simulation and generation of alternatives and verification of the

formulated properties through the use of ICAS-MoT (also available in ICAS), that essentially is a modelling tools able to generate, analyze and simulate mathematical models without extra programming efforts. Afterwards, predicted product behavior is compared and a sustainability analysis might be performed in order to evaluate the environmental and economical impact for the production and performance of the product.

Another of the needs in the modelling framework is the software architecture that provides the means for integration and merging of methods and tools from different sources.
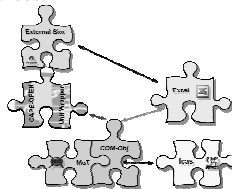
Figure 2: Integration of computational tools.

This architecture needs to accommodate models used for the prediction of the product behavior/performance. Here, ICAS-MoT is the main modelling tool, which is able to have an interaction (see figure 2) with modelling engines, external software through the use of COM-objects, and also with external simulators through with the use of CAPE-OPEN standards. More details about this synergy is described by Morales-Rodríguez et al. [4].

Multiscale Modelling, what is it?

Multiscale modelling approach basically consists of the division of a complex problem/model into a set of sub-problems/models that are described at different scales on length or/and time, in order to improve the degree of details of the phenomena that the set of mathematical model is describing in product-process design.
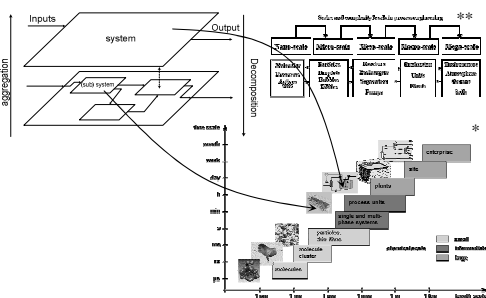
Figure 3: Multiscale modelling structure, chemical supply chain [1]*, scales and complexity levels in process engineering [2]**

Figure 2 illustrates the classical multiscale modelling structure, chemical supply chain and finally, the scales and levels in process engineering. This figure is useful to explain how multiscale modelling works; for example, block-system is depicting an unit operation at

the meso-scale level (reactors, exchangers, separators, pumps and so on) what is described for a mathematical model and also provided results of the behavior of the unit operation. Further details of some properties included in this unit are obtained if a connection between block-system and sub-system exist. This further description at the micro-scale level (particles, droplets, bubbles, eddies and so on) allow to get more fundamental knowledge with more details of the phenomena taking place at different scales.

Application of Multiscale Modelling Framework: Virtual Product-Process Design Lab

A software called the "Virtual Product-Process Design Lab" has been developed by implementing the model–based framework for chemical product-process design. Currently, the software contains model-based libraries for design/analysis of controlled release, pesticide uptake, fuel cells and microcapsule controlled release.
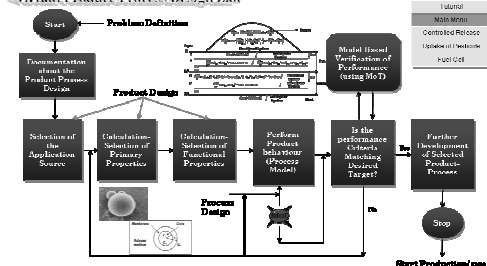
Figure 4: Virtual Product-Process Design Lab.

Pesticide Uptake Design.

The pesticide uptake example has been chosen due to its multiscale features from the modelling point of view.
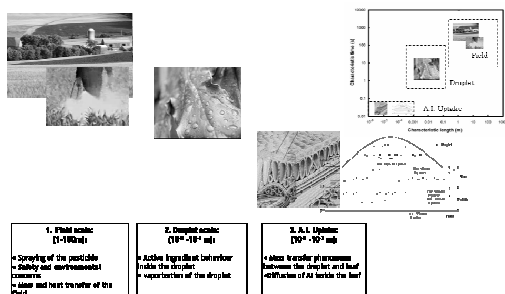
Figure 5: Multiscale description of pesticide uptake.

Figure 5 shows that the modelling of the pesticide uptake can be carried out in a complete field that basically corresponds to the macroscale; an analysis in a droplet scale can be also performed, that is, the behavior of the active ingredient inside the droplet as well as the vaporization of the liquid phase can be predicted and play an important role in pesticide uptake; further details can be analyzed in a smaller scale (the behavior of the pesticide uptake inside the leaf can be predicted),

here, the pesticide mass transfer phenomenon between the droplet and the leaf as well as inside the leaf are important issues to consider.
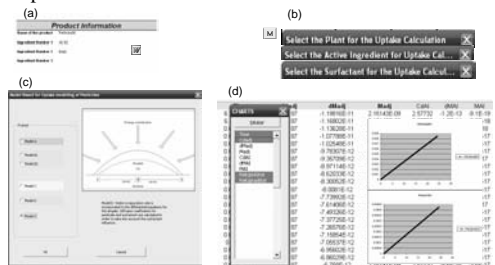
Figure 6: Design of a pesticide using the Virtual Product-Process Design Lab.

Implementation of this pesticide uptake design/problem has been done in "Virtual Product-Process Design Lab". Figs. 6a-6d depict the workflow for the design of one pesticide and the models needed at various scales - the droplet scale to the pesticide uptake. Figure 6a shows the step where the generation of information related with the product is carried out and also saved in a documentation file. Figure 6b shows the selection of the plant where the pesticide will be applied, also the selection of the pesticide to be used in the designed product as well as the surfactant. All the information that is collected in this part is transferred to the modelling tool. Figure 6c shows the different mathematical models [3] that are stored in the model-based library, each model take into account different phenomena as well as different assumptions allowing the user have a wider range of applicability in the pesticide design, this one of the most important part of having a large model-based library. Once the virtual design has been done, a product behavior performance evaluation is carried out; Figure 6d depicts the results highlighting the calculated amounts of pesticide uptake by the leaf. Here, it is allowed to ask if the performance criteria have been satisfied. If "Yes" a new product alternative has been developed and verification by experiment can be performed, if necessary. Otherwise, it is possible to return to the appropriate product design step and repeat with other options until the desired performance criteria are matched.

The size of the mathematical model depends on the scenario being evaluated and the number of discretization points. The model consists of a set of differential and algebraic equations representing the phenomena of evaporation rate of the droplet, mass transfer of pesticide and solvent through wax and cuticle layers of the leaf. It is important to note the multidisciplinary nature of the problem (different sources of information from different parts or fields of science, for instance, the information about the leaf conformation, diffusion coefficients for biological systems, weather conditions that effect in the behaviour

of the plant, etc.) and the multiscale characteristics of the model.

Direct Methanol Fuel Cell Design.

A design of a direct methanol fuel cell is also illustrated using the virtual product-process design lab.
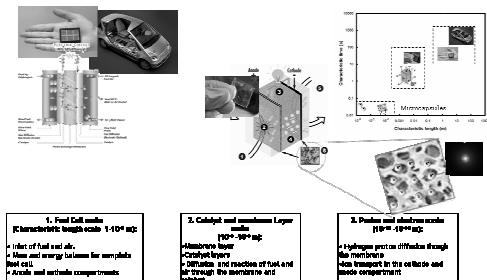
Figure 7: Multiscale description of fuel cell.

Figure 7 shows that the modelling of fuel cell can be carried out to see the performance of one car, battery, etc., which basically corresponds to the macroscale; an analysis in the membrane and catalyst layer can be also performed, that is, the behavior of the mass transfer and chemical reactions are important a this level of abstraction; further details can be analyzed in a smaller scale, for example the charge transfer between inside the membrane that belongs to the nano-scale.
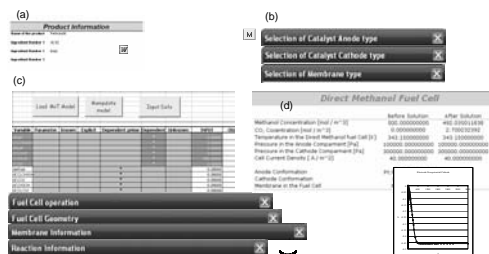
Figure 8: Design of a fuel cell using the Virtual Product-Process Design Lab.

The application of the design of the direct methanol fuel cell using the virtual lab starts with the generation of information related with the product that is made (see figure 8a). Figure 8b shows the selection of the material for the catalyst layers at the cathode and anode as well as the material of the membrane that want to be used. All the information that is collected in this part is transferred to the modelling tool. Figure 8c shows the computer-aided modelling tool that helps in the solution of the problem, this interface helps to the user to solve the problem in a easier way. Once the virtual design has been done, a product behavior performance evaluation is carried out; figure 8d depicts the results of the design of the fuel cell. Here, again it is allowed to ask if the performance criteria have been satisfied. If "Yes" a new product alternative has been found and verification by experiment can be performed. If "No", it is possible to return to the appropriate product design step and do again with other options until the desired performance criteria are matched. More details about the systematic multiscale modelling framework for chemical product-process design of microcapsule controlled release of active ingredients can be found in other publication [11].

Conclusion

A systematic multiscale model-based framework for product-process design has been developed and its application illustrated through the design/analysis of pesticide uptake and fuel cell. The usual trial and error experimental-based approach has been replaced with a virtual product/process lab, which allows some of the time consuming and repetitive steps to be performed virtually through the model/based framework. In this way, the resources of experimental work can be reserved for the final verification of the product, after a small number of candidates matching the desired end-use characteristics of the product have been identified. Finally, for the virtual product-process design lab to succeed, reliable multiscale models must be available in a model-library and used through an appropriate model-based framework, that can also help to generate models, when they are not available.

References

1. Grossmann,I.E., Comp.Chem.Eng. 29(2004) 29-39.
2. Charpentier, J.C., Chem Eng Sci, 57 (2002) 4667-4690.
3. Rassmusen, J.K., Prediction of Pesticide Uptake in Plants, Master Thesis, Department of Chemical and biochemical engineering at DTU.

List of Publications

4. Morales-Rodríguez, R., Gani, R., Déchelotte, S., Vacher, A. and Badouin, O., Chem. Eng. Res. Des., 86 (2008) 823-833.
   #### Conference Contribution
5. R. Morales-Rodriguez, A.M. Sales-Cruz, R. Gani, S. Déchelotte, A. Vacher, O. Baudouin, AIChE meeting (2006), 489c.
6. R. Morales-Rodriguez, R. Gani, CACE 24 (2007) 207-212.
7. R, Morales-Rodriguez, R. Gani, ECCE 6 (2007).
8. Morales-Rodríguez, R., Gani, R., Déchelotte, S., Vacher, A. and Badouin, O., ECCE6 (2007).
9. V. Soni. R. Morales-Rodriguez, E. Conte, R. Gani, AIChE meeting (2007), 496e.
10. R. Morales-Rodriguez, R. Gani, A. Vacher, P. Castelain, S. Dechelotte, AIChE meeting (2007). 344d.
11. Morales-Rodríguez, R. and Gani, R. Proceedings of Chempor Conference. Braga Portugal, 2008.
12. R. Morales-Rodriguez, R. Gani, AIChE meeting (2008), 545c.
13. E. Conte, R. Morales-Rodriguez, R. Gani, AIChE meeting (2008), 697b.

Anders Rooma Nielsen

Phone:	+45 4525 2831
Fax:	+45 4588 2258
E-mail:	arn@kt.dtu.dk
WWW:	http://www.kt.dtu.dk
Supervisors:	Kim Dam-Johansen
	Peter Glarborg
	Morten Boberg Larsen, FLSmidth A/S

Industrial PhD Study in corporation with FLSmidth A/S

Started:	April 2008
To be completed:	March 2011

Fuel Flexible Rotary Kilns for Cement Production

Abstract

The aim of this PhD-project is to investigate the combustion of solid, alternative fuels, fired into the inlet of cement rotary kilns. The investigations should clarify how parameters such as kiln atmosphere, mixing efficiency and fuel particle characteristics will affect the occurrence of local reducing conditions in the rotary kiln, as well as the release of inorganic volatiles and the emission level. These investigations should contribute to pave the way for a safe introduction of alternative fuels in the cement industry, while lowering negative impacts on kiln operation, product quality and emissions.

Introduction

Cement production is highly energy intensive. The energy consumption by the cement industry is about 2% of the global primary energy consumption [1]. Coal and coke have traditionally been the primary fuels in the industry, but increasing fossil fuel prices and environmental concerns make other fuels attractive. Since energy costs accounts for at least 30-40% of the total costs of cement production, there is a great potential to reduce the overall production costs by replacing fossil fuels with alternative fuels[1]. Alternative fuels are typically cheaper than fossil fuels and in some cases the cement producer may even be paid to receive the alternative fuels.

Substitution of fossil fuels with alternative fuels offers the following major advantages:

1. Fossil fuel reserves are saved.
2. Landfill problems are solved.
3. Alternative fuels may be CO_2 neutral.
4. Solid residues from the alternative fuels are incorporated into the cement clinker.
5. High flame temperatures and residence times provide good conditions for destruction of organic compounds.

---

[1] In this context "alternative fuels" refers to all non-fossil fuels and waste from other industries. Secondary, waste or replacement fuels are often used as synonyms for alternative fuels.

In the recent years the use of alternative fuels has increased. In Germany, for example, the share of alternative fuels is today higher than 50%, while it was only 4% in 1987 [2]. It is expected that the share of alternative fuels will continue to increase in the coming years, which will create a need for new technology to handle, treat and combust these fuel types [3].

Many types of alternative fuels are applied in the cement industry. The majority of the alternative fuels are on solid form, while liquids and gasses are less common. Some of the most common alternative fuels are refuse derived fuels (RDF), tyre derived fuels (TDF), meat and bone meal (MBM) and waste wood [4]. Price and availability are typically the determining parameters for the type of alternative fuel that will be utilised at a specific cement plant.

The main challenges by changing from traditional fuels to alternative fuels are to:

1. Maintain a stable kiln operation.
2. Ensure a good cement clinker quality.

A key to control these challenges may be to avoid reducing conditions in the material charge in the kiln system and ensure complete alternative fuel burnout. However, this requires a solid knowledge about the combustion behavior of the specific fuel in the kiln system.

Specific Objectives

The overall objective with this project is to improve the knowledge about combustion of solid, alternative fuels in cement rotary kilns. More specific, the project will focus on feeding of alternative fuels through the inlet to the rotary kiln, see figure 1.
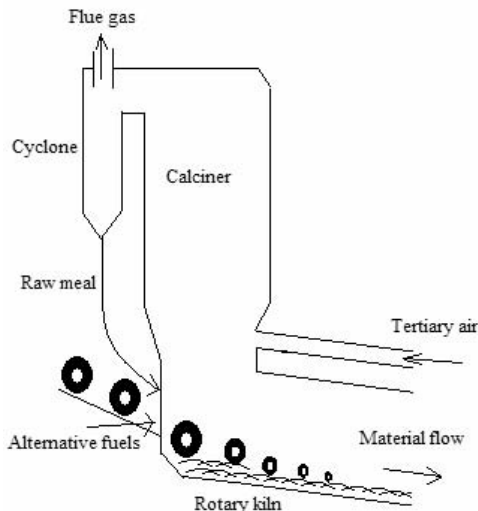
Figure 1: Calciner and rotary kiln inlet.

An important advantage with this feeding point is that the need for shredding of the solid fuel can be minimized, thereby saving this expense.

The project shall clarify how local reducing conditions may be minimized. Furthermore, it is desired to study the release of inorganic volatiles, in particular sulphur, when alternative fuels are combusted. Finally, it is desired to investigate if a shift to alternative fuels has any effect on the NO_x emission level.

The alternative fuel types of interest in this project will be waste wood, tyre derived fuel and poly propylene plastic.

The parameters that will be systematically investigated are:

- Kiln atmosphere
- Mixing efficiency (rotational speed and kiln filling degree)
- Fuel particle type/size/shape
- Amount of alternative fuel (substitution degree)

The investigations will be performed via a mix of literature study, laboratory/pilot scale experiments, mathematical modeling and full scale measurements.

Results

Until now, preliminary laboratory scale experiments have been made in a fixed bed reactor, where mixtures of tyre char and calcined cement raw materials have been exposed to an atmosphere similar to the atmosphere in a cement rotary kiln. The purpose with these experiments is to investigate the relationship between the mixing efficiency and a) the fuel burnout behavior, and b) the release of sulphur. In these experiments, the measured SO_2-signal is taken as a measure for the sulphur release.

A corporation with a relevant cement plant has also been established. This cement plant feed alternative fuels into the calciner, and these fuel particles falls into the kiln inlet before they are completely burned out. Solid material samples at relevant positions around the cement plant have been collected. The samples will be chemically analyzed, and will together with gas measurements help to establish a mass balance for sulphur, chlorine and alkaline metals throughout the cement plant. Furthermore, the content of organic carbon at the different positions in the kiln system will also be determined. This information may help to optimize the performance of the kiln system.

Conclusion

This industrial PhD project deals with combustion of solid, alternative fuels, fired into the inlet of cement rotary kilns. The project is composed of four main components: Literature study, mathematical modeling, laboratory/pilot scale experiments and full scale measurements, which all should contribute to an improved understanding of the combustion process of alternative fuels when used in the cement production.

The PhD project should contribute to ensure that FLSmidth A/S will maintain a position as the leading technology supplier to the cement industry.

Acknowledgements

References
1. S. R. Asthana, R. K. Patil, Use of alternative fuels in Indian cement industry, Advances in Energy Research (2006) 347-349.
2. M. Schneider, Activity Report 2005-2007, Verein Deutscher Zementwerke (2007), www.vdz-online.de.
3. J. H. Rasmussen, FLS skruer op for alternativ energi (2008), http://borsen.dk/nyhed/145258/. 18/11 2008.
4. C. Ochsenreiter and H. Z. Kuyumcu, Production of secondary fuels from waste materials and their application possibilities, Aufbereitungs Technik, (1999) 40, No. 11, 538-551.

Hanne Hostrup Nielsen

Phone:	+45 4525 2838
Fax:	+45 4525 2258
E-mail:	hhn@kt.dtu.dk
WWW:	http://www.chec.dtu.dk
Supervisors:	Peter Glarborg
	Sønnik Clausen
	Stefan Mayer, MAN Diesel SE

Industrial PhD Study
Started: March 2006
To be completed: August 2009

In-Situ Investigations of the Combustion in Large, Two-Stroke Diesel Engines

Abstract
Due to restrictions on the emission levels from marine engines, MAN DieselSE is conducting thorough research in areas connected with combustion optimization and emission reduction. An important tool in the combustion investigations is numerical analysis of the various combustion phases, but a lack of reliable experimental data provides an obstacle in validation and optimization of the developed code. For years, various optical analysis methods have been applied for investigations of the combustion in smaller engines, but due to the more restricted access, extremely sooting combustion, and very high heat loads, similar investigations undertaken at larger engines under realistic combustion conditions are limited.
This project considers optical in-situ investigations on a large, two-stroke Diesel engine. The aim of the investigations is to provide experimental data for the combustion under realistic running conditions and to use these data for validation and optimization of an existing CFD-code.

Introduction

Large, marine engines are responsible for approximately 2 % of the total world fuel consumption, and many of these engines are two-stroke Diesel engines. Strong restrictions are expected to be imposed on the industry in near future, thereby forcing the leading engine manufactures to focus further on emission reduction and engine performance optimization in general.

The costs of performing physical tests on marine engines are very large, which makes numerical analysis a natural choice. Obviously, experimental data are necessary for validation of the numerical codes, and the developments in optical methods within the areas of measurements of complex flows make these a natural choice. These methods have been used for several years in smaller engines, though the transient characters of the combustion and the large and fast variations in pressure and temperature have provided several challenges in the design of both optical accesses and experimental equipment.

Unfortunately, the results obtained on smaller engines cannot be scaled up to the conditions present in the larger engines. This is mainly due to large difference in both length and time scale of the engine processes and the use of different types of fuel.

Specific Objectives

The aim of the present Industrial Ph.D.- project is to develop an optical access to the test engine located in the Test Centre at MAN Diesel SE in Copenhagen, and with this to provide experimental data from the Diesel combustion for validation and optimization of the in-house developed numerical models.

As opposed to many of the investigations undertaken so far, this project focuses on in-situ measurements under realistic conditions, thereby enabling validations of local character for real-size, two-stroke, marine engines.

Diesel combustion

The combustion cycle in a two-stroke, marine Diesel engine is complex and consists of several different stages. The following paragraph will give a very short introduction to these, in order to demonstrate the many different aspects of the Diesel combustion.

During the compression of the last parts of the scavenging air from the former combustion cycle, pressure and temperature in the combustion chamber is increased considerably. Diesel fuel is sprayed into the combustion chamber at high pressure and, due to the conditions, quickly vaporizes. The fast vaporization and the swirling motion of the scavenging air ensures that fuel and oxygen is mixed, which causes the auto-ignition processes to proceed.

The fuel and air mixture often ignites several different places in the combustion chamber more or less at the same time, and spreads quite fast to the remaining parts. During this premixed, turbulent combustion, more fuel is still being injected into the combustion chamber. The fuel being injected is now ignited, causing a non-premixed, turbulent flame. When the injection is stopped, the last parts of the spray is mixed with air and finally burned out. Subsequent scavenging with air removes the combustion gases from the cylinder.

The dynamic and complex manner of the Diesel combustion illustrates the troubles encountered when trying to either control the formation of unwanted components or describing it numerically. It also emphasizes the possible shortcomings of the data obtained from simplified laboratory equipment or ideal reference fuels, and hence confirms the need for reliable data recorded at real engines under realistic conditions.

Optical investigations in engines
The predominant method for optical investigations of the combustion in engines is by use of a special designed laboratory 1-cylinder engine constructed with large parts of the cylinder walls made of a transparent material. Due to the very large heat stresses in the larger engines, this approach is impossible for large marine engines.

Alternatively, an endoscope can be used for looking into a more limited space of the engine. An endoscope can be introduced through an existing opening of the engine, but also limits the view of the combustion chamber, when comparing to an ideal laboratory cylinders. This can though partially be solved by the wide range of industrial endoscopes available today, allowing for various directions and angles of view. Further, using existing openings, the modifications of the engine from the standard set-up are minimized, thereby providing experimental data obtained under as realistic conditions as possible.

Establishing a useful and reliable optical access to a large, marine engine is rather troublesome, due to the very harsh environment inside the engine cylinder during the combustion cycle.

Challenges include:
- Heavy sooting, which causes:
  - intense heat radiation
  - soot depositions on the window
- Low speed, which gives long periods of time with high heat loads
- Two-stroke engines have no cooling stroke, which could otherwise lower the thermal stresses.
- The safety risks connected with a window breaking during running of the engine are high, and considerable care must be taken during both the design phase and experiments.

With a functional optical access, various optical methods of investigations are possible. A typical method for basic information on the combustion process

is doing direct imaging of the combustion. This means high speed images of the natural combustion light, which in the case of the non-premixed turbulent flames of the Diesel combustion means images of the soot being formed during the combustion.

The surfaces of the soot particles radiate light continuously throughout the UV, the visible and the IR spectral regions, with an intensity corresponding to the surface temperature.

Due to the direct injection of fuel, the soot formation is very intense during the non-premixed turbulent combustion phase. However, because of the large overall air excess values, the final engine out emissions of soot in heavy marine engines is quite low, relatively speaking, when comparing to smaller Diesel engines.

Experimental set-up
The investigations are undertaken at the MAN Diesel test engine in Copenhagen. This is a real engine run under realistic conditions, but also heavily experimentally equipped. In Table 1, a few data for the test engine can be found

Table 1: A few characteristic data for the MAN Diesel test engine used for investigations.

Characteristics	Data
Engine type	Diesel, 2-stoke
No. of cylinders	4
Cylinder diam. [cm]	50
Stroke [cm]	220
Power [MW]	~ 8
Power [hp]	~ 10.000
Max. speed [rpm]	123
Adiabatic. gas temp. [°C]	~ 2400
Max pressure [bar]	~ 180
Overall air excess ratio [-]	~ 2

In Figure 1, the optical set-up used in the investigations on the MAN Diesel test engine is depicted. The optical access gives a view across the top of one of the four cylinders, and is constructed inside the starting air valve. As the engine can be started without starting air on this cylinder, the access minimizes the influence on the combustion conditions. The optical assess involves the following components:
- Sapphire window shielding the optics from the combustion environment
- Endoscope guiding the image from the inside of the window to the outside of the valve
- A mirror directing the image towards to capturing equipment
- A standard 50 mm. Nikon lens
- Photron APX High Speed Camera, capturing light with wave lengths in the 400-1000 nm spectral range (visible region).
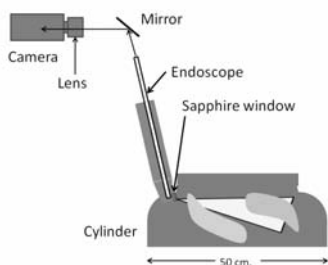
Figure 1: Sketch of the optical set-up for doing direct imaging of the combustion in the MAN Diesel test engine. The endoscope view covers approximately 53 degrees and looks across the top of the cylinder .

The choice of using the starting air valve for the optical access, along with the design of the cylinder cover and the optical access, pre-determines the view within the cylinder. The fuel is injected directly into the combustion chamber through two fuel nozzles, placed almost directly across from the optical access and next to the optical access, respectively. This means, that when doing imaging of the sooting flame, the initial images will show the flame propagating from the fuel nozzle across the cylinder. Shortly into the combustion process, the sooting flame from the injector next to the optical access will have developed into covering the entire field of view, giving a close-up image of a non-premixed turbulent flame, see Figure 2.
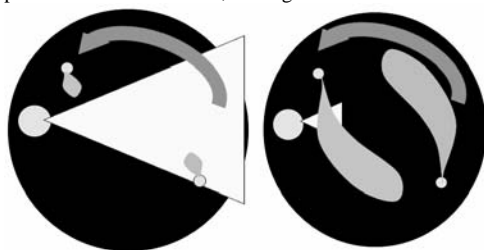
Figure 2: Top view of the flame development and optical field of view within the cylinder during combustion. The large triangle represents the field of view through the optical access, and the arrow the swirl direction.

The images of the combustion are captured with a Photron APX High Speed Camera, which is a CMOS camera recording in light within 400-1000 nm spectral region. The camera has built-in functions for only using part of the chip (reducing field width) and triggering the camera for recording for a limited period of each cycle. This facilitates the recording of several cycles in a row without compromising with a good temporal resolution. In Table 2, a typical set-up for high speed recordings of a 75 % load run are listed.

Table 2: Recording settings for direct high speed imaging of the combustion during a 75 % load run.

Recording parameter	Data
Engine speed [rpm]	111
Framing speed [fps]	16800
Image resolution [-]	384x368
Shutter speed [1/s]	1/252,000
Images pr. cycle	1000
Consecutive cycles recorded	14
Time covered pr. cycle [ms]	~60

Results

In Figure 3, an example from the combustion during engine run of 75 % load can be seen. The image is captured approximately 3 ms. after the fuel injection has been initiated. In the lower right hand side of the image, the turbulent flame from the injector across the cylinder can be seen. From the left side of the image, the flame from the injector next to the optical access can be seen evolving, soon after to cover the entire view.
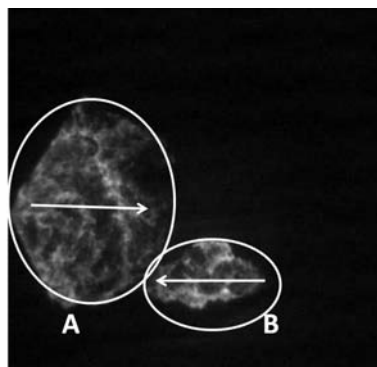
Figure 3: Image from the combustion process. In circle A, the turbulent flame from the injector right next to the optical access can been seen developing into the position, where it covers the entire field of view. In circle B, the flame from the fuel injector across the cylinder is evolving. The arrows indocate the jet directions.

The light that can be seen in the image stems from very hoot soot particles, with the light intensity scaling roughly with the particle temperature. The darker areas in the flames should thus be interpreted as areas with lower temperatures.

The timing of the combustion event is crucial in the Diesel combustion control, and can be investigated by comparing the cycle-to-cycle variations. In Figure 4, a image from the same temporal position in the combustion cycle as given in Figure 3 can be seen for 9 consecutive cycles.
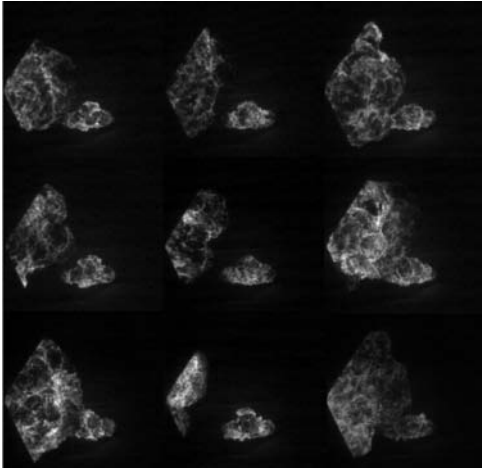
Figure 4: 9 Images from the combustion process approximately 2 ms. after the fuel injection has been initiated. Each image represents the same timing in 9 consecutive cycles.

As can be seen, the shapes of the evolving flames varies a bit, though some features are constant. Future work will include comparison between the observed timing and geometrical features of the flames and the numerically calculated features induced by injector design.

The intensity of the light registered in each pixel will depend on a number of factors:

- The soot particle surface temperature. The total energy radiated per area and time depends on the temperature to a factor of four.
- The concentration of soot particles in the entire depth of the volume observed. The soot particles closer to the window will contribute more than those further away
- Absorption or blocking of the light somewhere in the path of sight from the soot particles to the optical equipment. Blocking of the light can be due to a "optically thick" environment, like the heavily sooting flame.
- The attenuation of the light intensity due to the optical equipment – the intensity is lowered when passing through the sapphire window, the endoscope and when reflected by the mirror.
- Finally, the spectral sensitivity of the camera chip obviously also determines the recorded pixel values. If the soot luminescence intensity is to be used temperature measurements, the spectral sensitivity of the chip must be accounted for.

Of the influencing parameters mentioned here, the fact that the direct imaging technique try to picture a 3D phenomenon in 2D is the most troublesome. This means, that each pixel sum up the contributions from all emitters along the line of sight. Assuming that the conditions along the entire line of sight are homogeneous, this can be corrected for, but that is not a valid assumption for the combustion under the given conditions.

In Figure 5, the average pixel value from the entire image is depicted as a function of CAD (crank angle degrees). The graph also shows the opening of the fuel valve along with the pressure in the cylinder. As can be seen, the onset of the hot soot luminescence has a short delay from the opening of the fuel valve.

Also noticeable is the correlation between the pressure and the pixel intensity. After approximately 10 CAD, where the fuel injection is still at its maximum level, the average pixel intensity begins to decrease. The most likely cause of this is a decrease in temperature, due to the gas expansion. As can be seen from the cylinder pressure trace, the timing of the onset of the decreases matches the cylinder pressure peak.
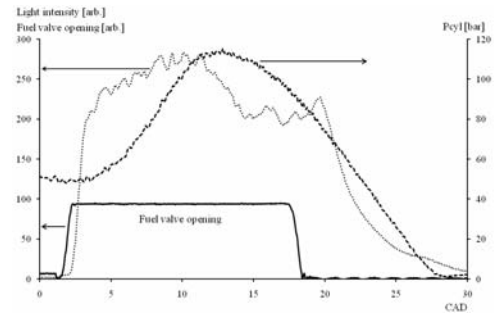
Figure 5: Fuel valve opening (solid line), cylinder pressure (large dots) and average pixel intensity (smaller dots) as a function of crank angle degree (CAD) for direct imaging of the combustion at 75% load.

The timing of the decrease of the soot luminescence is one of the factors that are to be compared with the results of the numerical analysis undertaken at MAN Diesel SE. These investigations includes predictions of the soot formation, which numerically will be converted into a soot luminescence, taking factors like soot surface temperatures into account.

Conclusions

The work presented in this paper have shown the results obtained with in-situ optical investigations of the combustion in the cylinder of a large, two-stroke Diesel engine.

The investigations have proven the applicability of the experimental set-up for doing robust, reliable and highly temporal resolved direct images of the soot luminescence during the Diesel combustion, even when running the engine under realistic conditions.

Future work includes comparisons with numerical predictions for the soot luminescence and geometrical fuel jet observations.

Rudi Pankratz Nielsen

Phone:	+45 2210 2522
Fax:	+45 8830 3211
E-mail:	rpn@kt.dtu.dk
WWW:	http://www.ivc-sep.kt.dtu.dk
Supervisors:	Erik G. Søgaard, Aalborg Universitet
	Steen B. Iversen, SCF Technologies A/S
	Kaj Thomsen
	Nicolas von Solms

Industrial PhD Study

Started:	May 2006
To be completed:	April 2009

The Physical Chemistry of the CatLiq® Process

Abstract

The CatLiq® process converts aqueous biomass into oil at high pressure and temperature. Due to changes in the properties of water especially with regards to solubility of salts it is important to determine if salts precipitate at process conditions. Also it is of interest to determine the phase distributions and compositions at process conditions, to ensure operation is in the single phase region. To do this models are being developed to allow for these calculations.

Introduction

The CatLiq® technology is a method for conversion of aqueous biomass to oil compounds. The process window is at near critical water conditions and the overall process may be described as a catalytic step followed by a separation step, which is illustrated in figure 1, where biomass is fed into the system and resulting in a gas stream as well as a liquid stream as the products.
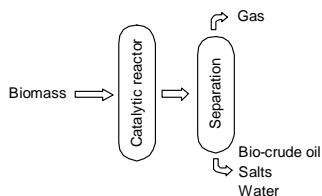
Figure 1: The Cat-Liq® process

The CatLiq® process is a catalytic process, and incorporates both homogeneous as well as heterogeneous catalysts.

Specific Objectives

The objective of the Industrial Ph.D. study is to model the system, especially with regards to phase distributions and salt precipitations. The process is investigated in a pilot scale plant at SCF Technologies A/S, as well as in a lab scale set-up at Aalborg University.

Results and Discussion

The process streams in the CatLiq® process are composed of a large number of components. Due to this it is preferable to model the system using lumped pseudo-components, which will facilitate calculations. Table 1 illustrates the reduction of the number of components by using pseudo-components.

Table 1: Reduction of the number of components

Components	Pseudo-components
Methanol	
Ethanol	Ethanol
Propanol	
Acetic Acid	Acetic Acid
Propanoic Acid	
Decanoic Acid	
Dodecanoic Acid	Dodecanoic Acid
Hexadecanoic Acid	Hexadecanoic Acid
Octadecanoic Acid	
Unknown fraction	Unknown Fraction

To determine the composition of the streams using pseudo-components GC and GC/MS analysis is utilized at Aalborg University to investigate the composition of the actual process streams.

The properties of water change significantly at near-critical conditions. The decrease in the dielectric constant is of interest as solubility of salts will decrease significantly [1][2]. To model if salts will precipitate at process conditions the saturation index (SI) is calculated. Equation 1 gives the saturation index as the

relationship between the solubility constant K_{SP} and the activities.

$$SI = \frac{\ln K_{SP}}{\sum a_i{'}} \qquad (1)$$

Due to process conditions the solubility constant must be corrected for pressure and temperature. Equations 2 and 3 show the corrections as described by [3] and [4] respectively, while figure 2 (left) shows the algorithm.

$$\ln K_{SP,i} = \ln K_{SP,0} - \frac{\Delta_{dis} V_{P_0}}{RT}(P - P_0) + \frac{\Delta_{dis}}{2RT}(P - P_0)^2 \qquad (2)$$

$$\ln K_{SP} = R \cdot \ln K_{SP,T_0} - \Delta H_{T_0}^0 \left(\frac{1}{T} - \frac{1}{T_0}\right) + \Delta a \left(\ln \frac{T}{T_0} + \frac{T_0}{T} - 1\right)$$
$$+ 0.5 \Delta b \left(\frac{(T - T_0)^2}{T}\right) + \frac{\Delta c}{T}\left(\frac{T - T}{T} \cdot \ln \frac{T - T}{T_0 - T} - \ln \frac{T}{T_0}\right) \qquad (3)$$

Besides determining salt precipitation it is of interest to be able to model the phase distribution at process conditions. For this model the pseudo components are used to describe the system.

The multiphase flash routine will be based on cubic equations of state with a multistep Rachford-Rice procedure for calculation. Figure 2 (right) shows the algorithm for the multiphase flash routine.
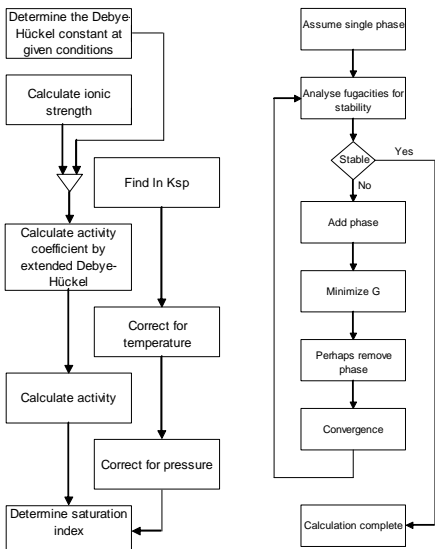
Figure 2: Model algorithms, Salt precipitation (left) and multiphase flash (right).

The reason to use a cubic equation of state and not more advanced equations of state such as SAFT, which has been shown by Feng et. al. [5][6] to work for high temperature and high pressure conversion processes, is

that the complexity of the feed and product streams will require extensive parameter estimation from experimental data.

Conclusions
CatLiq® is a high pressure high temperature catalytic process for conversion of aqueous biomass into oil.

Due to changes in water at these conditions it is important to be able to determine if salts will precipitate during processing. To be able to do this a model is developed to determine the saturation index based on activities and the solubility constant corrected for pressure and temperature.

Phase behavior at process conditions is modeled based on a cubic equation of state. This model uses pseudo-components instead of the actual composition to facilitate calculations, due to a very large amount of components in the actual process streams.

References
1. Savage, P.E., Reactions at Supercritical Conditions: Applications and Fundamentals, AIChE Journal 41 (1995) 1723.
2. Peterson, A. et. al., In situ visualization of the performance of a supercritical water salt separator using neutron radiography, J. of Supercritical Fluids 43 (2008) 490.
3. García, A. et. al., Prediction of Mineral Scale Formation in Geothermal and Oilfield Operations Using the Extended UNIQUAC Model Part II. Carbonate-Scaling Minerals, Geothermics 35 (2006) 239.
4. Thomsen, K. et. al., Correlation and Prediction of Thermal Properties and Phase Behaviour for a Class of Aqueous Electrolyte Systems, Chem. Eng. Science 51 (1996) 3675.
5. W. Feng, et. al., Phase Equilibria for Biomass Conversion Processes in Subcritical and Supercritical Water, Chemical Engineering Journal, 98 (2004) 105
6. W. Feng et. al., Biomass Conversions in Subcritical and Supercritical Water: Driving Force, Phase Equilibria, and Thermodynamic Analysis, Chemical Engineering and Processing 43 (2004) 1459

List of Publications
1. Nielsen, R.P., Iversen, S.B., Thomsen, K., von Solms, N., Larsen, T., Søgaard, E.G.: Thermodynamic Modeling of Production of Biofuel by Catalytic Conversion at Near Critical Conditions in Aqueous Solution, Proceedings of the 16th European Biomass Conference and Exhibition, ETA-Florence Renewable Energies (2008), 1779.

Sidsel Marie Nielsen

Phone:	+45 4525 2983
Fax:	+45 4525 2258
E-mail:	sa@kt.dtu.dk
WWW:	http://www.ivc-sep.dtu.dk
Supervisors:	Erling H. Stenby
	Alexander Shapiro
	Michael L. Michelsen

PhD Study
Started: September 2006
To be completed: July 2010

Modeling Microbial Enhanced Oil Recovery

Abstract

A potential method for enhancing oil recovery is to utilize the activity of microorganisms which are either present in or injected into the oil reservoirs. Microbial enhanced oil recovery is an emerging method for further exploitation of existing but non-productive oil fields to mobilize more residual oil. One of the important effects is reduction of viscosity. In order to mobilize residual oil, the effect of surfactant has been implemented in 1-D simulator. The reduction of residual oil affects the relative permeability curves, where different methods have been investigated and interpolation methods are mostly the case. Finally, this project is concerned with inclusion of a generic model for microbial activity into an existing simulator.

Introduction

The principle source of fluid fuels is and will be the hydrocarbon resources. However, the finite nature of our hydrocarbon reserves has been discussed as discoveries of new oil reservoirs decrease. For the present techniques of oil recovery, a large amount of oil remains in the reservoir after water flooding, but the oil reservoirs must be abandoned as the production is no longer economically feasible. Methods of enhanced oil recovery (EOR) have been developed, but in many cases they are economically unattractive.

The biotechnology research has advanced and the oil industry has matured to consider microorganisms in the context of oil production. The oil reservoir may already contain indigenous microorganisms, which can be used for MEOR. Both indigenous and injected microorganisms are used and it depends on their applicability of the specific reservoirs. In MEOR, bacteria are often used as they are small and have different useful features. For bacterial growth and metabolite production, the requirements are different nutrient, which are led to the reservoir. In some cases, the carbon source is residual oil.

The MEOR purpose is, like other EOR methods, to mobilize the residual oil and thus reduce its content and/or increase the volumetric efficiency. MEOR address the same physical parameters as chemical EOR, where they are subject to the same *in situ* technical difficulties. The essential difference between MEOR and chemical EOR resides in the method of introducing the recovery-enhancing chemicals into the reservoir.

Enhancement of the oil recovery through microbial action can be performed through several mechanisms as follows:

- Reduction of oil-water interfacial tension and alteration of wettability by surfactant production and bacterial presence.

- Viscosity reduction by gas production or degradation of long-chain saturated hydrocarbons.

- Selective plugging by bacteria and their metabolites.

- Generation of acids that dissolve rock improving absolute permeability.

MEOR is considered a potential 'high risk, high reward' process, where the high risk originates from the many performance constraints of the process. The reward is that the implementation difficulties and the cost resemble those of water flooding than those of chemical EOR.

An oil reservoir is a harsh environment, which can have high temperature, high salinity and low pH (3-7). In general, this extreme environment should be taken into account when selecting bacteria and nutrient media. As the reservoir conditions change from reservoir to reservoir, an extra effort has to be put on selecting and developing suitable bacteria and nutrient media for each reservoir, which has the potential to undermine microbial process economic viability.

Specific Objectives

The specific objective of the project is the investigation of the MEOR method through modeling. A 1-D MEOR flow and reaction model is setup and solved numerically. The most important effects should be incorporated in several ways in order to explore these MEOR effects.

After investigation and analysis of the MEOR effects, the MEOR should be incorporated in an existing simulator, which should be either a streamline or a black oil simulator.

Transport Equations for 1-D Flow System

The reservoir is considered to be 1-D with two flowing phases with a total of five components, which is also depicted in *Figure 1*.

- Water phase
    - Water
    - Bacteria
    - Substrate
    - Metabolite (surfactant)
- Oil phase
    - Oil
    - Metabolite (surfactant)

The transport equations are given as below consisting of an accumulation, convection and reaction term. This is the mass conservation balance without a diffusion term given for each component:

$$\frac{\partial}{\partial t}\left(\sum_{j=1}^{np} C_{ij}\, \rho_j s_j \right) + \frac{\partial}{\partial x}\left(v \sum_{j=1}^{np} C_{ij}\, \rho_j f_j \right) = q_i \qquad (1)$$

for $i=1...nc$.

where j is the phase, i is component, nc is number of components, C_{ij} is mass concentration for component i in phase j, s_j is saturation of phase j, np is number of phases, v is linear velocity, ρ_j is density of phase j, f_j is fractional flow function of phase j, x is length variable, t is time, p is porosity, and q_i is the source term for component i.
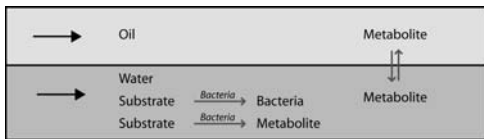
Figure 1: Sketch of the flow system, where a water phase and an oil phase exist. Substrate and bacteria exist only in the water phase, where bacteria convert substrate to metabolite and more bacteria. The metabolite can be distributed between both phases depending on the distribution coefficient.
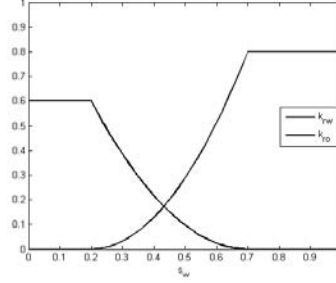
Figure 2: Relative permeability curve for water and oil with $s_{wi}=0.2$, $s_{or}=0.3$, $k_{rowi}=0.6$. and $k_{rwor}=0.8$.

As shown in Figure 1, two autocatalytic reactions occur, where bacteria convert substrate to metabolite and more bacteria. The rate expression is e.g. a Monod type with or without inhibition of substrates and products and 1-2 limiting substrates.

In this case, metabolite is surfactant. Metabolite can be distributed between both phases, where a coefficient K_i determines the distribution in relation to masses of water and oil.

The fractional flow function describes the flow of the phase j and is dependent on the saturation of phase j. Generally, the larger water saturation, the larger a fractional water flow. However, f_j depends on the relative permeability curves for water and oil, k_{rw} and k_{ro}, and their phase viscosities, μ_w and μ_o.

Fractional flow function for water

$$f_w = \frac{\frac{k_{rw}}{\mu_w}}{\frac{k_{rw}}{\mu_w} + \frac{k_{ro}}{\mu_o}} \qquad (2)$$

and the fractional flow function for oil

$$f_o = 1 - f_w \qquad (3)$$

The relative permeabilities describe the ease of a fluid to pass through the porous media. Figure 2 shows the relative permeability curves. The relative permeability curves used are the Corey type, which is a polynomial in the water saturation s_w. With s_{wi} is the irreducible water saturation and s_{or} is the residual oil saturation, a scaled saturation value can be defined:

$$s^* = \frac{s_w - s_{wi}}{1 - s_{wi} - s_{or}} \qquad (4)$$

and the approximations of Corey type of relative permeabilities of water and oil then becomes;

$$k_{rw} = k_{rwor}(s^*)^{pw} \quad \text{and} \quad k_{ro} = k_{rowi}(1 - s^*)^{po} \qquad (5)$$

where *pw* and *pw* can be obtained from measured data. Often p_j=2 is a suitable value.

Numerical Solution Scheme
Slim-tube type approach is used, where the reservoir is subdivided into a number of volumes.
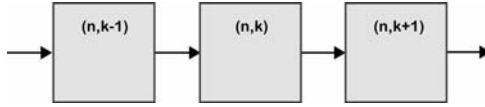
All *k* volumes for one time n are solved. Then, the next time step (n + 1) is solved. Each block is solved using total volume balance and component mass balances. Each block has the composition from the previous time step (n − 1, k) and what enters from the beforehand block (n, k − 1) at this time step. The flow between the blocks depends on the fractional flow function as the system is considered non-compressible. The flow from block *k* to block *(k+1)* is a function of the saturation of block *k* introducing implicitness into the system.

After equilibration calculation and iterations, the block composition and thus the efflux is known. The volumes when mixing the components of the model is considered as *no volume change on mixing*.

In order to solve converge the system of equations, the multivariable Newton method using a numerical Jacobian is applied. The variables are masses of water, oil, total metabolite, substrate and bacteria, but also the volumetric flow pr. time. Masses are used to be able to have mass conservation.

Surfactant Effect
One of the most important effects is *in situ* production of surfactants, which can enhance the oil recovery. Residual oil is trapped in the pore space and can not be displaced by the injected fluid (see Figure 3).
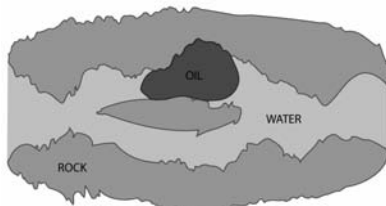
Figure 3: Residual oil drop is trapped in the pores. The injected fluid can not displace the oil unless the interfacial tension is decreased.

Surfactant decreases the interfacial tension (IFT) between water and oil. As a result, the residual oil can to some extent become mobilized and thus displaced by the injected fluid.
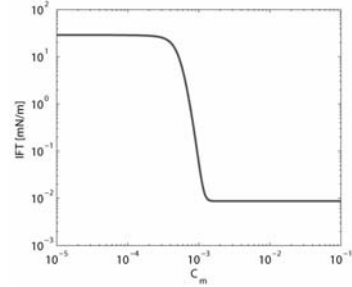
Figure 4: Typical correlation between metabolite mass concentration C_m and interfacial tension (IFT).

Relative Permeability Curves
In the model, the surfactant decreases IFT. A correlation between surfactant concentration and IFT is used, but the correlations are very much dependent on the type of surfactant. A very common correlation type is shown in Figure 4. The lowered IFT affect the shape of the relative permeability curves, where it is generally assumed that the curves become linear and residual water and oil saturations decrease.

Different methods have been proposed by different researchers, but they use the same general idea, where the interpolation between two curves at different IFT using an interpolation function $g(\ )$.

$$k_{rj} = g(\ )k_{rj(base)} + [1 - g(\ )]k_{rj(misc)} \qquad (6)$$

$$s_{or} = g(\ )s_{or(base)} \qquad (7)$$

$$s_{wi} = g(\ )s_{wi(base)} \qquad (8)$$

where $j=\{w,o\}$. The base curve is at the base case with the highest IFT, $_{(base)}$, and the miscellaneous curve often being straight line curves from corner to corner in the plot.

A common interpolation function is a function of the capillary number, which is a function of water viscosity $_w$, linear velocity *v* and IFT $_{ow}$ between oil and water:

$$N_{CA} = \frac{_w v}{_{ow}} \qquad (9)$$

There exist many versions of the capillary number interpolation function reasoning that it is not shown here. Another function is a simple interpolation function of the IFT.

$$g(\ ) = \left(\frac{}{_{(base)}} \right)^{\frac{1}{n}} \qquad (10)$$

Results

Different cases have been investigated at the 1-D simulator. The surfactant affects the relative permeability curves, where saturation profile and recovery of oil are changed. In the following, the N_{ca} method is used.

Figure 5 shows pulse injection of surfactant, where nor bacteria neither substrate are present. The water phase saturation profile s_w, residual oil saturation being used in the relative permeability curves s_{or} and total surfactant saturation v_m are shown at the dimensionless time $ = 0.34$ being pore volumes injected. The analytical solution for the reservoir, where only water flooding has occurred.

The MEOR water saturation front (blue) moves slower than the waterflooding front, which is a result of the surfactant is mobilizing residual oil, i.e. s_{or} decreases. The water phase displaces oil, where oil is moving instead of water and thus the blue water phase front is delayed.

Figure 6: MEOR profile showing water phase saturation (blue), bacteria (light green), substrate (dark green), metabolite (pink) and s_{or} (dotted).

Figure 5: The water saturation profile s_w (blue), residual oil saturation being used in the relative permeability curves s_{or} (pink,dotted) and total surfactant saturation v_m (pink, multiplied by 30) are shown at the dimensionless time $ = 0.34$ PVI. The analytical solution (red) for the reservoir, where only water flooding has occurred.

In figure 6, bacterial reaction converting substrate to surfactant and more bacteria is investigated. This case shows injection of 5% bacteria and 10% substrate. At the reservoir entrance, reactions start; substrate is consumed, more bacteria is produced, and surfactant is slowly formed. Around $ = 0.2$ enough surfactant is produced and the residual oil saturation used to estimate the relative permeability decreases. Thus, more oil can be displaced. In general, water phase saturations above $(1-s_{or})$ indicate that more oil is produced.

Another measure for the recovery methods are the recovery factor describing the amount of oil recovery to the original oil in place. Figure 7 depicts the recovery factor, where waterflooding is compared to MEOR (the profile shown in figure 6). The waterflooding can maximum recover 60% and MEOR recovers around 80%, where MEOR clearly enhances oil recovery.

Figure 7: Recovery factor (RF) describing the amount of oil recovered compared to the original oil in place.

Future Work

The 1-D simulator has been built and is working properly. The next step is to investigate and choose the simulator in which, the presented MEOR effects should be incorporated. Still, we are looking for data to validate the 1-D simulator. These data could for instance be laboratory data for different reservoir cores.

The other important effects should be also be investigated further as the program are to be built to comprise more levels on MEOR.
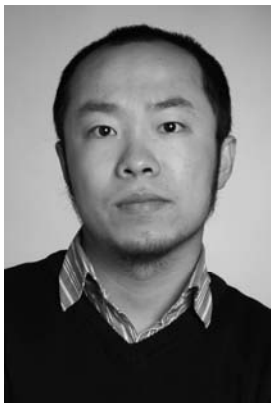
Ben Niu

Address: Building 229
Phone: +45 4525 2895
Fax: +45 4525 2258
e-mail: ben@kt.dtu.dk
www: http://www.ivc-sep.kt.dtu.dk
Supervisors: Alexander Shapiro
                Erling H. Stenby
                Wei Yan

Ph.D. Study
 Started: September 2006
 To be completed: September 2009

Carbon Dioxide Injection in the Carbonate Reservoir

Abstract
Carbon dioxide injection is a widely used EOR (Enhanced Oil Recovery) method. During the injection of carbon dioxide into reservoir at the MMP (Minimum Miscible Pressure), it will be become miscible with original oil. The compositional simulation including the reaction between carbon dioxide and carbonate matrix will also be investigated. The experiments will be conducted with CT scanner and ROP flooding rig under high temperature and high pressure conditions.

Introduction
Today's largest global challenges are climate changes and security of energy supply. With its efficient power plants located near the coast and the North Sea Denmark has a unique position to enable the development of methods to combine the utilization of CO_2 with enhanced oil recovery (EOR). This project is a part of the main project, "Enhanced Oil Recovery through CO_2 utilization" which is to ensure the build-up of knowledge within EOR in Denmark.

During laboratory and field studies, several problems become significantly important. The thermodynamic equilibrium under the circumstance of chemical reaction and the appearance of different ions in the saline water has a direct relationship with the prediction of various parameters in the oil production. The relative permeability between different phases could influence the breakthrough time of different zones, and further the longevity and cost of the whole project. The reaction between carbon dioxide and carbonate matrix will change the porosity and permeability of rock matrix, and further influence the injectivity, and finally limit the longevity of the whole project. The numerical method and algorithm varies with the different dimensions and the complexity of the model, which has significant influence on the robustness, efficiency and accuracy of the model.

The aim of this project is to investigate problems induced by carbon dioxide injection. The current research is focused on the experimental and modeling work.

Process description
The injection of CO_2 into a petroleum reservoir will result in either a miscible or immiscible displacement. If under the prevailing reservoir temperature and pressure, the injected gas is miscible with the reservoir fluid in all proportions, this type of displacement is called first – contact miscible (FCM)[1]. If the injected gas is enriched enough to be completely miscible with reservoir fluid at the front, this kind of displacement is referred as multicontact miscible flood (MCM)[1]. The last type of displacement is in which phases at the gas-oil front can not be miscible. Because the first two kinds of displacement finally achieve similar high recovery efficiency, the MMP has become an important optimization parameter in CO_2 injection.

Experimental Work
The experimental work is mainly conducted with CT scanner (figure 1) and ROP rig (figure 3) in IVC-SEP. In the oil industry, x-ray computed tomography (CT) has been accepted as a routine core analysis tool and mainly used to fundamental studies and recovery mechanisms, like saturation studies, improved recovery, hydrated studies, recovery of viscous oil, formation damage studies, acid treatment and stimulation[2].The saturation distribution of different phases during or after the flooding can be calculated based on the images from CT scanning.

Figure 1: CT scanner

In the recent experiment, three phases flooding in chalk sample is conducted by using CO_2, doped isopar-L and doped water under medium pressure, 6.5Mpa and room temperature 37C. In figure 2, Adsorption of the dopant at the inlet of the core is detected. Light color represents high density zone, which is filled with dopant. This result suggests the sensitivity of chalk sample to different dopants, which is not well-studied yet.
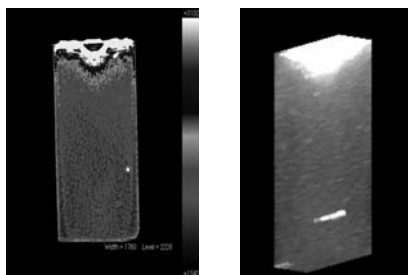
Figure 2: Adsorption of the dopant at inlet

With the analysis of CT images and mass conservation calculation, the experimental results indicate that the three phase experiments with two doped phases are difficult and complex and need further attentions. The choice of dopant is the key to success.

ROP flooding rig is an effective tool for the measurement of multiphase permeability. As in figure 3, the most important and sensitive part of the equipment is the three phase optical separator, which can separate three phases under medium pressure up to 11.5Mpa.
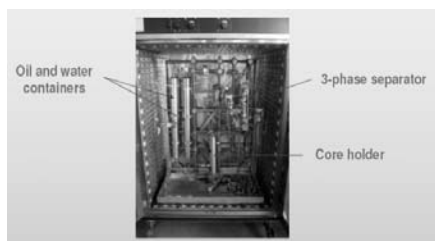
Figure 3: ROP flooding rig

The test experiment with ROP rig reveals that the wettability of glass tube in 3-phase separator can probably change from water wet to oil wet, which affects the final results.

Modeling work

The chemical reactions and multiphase flow in CO_2 flooding are considered in the model, which will be updated step by step.

For a carbonate system the kinetically controlled reactions is[3]:

$$H_2O + CO_2 + CaCO_3 \leftrightarrow Ca(HCO_3)_2$$

The reaction can change the porosity and permeability at the same time, and correspondingly the mechanical properties of the whole reservoir. The change is complex due to its dependence on rock type and the injection scheme. Suitable amount of icons and reactions will be chosen based on the time scale of the whole process and their individual importance.

Multiphase flow in CO_2 flooding could contain four phases, gas, two liquid hydrocarbon phases, and water. The importance of the second liquid hydrocarbon phase is still not fully clear, as mentioned many literatures[4, 5, 6]. This mechanism will be considered in the model.

At current stage, one dimension model has been proposed and in updating.

Future Work

Future research will be focused on multiphase flow and chemical reaction in carbonate reservoir. Flooding experiment will be mainly conducted under high pressure and high temperature conditions with CT scanner. Numerical simulation will mainly focus on the chemical reaction and the corresponding changes in petro-physical properties.

References
1. S. Haynes Jr. and R.B. Alston, SPE/DOE 20190 presented at SPE/DOE Seventh Symposium on Enhanced Oil Recovery, Tulsa, Oklahoma, 1990
2. E.M. Withjack, C. Devier, and G. Michael, SPE 83467 presented at SPE Western Regional/AAPG Pacific Section Joint Meeting, Long Beach, California, 19-24 May 2003
3. O. Izgec, B. Demiral, H. Bertin and S. Akin, SPE 100809 presented at the SPE Annual Technical Conference and Exhibition, San Antonio, Texas, USA, 2006
4. Nghiem, L.X., and Li, Y.K., SPE Reservoir Engineering, Volume 1, Number 4, 414-422, July 1986
5. Fanchi, J.R., SPE Annual Technical Conference and Exhibition, Dallas, Texas, 27-30 September 1987
6. K.K. Mohanty, W.H. Masino Jr., T.D. Ma, and L.J. Nash, SPE Reservoir Engineering, Volume 10, Number 3, 214-221, August 1995

Albert E. Cervera Padrell

Phone:	+45 4525 2861
Fax:	+45 4593 2906
E-mail:	acp@kt.dtu.dk
WWW:	http://www.bioeng.kt.dtu.dk
Supervisors:	Krist V. Gernaey
	Rafiqul Gani
	Søren Kiil
	Tommy Skovby, Lundbeck A/S

PhD Study
Started: August 2008
To be completed: July 20011

Moving from Batch towards Continuous Organic-Chemical Pharmaceutical Production

Abstract
Organic-chemical pharmaceuticals have traditionally been produced in batch reactors, and it is custom to tailor the synthetic routes to work well in these reactors instead of using reactor set ups designed to handle the relevant chemistry. The aim of this PhD project is to develop continuous operation units optimized for a certain type of reaction or separation process, ideally preserving flexibility. Such approach should yield a methodology and a set of toolboxes applicable to similar design problems.

Introduction
A major problem of many batch reactions for pharmaceutical production is that the process is typically based on a long sequence of reactions, which thus results in time-consuming production processes that often need expensive storage of reaction intermediates as well. As such, batch production also implies that the full benefits of the Process Analytical Technology (PAT) initiative of the FDA cannot be realized in the pharmaceutical production process.

In contrast, a continuous production environment may potentially lead to improved safety against e.g. runaway reactions, higher productivity and reduced costs, and reduction or elimination of stocks. Furthermore, continuous production inherently implies an improved capability to react on process disturbances (e.g. changes in the quality of the raw materials used) via appropriate control loops, thus resulting in a more robust production process and a more consistent product quality.

Specific Objectives
In this project a model reaction with known reaction mechanism will be studied. More specifically, it will be attempted to eliminate intermediate production steps (in this case a crystallization step) in order to obtain a less time-consuming and less complex production process. That means in practice that it will be attempted to change the production from batch to continuous.

The following factors need to be investigated in detail in a first project phase: reaction selectivity and yield, impurity profiles, process stability, process safety.

The techniques to be used are a literature survey, laboratory experiments, and development of mathematical models – for example in Matlab/Simulink – or use of existing simulation packages (e.g. ICAS, COMSOL). During the model-building step, the models will be refined by applying sensitivity analysis and optimal experimental design (OED), where the OED will be specifically helpful in designing experiments that will provide the highest information content for model identification, thus reducing the amount of experimental work to be conducted.

Based on the results of the first project phase, suggestions for improved continuous reactor design and operation will be tested in a second project phase. These tests will be based partly on process simulation, partly on experimental work in a lab-scale set-up. Considering the scale of operation that is relevant for Lundbeck, the potential of microreactors (with laminar flow) might be examined in this project phase. Assuming that the reaction mechanism is known from project phase 1, topology optimisation could be applied to find out what reactor shape and reactor operating parameters are most suited at the microscale for achieving the highest productivity (or the lowest amount of impurities, depending on the objective that is given the highest priority). Results for process design of microreactors will be compared with traditional process design, to find out which production scale is most promising. If successful, this project phase might be the start of the establishment of a continuous pilot plant for pharmaceutical production at the Department of Chemical and Biochemical Engineering at DTU.

If time allows, the focus in the third and final phase of the project will be on the development of a proposal for appropriate process monitoring and control strategies that can guarantee the desired product quality in a continuous process for organic-chemical pharmaceutical production. This monitoring and control system (or PAT system) should live up to 2 demands: (1) reliable performance, and (2) limited complexity. Development of this system can be based on the results of the PhD project of Ravendra Singh – aiming at the development of computer-aided tools for design of a PAT system – which is to be finished in the summer of 2009. Testing of the monitoring and control system will be simulation-based. The practical relevance of the simulations will be improved by including appropriate sensor and actuator models, for example based on Markov chains, such that the process performance can be simulated for normal operation and for a number of relevant process fault states. The expected outcome of this project phase is a proposal for an appropriate PAT system (minimum complexity, maximum reliability).

Brian Richard Pauw, M. Sc.

Phone:	+45 4525 6864
Fax:	+45 4588 2161
E-mail:	bp@kt.dtu.dk
WWW:	http://lookingatnothing.com/
Supervisors:	Martin E. Vigild, DTU
	Kell Mortensen, KU
	Jens W. Andreasen, Risø DTU
	Enno A. Klop, Teijin Aramid

PhD Study

Started:	Oct 2006
To be completed:	Sep 2009

Nano Pores in Micro Filaments

Abstract

This research aims to provide a novel and well-validated methodology to the determination of the nanostructure of high-performance polymer materials. The main applied technique is Small-Angle X-ray Scattering (SAXS). The advantages and disadvantages of the technique will be discussed, and data analysis methods will be treated and updated where required. These data analysis methods are utilized to characterize the microstructure of high-performance aramid yarns.

Introduction

High performance polymers, such as the aramid yarn, are put to use in a variety of applications such as ballistics, structural reinforcements and heat- and cut-protective clothing. These yarns (as the main focus of this research) have been investigated in detail since their appearance in the marketplace approximately 30 years ago. They have been scrutinized on the macroscopic, microscopic and atomic levels. Much less common, however, are the nano-structural investigations that focus on structural elements with sizes bigger than what can be observed by crystallographic techniques, but smaller than the optical limit. Especially the nanopore structure, with structural elements (nanopores) in the range of 1-100 nanometers, is a less well known area [1]. The characteristics of these pores have been shown to correlate to (macroscopic) physical parameters of carbon fibres [2], indicating that a good understanding of the nanopores may lead to better tuning of the fibre characteristics, a statement reiterated by Dobb et al. [3] based on their findings for commercial aramid fibres.

Approach

One of the main techniques to investigate such nanoscale structures, is Small-Angle X-ray Scattering (SAXS). This is the only technique that can determine such structural elements without destructive sample preparation, and above all, delivers parameters that are valid over the entire irradiated volume ($\approx$1mm^3) [4]. The analysis of the nanostructure present in the high-performance polymer yarn, however, requires a new fitting function in order to extract detailed structural parameters. This new function is described and validated using simulated scattering patterns from real-space 3D simulations (c.f. *Figure 2*).

Measurements

The measurements (e.g. *Figure 1*) show patterns characteristic for aligned scatterers with a high aspect ratio (i.e. their width is not equal to their height).
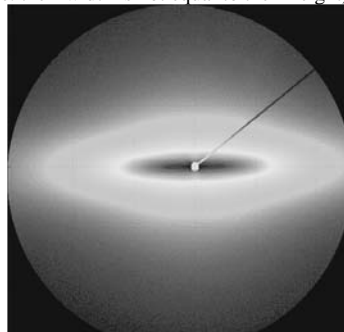
Figure 1: A scattering pattern measured at MAXLAB of a bundle of Twaron 1000 filaments.
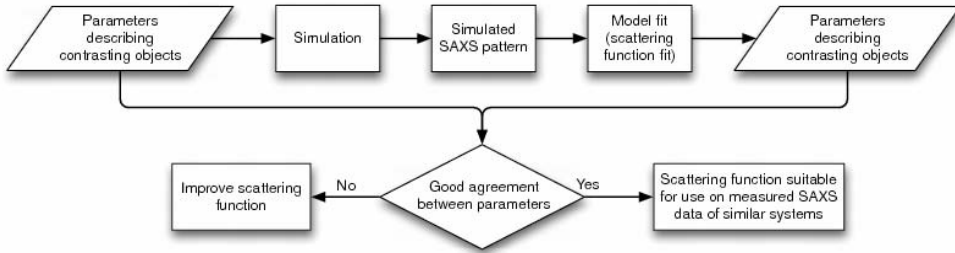
Figure 2: Validation methodology

Models

A nanostructure was modeled based on parameters for the size distributions of the scatterers obtained from the application of the yet unvalidated model to the scattering pattern. From this simulated nanostructure, shown in **Figure 3**, a scattering pattern was computed.

Figure 4: A comparison between the input into the nanostructure simulation routine and the output of the SAXS pattern fitting function shows good agreement.

Conclusion

We now have a fitting function that can be applied to the data, in order to extract nanostructural parameters of systems consisting of polydisperse, aligned scatterers shaped (mainly) as ellipsoids-of-revolution. This function is validated and determined to deliver the correct response for the measured pattern.

Outlook

We want to be able to also describe imperfectly oriented systems, so this has to be integrated in both the simulation of the nanostructure as well as the fitting model. We also want to apply the function to real measurements to complete the goals of the project.

Figure 3: A simulated nanostructure, consisting of 10 volume percent of polydisperse, aligned ellipsoids-of-revolution. From this structure, a scattering pattern can be computed.

Validation

We can verify that we can indeed re-determine the size distribution parameters that went into the modeled nanostructure, from its scattering pattern using the newly developed fitting function. In other words, we know that for structures similar to the simulated nanostructure, we can obtain the structural parameters from the SAXS pattern, as shown in **Figure 4**.

References

1. W. Wang, W. Ruland, and Y. Cohen, Acta Polymer 44, 273 (1993).
2. W. Ruland, Applied Polymer Symposia 9, 293 (1969).
3. M. G. Dobb, J. D. J., A. Ma jeed, and B. P. Saville, Polymer 20, 1284 (1979).
4. P. Debye and A. M. Bueche, Journal of Applied Physics 20, 518 (1949).

Mads Pedersen

Phone:	+45 4525 2943
Fax:	+45 4593 2903
E-mail:	map@kt.dtu.dk
WWW:	http://www.bioeng.kt.dtu.dk
Supervisors:	Anne S. Meyer
	Anders Viksø-Nielsen, Novozymes A/S

PhD Study
Started: April 2007
To be completed: March 2010

Lignocellulose Pretreatment for Maximal Enzymatic (Ligno) Cellulose Degradation

Abstract

Pretreatment of lignocellulose is an important step for the production of second generation bioethanol and other biomass derived products. Without pretreatment of lignocellulosic biomass the yield of fermentable monosaccharides is too low to make bioethanol production and other upgrading cost-effective. However, the fast and most effective pretreatment methods are energy demanding and thereby expensive in use. Therefore, it is one of the objectives of this project to evaluate the effectiveness of pretreatment and search for the most cost-effective treatment regarding energy consumption and yield.

Introduction

Degradation of lignocellulosic materials to fermentable monosaccharides can with time become an environmentally friendly alternative starting point for production of fossil fuels, gas and petrochemicals, thereby reducing the dependency of fossil fuel sources and reduce the release of green house gasses [1]. A part of the process is the pretreatment of the plant material which is an important step in making the production of bioethanol economically feasible. The purpose of the pretreatment is to make the cellulose (and hemicelluloses) more susceptible to enzymatic hydrolysis for production of fermentable monosaccharides [2], see Figure 1. The methods used for pretreatment (e.g. steam explosion and wet oxidation) often show to be energy, chemical and time consuming, thereby making the process expensive [3]. Strong acids and bases are also used for pretreating the plant material, but reduce the yield due to production of infermentable sugars and inhibitors. Due to the inhibitors formed and the demand of energy, the production of bioethanol is not economically feasible compared to the use of fossil fuels [4]. To make the biomass processing sustainable the pretreatment needs more attention regarding reduction of energy demand and reduction of the production of potential inhibitors. Therefore, more research is needed in the field of pretreatment of plant material and understanding the role of each polysaccharide forming the complex matrix of plant cell wall.

Specific objectives

The purpose of the project is to find possible improvements for the pretreatment of lignocellulose to enable more sustainable upgrading of lignocellulosic biomass. Initially, macroscopic and microscopic examinations of the substrates will be used to gain more knowledge on the effect of the pretreatment. Scanning Electron Microscopy (SEM) will be used to clarify the physical and chemical changes in the substrate due to fractionation and pretreatment.
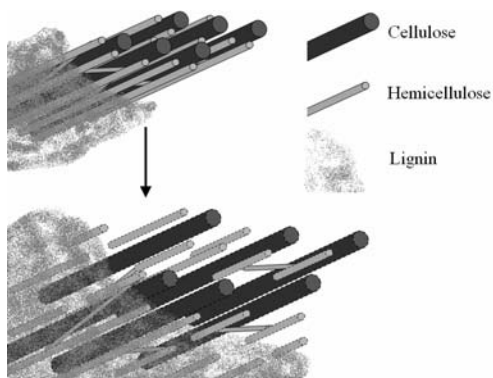
Figure 1: Pretreatment of the biomass resulting in opening of the plant cell wall biomatrix, thus making the biomass more susceptible to enzymatic degradation.

To increase the yield, factors such as viscosity, size of particles, surface and crystallinity needs to be drawn into consideration.

The project will include theoretically calculations on optimization of the pretreatment and scaling up the process for pilot plant. An important part of the project is to make the process ready for scaling the pretreatment up from a laboratory experiment to larger scale without loss of yield efficiency and still be cost-effective.

Experiments

To pretreat the wheat straw wet oxidation has been run at 195 °C for 10 minutes with 10 bar initial oxygen pressure [5].

Hydrolyses of the untreated and pretreated wheat straw were made by the commercial enzymes Celluclast 1.5L (Novozymes A/S) and Novozym 188 (Novozymes A/S) to evaluate the pretreatment. The hydrolyses took place in eppendorf tubes at 50 °C in a thermomixer with 2 % dry matter for up to 24 hours at pH 5 [6].

For analyses of the physical alteration of the wheat straw surface a Scanning Electron Microscope (SEM) was used.

Results and discussion

Figure 2 shows the alteration of the wheat straw surface. Before pretreatment the particles show clear line up of the fibers on the outer surface layer. However, when pretreating with wet oxidation the line up of the fibers seems disrupted and the material looks swollen. This disruption and swelling of the material is thought break down the biomatrix to increase the accessibility of the hydrolyzing enzymes and thereby increasing the yield in glucose.

Figure 3 shows the glucose release from hydrolyses of pretreated and un-pretreated wheat straw. The pretreatment showed a positive effect on the release of glucose. Noticeably, the reduction of the particle size also had an increasing effect on the glucose release.
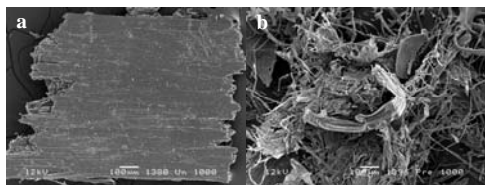
Figure 2: SEM images of wheat straw particle when (a) untreated and (b) pretreated.

Conclusion and future work

So far this project has shown that alongside with the increased release of glucose when pretreating the wheat straw, the reduction of the particle size also has a clear effect on the glucose release. However, energy balances are needed to confirm that the increase in yield also results in a cost reduction.
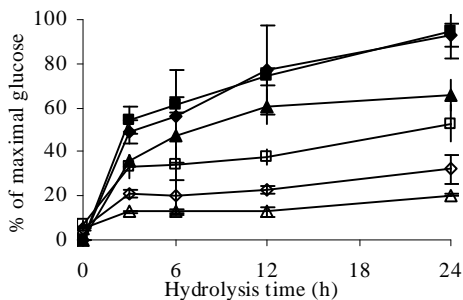
Figure 3: Percentage of maximal glucose release due to enzymatic hydrolysis of pretreated wheat straw (■: 53-149 μm, ♦: 250-500 μm, ▲: 707-1000 μm) and un-pretreated wheat straw (□: 53-149 μm, ◊: 250-500 μm, Δ: 707-1000 μm).

References

1. M.A. Kabel, G. Bos, J. Zeevalking, A.G.J. Voragen, H.A. Schols, Bioresource Technology 98 (2007) 2034-2042.
2. H.R. Sørensen, S. Pedersen, A. Viksø-Nielsen, A.S. Meyer, Enzyme Microb. Tech. 36 (2005) 773-784.
3. *N. Mosier, C. Wyman, B. Dale, R. Elander, Y.Y. Lee, N. Holtzapple, M. Ladisch, Bioresource Technology 96 (2005) 673-686.*
4. A. Esteghlalian, A.G. Hashimoto, J.J. Fenske, M.H. Penner, Bioresource Technology 59 (1997) 129-136.
5. A.B. Bjerre, A.B. Olesen, T. Fernqvist, A. Plöger, A.S. Schmidt, Biotechnology and Bioengineering 49 (1996) 568-577.
6. L. Rosgaard, S. Pedersen, J.R. Cherry, P. Harris, A.S. Meyer, Biotechnology Progress 22 (2006) 493-498.

List of publications

1. M. Pedersen, A.S. Meyer, Biotechnology Progress (in press, 2008).

Conference contributions

1. M. Pedersen, A. Viksø-Nielsen, A.S. Meyer, 7th European Symposium on Biochemical Engineering Science, Faro, Portugal (2008).

Nanna Petersen

Phone:	+45 4525 2861
Fax:	+45 4593 2906
E-mail:	nap@kt.dtu.dk
WWW:	http://www.kt.dtu.dk (no personal page)
Supervisors:	Krist V. Gernaey
	Anna Eliasson Lantz, DTU Systems Biology
	Stuart Stocks, Novozymes A/S

PhD Study

Started:	October 2006
To be completed:	June 2010

Data-Driven Modeling for Monitoring and Control of *Streptomyces* Cultivations

Abstract

Analytical methods utilizing electromagnetic radiation are non-destructive and provide the means of rapidly obtaining important information about fermentation processes. The absorbance in the near infrared region can be used to determine concentrations of relevant chemical constituents while the scattering properties of the broth contain information about the biomass concentration as well as the particle size distribution. The aim of this project is to examine the different methods for modeling these multivariable data sets, estimate reliable models and implement the models in a monitoring and control scheme on a *Streptomyces* cultivation.

Introduction

Measurements of physical, chemical and biological variables are indispensable for monitoring and optimization of fermentation processes. Traditionally, the sensors used for fermentation monitoring measure physical and chemical variables such as temperature, pH and oxygen concentration. Near-infrared spectroscopy can be used to determine the concentration of different biologically important variables such as glucose, ammonia, and biomass on-line in a fermentation process [1].

The morphology of filamentous organisms influences the viscosity of the fermentation broth and thereby also the mass transfer properties of the broth. Furthermore, the metabolism is often closely coupled to the morphology. It is therefore important to monitor and control the morphology of the microorganism. Laser diffraction provides the means of rapidly obtaining robust particle size data. The technique is based on the principle that a particle will scatter light at an angle that is directly related to the size of the particle. It infers a volumetric size distribution, reporting the sizes of spheres with equal volume to the particles actually present. It has the advantage of being much faster than more commonly used microscopy and image analysis. However, it fails to report morphological information such as roughness, compactness, or maximum dimension, which is obtained with image analysis.

The data sets – spectra or size distributions – acquired with NIR spectroscopy and laser particle sizing are very large which makes it difficult to simply visualize the data as well as to interpret them. Therefore, multivariate data analysis techniques are employed in the analysis of these data. Partial Least Squares Regression (PLSR) can be considered the industry standard for the analysis of multivariate data. It is a supervised learning method, which can be used to find correlations between output variables (e.g. biomass and substrate concentration) and a set of input variables (spectral data). PLSR is able to handle correlations in the data by reducing the dimensionality of the data. The data are projected to a subspace spanned by vectors determined to maximize the variance of the input data as well as the correlation with the output variables.

Specific objectives

A first project objective is to establish a data set consisting of a number of batch fermentations with *Streptomyces coelicolor* – a filamentous bacterium producing useful secondary metabolites such as antibiotics – as model organism, and using advanced on-line sensors (NIR) for data collection in addition to standard on-line measurements. The fermentation data set can then serve as a basis for finding and evaluating correlations between sensor data and the course of the submerged bioprocess. A second project objective is to provide a comparison of the performance of several data-driven modeling methods – linear versus non-linear, single model versus multiple local models – on this fermentation data set. A third project objective is to actively use the on-line process variable information

obtained from the advanced on-line sensor data in feedback control loops. Once feedback control using advanced on-line sensors is established, the project focus will shift towards fermentation process optimization.

Concurrently to the work on on-line NIR spectroscopy the multivariate analysis techniques will be used in the analysis of particle size distribution data in filamentous fermentation broths. Common to the work on the different measurement techniques is the focus on increasing the process knowledge, which is an essential part of the PAT initiative published by the FDA in 2004.

Results and discussion

NIR measurements
The first experiments with the NIR sensor have shown that implementing a NIR sensor on-line in a fermenter gives rise to several challenges. The concentrations of the analytes of interest are quite low e.g. for ammonia the range is between 0-0.1 M. This means that the absorbance signal is relatively low. Both air bubbles and biomass particles scatter the light. The scattering depends greatly on the biomass concentration but also on the size distribution of the bubbles and particles. The rapid flow of the air bubbles and particles through the measurement window results in very large variations in the measured light intensity as shown in figure 1.
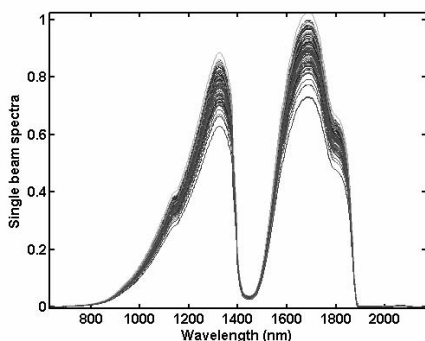
Figure 1. NIR spectra collected for one concentration of biomass, glucose and ammonia in an aerated and agitated fermenter.

The major challenge is to remove all of this unwanted variation while retaining the glucose, ammonia and biomass signal. Pretreatment methods such as multiplicative scatter correction exist which can remove a large part of the scatter effect in the data. The spectra after multiplicative scatter correction are shown in figure 2. The pretreatment has removed a large part of the variations in the data but not entirely. In the coming period different pretreatment methods will be investigated.

The analytes of interest absorb the light in specific wavelength regions. The chemometric modeling methods are developed for handling multivariable collinear data.
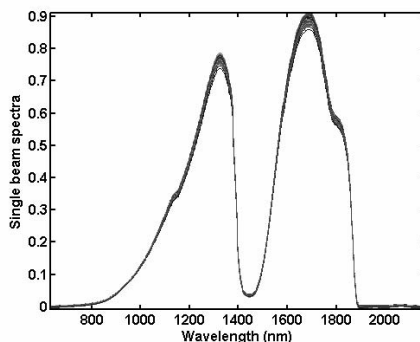
Figure 2. NIR spectra collected for one biomass, ammonia, and glucose concentration in an aerated and agitated fermenter after multiplicative scatter correction.

However, if too many non-informative variables are included in the model this may deteriorate the model quality. Therefore, an important part of modeling the spectral data is to choose which wavelength regions should be included in the model. To support this decision some simple experiments have been carried out in which the NIR absorbance spectra have been collected for different concentrations of ammonia and glucose. The wavelength regions identified for glucose and ammonia are shown in table 1. Interval PLS has also been used for the selection of wavelength regions.

Table 1. Important wavelength regions for glucose and ammonia absorbance.

	Glucose	Ammonia
Wavelength (nm)	1600-1800	1500-1600

When running a fermentation the concentrations of glucose, ammonia and biomass will be correlated due to the specific metabolism of the cell. This may cause problems in the calibration of the chemometric models as it will be uncertain whether the chemometric model is based on the signal of the analyte of interest or some correlation with a signal from another analyte. It will be investigated whether a spiking experiment can break this correlation and thereby improve the robustness of the chemometric models.

Size distribution
Analysis of particle size distribution data was carried out in collaboration with Novozymes A/S [2]. Samples from commercially relevant *Aspergillus oryzae* fermentations conducted in 550 litres pilot scale tanks were characterized with respect to particle size distribution, biomass concentration, and rheological properties. The data set consisted of 99 samples collected from 12 batches.

The size distributions of three different samples from a randomly selected batch are plotted in figure 3.

The multimodal shape of the particle size distribution illustrates that an average size of the particles can be an unsuitable measure of the particle size. There is a clear time dependency in the data. The proportion of larger particles decreases with increasing batch time, while the number of very small particles increases.
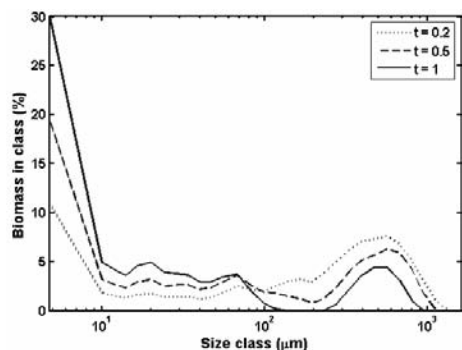
Figure 3. Particle size distributions of three samples taken at three different time points (0.2, 0.5, and 1 normalized batch time) during an *Aspergillus oryzae* fermentation. The graph shows the volume percentage of the particles in each of 31 size classes ranging from 4.75 μm to 1620 μm diameter.

A Principal Component Analysis (PCA) of the data from all 12 batches showed the same overall tendency in all of the batches. The first principal component captured the variation connected to the time development (figure 4) while the second principal component was related to the two different feeding strategies used. From the score plot it was possible to identify batch 5 as an outlier. A look into the process data revealed that a technical malfunction had in fact occurred in batch 5 resulting in a different morphology of the microorganism.

It was possible to correlate the size distribution data to the yield stress, consistency index and the apparent viscosity with PLSR. Validation on an independent test set yielded a root mean square error of 1.20 Nm^{-2} for the yield stress, 0.209 $Nm^{-2}s^n$ for the consistency index and 0.0288 $Nm^{-2}s^{-1}$ for the apparent viscosity, corresponding to R^2=0.95, R^2=0.94, and R^2=0.95 respectively.

Conclusion
NIR spectroscopy is a promising technique for monitoring of fermentation processes. However, several challenges must be overcome before the NIR sensor can be used in automatic control of *Streptomyces* fermentations e.g. low signal to noise ratio in on-line applications.
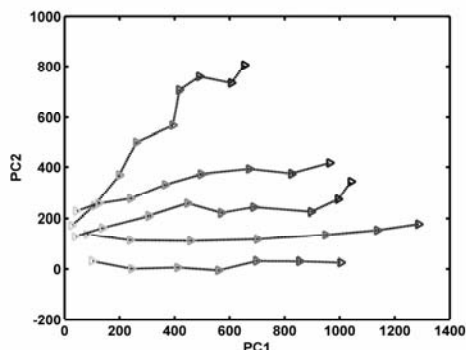
Figure 4. Score plot of the first two principal components in a PCA model of the size distribution data. Scores of the samples from five different batches (batch 5, 11, 9, 2, 1 from top to bottom) colored according to fermentation time from grey to black with increasing batch time. The lines connect samples from the same batch. The other seven batches show the same time development as is seen in the plot but are left out to ease the interpretation.

Chemometric methods can be used to extract valuable information from laser size distribution data. PCA can be used to provide an overview of the multivariate data, explore the data and reveal important correlations. This can be a valuable tool for monitoring purposes but may also help to increase the knowledge of morphology of filamentous organisms.

References
1. M. Scarff, S. A. Arnold, L. M. Harvey, B. McNeil. Near Infrared Spectroscopy for Bioprocess Monitoring and Control: Current Status and Future Trends. Critical Reviews in Biotechnology 26 (2006) 17-39.
2. N. Petersen, S. Stocks, K. V. Gernaey. Multivariate Models for Prediction of Rheological Characteristics of Filamentous Fermentation Broth from the Size Distribution. Biotechnology and Bioengineering, 100 (2008), 61-71.

List of Publications
1. Petersen N., Stocks S. and Gernaey K.V. Multivariate models for prediction of rheological characteristics of filamentous fermentation broth from the size distribution. Biotechnology and Bioengineering, 100 (2008), 61-71.
2. Sin G., Ödman P., Petersen N., Eliasson Lantz A. and Gernaey K.V. Matrix notation for efficient

development of first-principles models within PAT applications: Integrated modeling of antibiotic production with *Streptomyces coelicolor*. Biotechnology and Bioengineering, 101 (2008), 153-171.

3. Petersen N., Gernaey K.V., Padrell A.C., Eliasson Lantz A., Ödman P. and Stocks S. Analyse af NIR data fra *Streptomyces coelicolor* fermenteringer. Den første danske kemometri-konference (DSK.2008), January 10-11 2008, Nyborg Strand, Denmark. (oral presentation)

4. Petersen N., Stocks S. and Gernaey K.V. Chemometric modeling of filamentous broth rheology using size distributions from industrial fermentations. Advances in Process Analytics and Control Technologies 2007 Conference (APACT07), May 2-4 2007, Edinburgh, Scotland,.(oral presentation).

Katja Puder

Phone:	+45 2794 8731
Fax:	+45 4588 2258
E-mail:	pud@kt.dtu.dk
WWW:	http://www.chec.kt.dtu.dk
Supervisors:	Anker Degn Jensen
	Ole Simonsen, Novozymes A/S
	Christian Isak Jørgensen, Novozymes A/S

PhD Study
Started: January 2007
To be completed: December 2009

Mechanisms of Enzymatic Inactivation in the Animal Feed Pelleting Process

Abstract
For the development of new phytases, high pelleting stability is a key factor. In the animal feed pelleting process, steam application, and so temperature and moisture impact, stress the enzymes and they become susceptible towards unfolding, modifications of the proteins might occur and result in inactivation and therewith in a loss of activity. The aim of this project is to elucidate pathways of enzymatic inactivation in the pelletization by different proteomic and structural tools to get a better understanding of the protein's interaction with their environment. This will provide essential information of new formulations and of protective components which can enhance stability.

Introduction
Due to the lack of own intestinal enzymes, external enzymes are supplemented to monogastric animals' diet for providing enhanced digestion of cereal compounds [1]. One of the non-degradable compounds is phytic acid representing the major phosphor source in grains. The addition of the phytase granules into the animal diet catalyzes the hydrolytic degradation of phytic acid, generally yielding inorganic phosphate (Figure 1).
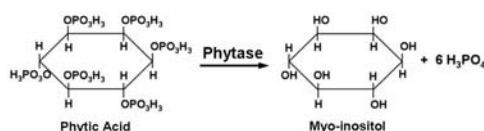
Figure 1: Conversion of Phytic Acid by Phytase

Phytase is applied in the animal diet as granule; a typical granule is composed of enzyme incorporated into a multi-phase core containing various binders, hydrophobic salt, and cellulose. For further stability issues the granule is often coated with polymers.
Animal feed is usually applied in pellets of presenting agglomerated compacted feed. The animal diet processing plant encompasses several main steps including mixing, conditioning, pelletizing and cooling. In the conditioning step, steam is applied providing heat and moisture to the diet for facilitating hygienization and compaction later. Anyway, the combined effect of high humidity (RH, up to 100%), high temperature (T, 70-100°C) and time (t, s-min) is detrimental to enzymes

even though proteins are incorporated in various formulations and coatings supporting stability. The process conditions result in a decline of enzyme specificity and reactivity, or the enzyme gets completely inactivated [2]. Key factors for solid-state stability are moisture and temperature as the stability decreased with increasing moisture utilized. Further on, the excipients in the granule, the impact of the mash and therewith their reaction at elevated temperatures and moisture affect protein stability. Solid-state protein stability is an important parameter which challenged researcher and determines the economic feasibility of phytases.

In general, the major driving forces for protein stability are the hydrophobic forces describing the sequestering of non-polar amino acids, strongly conserved by non-covalent forces, into a core. Meanwhile, hydrophilic moieties are situated on the surface [3]. Those interactions are disrupted at the exposure towards unfavorable environmental conditions; they unbalance the protein leading to unfolding and therewith to aggregation. In this case, the buried hydrophobic residues tend to become exposed to the solvent and interact with hydrophobic residues from other unfolding protein molecules to minimize their exposure. Unfolding can also cause chemical modifications meaning covalent alterations of a protein or amino acid residue producing new molecule via bond cleavage, bond formation, rearrangement, or substitution within the primary structure; but also chemical modifications might result in aggregation. So far, the mechanism for phytase inactivation is not known.

Specific Objectives

The scientific goal of this project is to get an understanding of the interactions of solid-state enzymes (lyophilized powder, granules) with temperature, relative humidity and time and correlate it to pelletization behaviour. Different analytical tools should be used to investigate physical and chemical modifications which should provide hints of the inactivation pathways. In dependence of the obtained results, components improving the stability should be proposed.

Experimental Set up

The set up (Figure 2) provides controlled conditions of RH, T, and t. A humid air stream is generated by evaporating water and adjusting the humidity by diluting the vapor with heated dry air. The mixed gas stream reached an open reactor which can be heated up to 120°C or cooled. The enzyme sample is situated in an aluminum pan placed on a metal holder which enters the reactor from the bottom. The enzyme granules and the lyophilized powder are directly in contact with the humid gas stream. So far, all trials are carried out at a total flow of 1L/min.
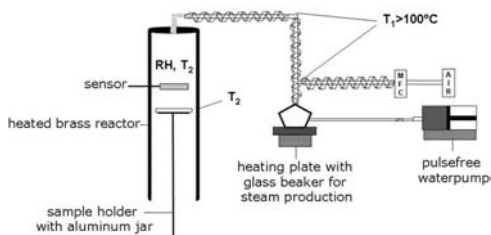
Figure 2: Sketch of Experimental Set Up

Results and Discussion

1. Investigation of Granules

Moisture Adsorption of Granule

Isothermal adsorption-desorption behavior indicated that due to the additional coating, a low moisture uptake of max 4.2% is observed at ambient temperature (Figure 3). An even lower water absorption value is determined at 50°C. A hysteresis loop suggested that moisture sorbed in the porous system can not be easily removed due to capillary forces.
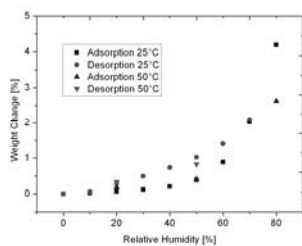
Figure 3: Isothermal adsorption & desorption of Phytase Granule 1. Hysteresis is observed

Effect of Temperature and Humidity

To study the impact of humid, hot air on enzyme stability, enzyme granules were investigated as a function of different temperatures, relative humidities and times. Stability plots are illustrated in Figure 4. Coated phytase granule 1 presents high stability at zero and low humidity exposure for 75°C and 85°C. At 85°C and above 50%RH, the activity drop is significant. At even higher temperature, the phytase activity is drastically reduced. This implies that at high humidity phytase granules become more susceptible towards inactivation.
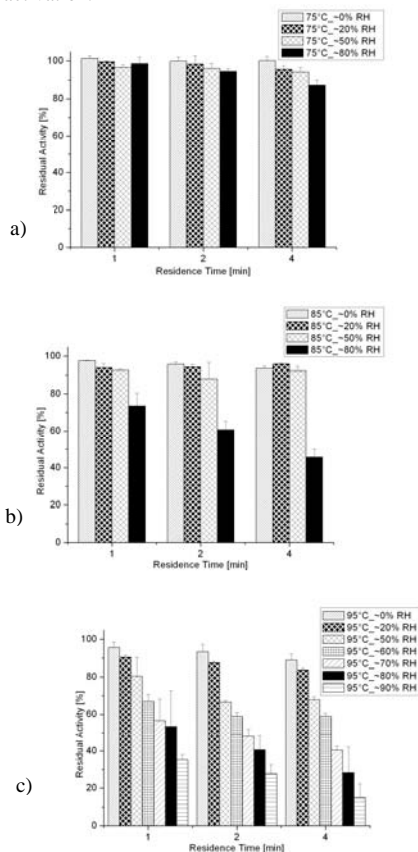
Figure 4: Effect of different temperatures, relative humidity and time on coated phytase enzyme granule 1 a) 75°C, b) 85°C, c) 95°C

The mechanisms behind moisture uptake are complicated due to the different chemicals utilized in the granulation process. At high temperatures the coating melts, and the moisture can get absorbed and diffuse in the granule. Eventually, some of the enzyme and/or matrix material might dissolve resulting in an increasing diffusion rate. When moisture diffuse into the granule, it can not be excluded that salthydrates are

produced or even saturated salt solution due to deliquescence which impacts protein stability [4].

Coated and uncoated granules
Further on, the behaviour of coated and uncoated phytase granule was examined. Figure 5 shows the results and indicate that at low humid air stream (up to 50%RH) the uncoated phytase granules are even a little bit more stabile compared to the coated granule. The hydrophobic salt in the granule might offer better protection towards moisture absorption in the low moisture range; while when the coating melts the moisture diffuse in and cause damage. Nevertheless, at high humidity concentrations, the activity dropped dramatically presumably due to the coating or enhanced and faster moisture absorption [4].
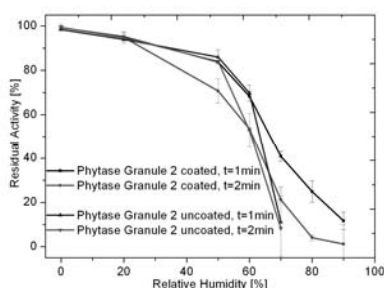
Figure 5: Activity Profiles of coated and uncoated Phytase Granules Exposed to 95°C

2. Investigation of Lyophilized Powder
Moisture Absorption of Lyophilized Powder
For comparison purpose, lyophilized enzyme powder formulated with only hydrophobic Na_2SO_4 (app. 80% salt) was produced. Dry protein rich material can absorb significant amounts of water and can be seen in Figure 6. In this case no hysteresis was observed, implying that moisture can be easily removed by drying.
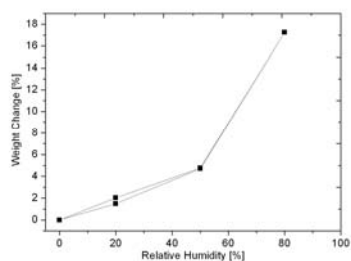
Figure 6: Isothermal adsorption-desorption curve for lyophilized phytase powder at 25°C. No hysteresis recognized.

Effect of Temperature and Humidity
Freeze dried powder was exposed to a hot humid air stream and activity was investigated (Figure 7). In freeze dried powder, proteins are not protected by stabilizers compared to granules. In absence of humidity, the loss of activity is already high. Increased humidity resulted in an enhanced mobility and chemical reactivity; water starts acting as plasticizer allowing unfolding and a loss of the native conformation and therewith reduction of phytase activity [5]; almost no activity is left after 80%RH exposure.
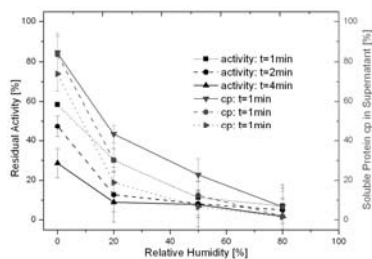
Figure 7 Activity and protein loss of exposed lyophilized powder to 85°C

Redissolving the treated powder showed aggregation. The higher the humidity treatment, the more aggregates where observed and the lower the protein concentration in the supernatant (Figure 7).

Further on, the treated samples were analyzed by SDS-PAGE where proteins were unfolded and separated according their molecular weight (Figure 8). The main band at around 48kDa represents phytase. The low molecular weight bands are impurities in the enzyme powder as they are present in the reference sample. A decrease in the phytase band could not be recognized. Complete dissolution of the treated powder in SDS-containing buffer implied non-covalent modifications. The treatment resulted probably in an unfolding process and eventually in aggregation.
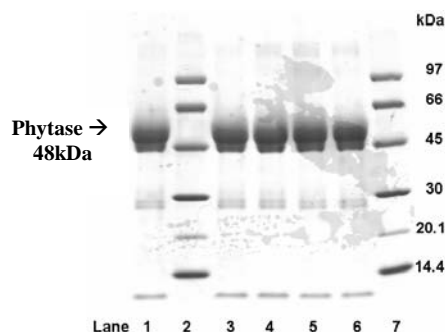
Figure 8: SDS-PAGE of lyophilized Phytase exposed to 85°C for 2 min and different RH's. Lane 2,7-Low Molecular Weight Standards, 1-reference sample, 3-0%RH , 4-20%RH, 6-50%RH, 7-80%RH

Size Exclusion Chromatography – UV (SEC-UV)
After removing the insoluble aggregates, the soluble aggregates in the supernatant were commenced analyzing via SEC-UV, where by chromatographic means proteins or macromolecules can be separated by their size (Figure 9). The middle peak presents the phytase monomer decreasing in the course of the treatment. The protein concentration dropped dramatically during the treatment; eventually, the small peaks left and right might be artifact peaks caused by up concentrating the samples. The aggregates might be lost in the column or the aggregates concentrations are still so low that they can not be caught by the UV-detector. An improved result might be obtained by coupling on the SEC a multi-angle light scattering instrument (SEC-MALS) to determine the absolute mass of the aggregates.
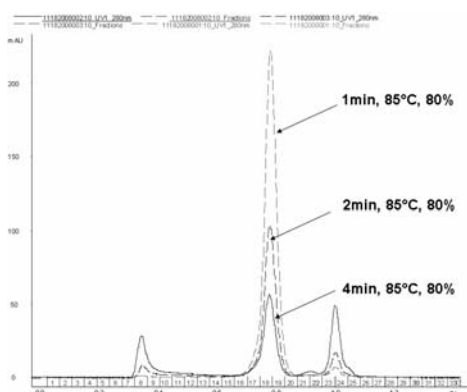
Figure 9: Chromatogram SEC-UV of differently treated powder, 5mg/mL applied; 0.5mL sample volume

Differential Scanning Calorimetry (DSC)
DSC was used to characterize thermal transitions of pretreated phytase powder as a function of temperature (Figure 10).
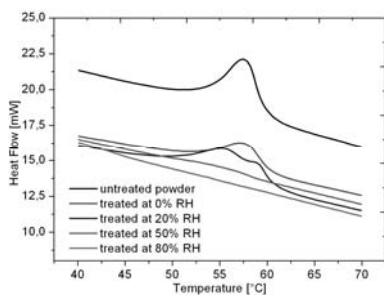
Figure 10: DSC thermogram of untreated and treated phytase powder (85°C, 2min, and different RH's)

The increase of inactivated enzyme could be followed by DSC as the unfolding enthalpy is lowered gradually. At 80%RH where almost no activity is detected, nearly all protein is already unfolded and inactive resulting that no unfolding transition can be detected.

Conclusion and Future Work

A method for controlled exposure of solid-state enzyme towards temperature, relative humidity and time was established. The impact of these parameters was investigated for phytase granules and lyophilized phytase powder. The combined effect of temperature and humidity is causing inactivation of phytase. First studies revealed that lyophilzed powder is probably inactivated by unfolding and followed by non-covalent aggregation.
Investigations of the formation of aggregates are ongoing. Further on, purifying phytase out of treated granule might provide more insight in the inactivation pathway.

Acknowledgements

References
1.   Kersten, J., Rohde H.R., Nef, E., 2005, Principle of Mixed Feed Production-Components, Processes, Technology, AGRIMEDIA
2.   Bhat, M.K., 2000, Cellulases and related enzymes in biotechnology, Biotechnology Advances, 18, p. 355-383
3.   Vielle,   C. &   Zeikus, G.J., 2001, Hyperthermophilic Enzymes: Sources, Uses and Molecular   Mechanism   of   Thermostability, Microbiology and Molecular Biology Reviews, 65, p. 1-43
4.   Kringelum, J., 2002, Measurement and Modelling of Water Sorption Kinetics in Enzyme Granules, Master Thesis carried out at Novozymes A/S
5.   Samborska, K., 2005, The influence of moisture content on the thermostability of Aspergillus oryzae alpha-amylase, Enzyme and Microbial Technology, 37, p. 147-174

Jamal El Bashir Ali Rashed

Address: CAPEC, Building 227, room 227
Phone: +45 4525 2811
Fax: +45 4525 2906
E-mail: jar@kt.dtu.dk
WWW: http://www.capec.dtu.dk

Supervisor: Rafiqul Gani

Ph.D. Study
Started: January 2006
To be completed: July 2008

Model-Based Retrofit Design and Analysis of Petrochemical Processes

Abstract
Driving force based models are developed for different separation and reaction processes for application in model based retrofit design and analysis of petrochemical processes. The design and analysis employs the reverse design approach and generates improved retrofit (design) alternatives. According to the reverse approach, the design variables that match the specified process targets for each unit operation in the process are determined by solving a new class of unit operation models based on the driving-force that "drives" the operation. The reverse approach has been developed and tested for vapor-liquid, liquid-liquid based separation processes and reaction operations.
To generate and screen feasible retrofit alternatives that produce the same products from the same raw materials but under more sustainable conditions, a systematic sustainable design methodology has been incorporated. This methodology is organized in three stages: 1. process analysis; 2. identify and design sustainable alternatives; and 3. final verification. In the first stage, process is analyzed in order to identify the design/operational weak points, indicating potential for improvement and thereby to identify design targets that may improve the process. Once the design targets are identified, the next stage is to identify and design alternatives that match the design targets. This identification of feasible process alternatives is based on thermodynamic insights. The process alternatives are generated through an analysis of the physico-chemical properties of the particular mixture present in the system and based on the relationships between properties and separation technique, a list of feasible sustainable alternatives for the particular separation task are generated. A reverse approach is used to identify the final design details for each alternative. In the third stage, sustainability metrics are calculated in order to select the best retrofit alternative.

Introduction
Competition in the petrochemical market has increased during the past decades. Therefore, to be still competitive, many existing production processes require constant improvements through retrofitting while new processes need to satisfy stricter regulations with concerns to pollution and process safety, thereby making the petrochemical processes more sustainable.

Different methodologies have been used for evaluating the retrofit potential of a chemical process with regard to one of these objectives. For example, Rapoport et al. (1994) presented a strategy using heuristic rules for the generation of retrofit options, while Jaksland et al (1995) presented a thermodynamic insights based synthesis method for generating process alternatives applicable to new processes, as well as existing processes. Ciric and Floudas (1989) used algorithmic approaches such as mixed integer nonlinear programming (MINLP). Also, combinations of these

methods have been developed, for example, Hostrup (2001) combined thermodynamic and mathematical programming methods.

In this project, a design algorithm to generate feasible retrofit process alternatives that will produce the same product from the same raw material but under significantly better conditions is developed. In this methodology, identification and selection of feasible separation techniques are made based on thermodynamic insights and sustainability metrics are used to generate better alternatives.

Specific Objectives
The main objectives of this project can be summarized as follows: The first objective is to analyze a class of current petrochemical processes and to identify their weak points from a point of view of operability, environmental impact, flexibility and energy efficiency. The second objective is to develop a systematic

methodology that can generate new and significantly better alternatives, and to identify from them, the optimal design. The third objective is to verify and validate the optimal design through further model – based analysis.

Methodology
The proposed methodology for systematic generation and screening of feasible retrofit alternatives is proposed in three stages; stage 1: Process analysis, stage 2: Identify and design alternatives and stage 3: final verification

Stage 1: Process analysis
In process analysis stage, process is analyzed in order to identify design/operational weak points and thereby define (design) targets for improvement. The analysis step employs the indicator based method developed recently by Carvalho et al. (2008). According to this method a set of mass and energy indicators are calculated from information of the process. The calculated indicators are used to locate the weak points in the process in terms of mass and energy flows within the process and their influence on the sustainability metrics, the safety metrics and other operational metrics thereby define design targets.

Stage 2: Identify and design alternatives
The purpose of this stage is to identify retrofit alternatives that match the targets for improvement and for each of these alternatives, to determine the important operational (design) parameters through a revere design approach. This stage has two main steps.
Step 2.1 Identify search space feasibility region. In this work, identification and selection of feasible separation techniques are made based on thermodynamic insights (Jaksland et al,. 1995). Jaksland et al. used thermodynamic insights combined with a set of rules related to physio-chemical properties to identify the most appropriate set of separation techniques for a given separation task. The method consists of two levels of calculations. In level 1, the mixture to be separated is analyzed, the binary ratio matrices for each property generated, the issues of the presence of azeotropes and use of mass separating agents identified and based on these, a list of separation tasks is generated. In level 2, the separation techniques are matched with the separation tasks and the sequence of separation tasks that need to be followed is determined, thereby generating an alternative feasible process alternative.

Step2.2 Design new alternatives: The purpose of this step is to design the process alternatives that match targets for improvement through a reverse design approach. First a target for improvement is matched with a corresponding maximum (attainable) driving force for any operation. For example, the driving forces for a separation of a mixture of compounds could be the composition differences in two co-existing phases. Since by definition, an operation is easy and less

expensive to operate if the driving force is higher, the use of the identified maximum driving force as the starting point for the design of an operation implies starting from a near optimal solution from which the important process design parameters are back-calculated. Therefore, the method is called the reverse design approach and does not require simulation and/or optimization to determine the near optimal solutions. Consider the situation where a given mixture is to be separated by simple distillation to specified product purity requirements. First the maximum attainable driving force for the specified separation task is determined. Then from the known value of the maximum driving force, the important design parameters for the distillation column (such as the reflux ratio, number of stages, feed stage location, etc.) are determined. Driving force based models have been developed for different separation and reaction processes for application in model based retrofit design and analysis of petrochemical processes.

Stage 3: Final verification stage
The purpose of this stage is to verify and evaluate the retrofit design alternatives through rigorous simulation. The sustainability metrics is used as the criteria for evaluation of the different alternatives. This stage involves two main steps:

Step 3.1 Simulation of the process with the new design parameters: The purpose of this step is to generate all the data needed to calculate the sustainability metrics. The results from stage 2 are used as initial estimates for the simulation, which therefore, provides a fast and efficient simulation of the process (retrofit) alternatives.

Step 3.2 Calculate the sustainability metrics: Sustainability metrics are calculated for all selected retrofit alternatives identified in stage 2. Use of the sustainability metrics follows the simple rule that the lower the metric the more effective the process. The impact of any retrofit alternative can be summarized in terms of environmental responsibility, economic return and social development.

Illustrative Example
A case study involving a process for styrene production is illustrated in this work. This process starts with the dehydrogenation of ethylbenzene in the reaction section. The reactor effluent is cooled to produce steam and then enters a three-phase separator followed by two distillation columns o separate 99.5% purity of styrene. Now the methodology will be applied in order to generate feasible retrofit alternatives that will improve the process and match design targets.

Stage 1: Process Analysis
Step 1.1 Identify design/operational weak points
The purpose of this stage is to define design targets that may improve the process. The separation of the desired styrene product from the light ends, heavy ends,

benzene and toluene is relatively easy, being accomplished by conventional sequential distillations. The separation of the styrene/ethylbenzene mixture by distillation, however, presents a considerably more difficult problem due primarily to their close similarity in volatility. The pure components boiling points are very close over a large range of pressure and they are difficult to separate by distillation. The separation of styrene and ethylbenzene by distillation is currently used in industry. In the reference process this distillation has large number of theoretical trays, (115 trays), and high reflux ratio.

The driving force indicates if the separation is easy or difficult with respect to normal distillation. If driving force is close to zero, high purity separation would require a large number of plates and energy consumption would be high, while if the driving force is close to 1.00, high purity separation would be easy and energy consumption would be minimal (see Figure 1). From this figure, It can be noted that the separation of styrene/ethylbenzene is difficult because driving force is close to zero, therefore, the separation of styrene/ethylbenzene mixture by distillation requires a high energy consumption. Therefore, from the analysis of the process from point of energy efficiency indicates that the separation of the styrene/ethylbenzene mixture by distillation is a very energy-intensive process comparing with other units in the process.

Step 1.2 Define attainable design targets
From step 1.1, the analysis step from point of view of energy efficiency shows that the separation of styrene /ethyl benzene is the most energy-intensive unit in the styrene production process separation. Using the reduction of the energy consumption as target for improvement, leads to a re-evaluation of the separation techniques used for the separation tasks in this section. That is, consider the changing of the separation techniques for the separation of the styrene/ethylbenzene mixture as the first alternative to improve the process.

Stage 2: Identify and design alternatives
Step 2.1 Identify search space feasibility region
The thermodynamic insights based method (Jaksland et al. 1995) is applied to generate the retrofit alternatives. The separation task involves the styrene/ethylbenzene mixture. Results from levels 1 and 2 are given below. All the calculations related to levels 1 and 2 have been performed through various tools available in ICAS (Gani, 2002).

- Mixture type: This mixture is a normal fluid system at low pressure
- Mixture state: This mixture is in the liquid state at 393 K and 1 atm
- Reactivity: at the specified conditions, the mixture is in chemical equilibrium
- Identification of an zoetrope: There is no zoetrope in this mixture (from the VLE for the styrene/ethylbenzene mixture).

- Predict relative volatility: It is close to unity, in such mixtures the mass separating agent or external separating agent could be used to separate such that mixture (Jacksland et al. 1995)
- Prediction of aqueous solubility: The aqueous solubilities of ethylbenzene in water is 5.997×10^{-4} g/cm^3 and for styrene 3.9×10^{-4} g/cm^3. That is to identify that the water is not a good solvent to separate this mixture
- Identification of eutectic points: Not interested to produce styrene as a sold

Identify separation technique: From the information of mixture analysis and the computed binary ratio are used together to identify the feasible separation techniques for the separation of styrene/ethylbenzene mixture. The following separation techniques have been identified: distillation, extractive distillation, and pervaporation.

In this work, extractive distillation is considered as alternative separation technique for the separation of styrene and ethylbenzene that may improve the process and match design target. Adiponitrile has been identified as good solvent to separate styrene and ethylbenzene by used ProCAMD.

Step 2.2 Design new alternatives
The reverse design approach has been used to identify the final design details for the extractive distillation column and solvent recovery column, by first determining the maximum attainable driving forces available for each separation task. The maximum driving force and the corresponding solvent to feed ratio to achieve the desired separation has been determined through an analysis of the phase compositions of ethylbenzene on a solvent-free basis as a function of the solvent to feed ratio. From the solvent free driving force shown in Figure 3, it is possible to select a solvent fraction of 0.8 to obtain a solvent free maximum driving force above 0.14. From the mass balance calculations and the solvent fraction it is possible to determine that an inlet of 1700 kmol/h of Adiponitrile is needed in the first column. From the driving force diagram generated for styrene/adiponitrile vapor-liquid system shown in Figure 4, the maximum driving force for the solvent recovery column is found to be 0.77. The design parameters for extractive and solvent recovery columns, back calculated to match these driving forces are listed in Table 2.

Table 2: Design parameters of the columns in the

	EB extraction	Solvent recovery column
Number of plates	30	7
Feed plate location	17	5
RRmin	2.77	0.312
Purity of light key	99.5	99.5
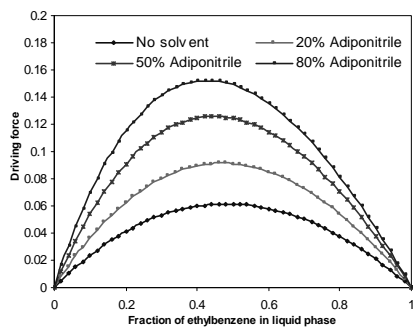
Figure 3: Solvent free driving force diagrams for styrene/ethylbenzene
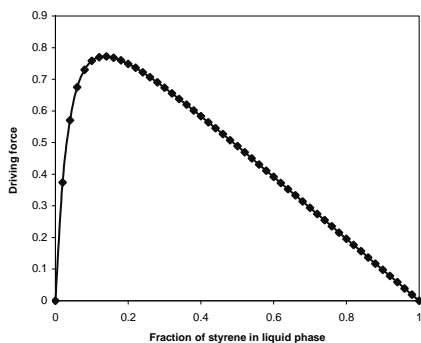
Figure 4: Styrene/Adiponitrile drivning force diagram at 1 atm. .

Stage 3: Final verification

HYSYS has been used to perform the rigorous process simulations. Sustainability metrics have been calculated and compared with the reference case (see Table 3).

Table 3: Comparison of existing process (reference design) and alternative design.

Indicator type	Indicator	Base case design	Alternative design
Energy	Total energy primary energy usage rate GJ/y	455.9×10^4	347.83×10^4
	Total net primary energy usage rate per kg product (kJ/kg)	4.32×10^4	3.3×10^4
Material	Total raw materials used per kg product (kg/kg)	1.53	1.53
	Hazardous raw material per kg product	1.53	1.53
Water	Net water consumed per unit mass of product (kg/kg)	253.34	206.59

The calculations are based on an 8000 h/year rate of work and a conversion factor of 0.8. As it can be seen,

the new alternative gives an improvement, especially for the energy consumption. For the environmental impact factors are calculated by WAR algorithm using the calculated stream compositions, temperatures and pressures of all input and output streams. The results from WAR algorithm (see Table 3), showing a slight improvement in the human toxicity potential by ingestion (HTPI), terrestrial toxicity potential (TTP), and Global warming potential (GWP). It is worth pointing out; however, that it has been possible to achieve design targets (reduction of energy consumption) without disturbing other variables, especially the environmental aspects.

Table 4: Indicators for WAR algorithm

	Base case	Alternative design
GWP	28.239	28.0544
HTPE	-75835	-75494
TTP	-75835	-75494
Total PEI	-2.24×10^6	-2.23×10^6

Conclusions and future work

The benefit of employing the reverse approach is that by solving for the constitutive variables directly from the balance equations of the process model, it is possible to define the design (retrofit) targets. Matching the target through a generate and test procedure then becomes relatively easy to achieve and does not require simulation and/or optimization to determine the near optimal solutions. A systematic design methodology for generating and screening retrofit alternatives has been developed to retrofit existing processes. Application of the methodology has been highlighted through a case study involving the styrene production process. Results from the case study indicate good potential for energy saving by replacing a distillation by extractive distillation as alternative for separate ethylbenzene from styrene in the styrene process.

Current and future work is looking for additional case studies from the petrochemical industry.

References

- Carvalho, A., Gani, R., and Matos, H., Design of sustainable chemical processes: PSEP, in press (2008).
- Ciric, A. R., and Floudas, C. A., Comp. Chem. Eng., **13**, 703 (1989).
- Gani, R. 2002, ICAS Documentations, PEC02-15, CAPEC, DTU, Lyngby, Denmark.
- Jaksland, C., Gani, R., and Lien, K., Chem Eng Sci, **50**, 511-530, 1995.
- Rapoport, H., Lavie, R. and Kehat, E., Comp. Chem. Eng., **18**, 743 (1994).

Louise E. Rasmussen

Phone:	+45 4525 2935
Fax:	+45 4593 2906
E-mail:	ler@kt.dtu.dk
WWW:	http://www.bioeng.kt.dtu.dk
Supervisors:	Anne S. Meyer
	Jens F. Sørensen, Danisco

PhD Study
Started: February 2007
To be completed: November 2010

Development of Quantitative Kinetic Models Describing Enzyme Catalyzed Heteropolysaccharide Degradation: Insoluble Arabinoxylan

Abstract

Enzymatic hydrolysis of arabinoxylan is of considerable interest for various biotechnological applications and an efficient exploitation of arabinoxylans as a carbohydrate source for fermentation to biofuels or for production of novel health promoting food ingredients requires a full understanding of the enzyme systems that effect their conversion. This study focuses on selective enzyme biocatalysis and –conversion of water insoluble arabinoxylan and other xylan structures to obtain uniform xylooligosaccharide products and an improved understanding of the enzyme kinetics and quantitative phenomena.

Introduction

Efficient enzymatic modification and degradation of natural plant cell wall polymers have significant implications in food, biofuel and paper processing and may open up for novel biological production platforms in various industries. Arabinoxylan is the main heteropolysaccharide of the hemicellulose fraction of the cell walls of higher plants where it accounts for as much as 35% of the dry weight [1]. Unlike cellulose, arabinoxylans are chemically heterogeneous molecules which consist of a backbone of β-1,4 linked D-xylopyranosyl residues. Depending on the source of the arabinoxylan and the procedure used for its extraction, the xylose units can be substituted at either the C(O)-2 or C(O)-3 or be di-substituted at both the C(O)-2- and the C(O)-3 position with L-arabinofuranose or 4-O-methyl glucuronic acid residues or they can be esterified with acetic acid. Furthermore, the L-arabinofuranosyl side chain residues can be esterified with ferulic and p-coumaric acid [2].

Due to their complex structure, degradation of arabinoxylans requires several enzymes. The major xylanolytic activities are those catalyzed by endo-1,4-β-xylanases, which hydrolyze the β-(1,4) xylosidic linkages in the arabinoxylan backbone, generating a mixture of arabino-xylooligosaccharides (Fig. 1). Other activities are α-L-arabinofuranosidase, α-glucuronidase, acetyl (xylan) esterase, ferulic acid esterases, and β-xylosidases, each having a specific function in the cooperative degradation process [1]. β-Xylosidase cleaves off the terminal xylose unit from the non-reducing end of the xylooligosaccharides arising from endo-1,4-β-xylanase activity [3]. Some of the enzymes acting on the backbone and side chains have been shown to operate synergistically leading to a higher degree of hydrolysis of arabinoxylan [4,5,6].
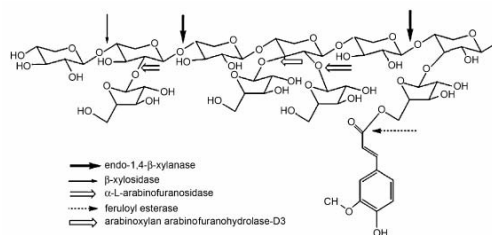
Figure 1: Chemical structure of arabinoxylan and the site of activity of different arabinoxylan degrading enzymes [7].

Enzymatic hydrolysis of arabinoxylan is of considerable interest for various biotechnological applications and an efficient exploitation of arabinoxylan as a carbohydrate source for fermentation to biofuels or for production of novel health promoting food ingredients are currently under intensive study. Xylo-oligosaccharides (XO) derived from partial hydrolysis of arabinoxylan are included among these new food ingredients. One of the most important features of XOs as food ingredients is mainly related to their effect on the gastrointestinal flora

where they stimulate growth of intestinal *Bifidobacteria* [7]. Therefore, XOs are considered as prebiotic, which are non-digestible food ingredients that beneficially affect the host by selectively stimulation the growth and/or activity of beneficial bacteria in the colon. Although the health effects of arabinoxylans are well documented, the effects of the degradation products, XOs, are less studied and therefore, an in-depth study of the prebiotic potential of XOs is warranted [8].

Specific objectives

This project focuses on enzymatic modification and degradation of water insoluble arabinoxylan and other xylan structures. Experiments will encompass use of selected individual xylanases and intelligently designed combinations of relevant enzymes in statistically designed reactions. In order to obtain uniform xylooligosaccharide products from insoluble arabinoxylan selected enzymes will be used and reaction parameters specified. Evaluation of topochemical equations will provide a better understanding of the enzyme kinetics and quantitative phenomena. Unraveling the quantitative kinetics will also encompass consideration of the heterogeneous structure of the substrate matrix and the changes occurring during the reaction.

A particular aim is then to study the prebiotic potential of the enzymatically released xylo-oligosaccharides derived from specific modification of the water insoluble arabinoxylan and other xylan structure on intestinal bacteria.

The hypothesis behind the project is that provision of a better quantitative understanding of the modification and degradation of insoluble arabinoxylan is a prerequisite for optimally exploiting enzyme reactions in new food and ingredient processes and for exploiting biomass rationally for production of value added products.

Experimental methods

Assessments of the enzymatic degradation are mainly accomplished by use of state of the art HPLC: High Performance Size Exclusion Chromatography (HPSEC) and High Performance Anion Exchange Chromatography (HPAEC) mainly focusing on the quantification of arabinose and xylo-oligosaccharides (Fig. 2).
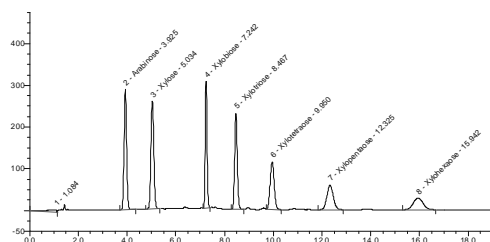
Figure 2: Chromatographic profile of arabinose, xylose to xylohexaose.

Current work

The current work encompasses systematic experimental evaluation of the hydrolysis of insoluble arabinoxylans by selected pure (mono-active) xylanolytic enzymes, including unraveling degradation products and enzyme kinetics. The hypothesis is that it is possible to catalyze the solubilization of isolated, insoluble wheat arabinoxylan and bran, by treatment with selected xylanases to obtain at least 65-75% and 50% of hydrolysis respectively.

The future work is directed towards a better understanding of the initial degradation and to optimize reaction parameters in order to obtain a more specific modification and efficient degradation in the initial phase.

Acknowledgements

References

1. N.M.E. Peij, J. Brinkmann, M Vrsanská, J. Visser, L.H.D. Graaff, Eur J Biochem 245 (1997) 164-173.
2. E.X.F. Filho, M.G. Tuohy, J. Puls, M.P. Coughlan, Biochem Soc Trans 19 (1991) 25.
3. J.A. Perez-Gonzalez, N.M.E. Van Peij, A. Bezoen, A.P. MacCabe, D. Ramon, L.H.D Graaff, App Env Microbiol 20 (1998) 1412-1419.
4. S.L. Bachmann, A.J. McCarthy, App Env Microbiol 57 (1991) 2121-2130.
5. H.R. Sørensen, A.S. Meyer, S. Pedersen, Biotech Bioeng 81 (2003) 726-731.
6. H.R. Sørensen, S. Pedersen, A. Viksø-Nielsen, A.S. Meyer, Enz Microbiol Tech 36 (2005) 773-784.
7. S. A. Hughes, P. R. Shewry, L. Li, G. R. Gibson, M. L. Sanz, R. A. Rastall, J. Agric. Food Chem 55 (2007) 4589-4595.
8. M.J. Vázquez, J.L. Alonso, H. Domínguez , J.C. Parajó. Trends in Food Science & Technology 11 (2000) 387-393.

Martin Hagsted Rasmussen

Phone: +45 4525 2923
Fax: +45 4525 2258
E-mail: mhr@kt.dtu.dk
WWW: http://www.chec.dtu.dk
Supervisors: Professor Kim Dam-Johansen
    Associated professor Stig Wedel
    Kent Thomsen, FLSmidth A/S

PhD Study
  Started: September 2007
  To be completed: September 2010

Reduction of SO$_2$ Emission from Modern Cement Plants

Abstract

The project concerns the emission of SO$_2$ from the preheater section of a modern cement plant, with primary focus on the reaction between CaO and SO$_2$. It has been found that the reactivity of partly calcined limestones is considerably larger than what has been observed for non-calcined limestones under similar conditions. Based on the results it was concluded that CaO may be of great importance for SO$_2$ adsorption in the top stages of the preheater tower.

Introduction

The most common way to produce cement today is by the dry process, illustrated in figure 1. In the dry process raw meal, which mainly consist of limestone and clay, is fed to the preheater tower which typically consist of 4-6 cyclones. Through the cyclone tower the raw meal is, step by step and counter-currently, heat exchanged with the hot flue gas from the calciner/kiln.

Figure 1: Illustration of the dry process for cement manufacturing.

The raw meal contains small amounts of sulfur, which is mostly found as pyrite (FeS$_2$). When pyrite is heated in an oxygen containing atmosphere, it will be oxidized to iron oxides and SO$_2$. This reaction takes place between 400 and 600 ºC [1]. The SO$_2$ formed can leave the preheater as part of the gas phase or react with the limestone in the raw meal, according to Eq. 1.

$$CaCO_{3(s)} + SO_{2(g)} + \tfrac{1}{2}O_{2(g)} \rightarrow CaSO_{4(s)} + CO_{2(g)} \quad (1)$$
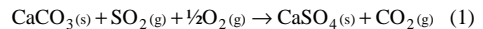
The reaction has been studied by Hu [2] under relevant conditions (relative low temperatures and short residence times). In his experiments Hu [2] found a maximum conversion of the CaCO$_3$ particles of about 0.25 mole % at a particle residence time of 0.35 s and a temperature of 700 ºC

It is also a possible that SO$_2$ formed reacts with CaO, which is formed in the calciner and transported upwards as a part of the flue gas.

$$CaO_{(s)} + SO_{2(g)} + \tfrac{1}{2}O_{2(g)} \rightarrow CaSO_{4(s)} \quad (2)$$
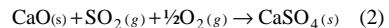
The atmosphere inside a preheater tower contains about 30 vol% CO$_2$ which means that carbonation of CaO will take place below 820 ºC [3]. For this reason CaO transported to upper cyclone stages will only be partly calcined, since it has reacted with the CO$_2$ in the flue gas and thereby carbonation and sulfation will be competitive reactions with regard to CaO.

Specific Objectives

The objectives of this PhD study are:

- To obtain kinetic data for the reaction between CaO and SO_2, under condition similar to those in a preheater tower.

- To develop a mathematical model that quantitatively can describe the reaction kinetics and transport processes.

- To investigate the possibilities for designing new preheaters for cement production with low SO_2 emission.

Experimental Procedure

Two different limestones have been investigated in order to determine their reactivity towards sulfation. The two limestones used were a Faxe bryozo limestone from Denmark and an Obajana limestone from Nigeria, in the following just called Faxe and Obajana, respectively. Both limestones were sieved to obtain a particle fraction between 63 and 180 micron. Each of the limestone samples was subsequently divided into three fractions which were partly calcined for about 1 s at 750, 800 and 850 °C. In the outlet of the reactor gas and particles were separated. Each particle fraction was transferred back to the entrained flow reactor particle feeder, one at a time, and reacted with SO_2. The linear gas velocity in the entrained flow reactor was 20 m/s in all cases. The particle feed rate during the calcination was 500 g/hr and during the sulfation the feed rate was 100-300 g/hr. All experiments were carried out in atmospheric air. The concentration of SO_2 in the sulfation experiments was 1000 ppm.

Results

The conversion of the partly calcined limestones is calculated from equation 1 and is based on the decrease in mole fraction of SO_2 that is observed in the reactor outlet, when particles are injected into the reactor.

$$X_{Ca} = \frac{\Delta x_{SO_2} PV}{RT} \frac{(M_{CaCO_3}(1-X_{cal})+M_{CaO}X_{cal})}{\omega} \qquad (1)$$

The molar mass of the particles is adjusted so that the calcination degree is taken into account. Since the particles are partly calcined the conversion is referred to as the conversion per mol of Ca injected.
In equation 1 Δx_{SO_2} is the mole fraction of SO_2 adsorbed by the injected particles, P is pressure, V is the volumetric flow rate, R is the universal gas constant, T is temperature, M_x is the molar mass of component x, X_{cal} is the calcination degree determined by TGA and ω is the particle feed rate. In figure 2 the Ca conversion for Faxe and Obajana, calcined at 800 and 850 °C and reacted with SO_2 for 0.5 s, is shown as a function of the sulfation temperature.
It is seen that both limestones has a maximum in conversion at 525 °C for the fraction calcined at 800 °C, whereas the fraction calcined at 850 °C does not reach a

conversion maximum for sulfation temperatures below 600 °C. It is also noticed that the fraction calcined at 800 °C and the fraction calcined at 850 °C show very similar Ca conversion at 450 °C and 525 °C.
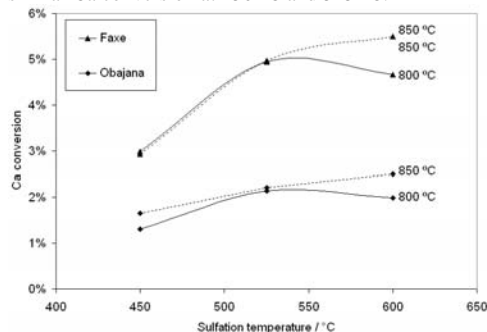
Figure 2: Ca Conversion as a function of temperature for partly calcined Faxe and Obajana limestone.

The maximum observed for particles calcined at lower temperature is due to blockage of the pore system formed during the calcination. The increase in temperature from 525 °C to 600 °C promotes the reaction rate, but is counteracted by the reaction products decreasing free CaO available for reaction, due to the larger molar volume of the product $CaSO_3/CaSO_4$. The leveling off observed for limestones calcined at 850 °C is due to only a partial blockage of the pore system, since in this case the secondary pore system is larger with larger pores and thus less susceptible to full pore blockage.
From figure 2 the Ca conversion of Faxe sulfated at 525 °C is about 5 %. If this conversion is compared to the maximum conversion (0.25 %) observed by Hu [2] in experiments with $CaCO_3$, it is seen that the Ca conversion obtained in these experiments is more than 20 times higher even though the temperature is about 200 °C lower. The present results indicate that CaO may be of great importance for SO_2 retention in the preheater section.

References

1. J.P. Hansen, SO_2 Emissions from Cement Production, Nørhaven Digital, Cph, Denmark, 2003.

2. G. Hu, Emission of SO_2 from Cement Production, DTU, Lyngby, Denmark, 2007.

3. B.R. Stanmore, P. Gilot, Fuel Processing Tec. 86 (2005) 1707-1743

Muhammad Riaz

Phone:	+45 4525 2877
Fax:	+45 4588 2258
E-mail:	ria@kt.dtu.dk
WWW:	http://www.ivc-sep.kt.dtu.dk
Supervisors:	Georgios M. Kontogeorgis
	Erling H. Stenby
	Michael L. Michelsen

PhD Study
Started: April 2008
To be completed: March 2011

Distribution of Complex Chemicals in Oil-Water Systems

Abstract
Chemicals are added to the oil and gas value chain at different positions during the physical flow from well stream to traded product. A fraction of added chemical goes into oil and remaining is discharged to the sea via produced water. It is important to know accurately, how much of an added chemical will go to the water in order to report to the environmental authorities and how much of the chemical will go to the oil. This is becoming increasingly important for down stream processing. The objective of this project is to develop a predictive model for oil-water partition coefficients of complex chemicals, over a wide range of conditions and with minimum input of experimental information.

Introduction
As crude oil resources decrease, the oil industry demands sophisticated methods for the exploitation of natural resources. As a result, the use of oil field chemicals is becoming increasingly important [1,2]. These chemicals belong to families like alcohols, glycols, alkanolamines, ethers, imidazolium salts and polymers. They are added for various purposes such as gas hydrate inhibitors, corrosion and scale inhibitors defoamers, demulsifiers and drag reducers.

Over the last years, the use of chemicals has increased as shown in figure 1. Here the production chemicals used at Statoil operated fields is shown on annual basis.
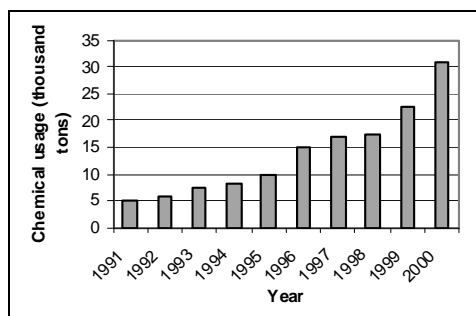
Figure 1: Trend in the use of production chemicals on Statoil operated fields [2].

In the past, calculation of oil-water partition coefficient (Koil) was based on octanol-water partition coefficient (Kow), but later on experiments have shown that oil-water partitioning does not always mimic well octanol-water partitioning [1]. A well stream containing oil water and different chemicals is separated in a series of separators as shown in figure 2. These chemicals generally are added in such small quantities that direct detection by analysis is extremely difficult and in many cases impossible. It is therefore, of interest to establish a relationship between octanol-water and oil-water partition coefficients and modelling for oil-water partition coefficients to develop a predictive model.
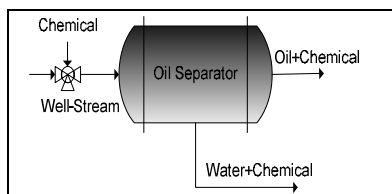
Figure 2: Addition and distribution of chemical in oil-water system

Oil-Water Partition Coefficient
The oil-water partition coefficient of a chemical i is the ratio of concentration of that chemical in the oil and aqueous phases respectively. Concentration of a chemical can be measured and it can be represented in different units. When it is given in term of mole

fraction, equation can be expressed as illustrated in figure 3.
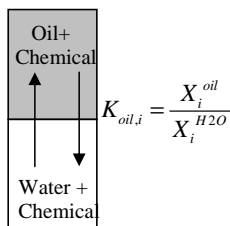
$$K_{oil,i} = \frac{X_i^{oil}}{X_i^{H2O}}$$

where

$K_{oil,i}$ = Oil water partition coefficient of chemical i

X_i^{oil} = mole fraction of chemical i in oil phase

X_i^{H2O} = mole fraction of chemial i in water phase

Figure 3: Oil-water equilibrium and definition of oil-water partition coefficient of a chemical

What is Oil?

Oil is a wider term with no specific general composition and usually mixture of thousands of hydrocarbon and other fractions like water, nitrogen etc. With existing chemical separation techniques we usually cannot identify the many hundreds or even thousands of components found in a reservoir fluid. Even if accurate separation were possible, the critical properties and equation of state (EoS) parameters of compounds heavier than C_{20} would not be known accurately. This problem can be solved by lumping, a number of heavier fractions into fewer fractions called oil characterization [3].

Thermodynamic Models

Cubic EoS such as Soave-Redlich-Kwong (SRK) and Peng-Robinson are the most widely used thermodynamic models for phase equilibrium calculations and physical property estimation in petroleum engineering. But in the presence of complex compounds such as water EoS do not perform very satisfactorily. To describe complex systems containing associating compounds, empirical/semi-empirical modifications of cubic EoS, or more rigorous EoS models explicitly accounting for association, are needed. The cubic plus association (CPA) EoS which is a combination of SRK and the Wertheim association term gives a better, more physical description of systems containing associating compounds compared with the empirical or semi-empirical modifications of cubic EoS. In addition, CPA has been successfully applied to water light hydrocarbon systems and calculation of phase equilibrium between reservoir fluids, water, and methanol or monoethylene glycol [4].

Specific Objectives

The general research issues to be addressed are the following:

- To identify the most important chemicals of interest to Statoil applications, group them into families, collect experimental data of octanol-water (Kow) and oil-water (Koil) partition coefficient and investigate if correlations exist between them.
- To check different thermodynamic models and correlations against experimental values of Kow and Koil and select one to be used in the study, the model selected may be CPA or another SAFT-variant.
- Extension of CPA to reservoir and refinery fluids.
- To perform experiments for obtaining required phase equilibrium data, this will then be used in model development.
- To calculate octanol-water and oil-water partition coefficient of complex chemicals and evaluation of selected model.
- Extend the study to ionic and polymeric materials depending on time.

Conclusions

A literature study has been carried out and investigation of correlations of Koil and Kow was also made. A preliminary calculation of Koil using CPA model was also made and compared with Statoil experimental data. After performing these tasks we have concluded.
1. Oil characterization is a useful tool to make phase equilibrium calculations of complex reservoir fluids
2. There is a real need for experimental Koil data and without it, correlation between Koil and Kow is not possible. Only very few Koil data sets were found in literature.
3. CPA has the capability to model complex associating fluids.

Future Work

1. Compare experimental data of Koil from Statoil to data from other sources for both reservoir fluid-water-chemical and well defined oil (alkane)-water-chemical system.
2. Investigate the effect of interaction parameter of model and characterization method on performance of CPA
3. To carry out experimental work to get Koil data and extend CPA to new chemicals of interest for Statoil

Acknowledgements

References

1. N. Ass, B. Knudsen, J. O. Sæten, E. Nordstad., Society of Petroleum Engineering International 2002(SPE No. 74083)
2. J. Fink, GP Press, 2003, p. ix
3. K. S. Pedersen, P. S. Pedersen, Taylor Francis, 2007, p.81
4. W. Yan, G. M. Kontogeorgis, E. H. Stenby, SPE International, 2007(SPE No. 110009-PP)

Alicia Roman-Martinez

Phone: +45 4525 2910
Fax: +45 4525 2906
E-mail: arm@kt.dtu.dk
WWW: http://capec.kt.dtu.dk
Supervisors: Rafiqul Gani
             John M.Woodley

PhD Study
 Started: August 2008
 To be completed: July 2011

Design of Intensified Bio-Chemical Processes

Abstract

Bio-chemical processes are faced with a strong demand for intensification and integration of process steps to increase yield, to reduce of process time and to cut down in running costs and capital expenditure. In bio-chemical process design and development, operational conditions have to be determined before the process is started, requiring substantial resources for development from the laboratory to the final plant. On the other hand, they provide renewable synthesis routes for the manufacture of important chemicals needed for many chemical-based product developments. Bio-chemical process design tasks have been done on a case-by-case basis, without using general rules for bioprocess selection. The main objective of this project is to develop a systematic model-based generic methodology for design and development of intensified bio-chemical processes to provide a step change in productivity and reduction of costs.

Introduction

The use of biocatalytic process technologies instead of conventional chemical synthesis has been a good option to achieve sustainable and environmentally benign processes. In addition, biocatalysis offers numerous advantages for achieving green chemistry goals: novel, high-yield, shorter processing routes, and lower temperature and pressure conditions. Biocatalysts, as well as the raw materials, are themselves renewable. Through the avoidance of high temperatures and pressures and large consumption of metals and organic solvents, the generation of mass and energy waste per unit of product is drastically reduced [1]. The implementation of an industrial-scale bioprocess, however, usually takes considerable time for development, due mainly to the following reasons:

First, bioconversions could be limited by substrate availability, due to inhibition caused by the starting substrate, its limited aqueous solubility and slow dissolution rate. Intermediates in chemical synthesis may also contain reactive groups that can inactivate or inhibit enzyme activity. Second, for many bioprocesses the major cost in manufacture lies in the downstream process operations where product separation and purification is carried out. The need for purification means that most downstream processes require many steps (each with a lost of product yield). In addition, the vast majority of bio-chemical processes are carried out

in dilute aqueous reaction conditions leading to an ineffective feed to the downstream process.

In many cases the achievable concentration of product is constrained by the biocatalyst. For small molecules in particular the biocatalyst will frequently loose activity at a relatively low product concentration. In reactors using immobilized enzymes as catalysts; there is in addition effect of mass transfer limitations on enzyme activity.

Many chemical and biocatalytic conversions involve reactions with an unfavorable equilibrium. Conversions where the product is unstable should be linked with the following process step to keep the yield as high as possible. Besides, biocatalytic reactions are most normally preceded and followed by a chemical conversion. With this in mind, implementation of an intensified bioprocess needs to consider the integration of the biocatalytic step with neighboring operations, which can be chemical reactions (one-pot synthesis) and/or separation operation (*in-situ* product removal).

In order to overcome these issues, the use of process engineering techniques, such as model-based and computer aided techniques, constitutes an alternative or complementary approach that has the advantage of being of general applicability to different biotransformation systems.
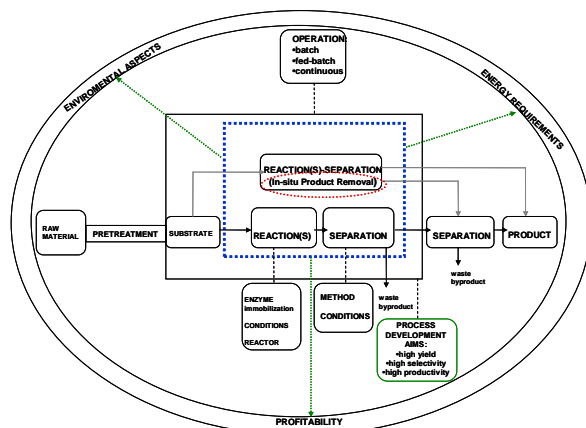
Figure 1. Bio-chemical Process Design Considerations

Objective

In this project, the general objective is to develop a systematic model-based generic methodology for design and development of intensified bioprocesses, considering the integration of chemical and enzymatic reactions (one-pot synthesis) and downstream processing stages (*in-situ* product removal); to provide process improvements by increasing yield, reducing processing time and reducing costs.

Specific objectives

The methodology to be developed will consider ISPR and one-pot synthesis procedures as well as technical and economical aspects, to achieve the goal of rational process development that will maximize the product yield, selectivity, productivity, biocatalyst stability as well as profitability, while trying to minimize energy requirements by employing fewer processing steps and higher yields in each step (Figure 1). Consequently, different routes of synthesis will be generated and evaluated and an optimal bioprocess configuration will be selected and validated.

Model-based strategies for hybrid bio-chemical processes design, supported by computer aided simulations [2], and combined with *a priori* knowledge of experimental data and constraints of the process defining the windows of operations [3] will be used to reduce the development time and systematically improve the process performance. Modeling must be oriented at the optimization task to be solved and must consider all the knowledge available about the biocatalytic system used.

Application of the developed model-based methodology will be validated for the following processes whose limitations are representative of a large number of biochemical processes. The second case involves the generation of an important chemical from renewable resources:

1. *Synthesis of N-Acetyl-D-neuraminic Acid (Neu5Ac)*

   The synthesis of Neu5Ac is attracting growing attention due to increased need for this compound in the pharmaceutical industry. In spite of this growing need there has been almost no advancement of the synthesis routes during recent years, although a number of problems like, unfavorable equilibrium, high amount of waste per kilogram of product and difficult downstream processing are encountered [4].

2. *Enzymatic isomerization of glucose to fructose*.

   The manufacture of HFCS (high-fructose corn syrup) is certainly the largest and one of the most important enzyme processes [5]. The large scale necessitates low manufacturing costs and thus very efficient processing. For this reason, improved process options will be investigated in more depth in this project.

References

1. A. S. Bommarius, B. R. Riebel, Biocatalysis, WILEY-VCH Verlag GmbH & Co. KGaA, (2004)
2. P. T. Mitkowsky, PhD Thesis, CAPEC, DTU, Denmark (2008)
3. J. M. Woodley N.J. Titchener-Hooker, Bioprocess Engineering, 14, 263-268, (1996)
4. V. Zimmermann, H. Hennemann, T. Dauβmann, U. Kragl, Applied Microbiology and Biotechnology, 76, 597-605 (2007).
5. H. S. Lee, J. Hong, Journal of Biotechnology, 84, 145-153, (2000).

Oscar Andrés Prado Rubio

Phone: +45 4525 2801
Fax: +45 4525 2906
E-mail: oap@kt.dtu.dk
WWW: http://www.kt.dtu.dk
Supervisors: Gunnar Eigil Jonsson
Sten Bay Jørgensen

PhD Study
Started: June 2007
To be completed: May 2010

Modeling of Electro-Enhanced Membrane Separation for Anion Recovery

Abstract

A dynamic model for transport of multiple ions through an anion exchange membrane is derived based on an irreversible thermodynamics approach. This model accounts for the convective transport of the dissociated and undissociated species in the channels with diffusion and migration across the boundary layers and membranes. Donnan equilibrium is employed to describe the potential discontinuity on the membrane-solution interface. The Nernst-Planck equation is used to model the ion transport though boundary layers and membranes. The model is tuned for Donnan dialysis recovery of several monoprotic carboxylic acids reported in literature. Simulations are performed to evaluate the potential enhancement of lactate fluxes under current load conditions, referred as Electro-Enhanced Dialysis (EED). Finally, lactate recovery under current reversal conditions is investigated.

Introduction

The work presented in this contribution is part of a study on the integration of a bioreactor and membrane separation processes, in order to optimize the design and operation of such an intensified process according to different objective functions, the selected case study is the lactic acid fermentation. Special attention has been paid to the modelling and simulation of multiple ion transport through anion exchange membranes.

Lactic acid is an interesting product since it is widely used in industry. Perhaps its greatest industrial potential is as feedstock for Polylactic acid (PLA) production. This monoprotic carboxylic acid can be produced synthetically or by Lactic Acid Bacteria (LAB) fermentation of carbohydrates, where the latter is the most used. The fermentation of lactic acid by LAB is normally impaired by product inhibition, similar to many other fermentation processes at a certain concentration level of the product or one of the bi-products [1]. Hongo *et al*. studied the inhibition of *Lactobacillus delbueckii* in the presence of different lactates with and without pH control, concluding that even neutralized lactates generate inhibition [2]. The inhibitory effect generated by the presence of lactates and low pH can be diminished by continuous removal of lactate from the fermentation broth combined with pH control, this will result in a higher productivity and product yield. In addition, continuous recycle of the biomass will allow obtaining higher cell densities which will minimize the risk of cell washout, thereby the fermentation can be operated at higher dilution rates than the specific growth rate of the organism.

Due to the lactic acid properties, conventional continuous separation operations such as distillation have limited potential. Therefore, research has focused on developing alternatives for downstream processing [3]. Since 1960's, membrane separation processes have been suggested as alternatives for the lactic acid extraction and biomass confinement. These processes are advantageous since they can be very selective, are capable of being operated aseptically and there are no by-products generation. The application of processes as Dialysis, Donnan Dialysis, Electrodialysis, Ultrafiltration, Nanofiltration, Reverse Osmosis, or their combination is well documented. From these techniques, Electro-Enhanced driven membrane separation processes are attractive, as *in situ* separation methods, since lactate can be selectively removed by ion exchange membranes during electrochemically pH-controlled electrodialysis fermentation.

Specific objectives

The objective is to model and investigate the recovery of anions, particularly monoprotic carboxylic acids using electro-enhanced membrane separation processes. The proposed separation method is Reverse Electro-Enhanced Dialysis (REED). This technique was recently designed; its performance suggests it to be a promising alternative for continuous removal of lactic acid during fermentation [4].

Modelling of Reverse Electro-Enhanced Dialysis

Since 1980's, when electrodialysis was proposed as an alternative for the continuous recovery of lactic acid from fermentation broth, several potential problems have been encountered: membrane fouling, scaling due to the presence of divalent cations and when bipolar membranes are used, for further recovery and concentration of lactic acid, then the presence of Calcium and Magnesium can damage or destroy these membranes [2,4].

Donnan dialysis appears as a promising process where the scaling and bipolar membrane degradation problems are avoided since only anion exchange membranes (AEM) are used. In addition, the fouling problem is reduced due to high flow velocities and a destabilization mechanism is generated by the hydroxyl flow through the membrane. The main drawback using Donnan dialysis is a rather low lactate flux, since the driving force behind the lactate transport is the hydroxyl concentration gradient in the opposite direction [5]. The REED design emerges as a potential method to enhance the lactate fluxes in conventional Donnan dialysis operation, this is done by imposing an external electrical field. REED combines elements from electrodialysis reversal (EDR) and Donnan dialysis (DD) operations.
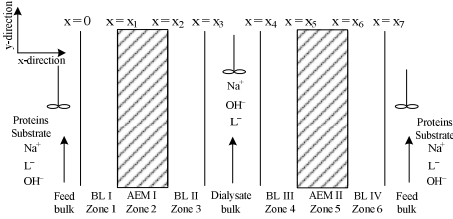
Figure 1: sketch of a cell in the REED module. BL: boundary layer, AEM: Anion exchange membrane

The REED module is composed of several cells in parallel. The transport of ions across anion exchange membranes in a REED stack cell is modelled (see Fig. 1). A cell consists of two feed channels with one dialysate channel in between. The different zones and the ions present in each zone are indicated in Fig. 1.

Model assumptions

➢ General: electroneutrality condition at any location in the system, the electrical current is carried by ions, ideal solution and the process is carried at sub-limiting current densities. Species included in the model are: carboxylic anion, hydroxyl, sodium, dissociated protein, carboxylic acid and undissociated protein.
➢ Membrane: there are diffusive and electrophoretic transports in the x-direction (Fig. 1), no convective transport, water transport by osmosis and electro-osmosis are neglected, there is no transport of uncharged species or big molecules through the membrane, the membrane surface is in equilibrium

with the solution and the influence of swelling on membrane dimensions is not included initially.
➢ Boundary layer: diffusive and electrophoretic transport in the x-direction are investigated, convective transport is neglected and the thickness of the boundary layer is constant for a given flow condition.
➢ Bulk channels: there is convective transport in y-direction in the bulk channels and a tank is series model is used in the y-direction.

Boundary layer and membrane transport

As general notation, the substances and the phases are denoted by the subscripts k and p, respectively. The phases are the channels, boundary layers and membranes. The mass balances for each phase are formulated in the following subsections. A component mass balance is formulated in these zones:

$$\frac{\partial C_{k,p}}{\partial t} + \nabla J_{k,p} - \Delta R_k = 0 \qquad (1)$$

The reaction term (ΔR_k) is used to introduce the acid dissociation into the model. The flux $J_{k,p}$ is estimated using the Nernst-Planck equation for ideal solutions, neglecting convective transport [5]:

$$J_{k,p} = -D_{k,p}\left(\frac{\partial C_{k,p}}{\partial x} + \frac{z_k F C_{k,p}}{RT}\frac{\partial}{\partial x}\right) \qquad (2)$$

Where $D_{k,p}$ is the diffusion coefficient, z_k the valence, F is the Faraday number, R is the ideal gas constant, T is temperature and ψ is the electrical potential. The potential gradient can be calculated using the assumption that the entire current I_d is carried by ions:

$$I_d = \sum_k z_k F J_{k,p} \qquad (3)$$

Bulk channel model

The bulk channel models are approximated using tanks in series model, where in each tank there is mass exchange with the adjacent membrane. The dissociation reactions are present as well. The mass balances for each tank in the feed channel is depicted in equation (4), where q is the flow rate and h, L, W are the height, length and width of the channel, respectively.

$$\frac{dC_k^{feed}}{dt} = \frac{q_{feed}}{h_{feed}LW}\left(C_k^{feed,in} - C_k^{feed}\right) +$$

$$\frac{1}{h_{feed}}\left(J_k\big|_{x=x_7} - J_k\big|_{x=x_o}\right) + \Delta R_k \qquad (4)$$

The model for the dialysate channel is completely analogous.

Boundary conditions at the interfaces

For sorption in equilibrium at the membrane surface, the electrochemical potential in the ionic solution and the membrane surface must be the same. Then the following relation arises for an ideal solution [5]:

$$\Delta \psi_{Don} = \frac{RT}{z_k F} \ln \left(\frac{C_k^s}{C_k^m} \right) \qquad (5)$$

Where $\Delta\psi_{Don}$ is the Donnan potential and the superscripts *s* and *m* correspond to solution and membrane, respectively. The Donnan potential gives the potential build-up at the membrane-solution interface, which is determined by the ionic distribution. Besides, the fluxes at the membrane-solution interfaces must be conserved since there is no accumulation.

$$J_k \big|_{x=x_j^-} = J_k \big|_{x=x_j^+} \qquad (6)$$

Finally, the electroneutrality condition affects the concentration distribution in both the membrane and the solution. On the solution side:

$$\sum_k z_k C_k^s = 0 \qquad (7)$$

On the membrane side:

$$\sum_k z_k C_k^m + z_{fix} C_{fix}^m = 0 \qquad (8)$$

Where the subscript *fix* is related to the fixed charged groups in the membrane. Finally, the assumption that the entire current is carried by ions remains.

Model solution

The dynamic model depicted above in equations 1-8, is based on first engineering principles for diffusion, migration, convection and reaction; it consists of a system of stiff partial differential and algebraic equations that must be solved simultaneously. The method of lines is used to discretize the partial differential equations. Sixth order Taylor expansion was employed, then seven point difference equations are derived for asymmetric centered differences. Due to the complexity of the model, an inconsistent set of initial conditions leads to numerical problems (index problems), Møllerhøj [6] proposed an initialization procedure in order to guaranty, to some extend, convergence.

Results and Discussion
Model tuning
The model parameters are tuned using experimental data taken from literature [7]. In that publication, the dialytic transport of carboxylic acids, through Neosepta-AMH, is investigated as function of the inlet base concentration in the dialysate channel. The derived model was simplified in order to reproduce the experimental conditions. Through a sensitivity analysis, the influence of several unknown parameters on carboxylic ion fluxes was investigated. Those parameters are: anion exchange capacity of the membrane, the boundary layers thickness and the water content of the membrane. From this investigation, the thickness of boundary layers and the anion exchange capacity of the membrane were fixed. The membrane water content has a significant influence on the fluxes, since the diffusion coefficients within the membrane are related to their value in solution by a steric factor, which is a function of the membrane water content. The Mackie and Meares equation (cited by [8]) is used. It has been evidenced experimentally that the membrane water content increases by increasing the average pH. However, if pH is very high membrane dehydration could happen [9]. In this study, a black box model is proposed for water content as function of the concentration of hydroxyl ions at the inlet of dialysate channel.

$$WC = \left(C_{OH}^{dia,in} \right) \qquad (9)$$

The methodology used for parameter estimation is a numerical method for large scale optimization, this algorithm is a subspace trust region method based on the interior reflective Newton method for non linear minimization subject to constraints [10]. The unknown parameters in the model were estimated for three different monoprotic carboxylic acids: acetate, lactate and propionate. The results are shown in Fig. 2. From the fitted simulation results, the agreement between experimental data and the predicted fluxes is clear.
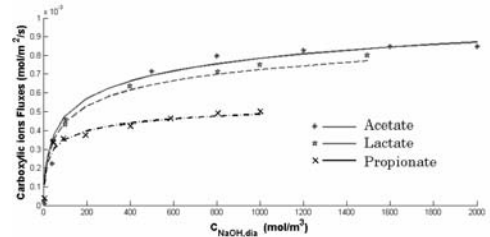
Figure 2: experimental and fitted simulated fluxes for acetate, lactate and propionate as a function of the inlet base concentration in the dialysate channel

Ions transport under current load conditions
As mentioned above, a drawback of Donnan dialysis operation is the rather low membrane fluxes. The REED design proposes to enhance ion fluxes by applying an external current, this way of operation is referred as Electro-Enhanced Dialysis (EED). The lactate flux enhancement generated by the imposed potential gradient is investigated next. Using the fluxes calculated for Donnan Dialysis operation as control, lactate flux is calculated for a range of current densities up to 260 A/m². In figure 3, the relative membrane flux enhancement is depicted.

It can be seen that there is not an apparent enhancement by applying low current densities, the

reason is that the flux is increased in one membrane but diminished in the other, then the total flux is nearly constant. Besides, the enhancement is higher for low hydroxyl concentration in the dialysate channel when the current density is increased. A large improvement of the lactate flux at low hydroxyl concentration means that fluxes for high current densities are almost independent of the base concentration.
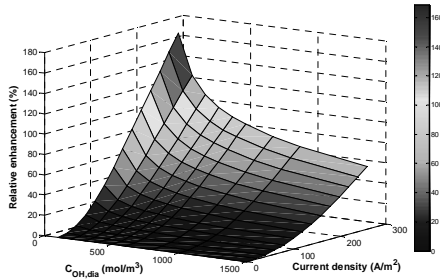
Figure 3: relative lactate flux enhancement as function of the current density and hydroxyl inlet concentration in the dialysate channel, 0% enhancement correspond to the Donnan Dialysis flux

Operation under current reversal conditions
Membrane fouling is an important factor since carboxylic acids are recovered from fermentation broth, which is characterized by high biomaterial content that easily can be adsorbed at the membrane surface. This is disadvantageous for a long term sustainable operation. REED minimizes the adverse fouling effect by reversing the current density periodically. REED is operated using constant current density, this implies that the strength of the external potential gradient must be increased with time. The lactate recovery under pseudo steady state operation is estimated as a function of the current reversal time, results are depicted in figure 4.
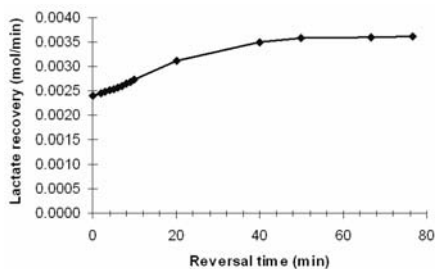
Figure 4: pseudo steady state lactate recovery for different current reversal times, t_{rev}=0 corresponds to Donnan Dialysis conditions

Higher recoveries are expected by increasing the current reversal time. At very high current reversal time, there is a plateau in the recovery since the concentration profiles are nearly developed in each period, which means that the maximum flux is achieved.

The price of high recoveries is the energy required to keep a constant current density. Then, the optimal operating point will represent a trade off between the carboxylic anion recovery and the energy consumption, subject to constraints.

Conclusions
Using first principles, the simultaneous transport of multiple ions through anion exchange membranes was modeled. The model consists of a system of multiregion partial differential equations. It was discretized using high order Taylor expansion. Employing experimental data for dialytic recovery of carboxylic anions, the parameters in a diffusion model were estimated. The predictive power of the model is limited to each ion type and the investigated membrane. It was estimated that the lactate fluxes can be enhanced up to 230% by imposing an external electrical field. This model was developed as a tool to optimize the design and operation of the REED module.

References

[1] Nielsen, J.; Villadsen, J. and Lidén, G. Bioreaction Engineering Principles. Kluwer Academic/Plenum Publishers, second edition. (2003).
[2] Hongo, M.; Nomura, Y. and Iwahara, M. Novel Method of Lactic Acid Production by Electrodialysis Fermentation. *Applied and Environmental Microbiology*, 52(2), (1986), 314–319.
[3] Hulse, J. Biotechnologies: Past History, Present State and Future Prospects. *Trends Food Sci. Technol.*, 15, (2004), 3–18.
[4] Rype, J. Modelling of Electrically Driven Processes. Ph.D. thesis, Technical University of Denmark. (2003).
[5] Strathmann, H. Ion-Exchange Membrane Separation Processes. Membrane Science and Technology Series, 9. Elsevier. (2004).
[6] Møllerhøj, M. Modeling the REED Process. Master's thesis, Technical University of Denmark. (2006).
[7] Zheleznov, A. Dialytic Transport of Carboxylic Acids through an Anion Exchange Membrane. *Journal of Membrane Science*, 139, 137–143. (1998).
[8] Jonsson, G. The influence of the Porous Sublayer on the Salt Rejection and Reflection Coefficient of Asymmetric CA Membranes. *Desalination*, 34, (1980), 141–157.
[9] Izák, P.; Hovorka, S.; Bartovská, L. and Crespo, J. Swelling of Polymeric Membranes in Room Temperature Ionic Liquids. *Journal of Membranes Science*, 296, (2007), 131–138.
[10] Coleman, T. and Li, Y. On the Convergence of Interior-Reflective Newton Methods for Nonlinear Minimization Subject to Bounds. *Mathematical Programming*, 67, (1994), 189–224.

Kaushal S. Sagar

Phone:	+45 4525 6825
Fax:	+45 4588 2161
E-mail:	kass@kt.dtu.dk
WWW:	http://www.licort.dk
Supervisors:	Professor Martin E Vigild
	Senior Scientist Sokol Ndoni
	(DTU Nanotech)

Started:	July 2008
To be completed:	July 2011

Polymer Design and Processing for Liquid Core Waveguides

Abstract

Today's current social scenario demands an attention to the growing need of quick, simple and low cost diagnostics of issues related to health, pollution, food safety. Diagnostics for high sensitivity quantitative measurements are to a large extent based on optical sensors. A perfect scenario would thus be able to perform on-site measurement capability, which are miniaturized for lab-on-a chip applications. The present project intends perfect focus on a sensor application by using liquid core waveguide technology.

Introduction

Optically based detection systems are widely used in analytical systems because of their high sensitivity to extremely low quantities of materials. There is currently much interest in basing miniaturize sensing systems on optical detection where the matter of interest is confined to a micro channel. The use of optical waveguides on-chip with the liquid core technology has opened the way for more advanced detection systems with improved limits of detection.

This work mainly focuses on the processing development for devices used for the above applications. This is materialized using the clean room facilities at DTU DANCHIP. This will lead to fabrication of the liquid core waveguides based on nanoporous materials [1, 2].

Experimental work

Liquid core waveguide phenomenon can be seen in scheme 1. As the refractive index (RI) values plays a crucial role in waveguiding phenomenon, the initial block copolymer upon etching reduces the effective RI to a greater extent.

Here the nanoporous polymers are prepared by initially solvent casting the *polybutadiene-polydimethylsiloxane (PB-PDMS)* block copolymer in *tetrahydrofuran (THF)* with 1 mol % of the cross-linker *dicumyl peroxide* wit respect to the number of double bonds of the PB component.[3,4] This is further cross-linked at 140 °C in an argon/nitrogen atmosphere for 2 hours. The etching

of the PMDS minority block is done by using *tetrabutyl ammonium fluoride (TBAF)* in 1:3 molar ratio of PDMS. The etching step lasts for 36 hours which is followed by the cleaning of etched matrix in THF and methanol for total 16 hours (Figure2)
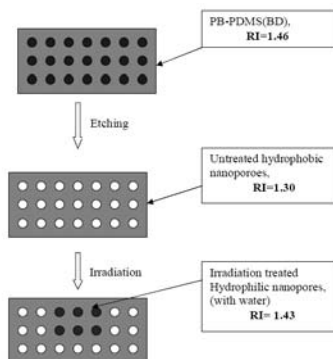
Where,
$RI_{PB} = 1.5$, $RI_{PDMS} = 1.4$, $RI_{water} = 1.33$, $RI_{air} = 1$

Scheme 1: Schematic diagram illustrating the working principle of liquid core waveguide

The nanoporous material is further turned selectively hydrophilic by irradiation technique which means that the exposed volumes will then take up water upon submerging of the sample into water. This is ready for further optical testing part as the contrast in the refractive index is now feasible.
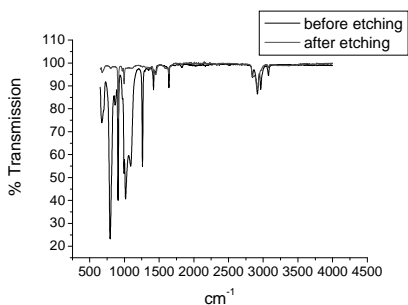
Figure 2: Fourier Transform Infrared spectra of nanoporous polymer, — unetched, — etched sample.

These samples are subjected to the optical testing set up. It consists of a laser light source of 655nm. Light at the other end of the curved hydrophilic waveguide is being collected by a spectrometer probe which shows the intensity of the out coming light signal (Figure 3).
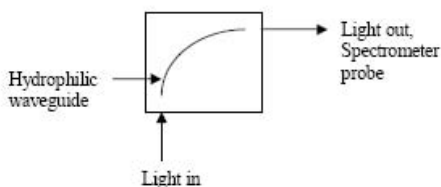
Figure 3: Schematic setup for the optical testing of waveguide

Results and Discussions
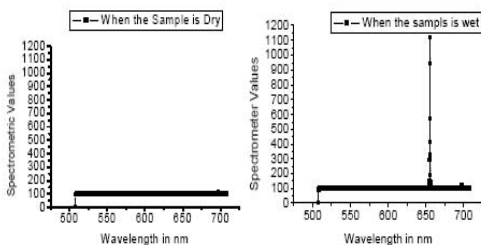
Figure 4: Light guiding experiment demonstrating the waveguiding phenomenon. Figure on the left is from a dry waveguide, Figure on the right is from a wet waveguide.

As can be seen from the Figure 4, a dry sample does not exhibit any significant peak at the ingoing wavelength but scatters the beam of light. On the other hand, when the water filled waveguide is subjected to the laser source it guides the light due to higher refractive index of the core than the surrounding material. It thus bends the light in the curved waveguide.

Thus the primary results indicate the demonstration of waveguiding of light. This can be further optimized in terms of performance of the waveguide. The primary task would thus be to enhance the performance of the waveguide by creating favorable conditions for better waveguiding. This requires work in the area of waveguide fabrication and the alterations in various reaction conditions of hydrophilising the polymer.

References

1. M.P. Duggan et al, A non- vasive analysis method for on-chip spectrometric detection using liquid-core waveguiding within a 3D architecture. Analyst, 2003, 128, 1336-1340

2. M. Holtz et al, small volume Raman spectroscopy with liquid core waveguide. Anal. Chem,vol 71,pp 2934-2939, 1999

3. S. Ndoni et al, Nanoporous materials with spherical and gyroid cavities created by quantitative etching of polydimethylsiloxane in polystyrene-polydimethylsoloxane block copolymer. J.AM. CHEM. SOC. 2003,125, 13366-13367

4. M. Hansen et al, Nanoporous crosslinked polyisoprene from polyisoprene. Polydimethylsilsiloxane block copolymer. Polymer Bulletin 51, 403-409 (2004)

Sara Bülow Sandersen

Phone:	+45 4525 2982
Fax:	+45 4588 2258
E-mail:	sbs@kt.dtu.dk
WWW:	http://www.ivc-sep.kt.dtu.dk
Supervisors:	Nicolas Smit von Solms
	Erling Halfdan Stenby

PhD Study
Started: May 2008
To be completed: April 20011

Enhanced Oil Recovery with Surfactant Flooding

Abstract
The aim of this Ph.D.-study is to investigate the phase behavior of single component surfactant systems at elevated temperatures and pressures for use in surfactant flooding for enhanced oil recovery. A literature study has been conducted to create a basis for the experimental work. Previously it has been common to use multi component systems for surfactant flooding, but as chromatographic separation takes place in the reservoir this is not a preferable approach. The mixed surfactant solution will then adsorb to the reservoir rock during flooding, which results in a surfactant blend that deviates from the optimal surfactant blend originally injected. Finally this results in poor oil recovery, which must be avoided.

Introduction
Many mature reservoirs still has about 50 % of the original oil in place despite that they are already using both primary and secondary oil recovery techniques.
One technique to attain higher oil recovery is chemical enhanced oil recovery (EOR), where surfactants are injected to the reservoir to reduce the interfacial tension (IFT) between oil and water. However, this technique encompasses several complex issues and the design of chemical EOR must be tailored to the reservoir rock and fluid. The principle of flooding is illustrated in figure 1.

RESIDUAL OIL
WATER
ROCK
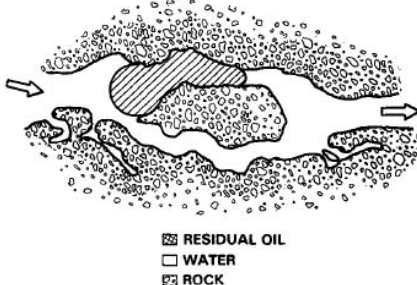
Figure 1: Principles of flooding, where residual oil is trapped in the reservoir, [1]. The residual oil trapped in narrow capillary pores is held back thanks to capillary forces and it is required to reduce the IFT between oil and water to 0.001 dynes/cm to mobilize the oil.

The primary goals in EOR operations are to displace or alter the mobility of the remaining oil, still present in the reservoir after conventional primary and secondary oil recovery techniques has been applied. Surfactant flooding EOR is a rather expensive technique and therefore it can only be justified when the oil price are relatively high. Usually the remaining oil is distributed in the pores in the reservoir, where the oil is trapped due to capillary and viscous forces. The mobilization of the residual oil is achieved through surfactants generating a sufficiently low oil/water IFT. Low IFT further gives capillary numbers large enough to overcome the capillary forces. The recovery efficiency is highly dependent on the capillary number which is defined as equation 1.

$$N_c = \frac{\mu_w \nu_w}{\varphi \gamma_{wo}} \qquad (1)$$

Where N_c is capillary number, μ_w is viscosity of the aqueous or displacing phase in [Pa Sec], ν_w is flow rate of the displacing fluid in [cm/sec], φ is effective porosity of formation and γ_{wo} is interfacial tension between water and oil in [N/m].
It is not unusual that co-surfactants are blended into the liquid aqueous solution to improve the properties of the surfactant solution. Co-surfactants serve as a promoter or help the blend to meet optimal conditions with respect to reservoir temperature, pressure and salinity. It is experienced that due to chromatographic separation during flooding it is very complicated to design a surfactant/co-surfactant solution that can perform

optimal throughout the reservoir. During surfactant flooding there will be losses due to adsorption and trapping to the rock.

Also it is essential to assure stability of the surfactant solution, which must resist physical conditions such as high temperatures, high pressures and high salinities. [2]

Specific Objectives

In this Ph.D.-project it is the purpose to investigate the potential of single component surfactant systems in contrast to the more ordinary systems with surfactants and co-surfactants.

Surfactant Flooding

EOR with surfactant flooding has been investigated for many years. Unfortunately, the economic reality of the process is that the technique is very expensive and therefore it has not yet been commercial employed, as it has not been tested successfully in full scale yet. [3]

Chemical EOR is introduced as this can contribute to improve oil recovery efficiency. The process is the injection of one or more specific liquid chemicals, the so-called surfactants, that controls the phase behavior properties in the reservoir. Injecting surfactants should entail that the IFT between the injected liquid and oil is reduced to 0.001Dynes/cm, which will then overcome the existing capillary forces and thus mobilize the oil towards the production well.

There is a great potential of chemical EOR with surfactant flooding, as this technique encompasses the possibility of designing a process where the overall displacement efficiency can be increased. It is also expected that surfactant flooding could be designed to increase the economic productivity, as the economic productivity for some mature reservoirs nowadays are low despite having 50-70% of the original oil still in place. [4] Surfactants in their common form take structures as depicted in figure 2.

Hydrocarbon 'tail':
Lipophilic and hydrophobic (nonpolar)

'Head' group:
Hydrophilic (polar)
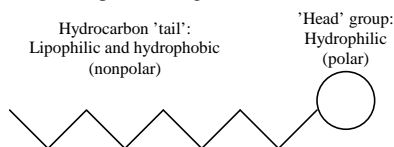
Figure 2: Surfactant molecule, whit the nonpolar hydrocarbon 'tail' to the left and the polar 'head' group to the right.

Surfactant flooding EOR involves microemulsions, where oil/water and water/oil micelles are formed. In the beginning of a surfactant flood the surfactant concentration is low and then the concentration increases as the amount of injected surfactant solution rises. At low surfactant concentrations the surfactant molecules are dispersed as monomers. As surfactant concentration is increased the surfactants molecules starts to aggregate and at some point the concentration will reach the critical micelle concentration (CMC). Any further addition of surfactants will form into micelles.

Surfactants are frequently classified by their ionic nature of the head group as anionic, cationic, nonionic or zwitterionic.

Anionic surfactants are the most widely used surfactants for surfactant flooding and according to Austad *et al.* (1996) [5] promising surfactants, for single component surfactant flooding, are branched ethoxylated sulfonates.

Phase Behavior

It is reported in literature that an increase in temperature increases the optimal salinity for the surfactant system.

Aside from the influence of temperature the effect of pressure on the phase behavior of the microemulsion is widely discussed as results from different researchers disagree. Reservoir conditions are typically at elevated pressures, why this is of importance.

Observing surfactant systems there are three types of systems to be considered.
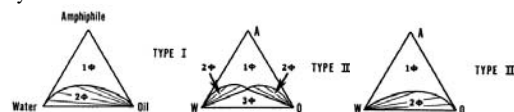
Figure 3: From left to right: multiphase region with lower-phase microemulsion with excess of oil, middle-phase microemulsion and upper-phase microemulsion with excess of water/brine.

Figure 3 represents the phase environment where surfactant/water/oil systems can equilibrate as either a single phase or as multiple phases. These generalized systems are often referred to as the so-called Winsor Type systems.

Current Work

It is the aim to begin phase behavior experimental activities in the nearest future. The objectives are at first hand to study single surfactant component systems behavior at different temperatures and pressures, where especially the pressure part is reported very little in literature. Also it is desired to observe correlations between surfactant structure and their phase behavior.

References

1. B.M. O'Brian, Journal of American Chemists' Society, 59(839a-852s), Houston, 1982
2. D.W. Green, G.P. Willhitw, Enhanced Oil Recovery, SPE Textbook Series, vol. 6, USA, 1998, p. 7
3. Y. Wu, P. Shuler, Y. Tang, W.A. Goddard, SPE 95404 presented at SPE Annual Technical Conference and Exhibition, Dallas, Texas, 2005
4. A.K. Flaaten, Q.P. Nguyen, G.A. Pope, J. Zhang, SPE 113469 presented Improved Oil Recovery Symposium, Tulsa, Oklahoma, 2008
5. T. Austad, H. Hodne, S. Starnd, K. Veggeland, Colloids and Surfaces, 108(253-262), Norway, 1996

Paloma Andrade Santacoloma

Phone:	+45 4525 2804
Fax:	+45 4593 2906
E-mail:	psa@kt.dtu.dk
WWW:	http://www.bioeng.kt.dtu.dk
Supervisors:	John M. Woodley
	Krist V. Gernaey
	Gürkan Sin

PhD Study
   Started: October 2008
To be completed: September 2011

Multienzyme Process Modeling

Abstract

Biocatalysis has been increasing considerably during the last years. Nevertheless, most of the kinetic studies concerning biocatalysis have been carried out using isolated enzymes (soluble or immobilized). Nowadays multiple enzyme mixtures are taking special attention in many industrial applications. Therefore, the aim of this project is to develop a mathematical model which describes multienzyme processes. In that manner, the best outcome of the process can be obtained by developing a thorough understanding of what modifications in the system and process design are required to optimize the use of the enzymes.

Introduction

In conventional synthetic chemistry, the development of new processes is achieved by established methods of data collection and model building such that the sensitivity of parameters can be evaluated rapidly. Enzymatic synthesis is now becoming an accepted means of achieving selective catalysis for some classes of reaction where conventional approaches are very difficult [1]. The potential of these biocatalytic processes is seen as an important tool for more sustainable synthesis, especially in the fine chemical industry. However in industrial biocatalysis, the reaction frequently operates far away from natural conditions and therefore inevitably some changes to catalyst and process are required.

Multiple enzyme mixtures are relevant in many industrial applications (e.g. pharmaceutical industry) [2]. It would indeed be advantageous to combine enzyme steps together in order to reduce operating time and cost as well as use of energy [3, 4]. Conventionally such enzyme sequences have been run inside living cells. However this whole-cell based approach to synthesis requires careful manipulation (genetic engineering) to achieve the required product in sufficiently high concentrations of the enzymes and in the correct ratio [5]. The use of isolated enzymes (which is now possible given increased expression levels) means that new combinations are possible. The matching water-based chemistry of the reactions makes this particularly attractive. Likewise in lignocellulose applications a cocktail of enzymes is required to break down the polymer efficiently and understanding the optimal ratio of enzymes would be highly beneficial.

Through several years of biocatalyst investigations, a valuable knowledge of the nature of enzyme catalysis has been obtained. However in terms of mixtures of enzymes, kinetic parameters have to take into account the interaction between substrates, enzymes, and products in order to obtain an adequate approximation of the global system behavior [6].

We believe that mathematical models of such multi-catalytic schemes can improve the potential benefit of this technology not only via simulation but also prediction of the analyzed system. Thus, the best outcome of the process can be obtained by developing a thorough understanding of what modifications in the system are required to optimize the use of the enzymes, (i.e. kinetics and operating strategies).

Specific Objectives

The aim of this project is to develop a generic mathematical modeling framework for describing multi-enzyme processes, and to validate the framework based on relevant conversions that have potential for industrial application using multiple enzyme mixtures.

Methodological framework

An extensive literature review, providing an overview of the state of the art of multi-enzymatic processes, will

form the foundation for the project. That literature review will be used also to select relevant case studies for the project. One essential criterion for selecting a case study from the literature will be that it shows appropriate dynamics and behavior for analysis.

Subsequently, a mathematical modeling of enzymatic processes will be formulated in a systematic way, based on first engineering principles, also known as deterministic modeling. Model validation will be done by using experimental data taken from the literature, as mentioned above. Furthermore, a case study will be performed including laboratory work. It will provide specific information to evaluate, analyze, and optimize operating conditions of enzymatic processes relying on multiple enzymes, (*see* Figure 1).

In order to perform an effective evaluation of the model, a standard engineering software tool such as Matlab/Simulink will be used for model building, simulation, parameter estimation, sensitivity analysis, multi-objective criteria evaluation and the like.
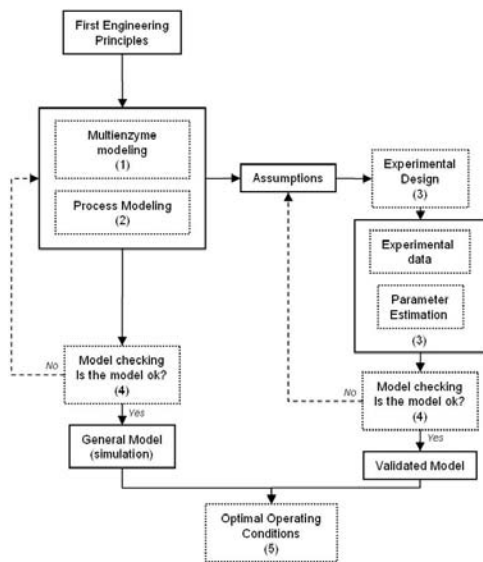
Figure 1: Methodological scheme proposed to develop the mathematical model for multi-enzymatic processes.

The suggested methodology for this project can be divided in five main stages, thus:

1. Multi-enzyme modeling
2. Process modeling
3. Experimental design and data analysis
4. Model validation
5. Evaluation of optimal operating conditions

The overall framework is described by considering Figure 1, which shows the individual elements and how they are interrelated. In general, the first stage (*multi-enzyme modeling*) will give the knowledge to interpret enzymes behavior obtained from the evaluation of different multi-catalytic schemes. In the second stage (*process modeling*), models for different types of bioreactors will be formulated according to desired operating conditions. Furthermore, model parameter estimation can be performed using experimental information reported in the literature. Knowing the system, experimental design and laboratory work can be developed in the third stage (*experimental design and data analysis*). Finally the last two stages (*model validation* and *evaluation of optimal operating conditions*) are proposed in order to obtain a more realistic definition of the most effective multi-enzymatic processes.

Expected results and perspectives
The expected result of this project will on the one hand be model building blocks implemented in Matlab/Simulink, which can be assembled in an overall model of a process in a user-friendly and flexible manner. On the other hand, the project aims at building a computational tool that can facilitate a faster workflow and accelerated scientific advancement in the development of multi-enzymatic biocatalytic processes.

The advantage of a software-based approach is that one can perform a large number of simulations of the process before testing reactor configurations in the laboratory. It also opens the possibility of studying different scenarios and conditions of the desired process, thus saving experimental time and effort. Consequently, knowledge of the systems will be acquired in a more efficient way. Improved formulations of experimental designs will further extend optimal applicability of multi-enzyme processes in real plants.

References
1. J.M.S. Cabral, D. Best, L. Boross, J. Tramper, Applied Biocatalysis, Hardwood Academic Publishers, Switzerland, 1994, p. 41.
2. D.J. Pollard, J.M. Woodley. Trends in Biotechnology 25 (2) (2007) 66-73.
3. S.J. Broadwater, S.L. Roth, K.E. Price, M. Kobašlija, D.T. McQuade, Organic & Biomolecular Chemistry 3 (16) (2005) 2899-2906.
4. B.H. Chen, A. Sayar, U Kaulmann, P.A. Dalby, J.M Ward, J.M. Woodley, Biocatalysis and Biotransformation 24 (6) (2006) 449-457.
5. K. Buchholz, V. Kasche, U.T. Bornscheuer, Biocatalyst and Enzyme Technology, Wiley- VCH, Germany, 2005, p. 283.
6. A. Cornish-Bowden, Encyclopedia of Bioprocess Technology: Kinetics, Enzymes. John Wiley & Sons, Inc. 1999.
7. D.Y. Murzin, R. Leino, Chemical Engineering and Design 86 (2008) 1002-1010.

Kavitha Chelakara Satyanarayana

Phone: +45 4525 2981
Fax: +45 4525 2906
E-mail: kac@kt.dtu.dk
WWW: http://www.capec.kt.dtu.dk
Supervisors: Associate Prof. Jens Abildskov

Prof. Rafiqul Gani

PhD Study
  Started: June 2006
  To be completed: May 2009

Multiscale Approach in Computer Aided Polymer Design

Abstract
A multiscale approach for designing a polymer is presented in this work. Here, the desired properties of a polymer is given as input, computer aided molecular design (CAMD) algorithm using group contribution plus models (macro-meso scale) gives out the polymer repeat unit structures satisfying the desired properties as output. The arrangement of polymer repeat unit structures to form a polymer chain and the properties corresponding to the generated polymer are studied in micro-scale approach. A case study using this multiscale approach is presented in this paper.

Introduction

The search for new polymeric compounds with desired end-user properties is an everyday problem in chemical, pharmaceutical and food industries. There is a number of different methods that can be used for designing new polymers with desired properties. But each method has its own set of advantages and limitation. For example some approaches are too time consuming (like quantum mechanics methods) while some are capital intensive (like laboratory scale preparation of many polymers). Integration of different approaches on the basis of the molecular descriptor used to describe the polymer structures (i.e. based on the time and length scale shown in figure 1) is considered in this work which is called a *multi scale approach* for computer aided polymer design.

The initial step in our approach is the identification of polymer repeat units, for the given target properties as input, using a Computer Aided Molecular Design (CAMD) algorithm (done in macro-meso level). While the arrangements of the identified repeat units in a polymer chain (for example how many number of repeat units, branching frequency, etc.) is studied in the micro-scale level.

Methodology

The required target properties are set as the input to this multilevel modeling methodology (see figure 2). Identification of a basic polymer repeat unit at macro/meso scale level requires an appropriate CAMD algorithm (where fragments are used to design the homopolymer repeat unit structures) and a set of property prediction models. Group contribution based property prediction models [1,2] are sufficiently simple and reliable for use in CAMD, but due to the limited availability of experimental data for polymer properties, one cannot expect to fill out the entire group parameter table. At times there can also be a polymer repeat unit structure that cannot be totally represented by groups for a specific group contribution method. This is overcome by a meso-scale approach, where an atom-connectivity index method is applied to determine the missing groups and their contributions automatically without the need for additional experimental data. This integration of the group and atom-connectivity index based models is called group contribution plus (GC^+) model and it has been proposed by Satyanarayana et al. [2].
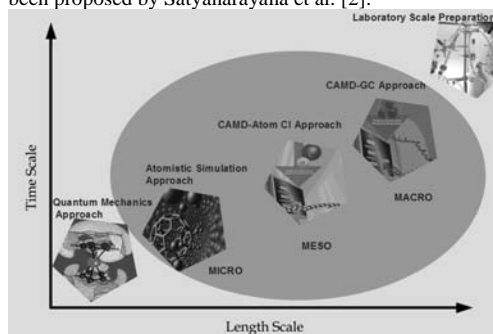
Figure 1: Multi scales for developing new polymer product on the basis of the required property.

A multi-step, multi-level hybrid CAMD algorithm by Harper and Gani [3], which suppresses the

combinatorial explosion problem and is also capable of generating a large number of structures has been modified for using the GC$^+$ models of Satyanarayana et al [4] and is employed in this work.

Bulk polymer models based on the identified basic repeat unit(s) (obtained from the CAMD algorithm) are then used as input in micro-scale step to generate a polymer chain with the desired number of repeat units. This is done in stage 1, where the pre-selected numbers of identified repeat units are used to build polymer chains using molecular modeling methods. A United Atom (UA) simulation approach is used to build and simulate the polymer chains to obtain well equilibrated configurations. Equilibrated structures are used in the second stage, where structures are converted from UA to all atom models by appending hydrogen atoms to them followed by the energy minimization procedure to overcome the steric overlaps. A short molecular dynamics simulation can be performed either to calculate/validate if the generated polymer chain (with the considered number of repeat units) has the required property or not. Dependency of the property on the varying chain length can also be studied in this micro-scale approach.

The obtained polymer configurations that have the required set of properties can then be tested in laboratory to verify that they satisfy the desired performance criteria.

Case Study

As a test case we consider here a problem referring to the design of a hermetic stopper for medical containers, which intend to secure against the entry of air or microorganisms and to maintain the safety and quality of the contents stored in their containers. There are a number of materials that are used as sealants such as natural rubber (can cause latex allergies), cork (varying pore size), etc. It would be interesting to design a polymeric material for use as a hermetic stopper (sealant) by retaining the advantages of existing stopper materials and overcoming their disadvantages.

*Application of the macro-meso-scale approach. T*he basic (homo) polymer repeat unit structures are identified in this approach that can be used as hermetic stoppers. This requires specifying initially a set of structural and property constraints.

Property Constraints: (a) Glass transition temperature (T_g) – the polymeric stopper is required to be elastic over a wide range of temperature, and it is preferred to be made of a rubbery amorphous polymer so that its T_g is less than or equal to the room temperature (300 K) [1]. The upper limit for T_g can be relaxed to 350 K. By doing this, the scope of missing some candidates that have the required property (but are not identified due to inconsistency of the experimental data reported and also considered while developing the property prediction models) is minimized to some extent. (b) Dielectric constant (ε) – some contents stored in the medical containers need to be constantly agitated with electrical agitators before use. It is therefore required that the

polymeric stopper should not conduct electricity and electrolyze the stored contents in the medical containers; this implies a low ε. Here, we impose a maximum constraint of 2.5 on the value of the ε. (c) Low permeation to moisture and air – the stopper should protect the contents stored from moisture and air, and to exhibit very low water (or moisture) absorption [1]. As the GC$^+$ model for predicting water absorptivity has not yet been developed, Van Krevelen's [1] group contribution model is used to predict this property (to verify if the identified repeat units have low water absorptivity or not) for the identified repeat units that satisfy both T_g and ε constraints. Moreover, low permeation to air implies low permeation to nitrogen (N_2) and oxygen (O_2). Since there is no direct group contribution method to study the solubility and diffusivity (the key factors determining permeation) in the polymer, the micro-scale approach is also used for determining these properties (along with the arrangement of repeat units to form a polymer chains).
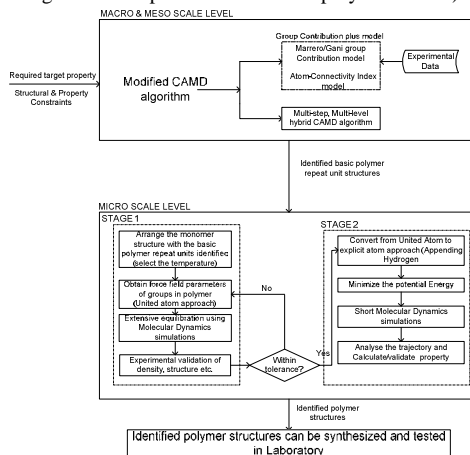
Figure 2: Schematic work-flow of the multiscale modeling.

Structural Constraints: Since the purpose of this case study is to design a polymer with low permeability to moisture, the polar and hydrogen bond forming functional groups should not be included in the basis set. The reason is that they often enhance chain-chain attractions, which tends to enhance crystallinity and tensile strength. Therefore, only the groups forming olefinic polymers are allowed. It is also known that the double bonds in polymers render them poor for weather resistance, thermal resistance, oxygen resistance and ozone resistance. This applies also to olefinic groups with triple bonds. Taking this into account, olefinic groups with double and triple bonds are excluded from the basis set, which is therefore limited to the CH_3, CH_2, CH and C groups.

Given the side chain forming groups (CH and C) that are included in the basis set and in order to avoid too many side chains in the basic polymer repeat unit, the number of times each group can occur in the repeat unit

is limited to 2 implying that the maximum number of groups that can occur with the combination of all the groups included in the basis set is 6. Thus;

$$2 \leq \sum_j n_j \leq 6 \qquad \text{(Eq. 1)}$$

where, n_j is the number of groups of type j.

As this case study aims at generating a basic homopolymer repeat unit that has two free ends, the criterion of having two free ends in each generated structure is also specified (based on valency and octet rule) as shown in eq. 2.

$$\sum_j (2 - v_j) n_j = 2(m - 1) \qquad \text{(Eq. 2)}$$

where n_j, v_j are the number and valency, respectively, of groups of type j and m =1, 0 or -1 for acyclic, monocyclic and bicyclic groups, respectively. As only olefinic groups are considered, m takes the value of 1.

Structural and property constraints were given as input to the CAMD algorithm. 112 candidates of basic repeat unit structures were designed and 106 candidates among them were selected based on the given constraints (including some isomers of the generated repeat units). Removing the isomers, 12 basic polymer repeat units that satisfy all constraints were chosen; they are listed here in table 1. The repeat unit structure of polyisobutylene (PIB) is one of the identified repeat units from the CAMD algorithm.

Table 1: Identified polymer repeat unit structures using CAMD algorithm

Structural Constraints	Min	Max		
Basis set CH3, CH2, CH, C				
Number of groups	6	2		
Property Constraints	Min	Max		
Glass Transition temperature (K)		350		
Dielectric Constant		2.5		
Basic polymer repeat units	T_g(K)	ε	W_{abs}	
-[-CH(CH$_3$)-]n-	302.51	2.48	0.00004	
-[-CH$_2$-CH$_2$-]n-	168.72	2.47	0.00004	
-[-CH$_2$-CH(CH$_3$)-]n-	257.91	2.37	0.00004	
-[-CH$_2$-C(CH$_3$)$_2$-]n-	*342.1*	*2.23*	*0.00003*	
-[-CH(CH(CH$_3$)$_2$)-]n-	303.13	2.28	0.00004	
-[-CH(CH$_3$)-CH(CH$_3$)-]n-	302.51	2.26	0.00004	
-[-CH((CH$_2$)$_2$CH$_3$)-]n-	235.61	2.25	0.00004	
-[-C(CH$_3$)((CH$_2$)$_2$CH$_3$)-]n-	307.43	2.12	0.00003	
-[-CH(CH(CH$_3$)CH$_2$CH$_3$)-]n-	275.75	2.14	0.00004	
-[-CH$_2$-CH(CH(CH$_3$)$_2$)-]n-	276.24	2.17	0.00004	
-[-CH(CH(CH$_3$)((CH$_2$)$_2$CH$_3$)-]n-	257.91	2.03	0.00004	
-[-CH((CH$_2$)$_2$-CH(CH$_3$)$_2$)-]n-	258.32	2.05	0.00004	

PIB is important elastomers with low T_g and high friction coefficient. From different literature sources [5-7] it is also reported that this polymer presents markedly low permeability properties to small gas molecules in comparison to other elastomers due to the presence of the two bulky pendant methyl groups on each basic repeat unit structure. Permeability is described as the product of solubility and diffusivity. Lower solubility and diffusivity values always correspond to low permeability. As it is highly time consuming to study the entire identified basic polymer repeat unit structures

at the micro-scale level (at this point of time), only PIB was addressed in the present case study.

Application of the micro-scale approach. Recently, Tsolou et al [8] undertook a systematic study of model PIB systems ranging in molecular length from 8 up to 80 repeat (monomeric) units per chain at different temperatures (from 600 K to 300 K). A key feature of this work was the development and implementation in the molecular simulations of a new UA force field for PIB, which reproduces faithfully the conformational, structural and thermodynamic properties of the polymer. Guided by Tsolou et al. [8], the first stage of the micro-scale approach of the present case study involved the execution of atomistic MD simulations with a C$_{320}$ PIB system (i.e., a system each chain of which contains 80 monomers or 320 carbon atoms) at several temperatures. The outcome of these simulations was an ensemble of well-relaxed configurations, which were used next as input to all-atom (AA) simulations (simulations in which the atomistic detail is restored with the insertion of the missing hydrogen atoms along each PIB chain) for the accurate prediction of the solubility and diffusivity properties of PIB to small molecules such as O$_2$ and N$_2$ of interest here. Through such an approach, Tsolou et al. [8], for example, obtained excellent predictions of O$_2$, N$_2$, He and Ar solubility in PIB as a function of temperature. In the present study, the approach was extended in order to calculate the diffusivity of O$_2$ and N$_2$ in PIB. Overall, the steps undertaken in the micro-sale approach are: (1) A 3-chain PIB system with 80 monomers per chain was subjected to long atomistic MD simulations in the NPT ensemble using the parallel LAMMPS code and the new UA model introduced by Tsolou et al. [8]. (2) Well-relaxed configurations from these UA simulations at four different temperatures (350 K, 450 K, 500 K and 550 K) were selected and converted to AA representations by re-inserting the hydrogen atoms that had been neglected in the UA simulations. (3) After a short energy minimization of the chosen PIB system, five O$_2$ molecules were randomly inserted at different positions inside the matrix at the temperature of interest, and the energy of the system was minimized again. (4) Long MD runs (up to 3 ns depending on the temperature) in the NPT statistical ensemble were carried out, which allowed us to monitor the time evolution of the 5 oxygen molecules. In all simulations with the all-atom model, the very detailed and accurate COMPASS force field was used.

The diffusivity of oxygen molecules in the PIB matrix was studied in terms of the time evolution of their mean square displacement (MSD) in the course of the MD simulation. The diffusion coefficient D can then be readily computed from the linear part of the curve through the Einstein relation [9]:

$$D = \frac{1}{6N} \lim_{t \to \infty} \frac{d}{dt} \sum_{i=1}^{N} \left\langle [\mathbf{r}_i(t) - \mathbf{r}_i(0)]^2 \right\rangle \qquad \text{(Eq. 3)}$$

where $\mathbf{r}_i$ denotes the position vector of the center of mass of the diffusant and angular brackets denote ensemble average over all five (i.e., N_a=5) O$_2$ molecules

and over all possible time origins in the course of the trajectory. Clearly, as the temperature decreases, the diffusivity of O_2 in PIB slows down considerably (see Figure 3). Indeed, by plotting log(D) versus 1/T, a linear plot is obtained whose slope provides an estimate for the activation energy of the diffusive process defined as:

$$E_a^{app} = -\frac{R}{0.434}\frac{\partial(\log D)}{\partial\left(\frac{1}{T}\right)} \qquad \text{(Eq. 4)}$$

The value obtained from the data of Figure 3 is 5.7 kcal/mol. This compares very favorably with the experimental value of 11.9 kcal/mol reported by Amerongen [8] from diffusivity data measured over a range of lower temperature values than the ones covered here by MD. In fact, Amerongen reports that the activation energy is not constant but increases with decreasing temperature; this indicates that the relatively higher value of E_a^{app} predicted from our micro-scale approach is quite reasonable.
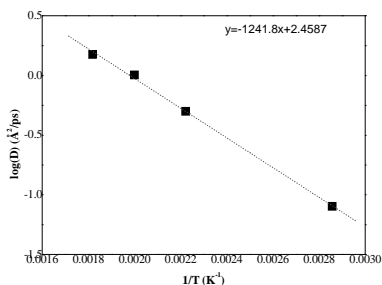
Figure 3: Log(D) versus 1/T for O_2 in PIB-C_{320} matrix

Case study results and discussion: The present case study has justified the success of the potential application of a multilevel approach to the design of a polymer with a set of pre-specified properties. Using the macro-meso-scale approach, a set of basic polymer repeat units promising to have the required target property (for the case study chosen here) is first obtained. Water absorptivity values (estimated using van Krevlen's [1] group contribution approach) for the identified basic polymer repeat units were comparatively lower as shown in table 1. On the other hand, the macro-meso-scale approach alone cannot decide about the optimal arrangement of the repeat units or the chain length; in the context of the proposed multi-level approach, this is the task of the micro-scale (atomistic or molecular modeling) component. In the present case, for example, we chose to simulate PIB with C_{320} (polymer chain with 80 repeat units) and compute its permeability properties to small molecules like O_2 and N_2. The simulation results from micro-scale work seem to verify the low permeability of O_2 in the designed polymer. Then, given that the molecular size of O_2 is smaller than N_2, we can safely conclude that PIB will also be characterized by low permeability to N_2. In a broader sense, this polymer will have a low permeability to air. Moreover other PIB systems with varying carbon number (C_{80}, C_{120} and C_{240}) will also be studied in the future to verify which system has lowest permeability to air. The next step is to recommend the polymer for laboratory scale synthesis, to experimentally validate the properties claimed here.

Conclusions

We have presented a multi-level approach for the design of polymers with a set of required properties, which can substantially help decrease the time for the development of new products (which traditionally has been based on the synthesis of a large number of compounds in laboratory and exhaustive testing). The approach relies first on the application of GC^+ property models in the CAMD algorithm for the identification of the polymer repeat unit structure properties; this greatly enhances the application range of problems that can be handled. Since the CAMD algorithm is not a stand-alone approach (it cannot, for example, give complete information on how the basic polymer repeat units should be arranged for the resulting polymeric structure to have the desired properties), a micro-level approach is also proposed to be employed; by providing the link to microstructure, this is capable of deriving reliable estimates of the desired properties based on the principles of quantum and statistical mechanics, and statistical thermodynamics. We have applied such a multilevel approach to a case study aimed at designing a polymer that can be used as a hermetic stopper. One of the basic polymers identified from the macro-meso-scale approach for such an application was polyisobutylene. In comparison to other elastomers and based on literature data, this polymer is characterized by a low glass transition temperature and markedly low permeability to O_2, N_2 and air). We concluded that PIB would be a candidate for constructing hermetic stoppers for use in medical applications.

References
1. D.W. Van Krevelen. Properties of Polymers, Amsterdam: Elsevier 1990.
2. K.C. Satyanarayana, R. Gani, J. Abildskov. Fluid Phase Equilibria, 261 (2007) 58.
3. P.M. Harper, R. Gani. Computers & Chemical Engineering, 24(2-7) (2000) 677.
4. K.C. Satyanarayana, J. Abildskov, R. Gani,. Computers & Chemical Engineering (2008) (in press).
5. K. Kamio, K. Moorthi, D.N. Theodorou. Macromolecules 40 (2007) 710-722.
6. C.F. Abrams, K. Kremer. Macromolecules 36(1) (2003) 260-267.
7. P.M. Harper, R. Gani, P. Kolar, T. Ishikawa. Fluid Phase Equilibria 158-160 (1999) 337.
8. G. Tsolou,V.G. Mavrantzas, Z.A. Makrodimitri, I.G. Economou, R. Gani. Macromolecules, 41 (16) (2008) 6228.
9. N.C. Karayiannis, V.G. Mavrantzas, D.N. Theodorou. Macromolecules 37 (2004) 2978.
10. G.J Van Amerongen. Journal of polymer science, 5 (3) (1950) 307.

Daniel Schäpper

Address:	Building 227, room 250
Phone:	+45 4525 2960
Fax:	+45 4593 2906
E-mail:	dsc@kt.dtu.dk
WWW:	http://www.kt.dtu.dk
Supervisors:	Krist V. Gernaey
	Anna Eliasson Lantz
	Stuart Stocks, Novozymes A/S

Ph.D. Study
Started: May 2006
To be completed: December 2009

Continuous Culture Microbioreactors

Abstract

The current microbioreactors mostly operate as fed-batch or continuous culture with *E. coli* as culture strain. This projects aims to design a microbioreactor running continuous cultures of *S. cerevisiae* in a reactor volume of approximately 100 L. The most important culture parameters can be measured on-line allowing for a high information-per-experiment ratio. Industrial relevance will be proven through comparisons of continuous culture microbioreactor experimental data with bench-scale experiments performed at DTU Systems Biology.

Introduction

Biotechnology plays an increasingly important role in production processes in the food, the chemical and the pharmaceutical industry. Well-known examples of biotech-based products that have an important function in the life of many people are enzymes used in laundry detergents, pharmaceuticals such as insulin, etc.

However, starting up a new biotechnological production is usually preceded by a tremendous research effort in which for example the productivity of different candidate production strains is compared (=screening). Usually, such screening is done in shake flask cultures. In a later stage of production process development, experiments done in bench scale reactors are performed to investigate the influence of process conditions on productivity.

Experiments done in shake flasks (typically with a volume of 100 mL to 1 L) are easy to set up. However, shake flask cultures only allow batch experiments, and the information gained per experiment is limited: typically only end-point measurements of for example the product quality are performed. If additional measurements are needed, manual sampling is required, which additionally disturbs the culture. Compared to shake flasks, bench scale reactors (typically with a volume of 1 to 10 L) have the advantage that they allow on-line measurements. Moreover, bench scale reactors are flexible since they can be operated in batch or fed-batch, but also as a continuous culture. However, the work effort needed to prepare, operate and subsequently clean bench scale reactors is vast.

Summarizing, biotechnological process development is expensive, for example because both traditional cultivation methods work with substantial volumes that in turn then require preparation of the appropriate amount of expensive nutrient media.

Motivation

Microbioreactors (µBRs) offer the possibility to circumvent many of the above-mentioned problems:

- The production cost of the µBRs is low, since they can be produced from polymers.
- The working volumes are very small (in the L/mL range), keeping costs for culture media low.
- On-line measurements are possible for the most important culture parameters (optical density (OD), dissolved oxygen (DO), pH).
- Batch, fed-batch and continuous culture conditions can be created in µBRs.
- The reactors are disposable after use and thus require no cleaning effort at all.
- Scaling out µBRs to systems with many parallel reactors allows for high-throughput screening, thus yielding a massive gain in information per experiment with continuously small working volumes.

The above advantages result in more-information-per-experiment (on-line measurements), financial savings (small volumes, less labor intensive) and the possibility to develop production schemes on the resource-saving micro-scale before scaling up a process.

Objectives

Currently, µBRs described in the literature are operated either as fed-batch or as continuous cultures, most often with *E. coli* as the culture strain. This project aims at the development of a continuous culture µBR that can perform experiments with yeast (*S. cerevisiae*). Compared to a batch experiment, the continuous culture has the advantage that steady-state conditions can be achieved. Additionally, it should be possible to induce step changes in the dilution rate, forcing the culture from one steady-state to the other with continuous measurement of the important culture parameters, thus leading to dynamic information on the behavior of the culture under well-controlled experimental conditions.

In the first part of the project, a reactor with the above features has been designed and fabricated, and a complete measurement & control setup was installed. The second step is now to prove the industrial relevance through comparisons of experimental µBR results with larger-scale data from the literature and from *S. cerevisiae* cultivations performed at DTU Systems Biology.

Naturally, µBR construction also poses some challenges. Proper mixing for example is very essential for good cultivation results, since substrate gradients in the culture might otherwise lead to a varying (location dependent) metabolic state of the culture. In the projected volume range turbulent flow is difficult to achieve due to the small Reynolds numbers. On the other hand the volume is too large to be able to rely on diffusion alone. Therefore one of the challenges in the project is to find a mixing regime which efficiently reduces diffusion distances.

Another challenge is the mechanical integration of the various sensors, a mixing apparatus and the aeration system into the small volume in such a fashion that the device is easy to manufacture.

Microbioreactor Technology

The current reactor is designed to have a working volume of 100 L which is sufficiently large to allow enough space for the sensors and actuators but is still small enough to considerably reduce the amount of media needed.

Contrary to conventional reactors which are mostly aerated by means of bubbles, microbioreactors are designed to work bubble-free. Aeration is done through a semi-permeable silicone membrane which allows both the incoming transport of oxygen and the outgoing transport of CO_2.

DO and pH are both measured with fluorescent sensor spots which change both the amplitude and the phase of the emitted light with a change in the sensitive variable. A lock-in amplifier measures the phase difference and thus quantifies the measured variable.

Optical density is continuously measured both in the reactor itself and in the outflow channel. Light from a LED is guided into the reactor with optical fibers, sent through the substrate and then guided to a photo detector (**Figure 1**).
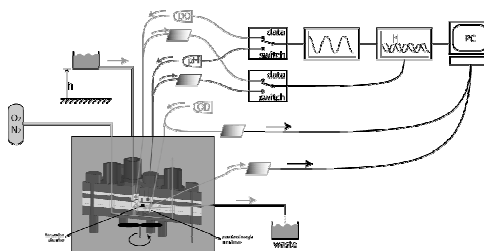
Figure 1: Schematic of a µBR setup

The flow rate is currently adjusted by a syringe drive. Both continuous and step changes in flow rate are possible which allows for various changes in dilution rates.

The reactor is currently fabricated out of poly(dimethylsiloxane) (PDMS), which is a cheap material. Additionally, no clean room fabrication steps are necessary which allows for cheaper manufacturing. Indeed, it means that the final product can be mass-produced, sterilized and pre-packaged similar to syringes.

Work Done

On the one hand a reactor was designed and fabricated, on the other hand the supporting systems have been developed. These include tempering & aeration of the broth and measurements of optical density and dissolved oxygen. Also the LabView system that measures and controls the system has been set up..

Mixing had been one of the larger problems which had to be solved – this has now been done with a surprisingly simple solution. Additionally, pH measurement and control has been set up and is working in a separate system.

The handling of the current system is now pretty rugged such that the risk of incorrect handling is getting smaller. With the current set-up batch cultivations of *S. cerevisiae* can now be performed and exhibit reasonable growth characteristics.

Next Steps

Currently cultivations shall be run which first prove the comparability of this system with bench-scale reactors; in parallel the existing pH measurement and control system is going to be integrated into the µBR.

The generation of a wash-out curve both in the µBR and in a bench-scale reactor will allow for the determination of the growth rate in both systems.

Acknowledgements

Ravendra Singh

Address:	Building 227
Phone:	+45 4525 2911
Fax:	+45 4593 2906
E-mail:	rs@kt.dtu.dk
WWW:	http://www.capec.kt.dtu.dk
Supervisors:	Rafiqul Gani
	Krist V. Gernaey

PhD Study
Started: September 2006
To be completed: August 2009

ICAS-PAT: A New Software Tool for Design of PAT* Systems

Abstract

A well-designed process monitoring and analysis system (PAT system) is necessary to consistently achieve a predefined end product quality. Systematic computer aided methods and tools provide the means to design the necessary process monitoring and analysis systems and/or to validate any existing monitoring and analysis system. A software to achieve this has been developed, including two supporting tools: a knowledge base (summarizing the available process knowledge as well as the knowledge on measurement methods & tools), and a model library (consisting of the process operational models). These supporting tools have been extended rigorously, and were integrated with the user interface to make the software more generic and applicable to a wide range of problems.

---

* PAT: Process Analytical Technology

1. Introduction

The necessity of the design of a suitable process monitoring and analysis system – (also called Process Analytical Technology system, or PAT system) for systematic product quality monitoring and control has been widely accepted following the publication of the FDA Process Analytical Technology guideline [I]. As reported by Singh et al. [5], the design of a PAT system involves the identification of the critical quality parameters, selection of economical and reliable on-line measurement tools and integration of these on-line sensors with the control system. Singh et al. proposed a computer-aided framework including the methods and tools through which the PAT system for product quality control can be designed, analyzed and/or validated. Based on the proposed framework, a software for design of PAT systems was developed. The software consists of two main supporting tools: an extended knowledge base of methods and tools for monitoring/analysis to provide the necessary information/data needed during the design of the PAT system and an extended model library to supplement the gaps in the knowledge base.

2. Specific objectives

The main objective of the project is to develop a software for design of process monitoring and analysis systems (PAT systems).

3. Extended design framework

As shown in fig. 1, the general supporting tools (protected general knowledge base and model library) as well as the user specific supporting tools (specific knowledge base and model library developed by the user) are integrated with the general user interface. The flexibility exists to either use the general supporting tools or the user specific supporting tools. The user specific supporting tools can be developed, extended and managed according to the user's needs while administrator rights are needed to edit/replace the general supporting tools. In either case a problem specific supporting tool (consisting of the problem specific knowledge and models) can be generated and can be used for design of a PAT system. The use of problem specific knowledge/data and models reduces the data retrieval time, and thus the final PAT system can be designed faster. As shown in fig. 1, the starting point for new PAT design problems is to provide the problem specifications, followed by the creation of the problem specific supporting tools and then to design the PAT system according to the methodology proposed by Singh et al. [5]. For the existing case specific problems the design methodology can be used directly, or earlier case studies can be opened and consulted.

3.1. Extended supporting tools

The knowledge base and the model library are the two main supporting tools of the design methodology. The knowledge base contains useful information needed for design of PAT systems. The extended knowledge base covers a wide range of industrial processes such as tablet manufacturing, fermentation, crystallization and
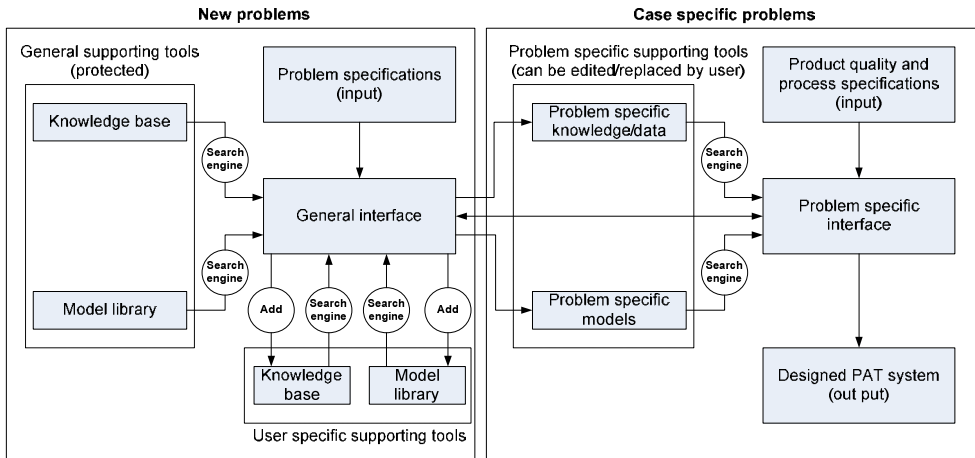
Figure 1: Overview of the extended PAT design framework which was implemented in a software
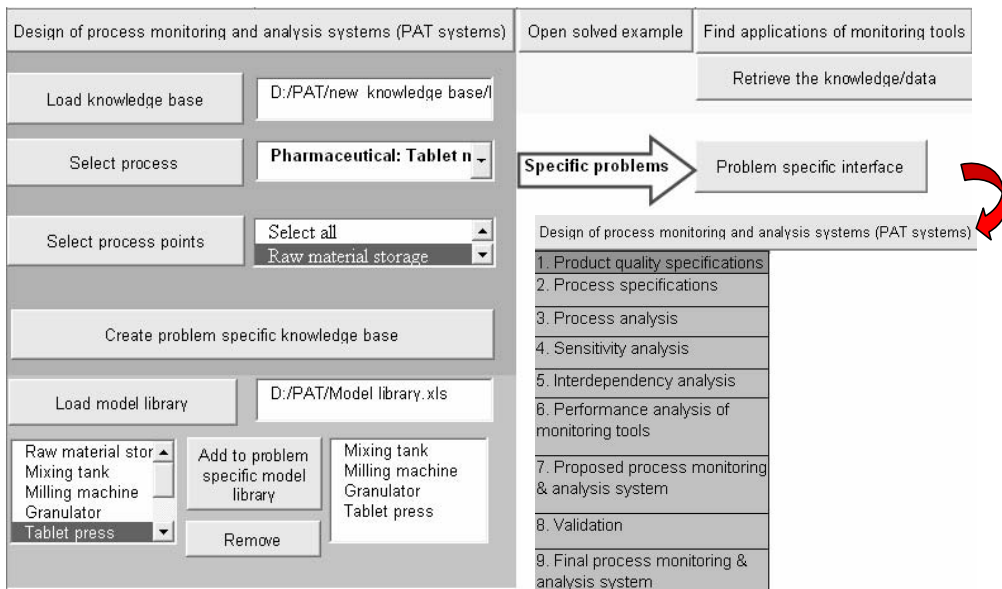
Figure 2: Software overview

a cheese manufacturing process. It contains information on typical unit processes in terms of the type of operation they perform, the process variables involved, the corresponding manipulating variables (actuators), the equipments typically used for on-line measurement of data (type of equipment, accuracy, precision, operating range, response time, resolution, drift, cost etc.). The model library contains a set of mathematical models of different form (steady state and dynamic) for different types of unit processes, sensors and controllers. They are used to generate data (e.g. in case measured data are not available) as well as for

verification of the performance of the closed-loop controlled process. Similar to the knowledge base, it covers a wide range of industrial processes (fermentation, crystallization, tablet manufacturing, cheese manufacturing).

3.2. Software overview

The overview of the software is shown in fig. 2. Through the main interface, the problem specific supporting tools can be generated (see fig. 2, left) and then the PAT system can be designed through the problem specific interface (see fig. 2, right). The main feature of the software is the design of PAT systems.

158

The design procedure consists of 9 steps [5] (see fig.2, right, bottom). In the first step the desired product quality is defined. Process information needs to be provided through step 2. Step 3 involves the listing of the possible process points (in general the process equipments are considered as the process points) and corresponding process variables where monitoring and control equipments might be needed. Critical process points and the critical process variables need to be identified through step 4. Step 5 provides the actuators for each selected critical process variable. The appropriate monitoring techniques and tools for each selected critical process variable can be found through step 6. Based on the outcomes of steps 3 – 6, a PAT system can be proposed in step 7. The proposed PAT system consists of the list of critical process variables and the corresponding actuators and monitoring tools for each critical process variable. The performance of the proposed PAT system can be verified in step 8. Step 9 provides the final PAT system. Note that each design step consists of a specific interface (window) through which the required input can be provided, and the results can be accessed and analyzed. The additional features of the software provide the options to open and analyze the solved examples, to find the applications of the monitoring techniques/tools and to retrieve the knowledge/data stored in the knowledge base.

4. Case study: Tablet manufacturing process

The process flowsheet (fig. 5) is adopted from the literature [II].

Step 1. Product property specifications: The desired product is a pharmaceutical tablet with the following predefined qualities: weight: 5E-04 Kg/tablet; water content: 5E-03 % w/w; coating: 1E-05 Kg/tablet; coating thickness: 1E-04 m; hardness: 145 Mpa; solubility: 14 Kg/m^3; volume: 5E-07 Kg/m^3; tablet thickness: 4E-03 m.

Step 2. Process specifications: The basic raw materials required include: USP Water, sucrose, API, stabilizer, excipient, mannitol, flavoring, OpaDry and air. The process equipments include: Mixing tank, milling machine, granulator, tablet press, storage tank, tablet coater

Step 3. Process analysis: This step involves the retrieval of process variables from the knowledge base corresponding to each process point. For example in the process point mixing tank, the retrieved process variables are: stirrer speed, stirring duration, homogeneity. Process variables for other process points are retrieved similarly.

Step 4. Sensitivity analysis: The process variable homogeneity in the mixing tank is considered to provide an example for the sensitivity analysis. Open loop simulations (fig. 3) show that the achieved homogeneity violates the lower limit indicating thereby that this variable needs to be monitored and controlled in order to guarantee final product quality. Repeating this procedure for all process variables yields the critical

process variables at each critical process point as shown in fig. 5 .
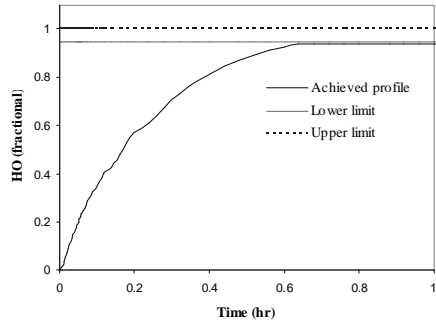
Figure 3: Sensitivity analysis

Step 5. Interdependency analysis: Interdependency analysis is performed for each critical process variable to select a suitable actuator. For example, fig. 4 shows the dependency of the moisture content of the granules on three actuator candidates. The moisture content is most sensitive to the binder flow rate and thus it is selected as an actuator for controlling the moisture content of the granules. Repeating the procedure for all critical control variables yields actuators as shown in fig. 5.
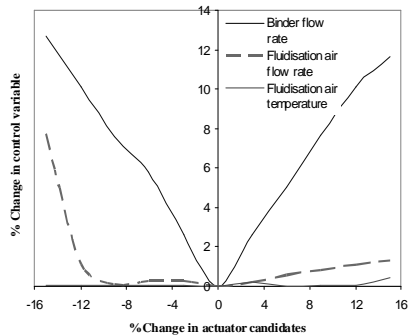
Figure 4: Interdependency analysis

Step 6. Performance analysis of monitoring tools: The performance of available monitoring tools (obtained from the knowledge base) for each measured variable is compared (based on the selected specifications) and monitoring tools are selected as shown in fig. 5

Step 7. Proposed PAT system: Based on the outcomes of the steps 3.3 – 3.6, a feasible alternative of a PAT system is proposed (e.g. Mixing tank – Homogeneity - Mixing time - NIR).

Step 8. Validation: A closed loop simulation has been performed to verify the performance of the control loop

and to validate the final product quality (see fig. 5, for final result).

Step 9. Final PAT system: A feasible alternative of the PAT system is shown in fig. 5. The critical process variables, corresponding monitoring techniques and actuators are shown in the figure.
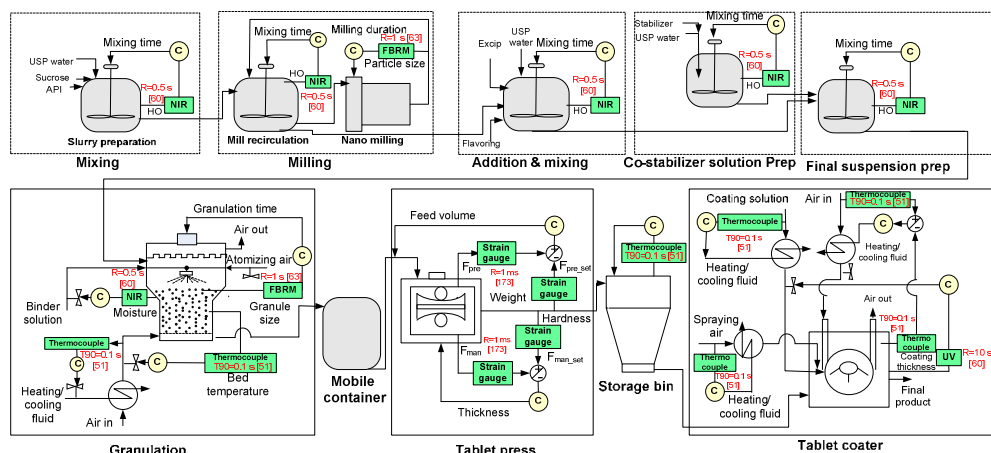
Figure 5: Tablet manufacturing process flow sheet with designed PAT system
c: controller, R: response time, T90: time for 90% response, HO: homogeneity

5. Conclusions

In this work a software for systematic design of PAT systems has been developed. The application of the developed software was demonstrated through a tablet manufacturing process case study.

6. Current and future work

The following case studies are being developed to further demonstrate the application of the developed methods and tools: Insulin production process which includes fermentation and downstream processing, crystallization process and a cheese manufacturing process.

Acknowledgement

References

I. FDA/CDER, 2005, Process Analytical Technology (PAT) Initiative, http://www.fda.gov/Cder/OPS/PAT.htm

II. V. Papavasileiou, A. Koulouris, C. Siletti, D. Petrides. Optimize manufacturing of pharmaceutical products with process simulation and production scheduling tools. Trans IChemE, Part A, Chemical Engineering Research and Design, 85 (A7) (2007) 1086-1097

Publications

1. R. Singh, K. V. Gernaey, R. Gani, "Model-based Computer Aided Framework for Design of Process Monitoring and Analysis Systems", presented at APACT-07, Edinburgh, UK, 01 - 04 May 2007

2. R. Singh, K. V. Gernaey, R. Gani, "Design of Process Monitoring and Analysis Systems, using a Model-based Computer Aided Framework", presented at ECCE6, Copenhagen, Denmark, 16 – 21 September 2007

3. R. Singh, K. V. Gernaey, R. Gani, "Design of Process Monitoring and Analysis Systems", presented at AIChE annual meeting (556a), Salt Lake city, Utah, USA, 3 - 9 November 2007

4. R. Singh, K. V. Gernaey, R. Gani, "Supporting Tools for Design and Validation of PAT system", presented at AIChE annual meeting (517m), Salt Lake city, Utah, USA, 3 – 9 November 2007

5. R. Singh, K. V. Gernaey, R. Gani. Model-based computer-aided framework for design of process monitoring and analysis systems. Computers & Chemical Engineering, 33 (1) (2009) 22-43

6. R. Singh, K. V. Gernaey, R. Gani, "Off-line design of PAT systems for on-line applications", Computer Aided Chemical Engineering, 25, (2008), 423-428

7. R. Gani, K. V. Gernaey, R. Singh, "A model-based framework for design and analysis of PAT systems", presented at EUROPACT, Frankfurt, Germany, 22 – 25 April 2008

8. R. Singh, K. V. Gernaey, R. Gani, "A model-based framework for systematic product quality monitoring and control", presented at AIChE annual meeting (710e), Philadelphia, PA, USA, 16 – 21 November 2008

9. R. Singh, K. V. Gernaey, R. Gani, "A software tool for design of process monitoring and analysis systems", presented at AIChE annual meeting, (577b), Philadelphia, PA, USA, 16 – 21 November 2008

Anna K. Sitarz

Phone:	+45 4525 2993
Fax:	+45 4525 2993
E-mail:	aks@kt.dtu.dk
WWW:	http://bioeng.kt.dtu.dk
Supervisor:	Prof. Anne S. Meyer

PhD Study

Started:	May 2007
To be completed:	April 2010

Biofuels from Important Foreign Biomasses

Abstract

Biomass is a renewable source of energy that is more sustainable than fossil fuels and more dependable than wind and solar. Moreover it provides the environmentally friendly and safe alternative for production of biofuels, especially when using the 2nd generation approach. In this project, the overall objective is to develop a method for the most optimal pretreatment of the biomass, leading to the low inhibitory content and the high yields of monosugars and produced ethanol.

Introduction

In the development of economically feasible conversion technologies for production of biofuels from renewable resources, the utilization of low cost biomass residues is of crucial importance. The most important parameters of these biomass residues are that they should contain a high amount of carbohydrates, which can be produced in large quantities [1]. Therefore the utilization of sugarcane bagasse will be the aim of the project.

The bagasse is a by-product from the sugar extraction process and is usually used in low-efficiency boilers at the processing plant. This lignocellulosic residue has a large content of relatively easily-available carbohydrates that could be utilized as substrate for 2nd generation bioethanol production. It is mainly composed of 40-50% cellulose and 25-30% hemicellulose with the remainder that is mostly lignin, minerals, wax and other compounds [2].

2nd generation bioethanol is made from residual lignocellulosic material. This approach of producing biofuels is beneficial in avoiding displacing agriculture for food and preventing from land clearing.

Lignocellulolytic materials are formed by three main polymeric constituents; cellulose, lignin and hemicellulose. Cellulose is linear and highly ordered (often crystalline) polymer of cellobiose (D-glucospyranosyl-β-1,4-D-glucopyranose). Hemicellulose is made up of different pentoses and hexoses polymers, which are often acetylated and generally form branched chains forming a matrix with cellulose fibrils. The third component, lignin, is a three dimensional network build up of dimetoxylated (syryngyl, S), monomethoxylated (guaiacyl, G) and non-methoxylated phenylpropanoid (p-hydroxyphenyl, H) units derived from the corresponding p-hydroxycinnamyl alcohols, which give rise to a variety of subunits including different ether and C-C bonds. Therefore lignin is very resistant toward chemical and microbial degradation.

Figure 1 shows the way of processing sugar cane. It begins with shredding the sugarcane with rotating knives and extraction of the juice to produce bagasse. This residual material is usually burnt to create heat. When the water evaporates from the juice, thy syrup is made. The seed crystals added to it will initiate the syrup to crystallize.

http://images.encarta.msn.com/xrefmedia/aencmed/targets/illus/ilt/T304793A.gif

Figure 1: Schematic processing of sugarcane with bagasse as the side stream.

Pretreatment as a method of improving sugars accessibility

Pretreatment is used to improve the biomass accessibility by destruction of harsh lignocellulosic structure and partially hydrolyzing the substrate. Current pretreatment methods, however, contribute to 30-40% of total costs of bioethanol production from lignocellulosic biomass. Hence, the pretreatment is one of the biggest bottlenecks for low-cost production of bioethanol. Therefore, the improvements in obtaining the most optimal parameters for disrupting the lignocellulose matrix will be investigated. In this project focus will be put on wet explosion, which is a combination of steam explosion and wet oxidation, applying both, the addition of oxygen and pressure release. The treated sample will be further hydrolyzed and fermented [3].

The hydrolysates released from the pretreatment are usually treated with enzymes in order to break down the cellulose and hemicellulose into hexoses and pentoses, which are later fermented to ethanol. The bottleneck of this process is the cost of the enzymes and the fact that enzymes can become inactive, due to the adsorption to lignin or shear stress. Therefore the need for finding ways to overcome those difficulties is needed. Hence, a new minimal cocktail of enzymes degrading lignocellulose material will be designed and evaluated [4].

Main objectives

The aim of the proposed PhD project is to develop the most optimal strategy and conditions for the pretreatment of lignocellulosic biomass, sugarcane bagasse, and obtain low yields of inhibitory compounds, high yields of free sugars, both xylose and glucose, and high yields of ethanol.

Acknowledgements

References

1. **A.**E. Wheals, L.C. Basso, D.M.G. Alves, H.V. Amorim, Fuel ethanol after 25 years, Trends Biotechnol. 17 (1999) 482-487
2. C. Martin, H.B. Klinke, A.B. Thomasen, Wet oxidation as a pretreatment method for enhancing the enzymatic convertibility of sugarcane bagasse, Enz. and Microb. Technol. 40 (2007) 426-432
3. P.F. Morjanoff, P.P Gray, Optimization of steam explosion as a method for increasing susceptibility of sugarcane bagasse to enzymatic saccharification, Bioethanol Bioengin. 29 (1987) 733-741
4. H.B. Klinke, B.K. Ahring, A.S. Schmidt, A.B. Thomsen, Characterization of degradation products from alkaline wet oxidation of wheat straw, Biores. Technol. 82 (2002) 15-26

Chutima Swangkotchakorn

Phone: +45 4525 2910
Fax: +45 4588 2258
E-mail: chs@kt.dtu.dk
WWW: http://www.capec.kt.dtu.dk
Supervisors: Rafiqul Gani
                John M Woodley
                Jan-Dierk Grunwaldt

PhD Study
 Started: September 2008
 To be completed: August 2011

Optimization of Tailor-Made Chemicals from Renewable Resources

Abstract
In the future, the chemical industry will need to be based on the conversion of renewable material, such as biomass and in particular lignocellulosic biomass. In order to meet the world's needs for industrial chemicals and liquid fuels, while minimizing the environmental impact, the economic and societal benefits would need to be maximized through the use of a new strategy. The objective of this strategy would be to develop a model biorefinery by matching a set of biomaterial feedstocks to an optimal set of end-point products (chemicals and fuels) through a range of sustainable processing routes. The optimal biorefinery model would be obtained by formulating and solving an optimization problem taking into account multiple criteria including biomaterial resources, product demands, processing routes and environmental impacts.

Introduction
The decrease in the world's crude oil production has caused fluctuations in the crude oil prices in recent years, and the price is expected to be higher in the future. Current chemical and energy industries are heavily reliant upon fossil fuel, and these fuels are unsustainable and contribute to economic and political vulnerability (US Department of Energy, 2003). At the same time, the potential to convert biomass to more valuable products has dramatically increased. It means that alternative strategies from renewable resources can start to compete for fuel and chemical production while minimizing environmental impact and increasing sustainability. The process for separation of biomass constituents and converting them to high value products is known as biorefining. The development of a model integrated biorefinery provides a good opportunity to provide new tools for application in the growing biorefinery manufacturing sector by creating new product streams [1].

For energy production a variety of alternative raw materials (wind, sun, water, biomass, nuclear fission and fusion) have been established. Industry based on conversion of sustainable material, would preferentially use biomass, in particular plant biomass. Generally, the biorefinery feedstocks can be classified into three types (i) sucrose-containing feedstocks (e.g. sugar beet), (ii) starchy materials (e.g. corn), and (iii) lignocellulose biomass (e.g. straw). The lignocellulose biomass is considered as the potential feedstock in this PhD project since it is a non-food feedstock and has low purchase cost, as well as desirable environmental and price attributes. Rather than burning residues, preferably cellulosic biomass (e.g. corn stover) should be converted into valuable products.

Figure 1 shows several possible ways of using lignocellulose and other biomass feedstocks for production of fuels and chemicals. One can differentiate between the production of syngas and the direct production of chemicals. These processes include pyrolysis, gasification, thermochemical liquefaction, hydrolytic liquefaction, fermentation, and chemical synthesis. Although most fundamental process steps are well-known, there is a need for a methodology capable of evaluating the integrated processes in order to identify the optimal set of products and the best route for producing them. Sammons *et al* [2] has proposed a framework for biorefinery production by using mathematical optimization and process utility integration to evaluate the profitability of different production routes while maximizing stakeholder value through global optimization of the supply chain. However, in this work, an optimal biorefinery model based on lignocellulosic biomass will be developed using techno-economic process simulation and optimization in order to locate the optimal production routes for a set of tailor-made chemicals based on maximizing profit, minimizing the energy utilization

and minimizing the resulting environmental impact. It should be possible to apply the developed techniques for different types of biomass feedstocks. Reliable optimization techniques coupled with process simulation of the identified routes will be applied and should answer a number of important questions, such as:

- For a given set of product prices, what should the optimal process configuration be, i.e., what products should be produced in what amounts and how?
- For a given product portfolio, can process integration methods be used to optimize production routes leading to a more sustainable alternative?
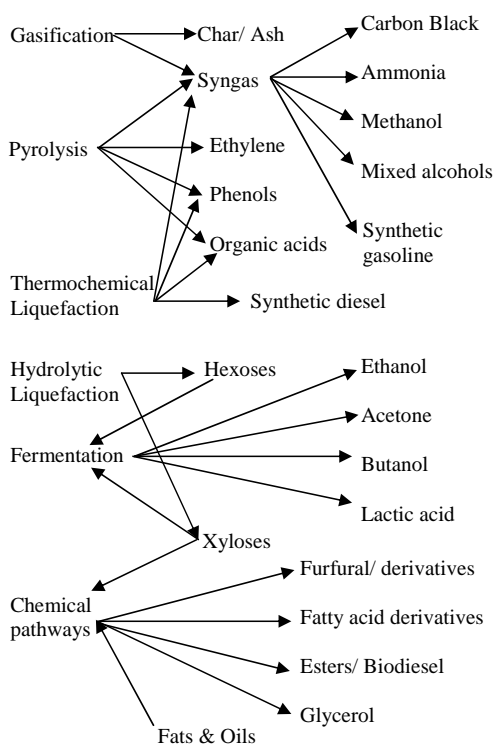
Figure 1: Biomass-derived industrial products [3]. Note: The different products may also be considered as platform molecules for chemical synthesis.

PhD-Project Objectives
The aim of this PhD project is to identify the potential routes for producing a set of precursor chemicals from biomass via biorefineries in order to replace the conventional processes from petroleum based refineries. Economic and environment impacts will be minimized through the optimal use of renewable and non-4. .

renewable feedstocks. To maximize economic and societal benefits, while the use of raw material and energy resources will be minimized.

Future work
The strategy to be employed in this work is illustrated in Fig. 2. The simulation models for positive economic potential process routes are to be developed by extracting knowledge from a database. Once the processing flow sheets are identified, process integration techniques and optimization models are to be used to minimize utility usage, maximize resource utility, and to optimize the utilization of biomass and energy. The environmental concerns, such as, green chemistry requirements and energy constraint will be considered in the models.
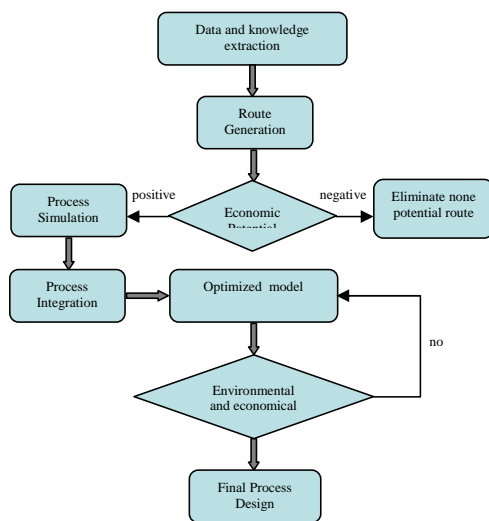
Figure 2: Strategy to identify the optimal route for tailor-made chemicals

References
1. Bridgwater, A.V., Renewable fuels and chemicals by thermal processing of biomass, Chemical Engineering Journal 91 (2003) 87–102.
2. Sammon, N.E. Jr., Yuan, W., Eden, M.R., Aksoy, B., Cullinan, H.T., Optimal biorefinery product allocation by combining process and economic modeling, Chemical engineering research and design 86 (2008) 800–808.
3. Kamn, B., Patrick. R.G., Kamn, M., Biorefineries-Industrial Processes and Products, WILEY-VCH, Germany, 2006, p. 124

Per Aggerholm Sørensen

Phone:	+45 4525 2927
Fax:	+45 4525 2258
E-mail:	pas@kt.dtu.dk
WWW:	http://www.kt.dtu.dk
Supervisors:	Søren Kiil
	Kim Dam-Johansen
	Claus Weinell, Hempel A/S

PhD Study
Started: February 2007
To be completed: January 2010

High Performance Anti-Corrosive Coatings

Abstract
One of the major modes of degradation of organic coatings immersed in sea water is called cathodic delamination. Cathodic delamination occurs on coating containing a defect, which allows corrosive species to react with the steel. Quantification of the most important steps responsible for cathodic delamination of organic coatings is an important step in indentifying the rate determining step. This knowledge may subsequently be used in the development of novel high performance anticorrosive coatings and lifetime predictions.

Introduction

Throughout the last decade, organic coatings have been widely applied for protection of metals against corrosion. Though various kinds of steel corrode at different rates, depending on their composition and the presence of mechanical stresses, the basic corrosion reactions are the same. On a steel surface some areas are anodic relative to other areas that are cathodic [1]. At anodes the following reaction takes place
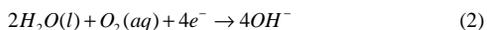
$$Fe(s) \rightarrow Fe^{2+} + 2e^- \tag{1}$$

and the cathode oxygen is reduced to hydroxyl ions

$$2H_2O(l) + O_2(aq) + 4e^- \rightarrow 4OH^- \tag{2}$$

According to Leidheiser et al. [2], reaction (2) is catalyzed by oxidized metals and does not occur to a significant degree in the absence of a solid.
The overall reaction can be written as

$$2Fe(s) + 2H_2O(l) + O_2(aq) \rightarrow 2Fe^{2+} + 4OH^- \tag{3}$$
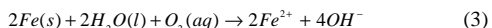
In the presence of dissolved oxygen, oxidation of ferrous hydroxide will lead to formation of hydrated magnetite, $Fe_2O_3 \cdot H_2O(s)$, known as rust.

$$Fe(OH)_2 + O_2(aq) \rightarrow 2Fe_2O_3 \cdot H_2O(s) + 2H_2O(l) \tag{4}$$
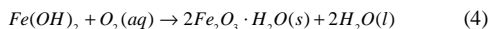
Despite significant improvement in existing coating technologies, problems continue to exist in the long-term protection of metal from aggressive environments. One of the main reasons for the lack of high performance anticorrosive coatings is the complexity of the coating-substrate system and the number of factors affecting the performance and durability of anticorrosive coating systems. Besides the composition of the coating, which consists of binder, pigments, solvents, extenders and additives, the performance and service life of anticorrosive coatings depend on several different parameters such as type of substrate, pretreatment of substrate, curing, coating thickness, adhesion between the coating and substrate as well as several external environmental parameters [3]. To perform its duty effectively, an anticorrosive coating must possess intrinsic durability, adhesion to the substrate, adequate flexibility and toughness to withstand impacts and cracking as well as maintain its appearance, when subjected to stress, swell, mechanical abuse or weathering.

Specific Objectives

If an anticorrosive coating containing a defect (e.g. a scratch or a scribe) is exposed to the environment, corrosion may initiate much more rapidly than for a defect-free coating. The cathodic delamination is one of the more important processes promoting the degradation of a defect protective organic coating immersed in neutral electrolyte solutions [3]. Cathodic delamination is the result of disruption of the bonds between coating and metal surface. Hence the bare metal is exposed to the surrounding environment, promoting corrosion and further degradation of the anticorrosive coating.

The reason for the cathodic delamination is proposed to be so-called polarization [4]. The cathodic polarization of the steel arises when the anodic and cathodic reactions take place at a defect in the coating. The process moves forward under coatings due to continuous migration of water and oxygen (necessary for the cathodic reaction) and positive ions, necessary in order to locally balance the electric charge [5].

Premature coating failure may decrease structural reliability and extreme expenses are associated with corrective repair. Hence it is important to be able to estimate the lifetime and performance of an anticorrosive coating system in a reliable fashion. The key to lifetime estimations and design of novel or improved formulations of anticorrosive coatings lies in the potential failure mechanisms. It is essential that the controlling mechanisms are identified and quantified through laboratory experiments

The purpose of this project is to obtain detailed knowledge on the mechanism of cathodic delamination and quantify the most important physical and chemical

Results and Discussion

The progress of the delamination front is proportional with the square root of time (see fig. 1). This suggests that interfacial diffusion along the coating-steel interface is likely to be the rate-determining step of the process of cathodic delamination because the mean diffusion length, $\overline{x}$, for a diffusion time, t, for linear isotropic and semi-infinite diffusion is given by

$$\overline{x} = 2 \cdot \sqrt{D \cdot t} \qquad (5)$$
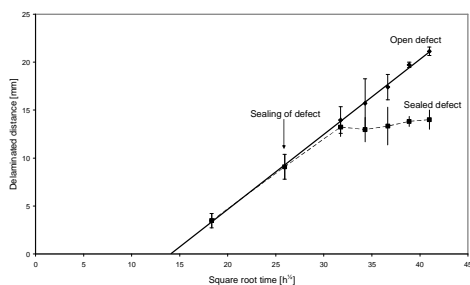
Figure 1: Delamination behaviour for an inert pigmented epoxy coating in aerated 0.5 M NaCl solution at 25°C with an open defect and a defect.

Interfacial diffusion of cations may very well be the rate-determining step in cathodic delamination because of the observed inhibition of the delamination when the artificial defect was sealed with a molten mixture of bee wax and natural gum rosin after four weeks exposure. This procedure represses the transport of cations along the coating-steel interface from the defect to the delamination front without affecting the transport of cations perpendicular to the coating (i.e. through the

intact or delaminated regions in the coating). Hence it is clear that the main route of the cations required for charge neutralization of the hydroxyl ions is along the coating-steel interface and not perpendicular to the coating system.

The inverse proportionality between the delamination rate and the tortuosity of the coating-steel interface given in figure 2 shows that cathodic delamination is a diffusion controlled process, where cations must migrate from a defect to the delamination front to neutralize the charge of hydroxyl ions generated by the cathodic reactions. This means that the migration of cations as well as the production and migration of hydroxyl ions along the coating-steel interface will determine the rate of cathodic delamination
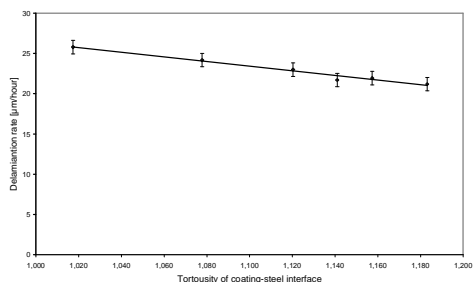
Figure 2: Effect of tortuosity of the coating-steel interface on the delamination rate of a commercial TiO_2 pigmented barrier coating.

Conclusions

The primary route of the cations which must be transported from the bulk solution to the defect is along the coating steel interface. This means that the tortuosity of the coating-steel interface, to some extent, can be applied to control and minimize the observed rate of cathodic delamination.

Acknowledgements

References

1. D. A. Jones, Principles and Prevention of Corrosion, Prentice Hall, U.S. 1996
2. H. Leidheiser, W. Wang, L. Igetoft, Prog. Org. Coat. 11 (1) (1983) 19-40.
3. T. Nguyen, J. B. Hubbard, J. M. Pommersheim, J. Coat. Tech. 68 (855) (1996) 45-56.
4. W. Funke, J. Coat. Tech. 55 (705) (1983) 31-38.
5. J. E. O. Mayne, Anticorrosion Methods and Materials 20 (10) (1973) 3-8.

List of Publications

1. P. A. Sørensen, S. Kiil, K. Dam-Johansen, C. E. Weinell, Prog. Org. Coat., In Press.
2. P. A. Sørensen, S. Kiil, K. Dam-Johansen, C. E. Weinell, J. Coat. Technol. Res., In Press.

Samira Telschow

Phone:	+45 4525 2952
Fax:	+45 4525 2258
E-mail:	ste@kt.dtu.dk
WWW:	http://www.chec.kt.dtu.dk
Supervisors:	Professor Kim Dam-Johansen
	Associate professor Stig Wedel
	Associate professor Flemming Frandsen
	Kirsten Theisen, FLSmidth A/S

PhD Study
Started: March 2008
To be completed: February 2011

Quality Dependence on Burning Conditions and Technology

Abstract

In the cement industry, reduction of the energy consumption and the CO_2 and NO_x emission levels while simultaneously increasing of the cement quality is of great interest. The aim of this project is to investigate the development of the cement properties, depending on process conditions. Special focus is on the clinker properties: product composition, porosity and crystal/particle size distribution.
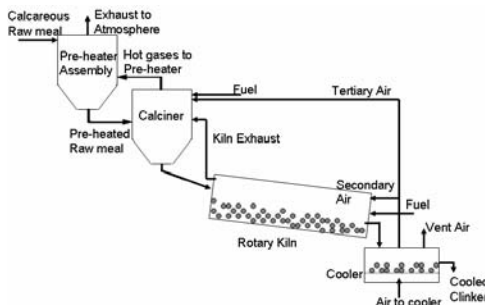
Introduction

Concrete is one of the most important materials in the construction industry world wide. The main component of concrete is cement, a hydraulic binder (characterized by its ability of hardening under water). The world production capacity of hydraulic cement was in 2006 3-5 Gt [1, 2]. One of the most common cement types is Portland cement, which consists of Portland cement clinker ground with ~5wt.% gypsum. By addition of granulated slag, pozzolan, sulfate or lime to Portland cement clinker, cement with special properties e.g. higher concrete strength or special resistance against aggressive agents is obtained. Examples are e.g. Blast-furnace cement, Pozzolan-lime cement or Supersulfated cement.

Figure 1: A flow diagram of a cement kiln system [3].

A typical raw meal is composed of a mixture of calcareous material, such as limestone or marble, and SiO_2/Al_2O_3-rich clays (kaolinite, illite) or shale, as well as iron ore. Additionally, minor compounds e.g. Mg,

Na, K, Ca as well as sulphates, phosphates, halogens etc. may be present in the raw materials [4-6]. The crushed raw materials are blended and ground, before the raw meal is fed into the preheater section (a series of cyclones). There the materials are heated up to 800°C by hot gases from the calciner and kiln. Water, which is contained in the raw materials, is released. In the calciner most of the limestone is decomposed at ~900°C, i.e. CO_2 is removed and CaO is formed [7]. The degree of calcination is approximately 90-95%. In order to achieve the necessary temperatures in the calciner, fuel is burned there. Thereafter the material enters the rotary kiln. The material moves along the kiln to the lower end and is heated by hot gases from the fuel combustion at the outlet from the kiln. In the hot zone at the lower end of the kiln (gas temperatures of ~1800°C) the mixture reaches a temperature of ~1500°C and melts partly [1, 7, 8]. In the kiln at temperatures of 1100-1500°C a series of reactions is occurring, resulting in the formation of the major phases in the clinker product: Ca_2SiO_4 (belite), Ca_3SiO_5 (alite) and the so-called liquid phase (melt) $Ca_3Al_2O_6$ (aluminate) and $Ca_4Al_2Fe_2O_{10}$ (ferrite) [4, 7].

In the cooler the hot clinker is rapidly cooled by heat exchange between the clinker solids and air, in order to recover the heat. The clinker product is ground with gypsum and possibly other additives, stored, packed and sold. The most important clinker phases, concerning the hardening and longevity of concrete, are alite and aluminate.

The production of cement is a highly energy consuming process, emitting various gaseous compounds. Typical compounds in the flue gas are CO, CO_2, NO_x, SO_2. The reduction of their concentration in the flue gas is of

great importance for the industry. E.g. five percent of the global anthropogenic CO_2 are released by cement plants. In 2006, German cement plants produced ~33 Mt cement, which caused an emission of 18 Mt CO_2 [2]. This is mainly due to the CO_2 release from limestone (66.8%), and consumption of thermal and electrical energy (33.2%) (German cement production = 1.3% of world production) [9].

The processes from drying of raw material till clinkerization consumes an average thermal energy of 3.1-3.5 MJ/kg of produced clinker [2]. Additionally, ~100 kWh/t of electrical power is necessary e.g. for grinding of the raw material and the cement product [10]. The highest proportion of the electrical energy is attributed to cement grinding due to the clinker properties (the different clinker phases and other clinker characteristics).

Specific Objective

Various technological improvements have been carried out in the last decades to increase the efficiency in all parts of a cement plant. Nevertheless, further optimizations are necessary. One possibility is to improve clinker properties (chemical, physical and mineralogical) by influencing the clinker formation in the reactor. A critical product property is the clinker hardness, which is mainly influenced by clinker composition, clinker porosity and product particle/crystal sizes. Decreasing the clinker hardness facilitates the cement grinding and reduces the energy consumption of this process, as well as the material attrition of the mills. Therefore, the focus in this project is on how these three properties are developed regarding different process conditions. These process conditions are among others:

- maximum burning temperature
- burning time
- raw mix composition
- raw mix particle size distribution.

The burning temperature and temperature profile influences the composition of the clinker product and also the crystal sizes of the different phases in the product. E.g. increasing temperatures may compensate for poor raw mix homogeneity as the rate of reaction depends on temperature. On the other hand high temperatures also cause crystal growth, which is not desired in terms of decreasing product hardness. The raw mix particle size distribution will influence the needed burning time and temperature, as smaller particles – all else being equal – will react in a shorter time.

It is also planned to investigate in which type of reactor these product properties may be controlled more precisely. The reactors in question are the rotary kiln and the fluidized bed reactor. Therefore, reactor specific conditions e.g. rotation velocity or fluid velocity will be included into the investigation of the product properties development. The overall goal of this project is to developed proposals, how the process pathway of clinker burning can be changed in order to reduce cement hardness, without degrading concrete properties such as, setting, hardness or longevity.

References
[1] U.S. Environmental Protection Agency, Inventory of U.S. Greenhouse Gas emissions and Sinks: 1990-2006, 2008.
[2] Verein Deutscher Zementwerke e.V., Forschungsinstitut der Zementindustrie, VDZ Activity report 2005-2007, Verlag Bau + Technik GmBH, Duesseldorf, 2008, p. 26, 74.
[3] A. Z. Jensen; Master thesis; Institute of chemical and biochemical engineering at DTU; 2008.
[4]G.C. Bye, Portland Cement-Composition, Production and Properties, Pergamon Press, Oxford, 1983, 8pp.
[5] F.P. Glasser, J.I. Bhatty, F. McGregor, S.H. Kosmatka, Innovations in Portland Cement Manufacturing, Portland Cement Association, Skokie, Illinois, 2004, p. 332.
[6] F. Nishi, Y. Takéuchi, I. Maki; Zeit. Krist. 172 (1985) 297.
[7] H.F.W. Taylor, Cement Chemistry, Academic Press Thomas Telford, London; 1997, 55pp.
[8] J. Klauss, ZKG international 53 (3) (2000) 132-144.
[9] Verein Deutscher Zementwerke e.V., Forschungsinstitut der Zementindustrie;Umweltdaten der deutschen Zementindustrie, 2007, p. 17.
[10] V. Johansen, T.V. Kouznetsova; 9th ICCC; New Delhi, 1992.

Lise Vestergaard Thomassen

Phone:	+45 4525 2979
Fax:	+45 4593 2906
E-mail:	lvt@kt.dtu.dk
WWW:	http://www.bioeng.kt.dtu.dk
Supervisor:	Anne S. Meyer

PhD Study
Started: April 2008
To be completed: March 2011

Enzymatic Production of Dietary Fibres and Prebiotics from Potato Pulp

Abstract
Dietary fibres and prebiotics are non-digestible carbohydrates that beneficially affect the host by selectively stimulating the growth or the activity of some bacteria in the colon. The cell walls of potato are a potential source of dietary fibres and/or prebiotics and by targeting the modification of potato plant cell wall material with monoactive enzymes it is possible to modify and produce specific structures.

Introduction
Potato pulp is a coproduct from the industrial production of potato starch. At the moment it is mostly used as a feed ingredient for cattle and therefore it has a low value.

Potato pulp consists of about 37 % w/w starch, 17 % w/w cellulose, 14 % w/w hemicellulose, 17 % w/w pectin and 4 % w/w protein/amino acids (relative to dry matter) [1]. Pectin is constructed of homogalacturonan, rhamnogalacturonan I (RGI) and rhamnogalacturonan II (RGII). In this project RGI is of main interest. RGI has a backbone consisting of altering α-(1$\rightarrow$2)-linked L-rhamnosyl and α-(1$\rightarrow$4)-linked D-galactosyluronic acid residues. The side chains are mainly composted of galactose and arabinose or a mixture of these. In potato pulp the side chains mainly consist of galactose (figure 1).
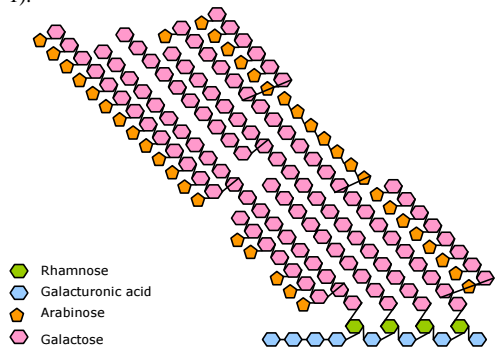
Figure 1: Stylised structure the RGI pectin in potato pulp.

Pectin is soluble in water and used in the food industry where it affects the functionally of products e.g. it is used as a gelling agent and stabiliser. Certain pectin fractions are also a non-digestible carbohydrate structures that might exert beneficial effects on the colonic bacteria.

Previous work
Meyer et al. 2008 has treated potato pulp from Andels Kartoffelmelsfabrikken Midtjylland (Brande, Denmark) with Termamyl 120L (95 °C, 30 min) and Alcalase AF 2.4 L (60 °C, 30 min) from Bacillus licheniformis, AMG 300L (95°C, 30 min) from Aspergillus niger, and Viscozyme® L (62.5 °C, 1 h) from Aspergillus aculeatus. The monosaccharide composition of the solubilised potato fibre is listed in table 1.

Table 1: The monosaccharide composition of solubilised fibre from potato pulp.

Monosaccharide	Amount (wt. %)
Rhamnose	0.6 ± 0.10
Fucose	0.1 ± 0.01
Arabinose	3.6 ± 0.00
Xylose	1.4 ± 0.00
Mannose	0.6 ± 0.001
Galactose	17.7 ± 0.10
Glucose	2.3 ± 0.85
Uronic acid	13.4 ± 0.00
Cellulose	21.7 ± 1.20
Starch	30.0 ± 2.12
Klason lignin	3.8
Uncharacterised	4.9

The molecular sized profiles showed that the solubilised potato fibres were distributed in four populations of different approximate average molecular weights: 911(31.4 %), 710 (12.7 %), 99 (49.9 %) and 14 (5.9 %) kDa [2].

Lærke et al. (2007) evaluated three different potato fibre products from potato pulp (concentrated (CF), soluble (SF) and insoluble potato fibre (IF)) by enzymatic treatment and compared their effect with cellulose (CEL) on rats. The SF fraction was prepared the same way as described by Meyer et al. (2008). One of the results from the experiment is shown in table 2.

Table 2: Approximate weight (g) development during ad libitum feeding of the experimental diets. *Significant different from CEL (P<0.05); #significant different from all other diets (P<0.05) (n=10) [3].

Day	CEL	CF	IF	SF
0	320	326	321	319
7	339	341	341	336
17	355	356	355	347
21	370	370	368	356*
27	377	377	374	362*
33	388	383	381	370#

As can be seen from table 2 there was a general trend for rats fed with the SF diet having a lower body weight than the other rats and from day 21 the body weight was significantly different from the rats fed CEL and CF diets.

The fermentation pattern in the differently fed rats that had consumed enzymatically solubilised potato fibres had larger pool of total organic acids and short chain fatty acid in their cecum. The results obtained in the in vivo studies with the rats indicate that the galactan rich fibres solubilsed from potato pulp are fermented to a significant degree in rats [3].

Specific objectives
The previous obtained results indicate that there exists an potential of production of prebiotics and/or dietary fibres from potato pulp. By intelligent combining monoactive enzymes it is the aim of the PhD project to produce specific modifications of pectin from potato pulp using the minimal number and concentration of different enzymes.

Acknowledgement

References
1. F. Mayer and J.-O. Hillebrandt, Potato pulp: microbiological characterization, physical modification, and application of this agricultural waste product, Appl Microbiol Biotechnol (1997) 48: 435-440
2. A. S. Meyer, B. P. Dam and H. N. Lærke, Enzymatic solubilization of pectinaceous dietary fiber fraction from potato pulp: Optimization of the fiber extraction process, Biochemical Engineering Journal, (2008) in press
3. H. N. Lærke, A. S. Meyer, K. V., K. V. Kaack and T. Larsen, Soluble fiber extraction from potato pulp is highly fermentable but has no effect on risk markers of diabetes and cardiovascular disease in Goto-Kakizaki rats, Nutrition Research 27 (2007) 152-160

Stuart R Tindal

Phone:	+45 4525 2950
Fax:	+45 4525 2906
E-mail:	st@kt.dtu.dk
WWW:	http://www.bioeng.kt.dtu.dk
Supervisors:	John M Woodley
	Suzanne Farid, UCL
	Helen C Hailes, UCL
	Ian Archer, Ingenza Ltd

PhD Study

Started:	September 2006
To be completed:	August 2010

Process Design for Biocatalytic Amino Acid Deracemisation

Abstract

Biocatalysis is an intensifying area of chemistry that offers novel and alternative synthetic strategies to a range of useful chemical products. In particular chiral intermediates represent a huge potential market for biocatalysis-based products. However, enzyme stability has hindered the implementation of many processes. Using an amino acid oxidase (AAO) based deracemisation platform as a test conversion, stability has been assessed. Stability was studied at different pH values to assess the effect of hydrogen peroxide nuecleophilicity. Significant improvements were observed under more acidic conditions. Knowledge of these factors will be used to develop a new reactor and process design which will minimise the destabilising effects of the enzyme.

Introduction

Biocatalysis contributes to just over 2% of the total $27 billion market for basic, intermediate, fine and specialty chemicals and polymers[1]. The potential for this to grow is considerable, especially given the current pressures to reduce waste and increase process sustainability, atom efficiency and product quality. A key area in which biocatalysis can challenge chemical catalysis is in the production of chiral molecule building blocks for use in the chemical development of new and existing pharmaceuticals[2]. One such example is the deracemisation of chemically produced amino acid racemates into their corresponding optically pure forms. The chiral raw materials and synthetic intermediates market currently stands at $15 billion and is growing at 9.4% annually [1]. The high enantio- and regioselectivity of biocatalysis is well suited to chiral organic synthesis and the progress of techniques in bioinformatics and microbial genomics are broadening the capacity and availability of new biocatalysts. A promising prospect is the synthesis of optically pure amino acids in a process that incorporates a hybrid chemoenzymatic reaction to convert a racemate into an enantio-pure material.

Technology

The principle reaction in this project is the conversion of one enantiomer of a racemate producing an enantiomerically pure solution[3]. Further, to improve the yield beyond 50% a non-selective chemical reducing agent is used to produce the desired enantiomer in excess of 99.5% e.e. as shown in Figure 1[4]. The production of these key building blocks is essential in

many important pharmaceutical products. Recently, the reaction has been scaled up to pilot level with some substrates and has shown potential to become a valuable biocatalytic synthetic process[5].
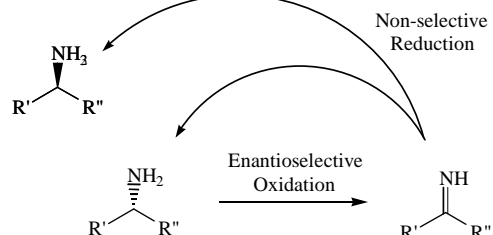
Figure 1: Generic deracemisation process using AAO. The AAO reacts much faster with one of the enantiomers oxidising it to the imine and the chemical reducing agent produces an equal amount of both enantiomers. Hence the unreactive enantiomer accumulates resulting in an enantiomeric excess above 99.5%[6].

The focus of this project is to quantify and model the factors affecting the stability of AAO using rational experimentation and Design of Experiments (DoE). The detrimental variables uncovered will become the focus of a stability improvement study, using process conditions, reactor design and biocatalyst modification.

Results and discussion

The individual affect of the chemical and physical factors that resulted in the loss of enzyme activity were quantified at varying pH values. The reactivity of the hydrogen peroxide increased as the prevalence of the anionic form (deprotonated) increased in alkaline

conditions. Loss of AAO activity and decomposition of hydrogen peroxide can be correlated and shown in figure 2. The rate of hydrogen peroxide breakdown is a related to the pH, concentration and reactive surface area.
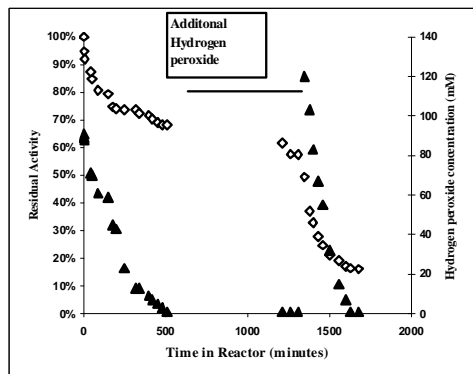
Figure 2; Shows the correlation between the breakdown of hydrogen peroxide in the reactor and loss of residual activity of AAO. Solid triangles [H_2O_2] and open circles Residual activity

Data compiled from the factorial stability studies will be used to construct the magnitudes and limits for the oxidation's process conditions. The enzyme's productivity will be judged by a comparison of the product to biocatalyst ratio (Kg/Kg). Improvements in the stability that maintain AAO activity will result in higher productivities and thus a higher yielding process.
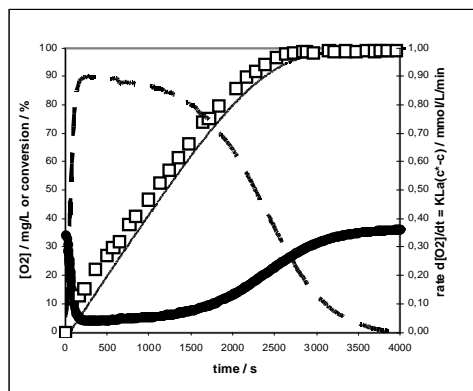
Figure 3; Shows the on-line and off-line measurements combined to follow a 100mM DL-amino butyric acid (aba) resolution. Dashed line $K_La(c^*-c)$/mmol/L/min, open squares represents the conversion of D-aba, thin grey line conversion base of area below $K_La(c^*-c)$/% and the solid black line is the DOT /mmol/L.

The oxidation will be monitored off-line as well as on-line with a combination of HPLC techniques and dissolved oxygen tension measurements. As an oxidation progresses and the substrate is converted to the imine the rate of reaction will slow as it shifts from being oxygen limited to amino acid limited. Knowing when and where the reaction is limited by the mass transfer of oxygen or availability of substrate or if the stability of the enzyme has been compromised is important to accurate on-line analysis. An oxidation profile can be seen in figure 3 with the various rates of reaction and off-line analysis of D-aba consumption.

Conclusions

The hydrogen peroxide stability experiments found that when the pH value shifts to a more basic pH the reactivity of hydrogen peroxide increases. This higher reactivity was more detrimental to the enzyme's residual activity. As a result, lowering the pH of the process gave improvements in stability. The effect of changing the pH has been quantified allowing the prediction of residual activity at other values. This model only takes into account the improvement of enzyme longevity and does not incorporate the activity of the enzyme at these differing pH values.

Hydrogen peroxide and other deleterious chemical and physical components found in an oxidation have each had their individual effect on stability, quantified. While these factors all contribute individually to the stability of the enzyme, synergistic effects can also be expected. Thus the next logical step forward is to combine the knowledge attained from the stability experiments such that the process conditions and controlling them within a window of operation can be achieved. That will improve the understanding of the oxidation of amino acids for implementation into the deracemisation technology.

Future work

The stirred tank reactor vessel is a robust and industrially common design in bioprocesses; unfortunately it introduces gas/liquid interfaces via aeration. Investigation into alternative reactor designs such that the deleterious gas/liquid interface is reduced or removed are ongoing.

Acknowledgements

References

[1]. Schmid A, Hollmann F, Park JB, Buhler B. 2002. *Current Opinion in Biotechnology* **13**:359-368.

[2]. Pollard DJ, Woodley JM. *Trends in Biotechnology.* 2007. **25**(2):66-73

[3]. Fotheringham I. 2006. *Biocatlysis* (November): 38-39.

[4]. Alexandre F-R, Pantaleone DP, Taylor PP, Fotheringham IG, Anger DJ, Turner NJ. *Tetrahedron Letters* 2002. **43**:707-710.

[5]. Taylor IN, Brown RC, Bycroft M, King G, Littlechild JA, Lloyd MC, Praquin C, Toogood HS, Taylor SJC. *Biochemical Society Transaction*s 2004. **32**:290-292.

[6]. Fotheringham I, Archer I, Carr R, Speight R, Turner NJ. *Biocatalysis Biochemical Society Focused Meeting.* 2006: 287-291.

Maja Bøg Toftegaard

Phone:	+45 9955 2910
Fax:	+45 4588 2258
E-mail:	mbt@kt.dtu.dk
WWW:	http://www.kt.dtu.dk
Supervisors:	Anker Degn Jensen
	Peter Glarborg, Peter Arendt Jensen
	Bo Sander, DONG Energy

Industrial PhD Study

Started:	April 2007
To be completed:	March 2010

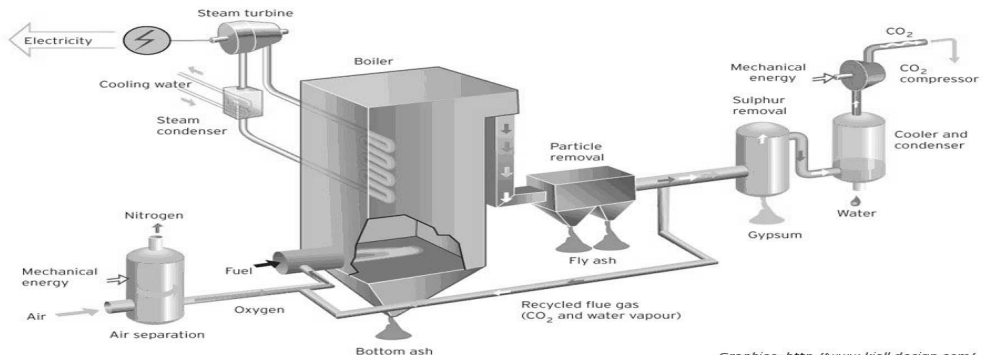# Oxy-Fuel Combustion of Coal and Biomass

Abstract

A drastic decrease of the CO_2 emission from power production is necessary to limit global warming. One of the promising technologies which will enable almost complete capture of CO_2 from power plants burning fossil fuels is oxyfuel combustion. There is a need for a more in-depth insight into the fundamental aspects of the effects of oxyfuel combustion regarding combustion chemistry and the effects on especially ash quality in relation to cement and concrete production. The PhD study includes an experimental and theoretical investigation of these aspects.

Introduction

Several technologies have been proposed and are investigated for carbon capture and storage (CCS), i.e. the removal of CO_2 from exhaust gases from e.g. power plants or other fossil fuel fired processes. Oxyfuel combustion is one of the more promising of these technologies [1]. Figure 1 shows the principle in oxyfuel combustion. The fuel, e.g. coal, biomass, or others, is burned in an atmosphere consisting of oxygen and recirculated flue gas (consisting primarily of CO_2 and water). The resulting flue gas has a CO_2 content of up to 95 % on a dry basis compared to about 14 % from a conventional plant. The CO_2 can be stored after cleanup and compression.

Generally, there is insufficient knowledge on many fundamental and practical aspects related to the change from the conventional to the oxyfuel combustion process. From a chemical engineering point of view this concerns among others the emission levels of CO, NO_x, and SO_2, the quality of the ash fractions, the risk of increased corrosion due to a change in the chemical composition of deposits, and the temperature and radiation in the boiler which are affected by the changed gas phase composition, i.e. the increased level of CO_2 and water vapour. Especially aspects regarding the effect of the flue gas cleaning strategy on fly ash quality and corrosion still need significant further investigations. Furthermore, the effect of using biomass as fuel in CCS has only been investigated experimentally by very few research groups [2,3]. This approach involves the possibility of operating power plants with negative CO_2 emissions.


Figure 1: Possible layout of an oxyfuel power plant showing the air separation, flue gas recirculation, and flue gas treatment new to the plant compared to a conventional air-fired power plant.

Specific Objectives

The aim of the PhD study is to strengthen the scientific basis for the development and application of the oxyfuel combustion technology to thermal power plants. Both experimental and theoretical investigations of the fundamental aspects of the combustion chemistry obtained when burning coal and biomass will be performed. Specific topics which will be addressed are:

- Ash composition and quality, especially related to sulphur retention – because of the application of fly ash in cement and concrete production this is a very important area of investigation.
- Deposits composition – the chemical composition is indicative of the risk of corrosion on heat transfer surfaces.
- Emissions of CO, NO_x, and SO_2 from the boiler – the recirculation of flue gas will play a role in the obtained levels of the emissive gas phase components together with the chosen strategy for flue gas cleaning
- The effect of co-firing coal with biomass (wheat straw)

The results obtained in the experimental investigations will be applied in a validation of a Computational Fluid Dynamics (CFD) model for oxyfuel combustion. The CFD model will be built as part of the PhD study and should be applicable for design and process optimization in full scale boilers.
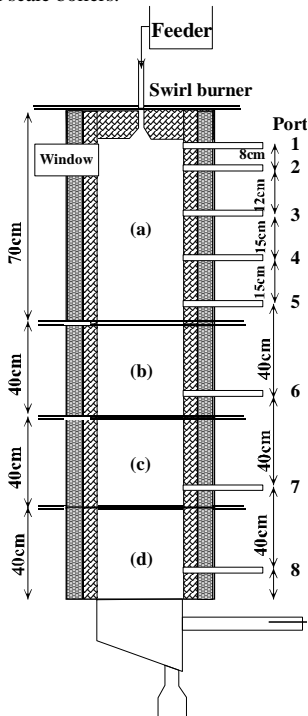
Figure 2: Sketch of the experimental setup – a 30 kW down-fired swirl burner.

Experimental setup

An existing experimental setup is applied in the investigations, see Figure 2. The setup consists of a cylindrical reactor (inner diameter 30.5 cm) with a swirl burner. The setup is equipped with a solid fuel feeder, a fly ash sample system (not shown), and 8 measuring ports for temperature and gas phase composition measurements. The setup can run at a thermal input of approximately 30 kW.

As part of the project the setup is being rebuilt to be able to run at oxyfuel conditions. In full scale, flue gas will be recirculated to adjust the temperature, but in the pilot plant flue gas recirculation is not applied. Instead, synthetic flue gas consisting of pure CO_2 from gas cylinders is used. Pure oxygen will likewise be delivered to the setup from gas cylinders and mixed with CO_2 in a special mixing panel. A system to enable addition of both N_2, NO and SO_2 to the CO_2 stream is likewise included in the setup. Addition of N_2 has two purposes. First, it can be used to simulate air entrainment in the setup, and secondly to investigate the effect of the purity of the oxygen, since oxyfuel power plants generally are assumed to be run on about 95 % pure oxygen the remaining being N_2 and Ar. Variation of the amount of NO and SO_2 in the oxidizer can be used to investigate the effect of different strategies for flue gas cleaning before and after the recirculation stream has been taken.

Conclusions

The work on rebuilding the setup is currently ongoing and the experiments will begin shortly.

Besides the experiments, a thorough survey of the available literature within oxyfuel combustion has been performed. The survey concentrates on the combustion process, emissions of primarily NO and SO_2, and ash formation.

References

1. B.J.P. Buhre, L.K. Elliott, C.D. Sheng,, R.P. Gupta, and T.F. Wall. Progress in Energy and Combustion Science 31 (4) (2005) 283-307
2. B. Arias, C. Pevida, F. Rubiera, and J.J. Pis. Fuel 87 (12) (2008) 2753-2759
3. L. Fryda, M.K. Cieplik, J.M. Jacobs, and W.L. van de Kamp. 16th European Biomass Conference & Exhibition, Valencia, Spain, June 2-6, 2008

Carlos Axel Díaz Tovar

Phone:	+45 4525 2808
Fax:	+45 4525 2906
E-mail:	adi@kt.dtu.dk
WWW:	http://www.capec.kt.dtu.dk
Supervisors:	Rafiqul Gani
	Bent Sarup, Alfa Laval

PhD Study
  Started: May 2008
  To be completed: April 2011

Modeling of Production Process for Vegetable Oils and Fats: Prediction of Melting Points

Abstract

The production of edible fats and oils, like many other chemical processes, involves a wide range of processing steps, from crude edible oil (vegetable) production to the final product. However, unlike the chemical processes, the state of the art in process modeling and simulation has only to a very limited extent penetrated this industry, due to the complex nature of the lipid systems involved.

Modeling and validation of physical properties of the most representative chemical species and their mixtures occurring on the edible oil industry, as well as of those selected unit operations and process sections are the main objectives of the PhD project. In this paper a new model to predict the melting point, based on the level of saturation of different types of fats and oils, is proposed. The accuracy of the model compared with those available in the literature is better; however the main contribution of this model is the capability of predicting melting points above 300K. Future validation work with other data bases will be done in order to corroborate the accuracy of the model.

Introduction and Specific Objectives

About 79% of the over 100 million ton of edible oils and fats produced worldwide annually are derived form plant sources and are referred to as vegetable oils [1]. Melting behavior is one of the properties of vegetable oils that influence their functionally in many prepared food products.

Unlike pure compounds, natural vegetables oils do not have true melting points. This is because fats and oils present in natural plant sources are mixtures of different types of triacylglycerols (TAG) [2]. Therefore, the complicated behavior of melting, crystallization and transformation, crystal morphology, and aggregation of real-fat systems is due in part to the physical properties of the components TAG's.

The aim of this paper is to develop a mathematical model capable of correlating the amount of unsaturated, mono saturated, and poly unsaturated TAG's of a specific oil and/or fat with the melting point (Tm).

Methodology

Experimental values of melting point reported in the literature for 52 different kinds of edible oil and fats such as soybean (crude and hydrogenated), palm oil (refined and hydrogenated), and olive oil, among others where used to develop a predictive mathematical model for this physical property.

The main difference between each one of these oils is the amount of saturated, mono unsaturated and poly unsaturated fatty acid chains attached to the glycerol group.

Equation 1 is the proposed model used to predict the melting point of different oils and fats based on the level of saturation of the most representative TAG's.

$$T_m(K) = T_{ref}(K) + bSS + cMM + dPP \qquad (1)$$

Where b, c, and d are adjusted parameters. SS, MM, and PP are the level of saturated, mono unsaturated, and poly unsaturated triacylglycerols presents in the oil respectively. Finally $T_{ref}(K)$ is the melting point of the shortest triacylglycerol (see Figure 1).

$$CH_2 - COO - CH_3$$
$$|$$
$$CH - COO - CH_3$$
$$|$$
$$CH_2 - COO - CH_3$$
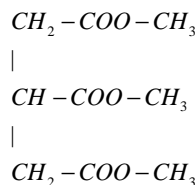
Figure 1: Schematic representation of Triacetin

175

The data base (DB1) [1,3,4,5] used in the regression consists of fifty two different oils and fats as well as their corresponding composition and measured melting point.

Results and Discussion
The computed values of the adjustable parameters of Equation 1 are showed in Table 1.

Table 1: Adjustable parameters of the predictive model.

Parameter	Value
B	0.4020
C	0.0464
D	-0.2978

A set of thirty three experimental values of different oils and fats (DB2) [6,7] was used to check the accuracy of the proposed model. Table 2 compares the accuracy of the model proposed in this paper with respect to the two models proposed by Fasina et al[1].

Table 2: Adjusted parameters of the predictive model.

Model	Data Base			
	DB1+DB2	DB2	FASINA	
This work	3.69	5.59	1.17	
Fasina 1	8.42	12.1	1.36	**ARD (%)**
Fasina 2	6.26	9.23	1.22	

The comparisson between the experimental and the predicted values obtained with each one of the three models are highlighted in Figures 2 and 3. Notice that the Fasina et al [1] models are not capable of predicting values above 282K.
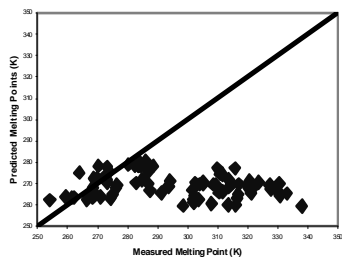
(a)
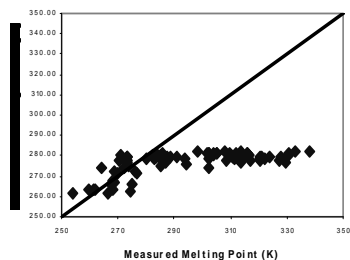
(b)

Figure 2: Comparison between measured melting points and predicted melting points computed with the Fasina et al models.
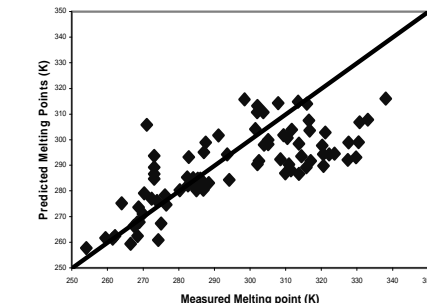
Figure 3: Comparison between measured melting points and the predicted melting points predicted with the model proposed in this paper.

Conclusions
More accurate predictive models of physical properties will provide more strong and reliable tools for the process and equipment design of the edible oil industry.
This paper provides a new and more accurate model to predict the melting point of different oils and fats based on the level of saturation of the TAG's. Future validation with other databases needs to be made before using this model for design and analysis of Production processes for edible oils.

References
1. O.O. Fasina,, M. Craig-Schmidt, Z. Colley, H. Hallman, LWT - Food Science and Technology 41(8) (2008) 1501-1505.
2. J. Qingzhe, Z. Ting, S, Liang, L. Yuanfa, W. Xingguo, Journal of the American Oil Chemists' Society 85 (1) (2008) 23-28.
3. R. T. Nassu, L. A. Guaraldo-Goncalves, Grasas y Aceites 50 (1) (199) 16-21.
4. E. Chiavaro, Journal of Agricultural and Food Chemistry 56 (2) (2008) 496-501.
5. A. Jimenez-Marquez, Grasas y Aceites, 54 (4) (2003) 403-409.
6. M.V. Gilabert-Escriva, Journal of the Science of Food and Agriculture, 82 (13) (200) 1425-1431.
7. F. C. Chiu, Journal of Applied Polymer Science, 107 (6) (2008) 79-87..

Chien-Tai Tsai

Phone:	+45 4525 2943
Fax:	+45 4593 2903
E-mail:	ctt@kt.dtu.dk
WWW:	http://www.bioeng.kt.dtu.dk
Supervisors:	Anne S. Meyer
	Anders Viksø Nielsen, Novozymes A/S

PhD Study

Started:	May 2008
To be completed:	April 2011

Physical and Chemical properties of Pretreated Lignocellulose

Abstract
The project focuses on the chemical and physical properties of pretreated lignocellulose as well as the relation between these properties and enzyme hydrolysis efficiency. The information facilitates developing new strategies improving the efficiency of lignocellulose deriving bioethanol production process.

Introduction
Due to the increasing demand for energy but the decreasing petroleum, and the deteriorating environment, seeking for alternative energy is more and more important. Biofuel made from plant biomass, oil containing plants or starch and sugar rich crops are alternatives. However, under the pressure for food, optimal utilization of agricultural residuals to produce fuel is crucially important.

Plant biomass is mainly composed of lignocellulose. Cellulose is a polysaccharide with D-glucose as monomer. The hydrolysis of cellulose to release D-glucose monomers for down stream fermentation is one of the key steps for producing ethanol. However, due to the recalcitrant properties of the biomass, until now there is no satisfying pretreatment. Hence, as a base for developing better pretreatment and enzymatic hydrolysis schemes the fundamental objective of the present project is to provide an improved understanding of the chemical and physical properties of pretreated lignocellulose as well as the relation between these properties and enzyme hydrolysis efficiency. The information facilitates developing new strategies improving the efficiency of lignocellulose deriving bioethanol production process.

Specific objective
In chemical reactions, the reaction area affects the reaction rate. Hence, for a heterogeneous enzymatic catalysis system, the pore size of the substrates determine the diffusivity of enzymes into the interior part substrate, and a main hypothesis of this project is that the accessible substrate surface area and hydrolysis efficiency depend on the pore size distribution of the substrate. In this part we will characterize the pore size distribution of wheat straw after pretreatments and evaluate the hydrolysis efficiency.

Due to the multicomponent nature of lignocellulose (cellulose, hemicellulose and lignin etc.), which are mainly polymers, after pretreatment destroying the organized tissue structure, the conformational structures and the interaction of these components in water should be very complicated. Until now, there is no research directly visualizing the conformation and interaction of these components in water. The substrate conformational change may be an explanation to rheological property of the pretreated lignocellulose and the efficiency of hydrolysis of cellulose. The rheological behavior of pretreated lignocellulose may correlate to its interaction with water. The aim of the research is also investigating the interaction between water and pretreated lignocellulose.

The viscosity of pretreated plant biomass is too high to process. It is necessary to add a large quantity of water to lower the viscosity, resulting in the sizes of processing facilities have to be enlarged to adapt the material containing so much water. Besides, more energy has to be put in to distil ethanol from the end product. All this increases the cost of processing and waste energy.

The research mainly consists of the following parts:

- Characterize the Pore Size Distribution of Wheat Straw after Different Pretreatments

- Visualize the Conformation and Interaction of the Components in Pretreated Lignocellulose

- Interaction between Water and Pretreated Lignocellulose

References

1. Mads Pedersen, Anne S. Meyer. Influence of substrate particle size and wet oxidation on physical surface structures and enzymatic hydrolysis of wheat straw. Biotechnology Progress (In press)
2. Lisa Rosgaard., Sven Pedersen, Anne S. Meyer. Comparison of Different Pretreatment Strategies for Enzymatic Hydrolysis of Wheat and Barley Straw. Appl Biochem Biotechnol (2007) 143:284–296

Rasmus Wedberg

Phone:	+45 4525 2959
Fax:	+45 4593 2906
E-mail:	raw@kt.dtu.dk
WWW:	http://www.kt.dtu.dk
Supervisors:	Jens Abildskov
	Günther H. Peters, DTU Chemistry

PhD Study

Started:	November 2007
To be completed:	October 2010

Molecular Simulation Routes to Properties of Solutions and their Interactions with Biomolecules

Abstract

The project deals with developing and improving the applicability of molecular modeling approaches to two different problems: prediction of thermodynamic properties of solutions via calculation of so-called Kirkwood-Buff integrals, and selection of solvent for biocatalysis of transesterifications. The project also deals with exploring rational approaches to force-field development.

Introduction

Molecular modeling methodologies play an increasingly important role in Computer-Aided Molecular Design (CAMD). Though computationally expensive, these methodologies have proven to be of great value in situations where conventional property-prediction methods fall short.

A relevant example is the prediction of thermodynamic properties of solutions, in particular phase behavior. Molecular modeling based tools focusing on this problem, such as Gibbs-Ensemble Monte Carlo and COSMO-RS, are gaining popularity.

Molecular modeling is also frequently employed to study biomolecules. Predicting relative protein-ligand binding free energies and the effects of site-specific mutations are common tasks. However, molecular modeling approaches are not yet exploited for the task of selecting solvent for biocatalysis. Organic solvents, are routinely used in industry for enzyme-catalyzed reactions [1]. However, in this context, solvent design is typically done on a 'trial-and-error' basis. The development of a CAMD approach to support the selection of solvent is thus desirable to practitioners in the field. Such an approach can benefit from the use of molecular dynamics (MD) and quantum mechanical/molecular mechanics (QM/MM) simulations [2] which allows one to study the interactions between the enzyme and the solvent in great detail, and extract properties, *e.g.* flexibility, that correlates with activity.

Specific Objectives

The project is composed of three parallel tasks, all of which attempt to advance the fundamentals of molecular modeling approaches and bridge the gap between CAMD and molecular modeling methods. The first part is concerned with predicting thermodynamic properties of solutions, via the so-called Kirkwood-Buff integrals. The objective is to improve the accuracy and robustness of the methods used to extract these integrals from simulations.

In the second part, Lipase B from *Candida Antarctica* (CALB) is studied in organic solvents with low water content through MD and QM/MM simulations. The enzyme-solvent interactions are characterized in different ways, *e.g.* via flexibility and solvent structure around surface residues. The results will be correlated with kinetics measurements of transesterification reactions carried out by collaborators.

The third part addresses rational approaches to force-field development. An attempt will be made to develop an accurate force field for lactones.

Results and Discussion

Calculation of Kirkwood-Buff Integrals

Thermodynamic properties of solutions can be expressed in terms of so called Kirkwood-Buff (KB) integrals [4]:

$$H_{ij} = \int \left(g_{ij}(\mathbf{r}) - 1 \right) d\mathbf{r} \qquad (1)$$

where ρ and g_{ij} denote the density and the radial distribution function correlating molecules of species i and j, respectively. Evaluating KB integrals of radial distribution functions obtained from MD simulations

has previously been explored as a method for predicting the excess Gibbs free energy of binary mixtures [4]. However, a key challenge is that the integral in eq. 1 converges slowly, and it is necessary to extend the $g(r)$ to a longer range of r, in order to obtain an accurate result.

A previously employed method for extension is to fit the tail of $g(r)$ from simulation to the analytical expression

$$g(r) \propto 1 + ae^{-b(r-c)} \sin\left(d\left(r-c\right)\right) \quad (2)$$

which allows for extending $g(r)$ to evaluate the integral. In order to evaluate the accuracy of this approach a number of MD simulations of pure alkane liquids were carried out and KB integration was used to compute the isothermal compressibility. The same quantity was also computed via the well established approach, in which one considers density fluctuations, in order to check for consistency between the two approaches.

The results show that the two approaches are well consistent with each other, which means that the KB integrals can be obtained accurately (see Wedberg *et al.* 2008). However, the results also hints that the approach is not completely robust and that the functional form in eq. 2 might not be optimal in all situations.

An alternative approach is to utilize the direct correlation function, $c(r)$, defined by the Ornstein-Zernike equation

$$h(\mathbf{r}) = c(\mathbf{r}) + \int c(\mathbf{r-r'}) h(\mathbf{r}) d\mathbf{r} \quad (3)$$

where $h(r) = g(r)-1$. In contrast to g, the long-range behavior of c is well known and is given by the random-phase approximation (RPA). In order to extend $g(r)$ beyond the simulation range, one seeks an extension such that the corresponding $c(r)$ has the correct long-range behavior. This approach is currently being explored.

Enzymes in Organic Solvents
MD simulations of CALB in water, hexane, acetone and tert-butanol are in progress. For the three latter, the simulation box also contains the water molecules present in the CALB crystal structure as determined by x-ray diffraction. The simulations will be analyzed to measure protein flexibility, interactions with hydration water and interactions with the solvent. The results will form a basis for further simulations and correlation with kinetics measurements.

In addition, a first step towards a quantum chemical study of CALB catalyzed ester hydrolysis was carried out. In this study, CALB was represented by five 'cut-out' residues of the active site, and the substrate considered was methyl formate. Semi-empirical calculations were carried out to study the mechanism of the proton transfer that underlies the reaction. This resulted in the estimate $6.1 s^{-1}$ of the turnover number, k_{cat}, which is of the same order of magnitude as values obtained from kinetics measurements, see *e.g.* ref. 5.

Rational Approach to Force-Field Development
A methodology [6] for determining the force-field parameters associated with intermolecular interactions, including Lennard-Jones (ε_X, σ_X) parameters and partial charges (q_X), is explored. Here, X denotes the atom type. In this method, the parameters are optimized with respect to the objective function:

$$Q\left(\varepsilon_X, \sigma_X, q_X\right) = \sum_i \left(f^{sim}\left(T_i, \rho_i\right) - f^{exp}\left(T_i, \rho_i\right)\right)^2 \quad (4)$$

Here, T_i and ρ_i denote various temperatures and densities, f^{sim} and f^{exp} denote a thermodynamic property evaluated from simulation using the current parameters respectively taken from data. The minimization is carried out using the Gauss-Newton method. One MD simulation is run for each statepoint and using relations from statistical mechanics f^{sim} is evaluated as well as its partial derivatives with respect to the parameters. Usually it is sufficient to perform a single Gauss-Newton step based on these simulations, in order to improve the parameters significantly.

As a first test of this methodology, the parameters of a very simple force field, the Lennard-Jones potential were optimized. The parameters were optimized so that the pVT-data of liquid argon were reproduced. The procedure turned out to be efficient and the parameters were significantly improved.

Currently, the methodology is further explored for slightly more complex molecules, namely 2-propanol and methyl acetate.

References
1. G. Carrea, S. Riva, Angew. Chem. Int. Ed. Eng. 39 (13) (2000) 2226-2254.
2. G. Colombo, G. Carrea, J. Biotechnol. 96 (1) (2002) 23-33.
3. J.G. Kirkwood, F.P. Buff, J. Chem. Phys. 19 (6) (1951) 774-777.
4. S. Christensen, G.H. Peters, F.Y. Hansen, J.P. O'Connell, J. Abildskov, Mol. Simulat. 33 (4-5) (2007) 449-457.
5. K. Blank, J. Morfill, H. Gumpp, H.E. Gaubb, J. Biotechnol. 125 (2006) 474-483.
6. E. Bourasseau, M. Haboudou, A. Boutin, A.H. Fuchs, P. Ungerer, J. Chem. Phys. 118 (7) (2003) 3020-3034.

List of Publications
R. Wedberg, G.H. Peters, J. Abildskov, Fluid Phase Equilibr. 273 (1-2) (2008) 1-10.

Hao Wu

Phone:	+45 4525 2927
Fax:	+45 4525 2258
E-mail:	haw@kt.dtu.dk
WWW:	http://www.chec.dtu.dk
Supervisors:	Peter Glarborg
	Kim Dam-Johansen
	Flemming Frandsen

PhD Study
Started: November 2008
To be completed: October 2010

Co-Combustion of Fossil Fuel and Waste

Abstract

Co-combustion of coal and waste offers a fast and low-cost opportunity to reduce the net CO_2-emissions from dedicated coal-fired plants, and at the same time to get rid of a certain amount of combustible waste produced from industry and household. In comparison with a conventional waste incineration plant, co-combustion of coal and waste in a pulverized coal-fired plant offers advantages such as improved electrical efficiency, increased waste disposal capability, and higher value of usable ash products. However, it can also lead to problems such as deposition, corrosion, fly ash qualities, and trace element emissions. The overall objective of this PhD-project is to identify suitable waste types, energy fraction and particle size that can be co-combusted in pulverized coal-fired power stations, and to optimize the co-combustion process through experimental and modeling studies.

Introduction

The emission of CO_2 has received enormous concerns in recent years due to its significant contribution to the world's greenhouse effect. Combustion of fossil fuels contributes to a major part of CO_2 emission worldwide [1]. To reduce the CO_2 emission, there is an increasing demand of replacing part of the fossil fuel consumption by biomass/waste which is considered to be completely or partly CO_2 neutral. Among the various technologies of utilizing biomass/waste energy, one of the most simple and promising ways is to co-combust a certain percentage of biomass/waste together with coal in existing pulverized coal-fired plants [2,3].

Besides the obvious effect on the reduction of CO_2 emission, co-firing of biomass/waste with coal in an existing pulverized coal-fired plant offers several other advantages such as improved efficiency of utilizing biomass/waste energy, high values of combustion residues, large biomass/waste treatment capacity, and high fuel feasibility [2-4]. However, problems are also related with co-combustion of coal and biomass/waste, such as severe deposition, corrosion and fly ash quality problems caused by the high alkali and chlorine contents in the biomass/waste and high emissions of trace elements due to the high trace element contents in the waste [2-4].

Denmark is one of the most active countries in promoting the co-combustion technology, especially on straw and coal co-firing. Through more than 10 years' researches and full scale demonstrations, it is now considered to be feasible to co-combust a certain percentage (<20 th%) of straw with coal in a pulverized coal-fired plant, without significant technical problems regarding emissions, deposition, corrosion, and fly ash qualities [5]. To promote the co-combustion technology even further in Denmark, the target now extends to co-firing a certain percentage of combustible waste with coal in existing pulverized coal fired plants. Therefore, there is a need to investigate and address the technical problems related with co-combustion of coal and waste.

Specific objective

The objective of this PhD-project is to identify suitable waste types, energy fraction and particle size that can be co-combusted in pulverized coal-fired power stations, and to optimize the co-combustion of coal and waste through laboratory, pilot- and full-scale experiments, supplemental by modeling work. The influences of co-firing on deposit formation, fly ash quality, gaseous emissions and trace element partitions will be the main focus. The mechanism governing the transformation and the partition of major- and trace elements during co-combustion of coal and waste will be studied through experiments and modeling.

Results

Co-firing experiments of coal and waste are carried out in an entrained flow reactor which is designed to simulate the combustion environment of a suspension fired boiler. Two coals (SAKLEI and COPRIB) and a

RDF (refuse derived fuel) which mainly consists of paper, plastic, and wood are selected as the fuels used in the experiments. Through the experiments, influences of co-firing on the gaseous emissions, burnout, deposits formation, and fly ash qualities are investigated.

Figure 1 shows the influences of co-firing on the NO emissions. The concentrations of NO are found to decrease with increasing percentage of RDF for both of the coals. One obvious reason for the observed reduction effect is that the RDF contains lower nitrogen content than both of the coals. However, through studying the percentages of nitrogen in the fuel released as NO at different RDF share, it is found that with higher share of RDF, lower percentage of the nitrogen in the fuel would be converted to NO. The presumable reason is that the high volatiles content of the RDF can restrain the formation of NO during the prolysis stage.
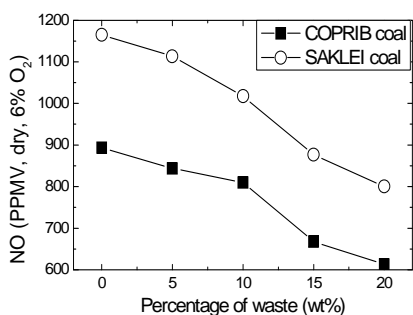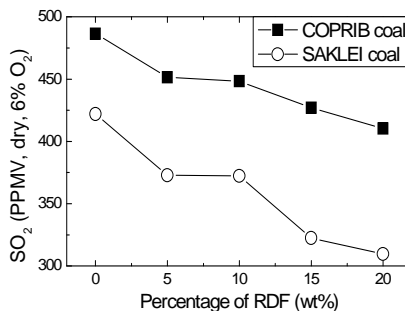

Figure 1: NO emissions from co-combustion of coal and RDF.

The concentrations of SO_2 generated during co-combustion of coal and RDF are presented in Figure 2. Similar as NO emissions, the emissions of SO_2 are found to decrease with increasing share of RDF for both of the coals. The reduction of SO_2 emissions at high share of RDF is partly due to the low sulphur content in the RDF. Besides, it is found that the percentages of sulphur in the fuel released as SO_2 also decrease with increasing RDF percentage. The main reason is probably the high Ca content in the waste which can react with SO_2 and retain the sulphur in the ashes.

The influences of co-combustion on the fuel burnout have also been investigated. The results indicate that co-firing of coal with less than 20wt% of RDF generally does not adversely affect the fuel burnout. However, in some cases, the fuel burnout can be slightly reduced at high RDF share since the agglomeration behavior of the fuel particles can become very significant with high percentage of RDF.

Through collecting deposits on an air-cooled probe, effects of co-firing coal and RDF on the deposit formation are studied in the experiments. The results show that ash deposition behavior during co-combustion varies significantly for different coals. For COPRIB coal and RDF co-firing, the deposit formation rate decreases slightly with increasing share of waste. For

co-combustion of SAKLEI coal and RDF, the deposit formation rate shows an increasing trend up to 10wt% waste share, and then starts to decrease at higher waste share ($\geq$ 15wt%). The change of the chemical compositions of the fly ashes is considered to be the primary factor that affects the deposition behavior of the fly ashes. However, other parameters such as ash particle size and the distribution of ashes in the flue gas may also influence the deposition of fly ashes on a probe. Further investigations are required in order to understand the results obtained in the experiments.

Figure 2: SO_2 emissions from co-combustion of and RDF.

Conclusion

Co-combustion experiments in an entrained flow reactor show that co-firing a certain percentage of RDF ($\leq$20wt%) with coal generally does not adversely affect the fuel burnout. With increasing share of RDF, the emissions of NO and SO_2 are decreased, both due to the low nitrogen and sulphur contents in the RDF and the positive synergy effects between coal and RDF. The deposit formation on an air-cooled probe is found to be highly coal-dependent during co-combustion of coal and RDF.

References
1. A. Demirbas, Prog. Energy Combust. Sci. 31 (2005) 171-192
2. B. Leckner, Therm Sci. 11 (4) (2007) 5-40
3. M. Sami, K. Annamali, M. Wood, Prog. Energy Combust. Sci. 27 (2001) 171-214
4. T. Nussbaumer, Energy Fuels 17 (2003), 1510-1521
5. P. Overgaard, B. Sander, H. Junker, K. Friborg, O.H. Larsen, 2nd World Conference on Biomass for Energy (2004)

Cheng Xu

Phone:	+45 4525 2935
Fax:	+45 4525 2258
E-mail:	cxu@kt.dtu.dk
WWW:	http://www.kt.dtu.dk
Supervisors:	Anne Meyer, DTU
	Jens Sørensen, Danisco A/S

PhD Study
Started: March 2007
To be completed: Feb 2010

Kinetic Models Describing Enzyme Catalyzed Degradation of Water Soluble Arabinoxylan

Abstract

The project focuses on modelling of the cooperative and synergistic action of the enzymes during modification, debranching and depolymerisation of differently substituted, water soluble arabino-xylooligosaccharides. The main purposes are to study the kinetics model of degradation with pure enzymes and to design a process in order to obtain target xylo-oligosaccharides with high prebiotics activity

Introduction

Native arabinoxylans are abundant in cereal plant cell walls and are composed of a backbone of (1,4)-linked-D-xylose residues to which -L-arabinofuranosyl residues can be single substituted at -1,3 or -1,2 and double-substituted at -1,3 and -1,2, [1,2]. Recent findings indicate that xylooligosaccharides stimulate the growth of probiotic, cecal bifidobacteria in vivo and exert inhibitory effects on precancerous colon lesions in rats. An overall aim of the PhD project is to use specific enzymes to design biofunctional xylooligosaccharides with defined substitution patterns and chain lengths, and in particular to quantify the rates of the different events by developing enzyme kinetic models. The enzymatic hydrolysis of arabinoxylan is a complicated process which requires the action of different enzyme activities for complete hydrolysis; These are first and foremost various α-L-arabinofuranosidases, endo-1,4-β-xylanase and β-xylosidase [3,4,5]. The enzymatic degradation of arabinoxylan, can be expected to depend on the degree of arabinose substitution, the position of glycosidic bonds and their distribution along the xylan backbone [3]. Purified microbial enzymes, including α-L-arabinofuranosidases, endo-1,4- -xylanases, and -xylosidase from various microbial sources will be systematically combined to obtain reaction rates for the different enzyme catalyzed reactions, e.g. removal of arabinose from singly versus from doubly substituted xyloses, and different patterns of xylan depolymerisation. The enzymes to be used are monocomponent enzymes, while some of the arabinoxylans have recently become commercially available. Rates of reactions will be determined from HPLC evaluation of arabinose, xylose, and xylo-oligomer release in timed enzyme experiments. In order to find better ways to reuse the enzymes to save costs, the effects and mode of removal of the monosaccharide products to eventually abolish product inhibition will also be assessed. The hypothesis behind the project is that provision of a better quantitative understanding of the events by modelling of the reactions is a prerequisite for optimally exploiting the complex, sequential enzyme reactions in new food and ingredient processes and development. With arabinoxylan, the results are particularly relevant in baking, brewing, prebiotics design, and in non-food cereal based processes.

Specific Objectives

The purpose of current study is to understand the enzyme kinetics in arabinoxylan degradation. The overall aim is that we can design and control the reaction optimally; a particular purpose of this study is to control the hydrolysis in order to produce specific xylo-oligsacchrides with high prebiotics activity.

Preliminary Result

Special attention is given to the action of α-L-arabinofuranosidases which are represented by the glycoside hydrolase (GH) families: 3, 10, 43, 51, 54 and 62. The enzymes catalyse the hydrolysis of α-1,2, α-1,3 and α-1,5 glycosidic bonds of α-L-arabinofuranosyl residues. Also the action of β-xylosidase is taken into account. β-Xylosidases catalyse the cleavage of xylobiose and attack the non-reducing ends of short xylooligosaccharides to liberate xylose [5]. β-xylosidase activity has been reported to be rate-limiting in arabinoxylan hydrolysis [6]. Enzymes exhibiting β-

xylosidase activity are categorised into the following seven different GH families: 3, 30, 39, 43, 51, 52 and 54. The synergistic effect of the enzymes acting on arabinoxylan was initially analysed with enzyme preparations from *Aspergillus niger*, *Bifidobacterium adolescentis* and the enzyme blend "Celluclast 1.5 L" (Novozymes A/S, Denmark).

Here, we use C+A represent the enzyme combination Celluclast 1.5 L and arabinofuranosidase from *A.niger* , C+B represent the enzyme combination Celluclast 1.5 L and Arabinofuranosidase from *Bi. adolescentis,* C represent pure Celluclast 1.5 L. Figure 1 shows the initial rate of xylose release in the arabinoxylan degradation on different substrate concentration.
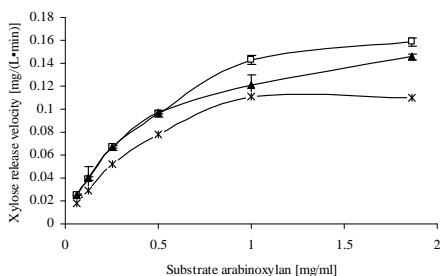
Figure 1: 2 The 20min reaction velocity for the enzymatic release of xylose plotted against substrate concentration treated with different enzyme combinations C+A (□), C+B (▲) and C (*)

The xylose release (beta-xylosidase activity) apparently follows the Michaelis-Menten kinetics curve. The reaction rate increases as substrate concentration increases. As arabinoxylan concentration gets higher, the enzyme becomes saturated with the substrate and the rate reaches the apparent Vmax, the enzyme's maximum rate on this substrate.

References
1. Izydorezynk MS, Biliaderis CG (1995). Cereal arabinoxylans: advances in structure and physicochemical properties. Carbohyd. Polym. 28: 33-48.
2. Dervilly-Pinel G, Tran V, Saulnier L (2004). Investigation of the distribution of arabinose residues on the xylan backbone of water-soluble arabinoxylans from wheat flour. Carbohyd. Polym. 55: 171-177..
3. Rasmussen LE, Sørensen HR, Vind J, Viksø-Nielsen A (2006) Mode of action and properties of the β-xylosidase from Taleromyces emersonii and Trichoderma reesei. Biotechnol Bioeng 94:869-876
4. De Vries RP, Visser J (2001). Aspergillus enzymes involved in degradation of plant cell wall polysaccharides. Microbiol. Mol. Biol. R. 65: 497-522.
5. Sørensen HR, Meyer AS, Pedersen S (2003) Enzymatic hydrolysis of water-soluble wheat arabinoxylan. 1. synergy between α-L-arabinofuranosidases, endo-1,4-β-xylanases, and β-xylosidase activities. Biotechnol Bioeng 81:726-731
6. Poutanen K and Puls J (1988). Characteristics of Trichoderma reesei β-xylosidase and its use in the hydrolysis of solubilized xylans. Appl Microbiol Biotechnol. 28: 425-432.

Linfeng Yuan

Phone:	+45 4525 2955
Fax:	+45 4593 2906
E-mail:	lfy@kt.dtu.dk
WWW:	http://www.capec.kt.dtu.dk/
Supervisors:	Gunnar Jonsson
	John Woodley
	Lars Korsholm, Novozymes A/S
	Sune Jakobsen, Novozymes A/S

PhD Study
Started: March 2008
To be completed: March 2011

Membrane Assisted Enzyme Fractionation

Abstract

An enzyme concentrate produced by fermentation will often contain two or more enzyme activities. From the application viewpoint then it can be necessary to remove the side activity. This can be done by a number of methods including chromatography or crystallization. The aim of this project will be to develop a suitable membrane fractionation process and to assess the economics of such membrane processes for industrial scale production and relevant applications such as pharmaceutical and dairy enzyme production.

Introduction

Large-scale economic purification of proteins is an increasingly important problem for the biotechnology industry. Separation of the desired protein from other proteins produced by the cell is usually attempted using a combination of different chromatography techniques. Adequate purity is often not achieved unless several purification steps are combined thereby increasing cost and reducing product yield. Consequently there is a need for processes that purify protein mixtures using fewer steps and without the need for a costly affinity step.

Membrane processes are widely used in the biochemical industry for separation and concentration of protein. Traditionally fractionation of enzymes using membranes due to the variation in size of the proteins is rather limited, which is partly caused by concentration polarization and membrane fouling.

Motivation

Recent publications have shown that by careful control of the concentration polarization, and use charged membranes, a dramatic effect can be seen on the separation efficiency of such membranes.

Enevoldsen et. al. has shown that by using an electrical field during crossflow ultrafiltration (EUF), a 3-7 times improvement in flux has been obtained. This indicates that using an overlaid electric field is an effective way to depolarize the membrane surface when operating with enzyme solutions [1,2]. It is possible that EUF can be used for the separation of two enzymes with opposite charge sign since enzymes can carry different charges by adjusting the pH of the solution. Another possibility is to separate the enzyme product from impurities in the solution by dragging the charged enzyme through the membrane. This could improve the purity of the enzyme product, which is desirable for new product markets where high purities may be required.

In addition Jonsson et. al. has shown that using high frequency backflushing of the membrane surface is very effective at reducing the concentration polarization and can further be used to tune the membrane selectivity and therefore on principle be used to make a fractionation of enzymes [3, 4].

Combining these techniques with the use of a charged membrane is expected to give the desired separation properties which can further be scaled-up to a feasible ultrafiltration membrane system.

Specific Obejctives

The project aims at developing and economically assessing a pilot scale membrane fractionation process as this might be more economical for bulk enzyme purification compared to current state of the art technologies.

The feasible membrane fractionation process to be considered or investigated will potentially include:

- EUF
- Charged membranes
- Membrane systems using high frequency pulsation and / or vibration

Feed solution properties such as pH, ionic strength, additives can be chosen as appropriate.

If an efficient process is developed then pilot up-scaling of the membrane fractionation process will be considered.

Electro-ultrafitration

To prevent direct contact between the enzymes and the electrodes, the EUF cell is configured according to Figure 1.
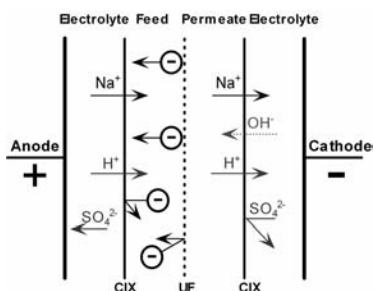
Figure 1: EUF module with an UF membrane placed between two cation exchange membranes[1].

The cell consists of four chambers. A UF membrane is placed between two cation exchange membranes (CIX), depending on the pore size of the UF membrane compared to the size of the enzymes, it either retains enzymes or let them pass through it. Flow spacers are used to enable adequate flow of the different streams. By using CIX membranes in front of both the anode and cathode it is possible to prevent an accumulation of salt ions in the feed stream.

The experiments are operated with full recycle by returning the concentrate back to the feed container. The electrolyte consists of 0.1 Na_2SO_4. The UF membrane is a 10kDa surface-modified PVDF ETNA 10PP membrane from Alfa Laval and the CIX membrane is a RELAX-CMH membrane from Mega. The membrane area is 10×10 cm^2

Work done

During the last 8 months, we have been using the EUF set-up to invesigate if it is possible for the separation of amino acids. The reason why we began with amino acid is that the low molecular weight of the compounds does not affect on membrane fouling. In order to study this, we divided the research into 3 parts. And we are now at the second part.

Firstly, 1g/L NaCl solution was used both in feed and permeate as a model solution to study how the permeate conductivity changes when applying an electrical field. This showed that the permeate conductivty of NaCl either increases or decreases depending on the position of the electrode. It also showed that the rate of change is dependent on the electrical field strength, while independent of the transmembrane pressure.

Secondly, charged phenylalanine by adjusting solution pH was used to study if the permeate conductivity and concentration change of a single amino acid follows the same trends with that of NaCl. It turns out that a single charged amino acid can mimic the same mass transport phenomina as NaCl.

Next Steps

In the very next step, the third parts which is the separation of two amino acid with different charges at a given pH will be carried out. Modelling of the mass transport for NaCl and amino acid will also be studied. The results from the amino acid studies will be used for further study on enzyme fractionation.

Finally, a charged membrane and membrane system using high frequency pulsation will also be tested for enzyme fractionation.

References

1. A.D. Enevoldsen Electrically enhanced ultrafiltration of industrial enzyme solutions, Technical University of Denmark, Ph.D. thesis, 2007
2. A.D. Enevoldsen, E.B. Hansen and G. Jonsson, Journal of Membrane Science 299 (2007) 28-37
3. S. P. Beier and G. Jonsson, Separation and Purification Technology 53 (2007) 111–118.
4. G. Jonsson, Fractionation of macromolecules by dynamic ultrafiltration, 7th World Conference on Chemical Engineering in CD, Glasgow, 2005

Dayang Norulfairuz Abang Zaidel

Phone: +45 4525 2861
Fax: +45 4525 2906
E-mail: daz@kt.dtu.dk
Web page: http://www.bioeng.kt.dtu.dk
Supervisors: Anne Meyer
                John M. Woodley

PhD Study
  Started: August 2008
  To be completed: July 2011

Enzymatic Production of Cross-Linked Plant Cell Wall Polymers

Abstract

This PhD project is based on the premise that improved emulsification and prebiotic effects in sugar beet pulp (SBP) and barley spent grain (BSG) can be achieved by cross-linking of feruloylated polysaccharide structures. The aims of the project are to establish the kinetic basis of the cross-linking reactions and characterize the macromolecular function of the resulting cross-linked polysaccharides in terms of their rheological properties and emulsion stabilizing effects.

Introduction

Recently, it has been recognized that polysaccharides, categorized as dietary fibres and prebiotic oligosaccharides, may exert potential physiological benefits beyond their classical effects. For instance, their ability to bind bile acids, cholesterol, and toxic compounds present in the digestive tract suggest that a number of oligosaccharides and polysaccharides may have an important preventative role against various chronic diseases such as coronary heart disease [1].

It is well established that many plant cell walls contain phenolic acids that are ester-linked to polysaccharides. They are mainly ester-linked to *0*-2 of the -(1→5)-linked arabinan chains and to *0*-6 of -(1→4)-linked type I of galactan chains [2]. It was reported that ferulic acid esters in plant cell walls could undergo oxidative coupling reactions to form dehydromers (diFA) [2-4]. This oxidative reaction can be catalyzed by various systems such as peroxidases (with hydrogen peroxide), polyphenol oxidases, including laccases, as well as some purely chemical systems [4]. From these reactions various diFA are formed: 5-5′, 8-O-4′, 8-5′ and 8-8′ (Figure 1). Formation of diFA enables covalent cross-linking of the polysaccharides they esterify. The previous studies indicated that the feruloylated polymers have an effect on the mechanical properties of plant cell wall *i.e.* a tightening effect on the plant cell wall (contributing to wall assembly, promotion of tissue cohesion and resistance against fungal penetration). This project is built on the premise that the cross-linked polysaccharides are able to enhance the emulsification stability of the polysaccharides [5].
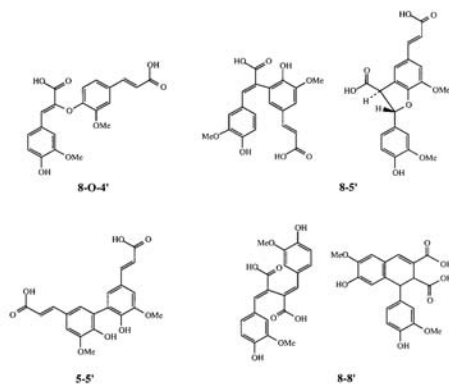
Figure 1: The six main structures of ferulic acid dehydromers

Objectives

The first objective of this project is to establish and describe the kinetic reactions of the enzymes involved in the *in vitro* cross-linking of the polysaccharides with the various substrates. It is expected that the concentration of ferulic acid substrate and the size of substrate affect the kinetics of the enzymatic reaction. The second objective is to characterize the

macromolecular properties of the cross-linked polysaccharides in terms of rheological measurements and then establish the correlation between the macromolecular function of the cross-linked polysaccharides and the reaction kinetics. Finally, it is aimed to investigate the effect of emulsification stability of the cross-linked polysaccharide.

Current Work

In this project, pectin from sugar beet (SBP) and arabinoxylan from barley spent grain (BSG) will be used as the examples. The content of phenolic acid in sugar beet pectin and arabinoxylan from BSG were determined by alkali extraction as described previously [6]. From Table 1, it can be observed that the content of phenolic acid in SBP and BSG were similar, about 8 – 9 mg g^{-1} dry weight.

Table 1: Phenolic acids content in SBP and BSG [6]. Results are shown as mean ± SD.

Sample	Total Phenolic (mg g^{-1} dry weight)
Sugar beet pectin	7.70 ± 0.03
Barley spent grain	9.17 ± 0.40

Information about the ability of ferulic acid to cross-link in pectin was obtained by using a UV-visible absorption measurement. The absorbance spectra of 0.1% (w/w) sugar beet pectin dissolved in aqueous phosphate buffer (pH 6; 20 mM) was measured at wavelengths between 200 and 500 nm. A maximum absorption spectrum at 325 nm was observed as shown in Figure 2, which indicates the presence of ferulic acid. This absorbance at 325 nm is used for the determination of the oxidative cross-linking of ferulic acid by peroxidase with hydrogen peroxide.
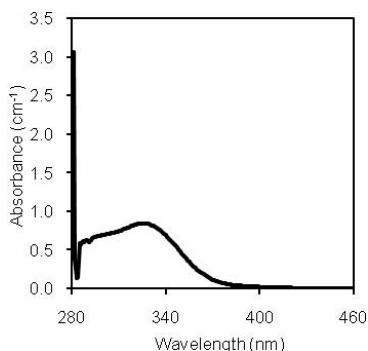
Figure 2: Absorbance spectra of sugar beet pectin (0.1% w/w) dissolved in aqueous phosphate buffer solution (pH 6; 20 mM).

Conclusion and Future Work

From this project, it is expected that a new enzymatic biocatalytis process will be developed, with a better understanding of the kinetics in order to improve the cross-linking of polysaccharides. This study will provide a distinctive contribution in the application of biological processes for the knowledge-based production of food ingredients, notably health promoting products. The knowledge gained will improve fundamental understanding of the molecular and kinetic basis of specific enzyme catalyzed processes.

Future work will be directed towards the establishment of enzyme kinetics of the cross-linked polysaccharides and their correlations with the macromolecular properties and emulsification stability.

References

1. T. Jalili, R.E.C. Wildman, Medeiros DM nutraceutical roles of dietary fiber. Journal of Nutraceuticals, Functional & Medical Foods. 2(4) (2000) 19-34.
2. M.-C. Ralet, G. Andre-Leroux, B. Quemener, J.-F. Thibault, Sugar beet *(Beta vulgaris)* pectins are covalently cross-linked through diferulic bridges in the cell wall. Phytochemistry. 66 (2005) 2800-2814.
3. K. Nishitani, D.J. Nevins, Enzymic analysis of feruloylated arabinoxylans (feraxan) derived from *Zea mays* cell walls. Plant Physiology. 93 (1990) 396-402.
4. L. Saulnier, J–F. Thibault, Ferulic acid and diferulic acids as components of sugar-beet pectins and maize bran heteroxylans. Journal of the Science of Food and Agriculture. 79 (1999) 396-402.
5. F. Littoz, D.J. McClements, Bio-mimetic approach to improving emulsion stability: cross-linking adsorbed beet pectin layers using laccase. Food Hydrocolloids. 22(7) (2008) 1203-1211.
6. J. A. Robertson, C. B. Faulds, A. C. Smith, K. W. Waldron, Peroxidase-mediated oxidative cross-linking and its potential to modify mechanical properties in water-soluble polysaccharide extracts and cereal grain residues. Journal of Agricultural and Food Chemistry. 56 (2008) 1720-1726.

Muhd Nazrul Hisham Zainal Alam

Address: Building 227, room 240
Phone: +45 4525 2993
Fax: +45 4593 2906
E-mail: mza@kt.dtu.dk
WWW: http://www.kt.dtu.dk
Supervisors: Krist V. Gernaey
              Anne Meyer
              Gunnar Johnson

Ph.D. Study
Started: July 2007
To be completed: June 2010

Continuous Membrane Microbioreactors for Development of Integrated Pectin Modification and Separation Processes

Abstract

The project aims at designing continuous membrane microbioreactors for the development of integrated pectin modification and separation processes. These microbioreactors should encompass the requirements to perform a continuous enzymatic reaction with simultaneous product separation and integration of optical sensors for on-line monitoring of relevant process variables. The project is linked to a new strategic research effort on enzymatic modification of pectins for producing pre-biotics initiated at the Department of Chemical and Biochemical Engineering at DTU.

Introduction

Pectin is a complex carbohydrate (heterosaccharide) mostly found in primary cell walls and intercellular regions of higher plants. Pectic substances are abundant in agro-industrial waste streams from sugar and potato starch production. Agro-industries are highly interested in converting these low-value waste streams into useful high-value products [1]. This conversion can be done by breaking down the pectin into oligosaccharides through the hydrolysis reaction catalyzed by combined action of pectinolytic enzymes, namely the pectinmethylesterase (PME) and polygalacturonase (PG). However; like any other enzymatic reaction, there is an abundance of factors dictating its reaction rate and kinetics [1 - 3].

Presently, the concept of microbioreactors to accommodate specific enzymatic reactions has been successfully demonstrated. However, most of the currently existing micro-scale systems for studying enzyme reactions are systems where the enzyme is immobilized [4]. Despite of its advantages in enzyme reutilization and elimination of enzyme recovery processes (recycle stream channel), this system is not suitable for the enzymatic depolymerization of pectin to oligosaccharides. This is due to the presence of multiple enzymes (PME and PG) and end-product inhibition. Under these circumstances, a free-cell system (stirred tank reactor) is most favorable. Microbioreactors (free-cell system) with a working volume ranging from milliliters down to nanoliters in different operating modes (batch, fed-batch and continuous operation) have been established. These microbioreactors are integrated with optical sensors for on-line monitoring of relevant

process parameters (OD, DO, pH) [5]. Nevertheless, currently existing microbioreactors were mainly designed to facilitate the fermentation processes of bacterial and animal culture strains.

The development of micro-systems for high throughput screening of enzymatic reactions and for on site production of expensive bioproducts at the point of demand is an on-going research activity. At this stage, a feasible continuous membrane microbioreactor for pectin modification processes has yet to be established. Therefore, development of such a novel continuous membrane microbioreactor for pectin modification and separation processes will be the goal of this research project.

Motivation

When evaluating new enzymes for novel enzyme-catalysed production processes, the costs and availability of the enzymes are often a limit, as the production of limited quantities of new enzymes is costly.

In this respect, microbioreactors offer a number of cost-reducing advantages for assessing enzymatic processes (particularly screening of new enzymes). First, the microreactors operate with very small volumes, even when operated as a chemostat as envisaged in this project, thus offering significant cost reduction for assays with expensive substrates (e.g. labeled substrates) or expensive enzymes. Second, by adapting technologies from polymeric bio-microsystems, microbioreactors can be made disposable to minimise reactor preparation efforts. Third, and

maybe most important, due to the small size, the microbioreactors can mimic in a controlled fashion a wide range of environmental conditions, which can be related to conditions in full-scale bioprocesses. Moreover, the microbioreactors can be scaled out to platforms of multiple reactors, thus greatly increasing throughput for elucidating enzyme behaviour under various relevant bioprocessing conditions. [5,6].

All in all, the continuous operation of the microbioreactors is precisely the technology that will enable conducting experiments to unravel the kinetics governing enzymatic conversion processes under conditions relevant for actual industrial processes.

Continuous membrane microbioreactor prototype
The current continuous membrane microbioreactor prototype was realized as a loop reactor [6] with a working volume between 100 to 200 L. The prototype (Figure 1) comprises both microbioreactor and micro membrane separation units pressed together in a housing made up of Polyethylene terephthalate (PETP). External microfluidic connections were established by standard Perfluoroalkoxy (PFA) tubing with commercially available chromatography fittings.

Figure 1. The continuous membrane microbioreactor prototype

The microbioreactor (MBR) counterparts merely consist of a Polydimethylsiloxane (PDMS) layer sandwiched between two Poly methyl methacrylate (PMMA) layers. Both materials are cheap and biocompatible. This significantly reduces the cost for fabrication. The feature of the MBR includes mixing, temperature control and pH measurement. Mixing was established by a micro impeller placed inside the microreactor chamber. Temperature is measured with a Platinum resistance thermometer (Pt 100) and controlled with a heater mat placed underneath the prototype. pH is measured with fluorescent sensor spots which change both the amplitude and the phase of the emitted light with a change in the sensitive variable. A lock-in amplifier measures the phase difference and thus quantifies the measured variable.

The micro membrane separation (UF) unit on the other hand, is simply consists of a Regenerated Cellulose membrane pressed between two PMMA layers for tight sealing. Both layers have the same geometry design. An optical pressure sensor is integrated for measurement of pressure on the retentate side of the micro UF unit. A micro-gear pump is used to regulate the flow rate in the micro UF unit in such a way

that a sufficiently large trans-membrane pressure for the separation process can be created. It is also used to establish the recycle stream for the entire system. Both units are illustrated in Figure 2.
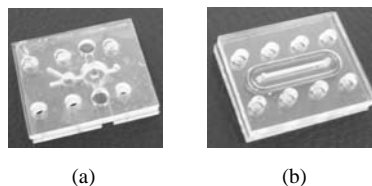

(a)   (b)

Figure 2. (a) Microbioreactor counterparts (b) Micro membrane separation unit in the continuous membrane microbioreactor prototype

Work Done
We have successfully designed and fabricated the first continuous membrane microbioreactor prototype. This prototype was designed considering several aspects (geometry design, mixing. sensors, separation processes, and establishment of control loops). The cheap fabrication method allows us to re-design (if necessary) and fabricate the microbioreactor in a very short period of time. The prototype is used as a basis in understanding the basic principles of the operation of membrane microbioreactors. Further testing is however required, before the prototype could be used for real biological work.

Next Steps
The next step of this research work will be on the establishment of a gaseous pH control concept for the continuous membrane microbioreactor. Focus will also be directed to the development of a micro Raman spectroscopy setup for the detection of desired compounds in the microbioreactor. Once these are established, a new continuous membrane microbioreactor prototype will be designed and fabricated in accordance to the requirements for the pectin modification and separation processes.

Acknowledgements

References
1. Todisco S. *et al.* (1994). *Mol. Cat.* . 92: 333 – 346.
2. Gallifuoco A. *et al.* (2003). *Ind. Eng. Chem. Res*. 42: 3937 – 3942.
3. Belafi-Bako K. *et al.* (2007). *Food. Eng*. 78: 438 – 442.
4. Miyazaki M. *et al.* (2006), *Trends. Biotechnol.*, 24 (10). 463-470.
5. Szita N. *et al.* (2005), *Lab on Chip*, 5, 819-826.
6. Muller D. H. *et al.* (2005), *Chem. Eng. Technol.*, 28 (12). 1569-1571.

Yuanjing Zheng

Phone:	+45 4525 2830
Fax:	+45 4588 2258
E-mail:	yjz@kt.dtu.dk
WWW:	http://www.chec.dtu.dk
Supervisors:	Anker Degn Jensen
	Christian Windelin, FLSmidth Airtech

Industrial PhD Study
Started: April 2008
To be completed: March 2011

Mercury Removal from Cement Plants by Sorbent Injection Upstream of a Pulse Jet Fabric Filter

Abstract

Strict emission limits of mercury from cement plants have been established. Despite that mercury removal by sorbent injection is the most promising and studied technology, fundamental investigations are still required before widely commercializing this technology. This project focuses on the kinetics and mechanisms of mercury retention by sorbents. Modeling of mercury removal by sorbent injection upstream of a fabric filter will be performed to optimize and get a better understanding of the process.

Introduction

There has been an increased focus on mercury emission from industry during the latest years as a consequence of the environmental impact and potential risk for human health of mercury compounds. Unlike most other trace elements, mercury is highly volatile, and exist almost exclusively in the vapor phase of combustion flue gas, either in the form of elemental mercury or mercury salts.

The US Environmental Protection Agency (EPA) sets the mercury emission limit from cement plants built or reconstructed after 2 December 2005 to 41 μg/Nm^3 dry gas @ 7% O_2 [1]. EU and Germany has set the limit value of 50 and 30 μg/Nm^3 dry gas @ 10% O_2, respectively, for cement plants firing waste [2-4]. The US EPA estimated that 25% of new cement plants in US will need emission controls to meet the mercury emission limit. A 90% reduction in mercury emissions from cement kilns may be expected over the next decade.

Due to rising energy costs and ever stricter energy and environmental regulations, alternative fuel technology is becoming an important factor in controlling costs. To gain a competitive edge, many cement and mineral producers worldwide have set ambitious targets for increasing their future usage of alternative fuels – both waste-derived fuel and biomass. High mercury containing alternative fuels such as chemical waste, domestic waste and sewage sludge are also incinerated in cement plants and high mercury emissions have been encountered. FLSmidth is committed to addressing all the technological needs of the global cement and minerals industries related to utilization of alternative fuels. To ensure that the mercury emission limit is met, FLSmidth has initiated research on mercury removal from cement plant.

Mercury can be removed from the flue gas by fuel cleaning and switching, raw material cleaning, sorbent injection, sorbent fixed bed, oxidation and removal by catalyst and wet scrubber. Activated carbon injection upstream of a particulate control device such as fabric filter has been shown to have the best potential to remove both elemental and oxidized mercury from the flue gas for coal-fired boilers not equipped with a flue gas desulphurization plant. Although activated carbon is the most studied sorbent for capturing mercury from gas stream, mercury adsorption by activated carbon is not clearly understood yet, research and development efforts are still needed before carbon injection is considered as a commercial technology for wide use. New sorbents need to be developed, the sorbent costs need to be reduced and the amount of sorbent injected needs to be kept to a certain level to avoid increased fly ash disposal costs. Furthermore, stability of mercury adsorbed by sorbents needs to be proved.

Extensive research has been carried out to reduce mercury emissions from coal combustion and waste incineration, but very little efforts have been concentrated on mercury removal in cement plant. The mercury removal not only depends on the sorbent but also on the speciation of mercury, flue gas composition and temperature, and the system configuration.

Compared to the flue gas from coal-fired boilers using low-NO$_x$ burners, the cement kiln flue gas contains less carbonaceous particles that contribute to mercury adsorption [5]. Recirculation of solid materials in the kiln system will cause release of the captured mercury. Thus the application of sorbent injection to cement kilns will be more challenging and knowledge obtained from mercury removal in power plant and incinerator might not be applied to cement plant directly.

Specific Objectives

The overall goal of this project is to develop and advance improved mercury control technologies using sorbent injection upstream of a pulse jet fabric filter for cement plants. Specific objectives are as follows:

1. To obtain updated knowledge of mercury control technologies relevant to cement plant by a comprehensive literature review.
2. To develop an experimental lab setup and screen sorbents for capturing mercury from cement kiln flue gas.
3. To develop an understanding of sorbent chemistry and provide mechanistic understanding and kinetic rates for sorbents of interest.
4. To demonstrate the ability of developed sorbents and technology to control emissions of mercury from a full-scale cement plant or FLSmidth Airtech pilot plant at Dania over a typical range of operating conditions.
5. To estimate the cost to implement mercury control by fabric filter at full-scale specific cement plant.
6. To develop a mathematical model that can describe mercury removal and predict mercury removal efficiency in cement plant by injecting sorbent upstream of a fabric filter.

Project status

The project is running smoothly according to the project plan and milestones. A comprehensive review of mercury removal from cement plants has been conducted and areas requiring further research and development were identified.

A lab-scale fixed bed reactor for screening the sorbents is being designed. Figure 1 illustrates the sketch of the proposed reactor system. The system consists of a mercury addition source, gas addition system, a gas-solid quartz reactor, an electrical heated oven, oxidized mercury to elemental mercury converter, a mercury analyzer, flue gas treatment units, and data sampling.

The applied mercury concentration in this project is very low (about 30 ppb) and a precise control of mercury addition is required. Both elemental mercury and HgCl$_2$ vapor will be added by a VICI calibration gas generator with mercury permeation tubes. Real-time mercury measurement is required to study the mercury capture kinetics and correlate operating parameters and sorbent performance. Commercially available mercury analyzers were reviewed and compared. Current mercury continuous emission monitors only measure

elemental mercury directly. The measurement of total mercury as well as mercury speciation can only be achieved indirectly by converting oxidized mercury to elemental mercury through a conversion system. In this project a thermocatalytic converter is proposed.
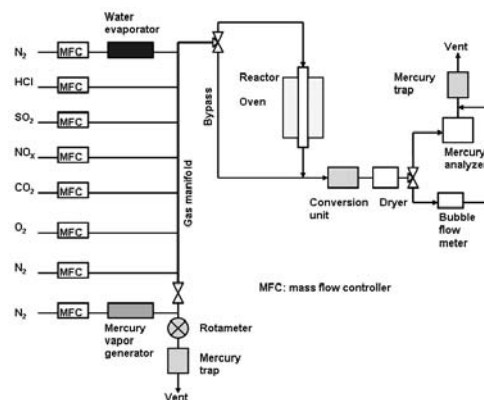
Figure 1: Sketch of the proposed fixed bed reactor system.

References

1. US EPA. National Emission Standards for Hazardous Air Pollutants from the Portland Cement Manufacturing Industry, 40 CFR part 63, EPA-HQ-OAR-2002-0051; FRLRIN 2060-AJ78, http://www.epa.gov/ttn/oarpg/t3/fr_notices/portland_finalamend_fr.pdf, accessed June 1, 2008.
2. The European Parliament and the Council of the European Union, Union directive 2000/76/EC on the Incineration of Waste, 2000.
3. German Cement Works Association, Environmental Protection in Cement Manufacture, VDZ Activity Report 2003-2005,
4. G. Ebertsch and S. Plickert, German Contribution to the Review of the Reference Document on Best Available Techniques in the Cement and Lime Manufacturing Industries, Part I: Lime Manufacturing Industries, 2006.
5. J. Richards, Capabilities and Limitations of Available Control technologies for Mercury Emissions from Cement kilns, PCA R&D Serial No. 2748a, 2005.